Modelling Nephron Autoregulation and Synchronization in Coupled Nephron Systems

Laugesen, Jakob Lund; Mosekilde, Erik

Publication date:
2011

Document Version
Publisher's PDF, also known as Version of record

PhD Thesis

Modelling Nephron Autoregulation and Synchronization in Coupled Nephron Systems

Jakob Lund Laugesen

October 25, 2010

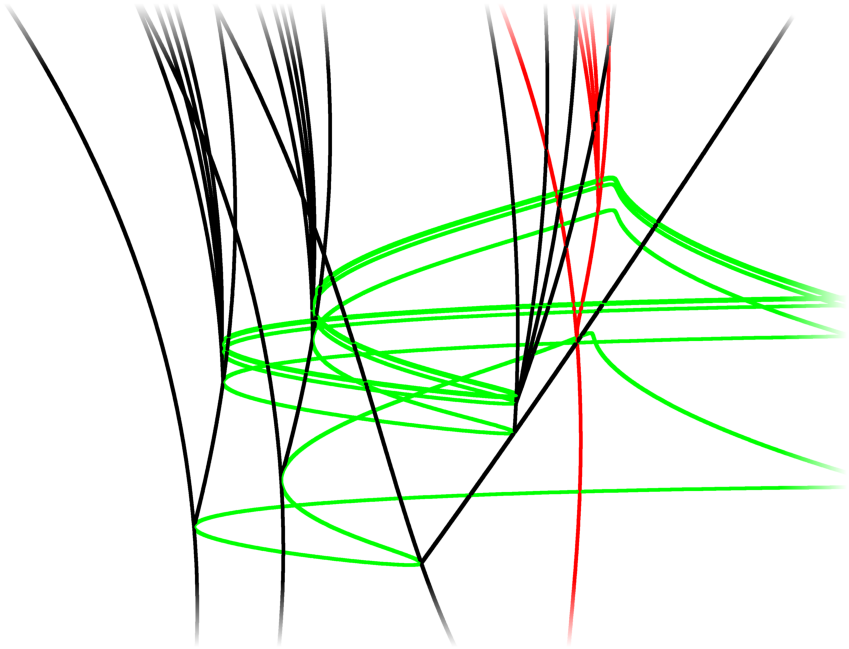

Supervisor: Erik Mosekilde

Technical University of Denmark

DTU

BioSim EU NETWORK OF EXCELLENCE

DTU Fysik
Institut for Fysik

Front figure: Bifurcation structure in the (ω, a_1) plane (rotated) of two coupled Rössler system, showing one period-doubling, three saddle-node and one torus bifurcation cascade.

Preface

This thesis presents the work I have produced during my PhD study at the Department of Physics at The Technical University of Denmark. The main part of the study was supported by BioSim - European Network of Excellence and has been conducted under supervision of Professor Erik Mosekilde.

The thesis collects a serie of bifurcation studies of a number of nephron models of different complexity, and the idea is to transfer the knowledge gained on the simple models to the complex and more physiological sound models. To me it has been very encouraging to work with the simple models because a much more detailed understanding of the phenomena can be achieved. Since the phenomena is generic to a large class of systems, the phenomena in simple models can be almost directly transferred to more complex models.

During my study I have had many collaborators, to whom I am very thankful. Many of the fruitful and exciting studies on the Rössler system was performed together with Professor Zhanybai Zhusubaliyev, Kursk State University. The most detailed nephron model was presented to me by Professor Donald Marsh from Brown University, Professor Niels-Henrik Holstein-Rathlou and Professor Olga Sosnovtseva, both from the Panum Institute, with who I have published a paper on our results. I would also like to give my thanks Alexey Pavlov, Saratov State University for performing a wavelet analysis for two of my papers.

I would like to give a special thanks to my supervisor Erik Mosekilde for the excellent guidance in general, and also to my co-supervisor Olga Sosnovtseva for always being encouraging. My thanks is extended to the administrators of BioSim Anne Marie Clemensen, Carsten Knudsen and Noami Dayan for their company and my PhD-colleagues Peter Larsen, Christian Bentzen, Per Greisen and all the other PhD-colleagues

and friends in the BioSim network for giving the research community a social angle as well (especially at the BioSim conferences).

Finally, I would like to give my tanks to my family for their support and understanding. My deepest tanks goes to my future wife Susanne, who also has been through the troubles of a PhD study, and hopefully we can now start a life not 600 km appart.

October 25 2010, Jakob Laugesen

Abstract

A successful mathematical description of the renal processes requires an understanding of the mechanisms through which these pressures take place. Part of the present thesis addresses the hypothesis that increased coupling between neighboring nephrons and increased strength of the tubuloglomerular feedback process can explain the experimentally observed irregular oscillations in the nephron pressures and flows. The hypothesis is put to test by calculating Lyapunov exponents of a high level mechanism-based model of a nephron and a similar model of two vascular coupled nephrons.

Synchronization between oscillating period-doubling systems is the topic of the larger part of the study. Since synchronization is a fundamental phenomenon in all sciences, it is treated from a general viewpoint by analyzing one of the most simple dynamical systems, the Rössler system, both in an externally forced version and in the form of two mutually coupled oscillators. The bifurcational mechanism to resonant dynamics and chaotic phase synchronization is described in detail. The transition from synchronized to non-synchronized dynamics is known to take place at a dense set of saddle-node bifurcations that run along the edge of the resonance tongue and appear also to be related to the formation of multilayered tori and torus-doubling bifurcations. A cyclic behavior of sub- and supercriticality of the period doublings in the neighborhood of the contact between period doubling and saddle-node bifurcations cause a set of torus bifurcations that take place at a very small range of parameters.

In coupled Rössler systems, the same torus bifurcations take a more global role. While a complete, but now folded, period-doubling cascade evolves, a cascade of torus bifurcations emerge from all the period doublings and run along side with three (due to the folding of the period doubling) sets of saddle-node bifurcations at the edge of the tongue. Through homoclinic bifurcations of tori with different periodicity, a second mechanism to phase synchronization is found to occur.

Similar bifurcation structures are shown to exist in an externally forced nephron model and in a model of two vascular coupled nephrons, underlining that the discussed phenomena are of a common nature to forced and coupled period-doubling systems.

Dansk resumé

En vellykket matematisk beskrivelse af nyrernes forskellige processer forudsætter en grundig forståelse af de mekanismer, hvorigennem disse processer finder sted. En del af denne afhandling undersøger en hypotese om at øget kobling mellem nabo nefroner og øget styrke i den tubuloglomerulære feedback-process kan forklare de eksperimentielt observerede kaotiske svingninger af tryk og væske strømme i nefronet. Hypotesen testes ved beregne Lyapunov eksponenter af en mekanisme-baseret nefron model samt en model bestående af to vaskulært koblede nefroner.

Synkronisering mellem oscillerende periode-doblings systemer udgør den største del af dette studium. Da synkroniseringen er et grundlæggende fænomen i alle naturvidenskaber, er emnet behandlet ud fra et generelt synspunkt ved at analysere en af de mest simple dynamiske systemer, Rössler systemet, både i en eksternt tvunget version og i en udgave hvor to oscillatorer påvirker hindanden gensidigt. De bifurkationer der optræder ved overgangen til resonans dynamik og kaotisk fase synkronisering er beskrevet i detaljer. Det er kendt, at overgangen fra synkroniseret til ikke-synkroniseret dynamik finder sted på en tæt mængde af sadel-knude bifurkationer der løber langs kanten af resonanstungen og synes også at være relateret til dannelsen af resonans tori organiseret i flere lag samt torus-doblings bifurkationer. En cyklisk opførsel af sub- og superkritiske perioden-doblinger i nærheden af kontakt punktet mellem periode-doblings og sadel-knude bifurkationer forårsager en række torus bifurkationer, der finder sted på et meget parametre område.

I koblede Rössler systemer, har de samme torus bifurkationer en mere global rolle. Mens en komplet, og nu foldet, periode-doblings kaskade udvikler sig, dannes en kaskade af torus bifurkationer som skabes på periodenfordoblingerne og udvikler sig side om side med tre (på grund af foldning af perioden-fordobling) sæt sadel-knude bifurkationer på kanten af tungen. I modsætning til det externt forcerede system finder overgangen til fasesynkronisering ikke sted ved sadel-knude bifurkationerne men derimod gennem homokline bifurkationer på tori med forskellige periodiciteter.

I analogi med de abstrakte Rössler systemer undersøges nefron modellen i en forceret og koblet udgave. Det vises at disse systemer har lignende bifurkationsstrukturer og at de derfor kan formodes at være typiske for forcerede og koblede periode-doublings systemer.

Contents

toregulation (Royal Society Interface Focus)

Manuscript M5: Synchronization of period-doubling oscillations in multi-dimensional systems (Chaos)

Publication P2: Coupling-induced complexity in nephron models of renal blood flow regulation (American Journal of Physiology)

Publication P3: Biosimulation and Computations in Systems Biology (Handbook of Molecular Biophysics)

CHAPTER 1

Introduction to the thesis

1.1 Motivation

During the past decades systems biology, including biosimulation, has become a rapidly growing approach to biological, physiological and medical research. A main characteristic of this approach is that it adopts a system's oriented view on the living organism rather than focusing on specific parameters or relations. In this way the approach introduces dynamics to the description while at the same time trying to bridge across the different hierarchical levels of the physiological system. Another characteristic feature of biosimulation is that its success requires contribution from a large number of different disciplines, including physics and complex systems theory.

Part of this research consist of experimental studies, that confirm results from modelling and also direct attribution to new questions and problems to be understood. The problem of understanding the dynamics of and mechanisms involved in blood flow autoregulation, which also include the understanding of how nephrons are coupled together and how the experimentally observed synchronization between coupled nephron take place, was suggested to me by Prof. Erik Mosekilde. On a longer term new knowledge of the physiological mechanisms in the nephron and on the coupling among nephrons, together with improved knowledge of the bifurcational mechanisms of the models, may provide the basis for larger models describing the kidney rather than the isolated nephron and its nearest surroundings. Let us also note that synchronization is a very fundamental phenomenon appearing in practically all kinds of natural sciences. This fact makes the phenomenon even more appealing as the research on synchronization between coupled nephrons may lead to wider consequences in other sciences.

1.2 Aims of the study

This thesis aims at shedding light on the processes taking place in connection with the kidneys role in blood flow autoregulation. Four main topics are addressed: 1) describing the dynamics of the single nephron, 2) establishing a bifurcational description of synchronization mechanisms in general, 3) examining the dynamics and synchronization mechanisms in coupled nephrons, and 4) confirming that irregular dynamics of coupled nephrons is related to an increased degree of coupling.

These four different wide goals are more specifically

1. To perform a more detailed bifurcation analysis in view of providing an overview of the transitions between different regions of mode-locking between the TGF and myogenic oscillations.

2. The theory of synchronization between period-doubling oscillators is not yet fully understood. We want to establish a precise description of the bifurcations that take place on the route to resonant and chaotic synchronization. This is expected to also give a better understanding of the behavior of more complicated systems such as the coupled versions of our nephron models.

3. The above more theoretical results will be shown to also be relevant to a description of synchronization in single and coupled nephron systems.

4. A detailed nephron model is used to test the hypothesis that hypertension is related to an increased strength of the tubuloglomerular feedback and an increased inter-nephron coupling.

1.3 Main results

At the moment of writing, many of the obtained results are either already published or they are in the review process. Below a list of all publications and manuscripts (submitted or will be submitted) is found and in the back of the thesis the full text is printed.

List of publications and manuscripts produced during the study:

M1 Laugesen, J. L., Mosekilde, E. and Zhusubaliyev, Zh.T., Bifurcation structure of the C-type period-doubling transition, *submitted to Physica D*.

P1 Zhusubaliyev, Zh. T. and Laugesen, J. L. and Mosekilde, E., From multi-layered resonance tori to period-doubled ergodic tori, *Phys. Lett. A* 374, 25342538, 2010.

M2 Mosekilde, E., Laugesen, J. L. and Zhusubaliyev, Zh. T., The edge of chaotic phase synchronization, *submitted to Eu. Phys. Lett.*

M3 Laugesen, J. L. Mosekilde, J. L., Bifurcation analysis of resource coupled Rössler systems, *J. Appl. Functional Analysis*, accepted for publication.

M4 Laugesen, J. L., Mosekilde, E. and Holstein-Rathlou, N.-H., C-type Period-Doubling Transition in Nephron Autoregulation, *submitted to Roy. Soc. Interface*.

M5 Laugesen, J. L., Mosekilde, E., and Holstein-Rathlou, N.-H., Synchronization of period-doubling oscillations in multi-dimensional systems, *submitted to Chaos*.

P2 Laugesen, J. L.,Sosnovtseva, O. V., Mosekilde, E., Niels-Henrik Holstein-Rathlou, N.-H. and Marsh, D. J., Coupling-induced complexity in nephron models of renal blood flow regulation, *Am. J. Physiol. Regul. Integr. Comp. Physiol.* 298, R997-R1006, 2010.

P3 Sosnovtseva, O., Laugesen, J. L., and Mosekilde, E., Biosimulation and Computations in Systems Biology. Chapter 25 in: *Handbook of Molecular Biophysics: Methods and Applications*, ed. H. G. Bohr, WILEY-VCH, Weinheim, 2009.

The first part of the study was mainly devoted to understanding of the single nephron and the possibility for chaotic dynamics in coupled nephrons. In short these results are:

- We have obtained a detailed bifurcation diagram for the single nephron model showing a number of separate period-doubling cascades each with different TGF:myogenic ratio. The existence of such a cascade broadens the working range of the model, since it has been shown that juxtamedullary nephrons have smaller locking ratios due to the greater length of Henle's loop.
  Described in: Manuscript M4 and section 3.2 in this thesis

- We have examined a spatially lumped version of Henle's loop with individual compliances and resistances in the compartments and successfully demonstrated how modelling can be used to describe the damping of pressures along the tubular system.
  Described in: Publication P3

- Calculation of Lyapunov exponents from simulated time series of the detailed nephron model support the hypothesis that hypertension is related to the strength of coupling between nephrons. A practically absent ability to show chaotic dynamics for any TGF-gain factor is found at zero inter-nephron coupling i.e., for a single uncoupled nephron. At physiological realistic inter-nephron coupling, chaotic dynamics emerge in a relative wide range of high TGF-gain values.
  Described in: Publication P2

Our studies on periodically forced and mutually coupled Rössler systems have resulted in a number of phenomena and generic bifurcation structures. Similar structures have been observed in corresponding forced and coupled nephron models

The main results of the study on forced systems are

- Detailed description for the formation of saddle-node bifurcations within the resonance zone, that limit the various stable and unstable solutions as a period-doubling cascade evolves inside the Arnol'd tongue.

Described in: Manuscript M1 in publication P2

- Outside the resonance zone a torus-doubling cascade evolves as a consequence the external forcing to the period-doubling cascade of the unforced Rössler system.
  Described in: Manuscript M1 and Manuscript M2

- We describe how multilayered tori are formed through period-doubling bifurcations of the node and saddle transverse to the torus. We also describe how these resonant tori are connected to the doubling of tori.
  Described in: Publication P1 and Manuscript M1

- Cyclic behavior of the sequence of sub- and supercritical period doublings at the edge of resonance, where the supercritical case leads to a torus bifurcation to close a small gap between two resonant regions not covered by a saddle-node bifurcation.
  Described in: Manuscript M1

- Consequently, a cyclic behavior of the saddle-node bifurcation along edge must exist. This leads to an accumulation of saddle-node bifurcations. The border between phase-synchronized chaos and non-synchronous chaos is located at that accumulation curve.
  Described in: Manuscript M2

Our study of coupled period-doubling systems extends the significance of the above findings, as the same phenomena are observed. In addition we also find that:

- The torus bifurcation takes a new and more global role, giving rise to a cascade of alternating torus bifurcations along the edge of synchronization together with the saddle-node bifurcation.
  Described in: Manuscript M5

- From the above finding follows an alternative mechanism to desynchronization of both the non-chaotic and chaotic resonance region, that take

place through a homoclinic bifurcation on the tori born at the torus bifurcations inside the tongue. We suggest that a cascade of homoclinic bifurcations exist as a consequence of Bogdanov-Takens bifurcations on the torus bifurcations.
Described in: this thesis.

All the above findings have also been found to be present in forced and coupled nephron models.

CHAPTER 2

Background: Introduction to the renal physiology

Nephrology covers a very wide range of topics all having to do with the functionality of the kidney. In this thesis emphasis is paid to the nephron's role in regulating its own incoming blood flow. Coupling between neighboring nephrons is believed to play an important role for the kidneys regulation of the blood flow and probably also other functions. To understand the nature of both the regulating mechanisms and the coupling mechanisms some basic knowledge of the anatomy and processes is required.

2.1 Anatomy, functionality of the kidney and its nephrons

Due to evolution of all mammals from the same species (presumable sea animals) we are largely alike regarding the organs. All mammals posses two kidneys', although the body only need one to function properly. Many different processes take place in the kidney among which the most well known are the kidneys 1) maintenance of the body's water and salt balance, 2) filtration and excretion of waste products through urine and 3) regulation of the blood pressure. Several hormonal processes also take place, such as hormones that control the body's calcium balance, a ion that is also important in the kidney itself.

The kidney is supplied with blood through the renal artery, which divides into the smaller arcuate arteries, then interlobular arterioles and then into afferent arterioles forming a tree like structure, see Fig. 2.1. Through this division, about 1 million (for the human) small arterioles are formed in each kidney. The number of branching levels are usually said to be about 6, hence the number of new vessels branching from one vessel is on average

$(10^6)^{1/6} = 10$. At the end of the branching the blood flows into the nephron, which is the functional unit of the kidney (at least regarding the regulation of blood pressure). The nephrons are sustained or contained in the medullary pyramids, that extend from the central part to the cortex of the kidney. In the nephrons the filtration of the blood takes place and the waste products flow with the redunant water via the ureter to the bladder. The functional

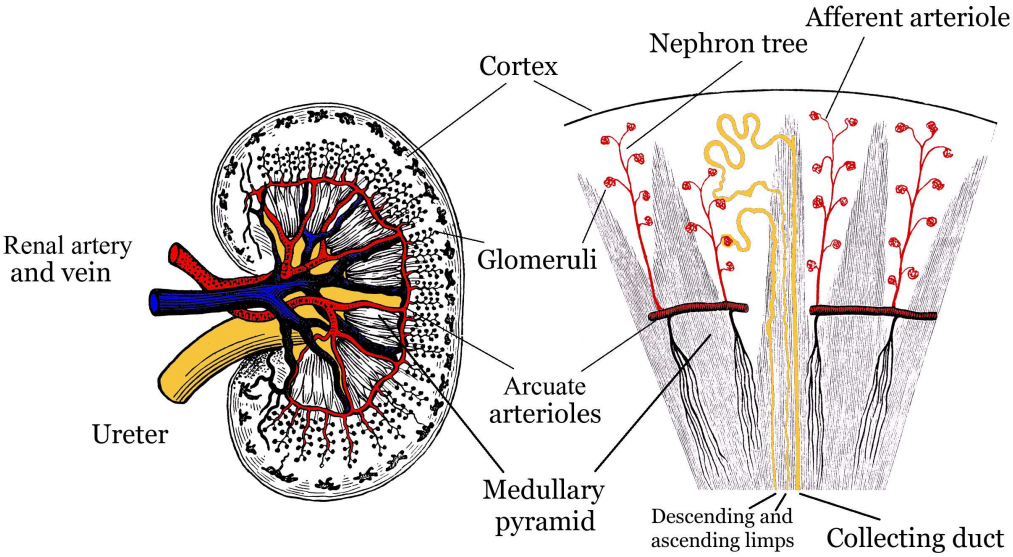

Figure 2.1 Anatomy of the kidney. The blood supply to the kidney starts at the arcuate artery that branch into smaller arteries and arterioles. Filtration takes place at the glomeruli, and the filtered blood is then returned to the blood system through the veins. The filtrate passes a tubular system in which part of the fluid is reabsorbed into the venous system. The nephrons (of which only the glomeruli are visible) are surrounded by tissue called medulla. Reabsorbed fluid first enters the medulla and from there it is absorbed into capillary veins.

units of the kidney are the nephrons, see Fig. 2.2. When the blood reaches the last level of the branching network, it flows from the afferent arteriole into the glomerulus, which extracts water and various substance, except blood cells and proteins. The extracted fluid flows further into the convoluted proximal tubulus. Nearby 70% of the glomerular filtrate is reabsorbed from the proximal tubule into the capillary network and collected by the outgoing venous system. This isosmotic process is controlled completely by a hydrostatic pressure gradient. The residual fraction becomes important for the feedback mechanism later in the filtration. The remaining 30% of the

filtrate enters the thin descending loop of Henle where additionally 15% of the water is reabsorbed giving rise to an increased concentration of NaCl as the limb is impermeable to salts. On passing the ascending limb the filtrate

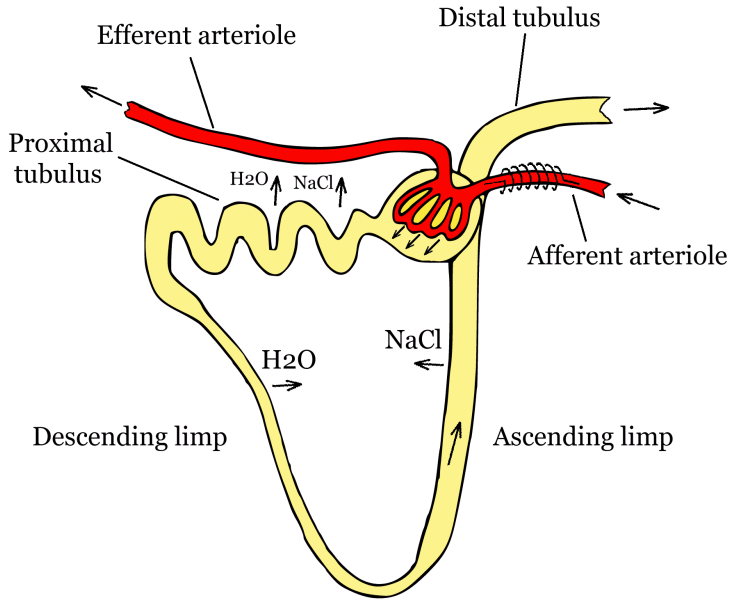

Figure 2.2 Sketch of the nephron with indication of the blood flow. The main processes involve filtration in the glomerulus, water and salt regulation along the loop of Henle, and feedback at the macula densa near the end of the ascending limp.

is again diluted as Na^+ and Cl^- are reabsorbed, while the limb is largely impermeable to water. At the end of Henle's loop, the tubulus comes into cellular contact with the afferent arteriole of the same nephron. At these points special cells, the so-called macula densa (MD) cells, sense the Cl^- concentration. If the rate of glomerular filtration, due for instance to an elevated arterial blood pressure, is too high, the active reabsorption of NaCl is not complete, and therefore the salt concentration at the macula densa is too high. The macula densa cells then produce transmitter agents that activates the smooth muscle cells in the arteriole causing a radial contraction of the arteriole whereby the flow resistance is increased, hence lowering the glomerular pressure and thereby reducing the filtration rate. This process is called the tubuloglomerular feedback mechanism (TGF). The TGF mechanism is seen as a way for the nephrons to protect their own function against variations in the arterial pressure. From the moment where the fluid is fil-

tered in glomerulus to moment where the afferent arteriole react 12-15 sec have passed. Since the reactive contraction of the arteriole to an increased flow is generally too high, there will be an opposite reaction (also too high) 12-15 sec later. This causes the TGF to be unstable and the oscillations are therefore sustained with a period of 30-40 sec, where and extra delay of approximately 5 sec has been include in order to account for the cellular processes in the arteriole.

A second oscillating mechanism that contribute to the autoregulation is the myogenic response of the afferent (and possibly the efferent) arteriole. Basicly it is an active response that counteracts increases in arteriolar pressure by increasing constriction of the vessel caused by the smooth muscle cells in the arteriolar wall. Inside the smooth muscle cells, oscillations in cytoplasmic Ca^{+2} tend to synchronize and cause the arteriolar wall to contract with a period of 4-6 sec. The two oscillatory modes are usually locked to a specific ratio, typical values for cortical nephrons are 1:4, 1:5 and 1:6.

CHAPTER 3

Nephron models

Three closely related mechanism-based nephron models and one fairly abstract but widely known model, the Rössler system, are analyzed in this thesis. They differ in their degree of complexity and therefore also in the amount of information they provide. In biology, all models are approximate, because of the high complexity of biological materials and processes. Spatial processes are often reduced to single compartment representations, whereby spatial variations are averaged. For many purposes such approximations do not change the qualitative behavior of the model. In order to get a little deeper into the physiology of the nephron than the short verbal description above, the processes is rephrased once again from a more physical point of view.

Two of the models do intent to include a spatial description of the water and salt balance. One of them, furthermore includes a representation of the myogenic mechanism on a cellular level. The last model is the Rössler system, that we will try to relate to the dynamics of the nephron. At the end of the chapter a discussion of coupling mechanisms is given.

3.1 A simple mechanistic single nephron model

The simplest single nephron model based on well-known physiological mechanisms and processes treated here was developed by K. S. Jensen, E. Mosekilde and N.-H. Holstein-Rathlou in 1986 [14, 13], but over the years several improvements have been introduced [3]. Other early models with the purpose of describing processes in the tubular segments only encompasses the TGF mechanism and appear to be unable to show chaotic dynamics. Since it is suspected, and well supported by experiments, that hypertension gives rise to an irregular time evolution of tubular pressure, it is assumed that a mathematical model represent this state by deterministic chaos.

The rate of change of the proximal tubular pressure P_t is given by the flow of filtrated fluid at the glomerulus F_{filt} substracted by the flow of reabsorbed fluid F_{reab} and the fluid flow continuing into the loop of Henle F_{Hen}, divided by the compliance C_{tub} of the proximal tubule

$$\frac{dP_t}{dt} = \frac{1}{C_{tub}}(F_{filt} - F_{reab} - F_{Hen}). \tag{3.1}$$

The reabsorption is assumed isosmotic with respect to water and salt, such that the salt concentration remains unchanged. It is also assumed that the reabsorption rate is constant, although it probably depends on the pressure. On the other hand this is justified because a pressure dependent reabsorption will only cause a damping of the pressure, and therefore corresponds to a slightly higher compliance of the tubule, so the pressure dependence can be said to be accounted for through C_{tub}.

By assuming that the pressure variations in the distal tubular pressure are small, the flow into the loop of Henle is given by

$$F_{Hen} = \frac{P_t - P_d}{R_{Hen}}, \tag{3.2}$$

where P_d is the distal tubular pressure and R_{Hen} is the total flow resistance along the loop.

Blood consists of plasma (water, proteins, minerals etc.) and blood cells. The blood cells occupy approximately 55% (the hematocrite) of the blood volume. Since protein molecules are too large to be filtered through the glomerular capillaries the amount of protein must remain constant, while the concentration must increase as part of the remaining plasma enter the capilaries. The plasma flow into the glomerulus is given by

$$F_a = \frac{P_a - P_g}{R_a}(1 - H_a), \tag{3.3}$$

where P_a is the arterial blood pressure, P_g the glomerular pressure, R_a the afferent flow resistance and H_a is the hematocrite. The glomerular filtration rate is

$$F_{filt} = F_a - F_e = F_a(1 - \frac{C_a}{C_e}), \tag{3.4}$$

where C_a and C_e are afferent and efferent protein concentrations. Note, that the conservation of protein ($C_aF_a = C_eF_e$) has been applied. An expression

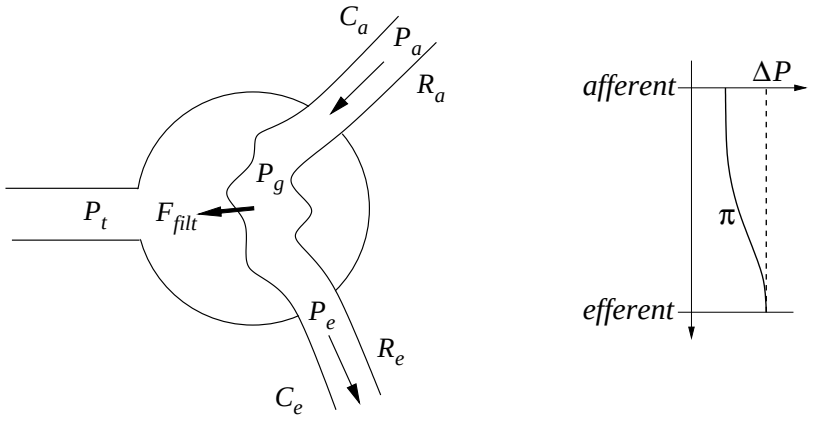

(a) Glomerulus **(b)** Capillary pressures

Figure 3.1 Physical quantities and parameters involved in the glomerular filtration rate. a) Glomerulus with the afferent and efferent arterioles. b) The evolution of colloid osmotic pressure $\pi(C_e)$ and the assumed constant hydrostatic pressure gradient $\Delta P = P_t - P_g$. At the efferent end pressure equilibrium is achieved.

for the glomerular pressure now follows from conservation of pressure and flow (Fig. 3.1)(a)) and by assuming a constant efferent flow resistance

$$P_g = P_e + R_e \left(F'_a - F_{filt}\right), \tag{3.5}$$

where $F'_a = (P_a - P_g)/R_a$ is the afferent blood flow.

In reality the protein content of the blood supply is time dependent, but this variation depend on mechanisms outside the kidney, mainly food consumption and physical activity. The beating of the heart is assumed to be damped so much that oscillations in the arterial pressure P_a can be neglected and the frequency ($\sim$ 1Hz) is fast enough for the vasomotion to be unable to react to such fast oscillations. Within the purpose of the model, which is to study mechanisms taking place in the nephron, the afferent protein concentration is defined to be constant. The efferent protein concentration, depends on the behavior of the filtration mechanism, which is an essential part of the functionality of the nephron, and therefore the mechanism behind the variation of this concentration must be included in the model. As mentioned earlier the filtration takes place through an osmotic process where the osmotic colloid pressure $\pi(C_e)$ gradually approach the hydrostatic pressure gradient $\Delta P = P_g - P_t$ across the capillaries, see Fig. 3.1(b). Based on exper-

iments on rats, Deen *et al.* [5] have shown that a second order approximation

$$\pi(C_e) = aC_e + bC_e^2, \tag{3.6}$$

to the colloid osmotic pressure $\pi(C_e)$, is sufficient in the physiological range of C_e. Parameters a and b are empirical determinants of the experimental study of Deen [4]. An expression for the efferent protein concentration in terms of P_g and P_t, which are explicitly stated above, follows directly from Eq. (3.6), by assuming that pressure equilibrium is reached at the efferent end ($\Delta P = \pi(C_e)$),

$$C_e = \frac{1}{2b}\left[\sqrt{a^2 - 4b(P_t - P_g)} - a\right]. \tag{3.7}$$

The processes taking place along the loop of Henle are not an issue for this model. Likewise the many processes on cellular level from sensing the Cl^- concentration at macula densa to the release of renin and signalling to the smooth muscle cells are left out from the mechanistic part of the modelling. However, all these processes take time and a delay between the flow into the loop of Henle to the response of the arteriole must be present. To take care of this slow signal, a third order delay of the fluid flow is introduced,

$$\frac{d\chi_1}{dt} = F_{Hen} - \frac{3}{\Delta T}\chi_1 \tag{3.8}$$

$$\frac{d\chi_2}{dt} = \frac{3}{\Delta T}(\chi_1 - \chi_2) \tag{3.9}$$

$$\frac{d\chi_3}{dt} = \frac{3}{\Delta T}(\chi_2 - \chi_3), \tag{3.10}$$

where ΔT is the total delay time and χ_i are intermediate flows. An alternative approximation to the actual delay is to increase the order whereby it approaches a discrete delay. However, a discrete delay corresponds to a system without damping of the flow, and since we know that there the amplitudes are approximately halved at the end of the loop of Henle, the third order delay is considered as a more reasonable approximation. To close the tubuloglomerular feedback loop the activation of the arteriole must be described in terms of the end flow χ_3. The activation of the smooth muscle cells is controlled by the Cl^- concentration at the macula densa (MD). As the flow through the tubular system is increased the NaCl concentration at the Macula Densa is increased. This causes activation of the smooth muscle cells, whereby the afferent arteriole is constricted, and the pressure and flow

in the glomerulus is decreased. By means of open loop experiments Leyssac *et al.* [21] have found that the salt concentration at macula densa to a high extent depends only on the early distal flow rate and that the relationship follows a sigmoidal curve of the form

$$\psi = \psi_{max} - \frac{\psi_{max} - \psi_{min}}{1 + \exp\left[\alpha(3\chi_3/(\Delta T F_{Hen,0}) - S)\right]}, \tag{3.11}$$

where $S = 1 - 1/\alpha \log(\frac{\psi_{eq} - \psi_{min}}{\psi_{max} - \psi_{eq}})$ is the displacement along the flow axis and ψ_{eq}, ψ_{min} and ψ_{max}, determine the equilibrium value of ψ and the limits of the curve. $F_{Hen,0}$ is a normalization parameter for the Henle flow. The parameter α determine the slope of the curve at ψ_{eq} and may be interpreted as the strength of the feedback. Since the afferent arteriole is most active at the glomerular end, it is divided into a passive and an active part. The total flow resistance is the sum of the individual resistances of the two parts

$$R_a = R_{a,0}(\beta + (1 - \beta)r^{-4}), \tag{3.12}$$

where β is the fraction of the arteriolar length is assumed passive with resistance $R_{a,0}$, and the quartic term in the normalized arterial radius r follows from Poiseuille's law. The average transmural pressure (average over length, not time) in the afferent arteriole is given by

$$P_{av} = \frac{1}{2}\left(P_a + P_g - (P_a - P_g)\beta\frac{R_{a,0}}{R_a}\right). \tag{3.13}$$

Aalkjær *et al.* [1] have experimentally shown that arterioles may display self-sustained oscillations in their wall tension due to oscillations in arteriolar radius, when the tension exceeds a certain level. A permanent high activation of the smooth muscle cells is assumed to be responsible for this vasomotoric or myogenic response. Several mathematical models (e.g. [8, 9]) support Aalkjærs explanation for this phenomenon.

As a simple model for the myogenic oscillations of normalized arteriolar radius r, may be a damped oscillator with a nonlinear external term representing the elastic and myogenic dependence on wall tension,

$$\frac{d^2r}{dt^2} + d\frac{dr}{dt} + \omega_m^2\frac{P_{eq} - P_{av}}{P_0} = 0, \tag{3.14}$$

where d is the damping factor, P_0 is normalization pressure, ω_m is the angular frequency tuned to the myogenic frequency. The last term include the response of the arteriolar wall to pressure variations.

The equilibrium transmural pressure is the transmural pressure at which the arteriolar wall would be in equilibrium at the present value of the radius and muscular activation ψ. This pressure is composed by an elastic P_{el} and an active part P_{act},

$$P_{eq} = P_{el}(r) + \psi P_{act}(r), \tag{3.15}$$

where ψ is the activation level given by Eq. (3.11). The following transmural pressure-radius relationships of both the elastic and active contribution was derived by Feldberg *et al.* [7]. Note, that Eqs.(3.15) and (3.14) constitude the connection between on one side the filtration and tubular mechanisms and on the other side the arteriolar dynamics.

The elastic part is due to the mechanical properties of elastin and collagen, which here are treated as one material. It behaves just like a rubber band, at small strains a linear stress-strain relationship exist, while at large strains the stress increase exponentially, $\sigma \propto e^{\epsilon\gamma} - 1$. A transmural pressure-radius relationship can be obtained by applying Laplace law, $dP = \sigma(1+\epsilon)/r dr$, where σ is circumferential stress to give

$$P_{el}(r) = P_1 \left[e^{\alpha_1 (r-1)} + b_1 (r-1) \right]. \tag{3.16}$$

Paul [25] suggest a piecewise linear, tent shaped relationship for the active part of the arteriolar stress-strain relationship. The active contribution also has a linear contribution to the total stress, however, when at some level of distention the stress decrease and contribute to a further distention or at least decreases the total stress, so that the reaction to the strain becomes smaller. Numerical integration and fitting to an empirical pressure-radius relation give the form:

$$\psi P_{act}(r) = \psi P_2 \left[\frac{1}{1 + e^{\alpha_2 (0.4 - r)}} + b_2 (r + 0.9) \right]. \tag{3.17}$$

Regarding the nephron autoregulatory mechanism all the equations above together form a minimum nephron model based on experimental observations describing both the TGF and myogenic mechanisms. While at the same time it is detailed enough to describe many of the characteristic features in nephron autoregulation, it is still simple and and low-dimensional enough to be analyzed with bifurcational methods such as continuation techniques.

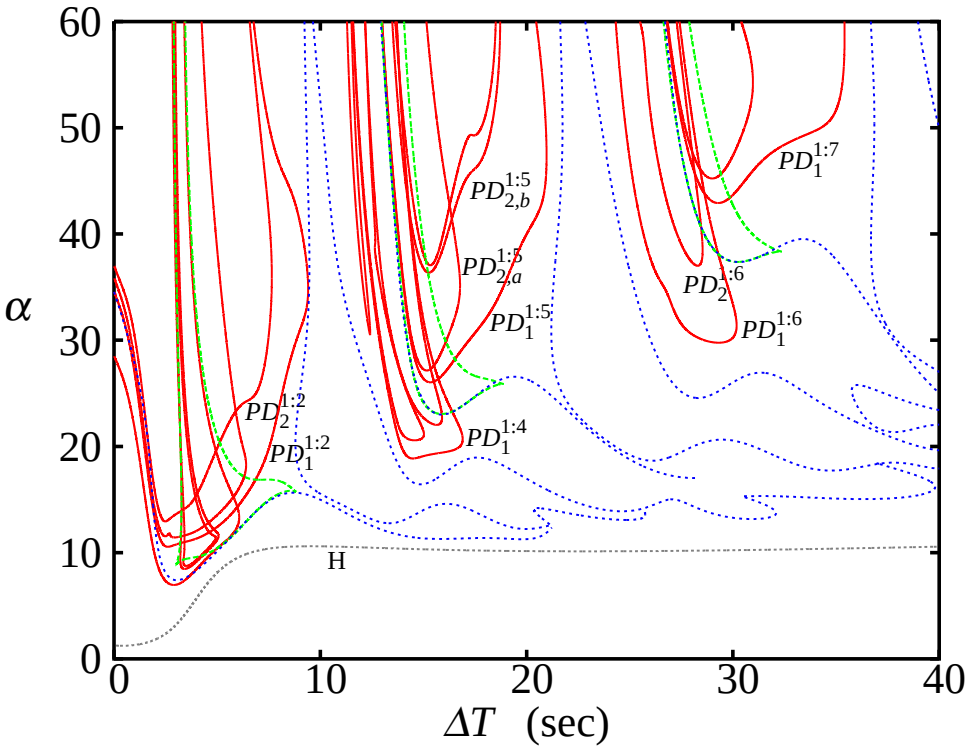

Figure 3.2 Overview of main bifurcations in the single nephron model. Red curves are period doublings, green are saddle-node bifurcations and the grey curve is the Hopf bifurcation giving rise to the oscillations in the TGF. Blue curves are soft transitions between regions of various locking ratios between TGF and the myogenic oscillations.

3.2 Model parameter values

Figure 3.2 shows a detailed two-dimensional bifurcation diagram of the above model, with the delay ΔT and TGF-gain α as bifurcation parameters and with all other parameters fixed according to Tab. 3.1. The parameter range especially of our interest is from $\Delta T = 12$ sec to $\Delta T = 18$ sec, since the model here oscillates with a period of the order $30 - 40$ sec, corresponding to the periods found in experiments. A value of $\Delta T = 12 - 18$ sec also agrees well with the experimentally observed phase shift between the proximal tubular pressure oscillations and the distal tubular NaCl concentration oscillations [10]. For normotensive rats typical experimental values for the gain parameter α in Eq. (3.11) are $\alpha = 11.4 \pm 2.2$, while spontaneously hypertensive rats

have $\alpha = 16.8 \pm 12$ [11]. Above the Hopf bifurcation different regions of mode-lockings are observed, limited by the dashed blue curves. Each mode-locking region is associated with a period-doubling cascade, and saddle-node bifurcations (green curves) cause pairs of period-doubling cascades to co-exist. Note, that a bifurcation is labelled with a subscript indicating the periodicity of the cycle that bifurcates. This label convention is used throughout the thesis. Within the first period doublings, $PD_1^{1:4}$ and $PD_1^{1:5}$, two individual period doublings are found for the 1:5 region these are $PD_{2,a}^{1:5}$ and $PD_{2,b}^{1:5}$, each leading to chaos through cascades of period doublings. For increasing ΔT the same period-doubling structure repeats for mode-locking pairs (1:6, 1:7), (1:8, 1:9) etc., but located at larger increasingly larger values of α.

Since the 1:4 and 1:5 mode-lockings are the most typical observed modes observed in experiments, we fix the delay ΔT to 16 sec, unless stated otherwise. Most of the parameters in Tab. 3.1 are experimentally determined. However, it is usual in modelling to adjust parameters to obtain a behavior of the model that resemble with experimental findings. Adjustments are justified by noting that many processes of the nephron are ignored in the model, giving rise to a displacement of bifurcations. In particular we consider one- and two-nephron models rather than the 30.000 nephron system by which the experimental data are produced. Other reasons to adjust parameters slightly is that experiments rather provide a parameter range, than a precise value mainly due to variations from animal to animal. This is the background for examining the system for values of the TGF gain factor α somewhat above the experimentally observed values.

3.3 Other nephron models

The degree of detail, level of scale and mechanisms included in a nephron model must be chosen to meet the individual aims of specific studies. For instance it is preferred to exclude mechanisms that are involved in salt and water balance if there is no need to know these quantities. On the other hand, such mechanisms must of course be included, and possible other mechanisms that are indirectly relevant, must be included in some studies. The single nephron model presented above does not involve the variation in salt concentration along the loop of Henle, although the TGF mechanism dependent on this concentration. Instead, an effective and experimentally determined relationship between the fluid flow and TGF-gain is applied.

Parameter	*Explanation*
$C_{tub} = 3.0$ nl/kPa	Proximal tubule elastic compliance (inverse stiffness).
$C_a = 54$ g/L	Afferent plasma protein concentration.
$H_a = 0.5$	Arterial hematocrite (the fraction of the total blood volume that consist of blood cells).
$P_a = 13.3$ kPa	Afferent arterial blood pressure.
$P_v = 1.3$ kPa	Venous (efferent) blood pressure.
$P_d = 0.6$ kPa	Distal tubule pressure.
$F_{Hen,0} = 0.2$ nl/s	Equilibrium flow in the loop of Henle.
$F_{reab} = 0.3$ nl/s	Proximal tubule reabsorption.
$R_{Hen} = 5.3$ kPa (s/nl)	Flow resistance in the loop of Henle.
$R_{a,0} = 2.4$ kPa (s/nl)	Equilibrium flow resistance of afferent arteriole.
$P_0 = 20$ kPa	Normalization pressure.
$\omega_m = 1$ s^{-1}	Mass-to-elasticity ratio for the arteriolar wall.
$d = 0.04$ s^{-1}	Damping parameter in arteriolar oscillation.
$q = 1$	Muscle activation amplification.
$\beta = 0.67$	Fraction of afferent arteriole with fixed radius.
$P_1 = 0.0439575$ kPa	Elastic equilibrium pressure for the afferent arteriole (AA).
$\alpha_1 = 10$	Parameter in non-linear elastic model for AA.
$b_1 = 36.39877$	Parameter in non-linear elastic model for AA.
$P_2 = 4.7$ kPa	Active equilibrium pressure for AA.
$\alpha_2 = 13$	Parameter in non-linear active model for AA.
$b_2 = 1.5319149$	Parameter in non-linear active model for AA.
$R_e = 1.9$ kPa (s/nl)	Flow resistance of efferent arteriole.
$a = 21.7\times10^{-3}$ kPa (l/g)	Protein concentration parameter.
$b = 0.39\times10^{-3}$ kPa (l/g)^2	do.
$\Psi_{min} = 0.20$	Lower limit in activation function.
$\Psi_{max} = 0.44$	Upper limit in activation function.
$\Psi_{eq} = 0.38$	Equilibrium in activation function.
$\alpha =$ control par.	The strength of the arteriolar response, i.e. determines the slope of the regulation curve ψ.
$\Delta T =$ control par.	TGF delay parameter.

Table 3.1 Parameter values used in all calculation with the simple nephron model presented in section 3.1.

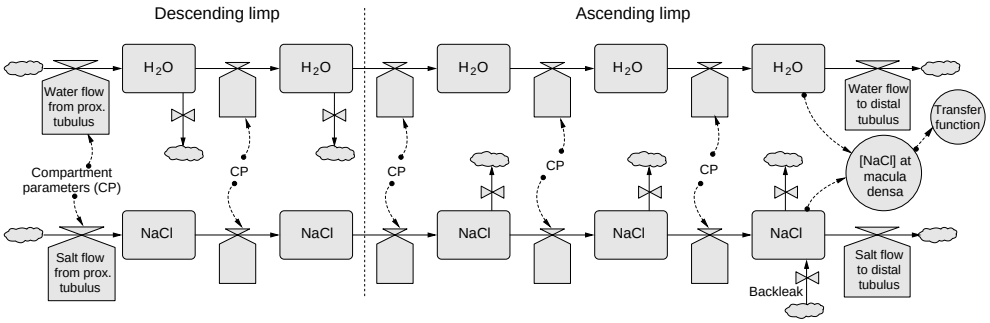

Figure 3.3 Flowdiagram illustrating the flow of water and salt in the descending and ascending limbs. Squares represents compartments and valves represent flows.

Two other mechanistic models have been studied in *Publication P2* and *Publication P3*, both take into account the dynamics of the concentration and one of them, furthermore, take into account the calcium dynamics behind the myogenic mechanism.

3.3.1 Lumped tubular system

An extension of the nephron model with the purpose of estimating the water and salt amounts at positions along the loop of Henle is presented in *Publication P3*. The idea is to divide the loop into a number of compartments and establish the equations for pressure, water and salt amount in each compartment. A schematic representation of the model consisting of two and three compartments for the descending and ascending limbs, respectively, are shown in Fig. 3.3. The supply of water and salt from the proximal tubulus is represented by the left valve and the first pair of boxes represent the amounts of water and salt in the beginning of the descending limb (the first compartment). The change in the rate of water and salt amounts are primary controlled by the local values of flow resistance, compliance, the pressure in the neighboring compartment and the reabsorption rate. The next three compartments represent the ascending limp, where an active reabsorption of salt takes place. The process on cellular level are very complicated and not the topic of this model. Here it is modelled by Michaelis-Menten kinetics as an averaged or effective process.

Up- and down concentration in the two parts of the limbs are visualized by valves on the water compartments in the descending compartments and

on the salt compartments in the ascending limb. At the other end of the sketch the final salt concentration is the input to the TGF-transfer function Eq. (3.11) modified to

$$\psi = \psi_{max} - \frac{\psi_{max} - \psi_{min}}{1 + \exp\left[\alpha(C_{md}/C_{eq} - S)\right]}, \tag{3.18}$$

where C_{md} is the salt concentration at the end of the loop (i.e. at macula densa) and where C_{eq} is the NaCl concentration at half the span of C_{md} and $S = 1 - \frac{1}{\alpha}\log\left(\frac{\psi_{eq}-\psi_{min}}{\psi_{max}-\psi_{eq}}\right)$ is a parameter used to guarantee that the inflection point is found at the point (ψ_{eq}, C_{eq}).

In principle any number of compartments can be made and in the limit of infinitely many, the tubular model effectively approach three partial differential equations, one for each quantity. In that sense this model is of intermediate complexity, compared to the simplified nephron model presented earlier and the detailed model to be mentioned in the next section.

3.3.2 Detailed single nephron model

An attempt to include most of the known mechanisms involved in nephron blood flow autoregulation into one comprehensive model has been made by Marsh *et al.* [22]. This is a quite ambitious task as the individual processes and interplays are not yet fully understood.

In this model the tubular delay of the simple nephron model or the compartments of the lumped nephron model are replaced by three partial differential equations (PDE) that each models the pressure, salt concentration and flow along the loop. Furthermore, the second order differential equation that represents the myogenic mechanism is replaced by a model for the calcium dynamics and phosphorylization of smooth muscle consisting of 6 ordinary differential equations. Since the arteriole display gradually increasing activity at the glomerular end, the arteriole is divided into three segments, one passive and two active segments. A total of 12 ordinary differential equations is therefore need to describe one arteriole. To simplify the processes described by the model a causal loop diagram is shown in Fig. 3.4. The right part of the diagram describe the processes involved in the TGF mechanism, while the left part represent the myogenic cellular processes. The model description of glomerular filtration is similar to the simpler nephron mode described in section 3.1. In the diagram, the tubular system encompasses the part from

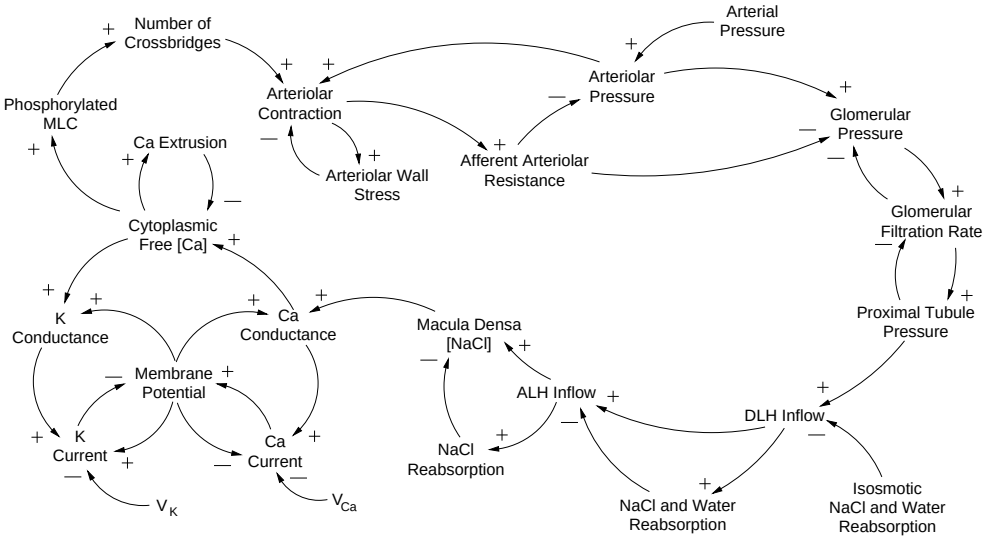

Figure 3.4 Causal loop diagram of the processes included in the detailed nephron model.

the "proximal tubular pressure" and until "macula densa [NaCl]". As mentioned above this part is represented by PDEs in pressure, salt concentration and fluid flow. A distinction between the equations for the descending and ascending segments is included to take care of the impermeability of water and active salt reabsorption in the ascending limb. Reabsorption of salt is again modelled by Michaelis-Menten kinetics. The salt concentration at macula densa follows directly from the PDE that describe salt concentration. The salt concentration then determine a muscular activation value from Eq. (3.18). This activation is the link to the myogenic mechanism and is established through the conductances of the arteriolar segments through

$$g_{Ca,tot} = (1 + \zeta\psi)g_{Ca} \tag{3.19}$$

where g_{Ca} is the native calcium conductance, ζ the coupling parameter and $g_{Ca,tot}$ the resulting calcium conductance. Basicly, the myogenic model describe the origin of the oscillations on a chemical level. The oscillations emerge due to an instability in the interaction between Ca^{+2} and K^{+} currents in the membrane of the smooth muscle cells. In the lower left part of Fig. 3.4 the interaction between membrane potential, ion-currents and conductances is shown. An increase in Ca-conductance caused by an increased Cl^{-} concentration at macula densa, will give rise to an increased Ca-current that builds up a membrane potential that in turn reduce the Ca-current. The increased

membrane potential further increases the Ca-conductance (increasing number of open Ca-channels), hence, this calcium dynamic is described by a positive feedback loop. The dynamics in potassium work oppositely on the membrane potential, but still in such a way that both conductances increase at increased membrane voltage. Since an increase in Ca-conductance gives rise to an increased inward Ca-current it also causes an increase in the cytoplasmic free calcium concentration. Inside the cell various calcium buffers reside that, together with the extrusion of calcium, contribute to maintain an oscillatory and restricted cytoplasmic calcium concentration. Removal of calcium from cytostol and the effect of the buffers is modelled by assuming a constant extrusion rate and assuming that the reaction between free unbound and bounded calcium is at equilibrium. As an increasing cytoplasmic free calcium concentration build up the chemical process of phosphorylation of the myosin light chains is enhanced. This process causes the formation of crossbridges between actin filaments (part of the smooth muscle cells) that create a stress and ultimately a contraction.

Note, that this explanation both covers the contractions caused by TGF and the self-sustained myogenic oscillations. Contractions due to TGF is triggered through the signal from macula densa, while the myogenic oscillations are due to the internal dynamics of the smooth muscle. Further information on this model may be found in the work by Marsh *et al.* [22] and *Publication P2*.

3.3.3 A very simple model

Having presented the main ideas of three nephron models of increasing complexity, the last model follows a completely opposite strategy. The model is simply the very well-known Rössler system, which is one of the simplest non-linear systems that may display chaotic dynamics. Of course this model is strongly limited in its ability to account for the many complicated mechanisms taking place in the nephron, and the purpose for studying this model is not to make any direct comparisons with the time course or phase-locking modes of nephron dynamics.

Otto Rössler [29] stated the system on the form

$$\dot{x} = -y - z \tag{3.20}$$

$$\dot{y} = x + ay \tag{3.21}$$

$$\dot{z} = b + z(x - c), \tag{3.22}$$

with the equilibrium points $x^*_\pm = (c \pm \sqrt{c^2 - 4ab})/2$, $y^*_\pm = -x^*_\pm/a$ and $z^*_\pm = x^*_\pm/a$. For $c^2 < 4ab$ there are no equilibrium points. At $c^2 = 4ab$ a saddle-node bifurcation gives rise to a stable and an unstable equilibrium point, of which the stable equilibrium (x^*_-, y^*_-, z^*_-) is located closer to origo. In the $x-y$-plane the parameter a controls the amplification of the excursions for an orbit emanating from the unstable equilibrium, and the parameter c controls the distance from the equilibrium point at which the orbit is re-injected close to the equilibrium, this means that large c generally cause a larger number oscillations in the $x - y$-plane for each re-injection.

Despite its simplicity and immediate lack of relationship with the nephron, it is possible to draw some links with the dynamics of the nephron. Like the physiological more realistic nephron models, the Rössler system has a fast mode (in the $x - y$-plane) that can be interpreted as the vascular oscillations and a slow mode (the re-injection) representing the TGF oscillations. The terms z and y in the first equation represent the TGF mediating and the vasomotoric feedback coupling, respectively. So, x and y are "vascular variables", that could represent the arteriolar radius and the rate of change of that radius, respectively. Variable z is associated with the slow dynamics, so that must be a "TGF variable", of which a possible choice could be the salt concentration at macula densa.

One of the clearest distinctions between this simple model and the more realistic models is that here there is only one oscillator, because the two modes are not independent, in the sense that they can not exist individually. But that does not really matter, because we are only using the Rössler system as a prototype for a period-doubling system. In that respect the nephron models and the Rössler system are comparable.

3.4 Coupling mechanisms between nephrons

Coupling is an interaction between two individual units. For instance, the periodically forced Rössler system can be considered as a Rössler system being distorted by a periodical change in surroundings (the forcing). The interaction is in this case a one way interaction, because the Rössler system does not influence the nature of the external forcing. Mutual coupling is very typical in biological systems. The coupling between TGF and vasomotion is an example of mutual coupling of two distinct systems.

In the present thesis coupling between neighboring nephrons in a nephron tree is central. Regarding regulation of blood flow, nephrons are mainly coupled through

- Hemodynamic coupling and
- Electrical (or vascular) coupling

Hemodynamic coupling arises when the radius of the afferent arteriole contracts in one of the neighboring nephrons. The flow resistance for that arteriole will increase and give rise to a decreased blood flow. During this process a surplus of blood become available for the neighbor nephron and if the arteriole is in a distended state the blood flow to this nephron increase. The distended arteriole start to react in response to the increased flow and gradually increasing pressure by initiating a contraction and affect the neighbor nephron in a similar way, and out-of-phase oscillations of the arterial flow, pressure and TGF contraction is established. For a larger system of many coupled nephrons, however, it is hard to think of a pattern of true anti-phase dynamics between all nephrons, because of the many different distances between even the closest nephrons.

In-phase synchronized variations in blood pressure of neighboring nephrons have been observed experimentally and it is actually more common than the out-of-phase synchronized situation. Holstein-Rathlou *et al.* [12] suggest that the domination in-phase dynamics arise in combination of the hemodynamic and vascular coupling.

Vascular coupling is due to the propagation of the electrical signal that activate the smooth muscle cells and cause the contraction along the afferent arteriole of one nephron to the neighboring nephrons. Since, the amplitude of the propagating signal decay exponentially, the strength of the coupling depends on the lengths of afferent arterioles. Typically a fraction of about 5% percent of the initial amplitude reach the afferent arteriole of the neighbor. Compared to the time scale of both TGF and myogenic oscillations electrical signals propagate quite fast. Therefore, vascular coupling typically induces in-phase variations of blood pressure. Due to the exponetial decay of the electrical signal, there is a spatial limit for the range where vascular coupling is in play and clustering of in-phase synchronized nephrons may for instance be due to a distribution of few nephrons with long arterioles among nephrons with shorter ones.

In the simple model treated in section 3.1, vascular coupling is modelled by letting the individual activation levels for each nephron depend on each other

$$\psi_{1,tot} = (\psi_1 + \gamma\psi_2) \tag{3.23}$$

$$\psi_{2,tot} = (\psi_2 + \gamma\psi_1), \tag{3.24}$$

where γ is the coupling parameter. However, the physiology behind the coupling take place at a much lower level. The electrical Ca-signal travels along the network of smooth muscle cells whereby changing the conditions for each cell.

In the detailed nephron model (section 3.3.2) the average effect of all smooth muscle cells within each arteriolar segment are modelled on the cellular level. The two-nephron model consists of two versions of the single nephron model, each solved separately, but with the arteriolar segments farther from the glomerulus coupled electrically [24]. These arteriolar segments were coupled to each other through an electrical node in the wall of the artery supplying the two nephrons with blood. Applying Kirchoff's law, balance of currents for all segments of both nephrons then allows for establishing the coupling between nephrons. Additional parameters needed for the coupled nephron model are the conductance coupling the two nephrons through the electrical node, and a conductance of the node to ground. Physically the strength of the coupling is controled by the lengths of the arterioles and a lot of properties of the arteriole. Effectively, the coupling is modelled by a coupling conductance. In this study, cortical nephrons were simulated, and both nephrons of the pair were assigned the same length with identical properties, i.e. both artioles have the same conductance.

CHAPTER 4

Numerical methods

Analysis of nonlinear dynamical systems may itself be a technical challenge. Development of integration routines, methods for detecting unstable solutions and detection of bifurcations, calculation of various characteristic measures such as phase and Lyapunov exponents and visualization of large multi-dimensional data are at a stage where relative complicated tasks can be approached. Many numerical methods exist, some are well suited for small and others are better for large systems. However, typically a more detailed analysis can be obtained for smaller than larger systems. In this thesis the models range from the simplest models to relative large, and therefore a broad range of numerical methods has been applied.

A short and mainly verbal description of the principles for continuing stable as well as unstable cyclic solutions and bifurcations on these solutions is presented in the first part of this chapter. In the second part the standard method for determining Lyapunov exponents of ordinary differential equations and estimation of the largest exponent of time series are presented.

4.1 Continuation method

Continuation is the theory of bifurcations put into numerics and computer language. Several books on the topic exist, and one of the most comprehensive description of the technique is due to Yuri Kuznetsov [20]. The main force of this method is that unstable solutions are obtained as easy as the stable ones, because it is based on the Newton-Raphson method for finding roots of a function. This is a great advantage as many bifurcational mechanisms of the stable solutions involve bifurcations taking place on the unstable solutions, and therefore knowledge of both highly improve the understanding of how and why the system change its behavior.

Let us here try to phrase the most important parts in a continuation step

of a limit cycle of the general system

$$\dot{x} = f(x). \tag{4.1}$$

For numerical reasons it is convenient to rewrite the problem as a boundary value problem

$$\dot{x} = T_0 f(x), \tag{4.2}$$

where T_0 is the period of the limit cycle and time is normalized $t \to t/T_0$. The periodic boundary and phase conditions are

$$x(0) = x(1), \quad \text{and} \quad \int_0^1 x(t)\dot{x}_{k-1}(t)dt = 0, \tag{4.3}$$

where $x_{k-1}(t)$ is a reference solution of period T_0. In a continuation step $x_{k-1}(t)$ may be considered as the solution of the previous parameter value. Assume that the solution of Eq. (4.2) is a period-K limit cycle denoted by $x(t) = \phi_t(x_0, t_0)$, where x_0 and t_0 are initial conditions located on the cycle.

Most continuation programs make use of several Poincaré sections $\sum_n$ (multiple shooting) distributed around the cycle, where the number of sections determines partly the accuracy and convergence of the Newton-Raphson iterations. Figure 4.1(a) illustrate the distribution of four Poincaré sections along a period-1 cycle. The intersections of the cycle with the surfaces are the only points that at this point is known numerically. In time the mesh of sections, are located at

$$0 = t_0 < t_1 < t_2 < t_3 = 1. \tag{4.4}$$

The parts between sections are then approximated by a piecewise- differentiable function, to be more precise, Legendre polynomials of degree m with appropriate coefficients such that the polynomia in each interval to within some small error are solutions to the problem Eq. (4.2) at m collocation points

$$t_0 = \zeta_0 < \zeta_1 < \zeta_2 < \zeta_3 < \zeta_4 = t_1, \tag{4.5}$$

where $m = 5$ in order to be in accordance with the figure. All this take place for a fixed parameter values.

Since the description follows the continuation of cycles it is necessary to define the map

$$F(x, \alpha) = P^K(x, \alpha) - x, \tag{4.6}$$

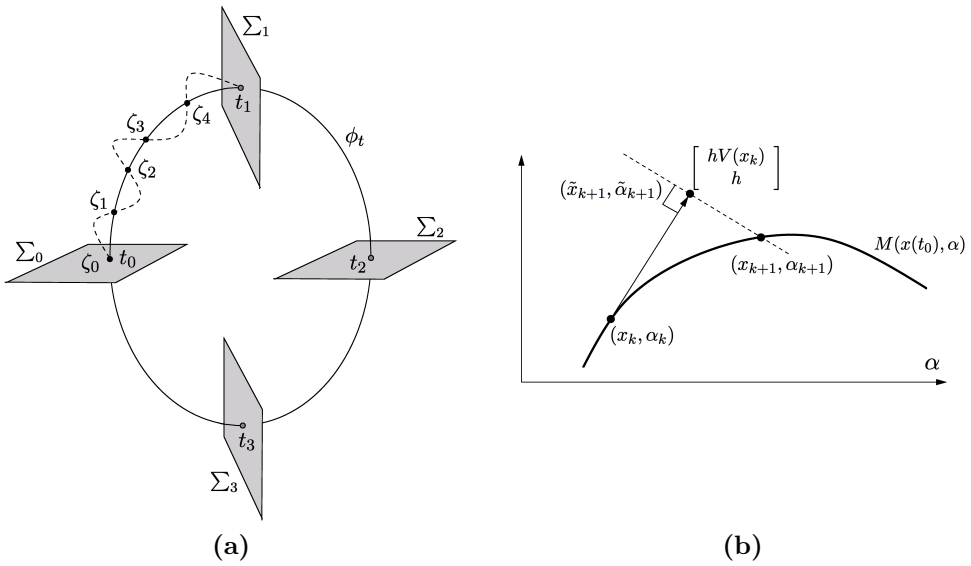

Figure 4.1 Continuation of limit cycles. a) The shooting method for a limit cycles with 4 Poincaré sections and 5 collocation points. b) Principle of the pseudo-arclength method.

where P is a Poincaré map and x is the fixed point of the K'th iterate.

Now we want to find the solution for some increment of one parameter. To make a first approximation the pseudo-arclength method is used. Consider the exact solution $M(x(t_0), \alpha)$, where α is a parameter of the system. Assume that we know the cycle ϕ_t for the parameter value α_0. Then the tangent vector of some specified length will point in the correct direction, but deviate from from the exact solution. Actually, the tangent vector is one step of an Euler integration, which is rarely a useful integration method for nonlinear system. However, the error is corrected by a number of Newton-Raphson steps in a plane normal to the tangent vector. Mathematically, the Euler step is expressed as

$$\tilde{x}_{k+1} = x_k + hV(x_k) \tag{4.7}$$

$$\tilde{\alpha}_{k+1} = \alpha_k + h, \tag{4.8}$$

where subscripts refer to the current and incremented solutions and $V(x_k) = \nabla F(x_k, \alpha_k)$ is the gradient in a Poincaré section, h is the step length by which α is incremented. The correction to the Euler step then take place through

the Newton-Raphson iterations

$$\begin{bmatrix} x_{k+1}^{i+1} \\ \alpha_{k+1}^{i+1} \end{bmatrix} = \begin{bmatrix} x_{k+1}^{i} \\ \alpha_{k+1}^{i} \end{bmatrix} + \begin{bmatrix} \delta x_{k+1}^{i} \\ \delta \alpha_{k+1}^{i} \end{bmatrix}, \tag{4.9}$$

where the $(\delta x_{k+1}^i, \delta \alpha_{k+1}^i)$ is determined from

$$\begin{bmatrix} D_x F(x_{k+1}^i, \alpha_{k+1}^i) \\ D_\alpha F(x_{k+1}^i, \alpha_{k+1}^i) \end{bmatrix} \begin{bmatrix} \delta x_{k+1}^{i} \\ \delta \alpha_{k+1}^{i} \end{bmatrix} = -F(x_{k+1}^i, \alpha_{k+1}^i), \tag{4.10}$$

where $D_x F$ and $D_\alpha F$ are variable and parameter Jacobians. Since the problem is underspecified an extra condition is needed. The pseudo-arclength method impose the constraint

$$[dx_k \; d\alpha_k]^T \begin{bmatrix} \delta x_{k+1}^{i} \\ \delta \alpha_{k+1}^{i} \end{bmatrix} = 0, \tag{4.11}$$

that ensure orthogonality of the iteration procedure. Step size control can be implemented by a requirement that the euclidean length of the correction must not exceed a certain length. If the length is too large or no convergence was found then above process must be repeated with a smaller step length h.

Since periodic solutions correspond to fixed points of a Poincaré map, stability and bifurcations are determined from the Floquet multipliers of the Poincaré map, either by direct inspection of the multipliers or by so-called test functions, which is a generalized formulation of the bifurcations dependence of multipliers. Each bifurcation type is attributed a test function, and usually it is defined so that it becomes zero at the bifurcation.

Two-parameter continuation of codimension 1 bifurcations follow the same principle as the one-parameter description. There are only two small differences: 1) the scalar α, is now a vector of two parameters, $\alpha = (\alpha_1, \alpha_2)$ and 2) the underspecified equation (Eq. (4.10)) is subject to the additional constraint that the corresponding test function must be zero.

The amount of memory and time consumption for a computer to solve this kind of problem is largely proportional to the dimension of the system, number of mesh intervals and number of collocation points. Also the accuracy of the bifurcation curves play a large role, though this mainly concern the time consumption and not the memory. Typically, the number of mesh points

must be doubled when switching from a cycle to a period-doubled cycle, therefore the mesh should be kept as small as possible, while still being able to detect bifurcation with a reasonable accuracy.

All continuation problems in this thesis was calculated by use of AUTO-07p [6].

4.2 Lyapunov exponents

Contrary to periodic dynamics, chaos differ by being sensitive to initial conditions, meaning that two arbitrary close initial conditions diverge in time. It may sometimes be difficult to judge whether a time evolution is chaotic, very high order periodic or quasiperiodic. To find out with great certainty Lyapunov exponents can be calculated. Lyapunov exponents is roughly a measure of the average divergence during a time serie, that is long enough for obtaining a converged average. For ordinary differential equations where the equations and Jacobian is accessible the exponents can be calculated directly during integration of the system. Assume the general system

$$\dot{x} = f(x,t), \;\; x(t_0) = x_0, \tag{4.12}$$

with the solution $\phi_t(x_0, t_0)$ and the variational equation

$$\dot{\Phi}_t(x_0,t_0) = D_x f(\phi_t(x_0,t_0),t)\Phi_t(x_0,t_0), \quad \Phi_{t_0}(x_0,t_0) = I. \tag{4.13}$$

The variational equation is the linearization of the vector field along the solution $\phi_t(x_0, t_0)$. During iteration with for instance a Runge-Kutta method the variational equation can be evaluated to yield the vector field at any wanted moment of time. In Fig. 4.2 the vector field around the solution ϕ_t is visualized at two instances $t = 0$ and $t = T_g$, where T_g is different from, but still of the order of the fundamental period of the system. For each integrated time interval T_g, the normalized length of the vector fields are logarithmically accumulated

$$\lambda_n = \frac{1}{KT_g} \sum_{k=1}^{K} \log(||v_n^k||), \tag{4.14}$$

where K is time integrated in units of T_g and v_n is the vector fields, i.e. column vectors of $\Phi_{t=T_g}\phi_t$. As time progress the vectors start to become very large, and since the vector field usually is composed of expanding and

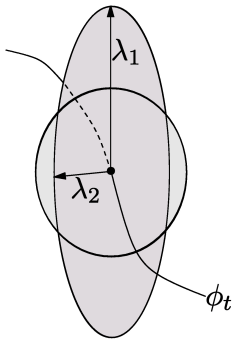

Figure 4.2 The rates of change of perturbations to the solution ϕ_t. The circle represent the initial perturbation of the orbit and the ellipsoid is the distorted after some time. The expansion due to λ_1 represent a positive Lyapunov exponent and the contracting direction λ_2 is a negative exponent.

contracting directions there is a tendency for the vectors to align, giving rise to inaccurate calculations. To avoid this problem the Gram-Schmidt orthonormalization procedure should be used at each time interval. From Eq. (4.14) it is easy to estimate the largest Lyapunov exponent because if the length of v_n typically is larger than one (expansion), then $\log(v_n)$ is on average positive giving a positive exponent. This means a general expansion of the dynamics and hence sensitivity on initial conditions.

Estimation of the Lyapunov exponent of time series obtained from for instance experiment or from integration of a system where the equations are not directly accessible is possible, if a reconstruction [30] of the attractor is possible. In the present work this method is used on the detailed nephron model, because the equations and their implementations are to complicated for a Jacobian to be evaluated.

The idea is to reconstruct the phase space attractor from the time evolution of just a single variable of the full system. Let us try to use the x-variable of the Rössler system as an example. Because variable x depend on y, which again depend on z, this variable must also contain information from both the y and z variables. To reconstruct the attractor we need a way to estimate how much the time course of x is due to the other two variables. Consider the time serie

$$\{x_1, x_2, x_3, ..., x_k, x_{k+1}, ...\}, \tag{4.15}$$

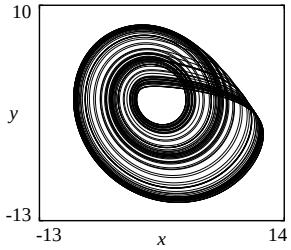

(a) Original

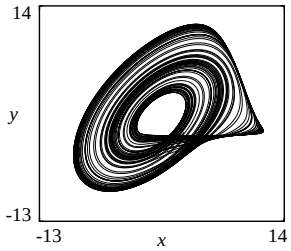

(b) Reconstructed

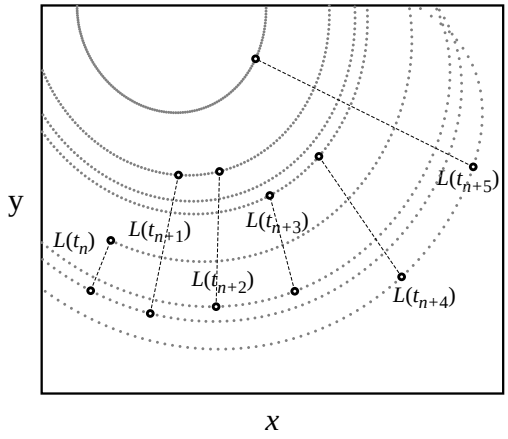

(c) Lyapunov exponent

Figure 4.3 Reconstruction of phase space and the largest Lyapunov exponent a) Chaotic Rössler attractor. b) Reconstructed chaotic Rössler attractor from variable x with a time lag $\tau = 100$. c) Principle of determining the largest Lyapunov exponent from the reconstructed attractor.

and define the estimate of x, y and z in terms of delayed coordinates to be

$$X = \left\{x_1, x_{1+\tau}, x_{1+2\tau}, ..., x_{1+(n-1)\tau}\right\} \tag{4.16}$$

$$Y = \left\{x_2, x_{2+\tau}, x_{2+2\tau}, ..., x_{2+(n-1)\tau}\right\} \tag{4.17}$$

$$Z = \left\{x_3, x_{3+\tau}, x_{3+2\tau}, ..., x_{3+(n-1)\tau}\right\}, \tag{4.18}$$

For some values of τ the phase space resample that of the Rössler attractor. A good choice of τ is typically to select a value such that the auto-correlation function between two reconstructed variables is zero. Figures 4.3(a)-(b) show the original chaotic attractor and reconstructed attractor for $\tau = 100$.

Lyapunov exponents can then be obtained by searching for the nearest neighbor to a point $B(t_i) = (X(t_i), Y(t_i), Z(t_i))$

$$L(t_i) = \min_{j=1..N}(||B(t_j) - B((t_i)||), \tag{4.19}$$

with the constraint $|t_j - t_i| > T/2$, and where $L(t_i)$ is the Euclidean distance and N is the number of sampling points during the average period T. At a

later time t_1 this length has changed to $L'(t_1)$. If the length has increased, this particular step contribute to an expansion of the system. Then the process is repeated from a new point in the sequence and each of the step is accumulated like for the analytical case

$$\lambda = \frac{1}{t_M - t_0} \sum_{i=1}^{M-1} \log \frac{L'(t_i)}{L(t_i + 1)}, \tag{4.20}$$

to cover the whole time serie in M steps. Note, that this procedure only supply the largest Lyapunov exponent.

CHAPTER 5

Chaos in a physiologically detailed model of coupled nephrons

The title of this chapter should *not* be interpreted as a proof for "chaos in the kidney". One thing is a model of a biological system, another thing is the real biological system. Of course it is the real system that is of most interest. So how can a model be used to indicate that a system behave chaotically under certain conditions.

Assume that the only mechanism that control the nephron's autoregulation of the blood flow are TGF and the myogenic mechanism. Then the real system behave solely according to these rules, and fluctuations not driven by the two mechanisms are completely due to noise from the outside. This means that if a mathematical model of the kidney is correct in the sense that it includes the mechanisms responsible for the behavior of the real kidney, then it should qualitatively reproduce its behavior. If under some distorted condition the kidney starts to behave chaotically, then the cause may be due to either a change in the surroundings (could be increased noise or some change in an other organ), a change in the a property within the kidney or both. When conditions outside the kidney cause the incoming blood pressure to be chaotic, it is not the kidney that induce the chaos, rather the dynamics of the kidney is a superposition of the kidneys regular dynamics and the irregular input. Thus, only if a internal parameter trigger the chaotic behavior, one can say the kidney is responsible.

5.1 Lyapunov exponents of coupled nephron models

In our *Publication P2* an attempt is made to give an indication of the presence of chaos in a system of two vascular coupled nephron. As described in

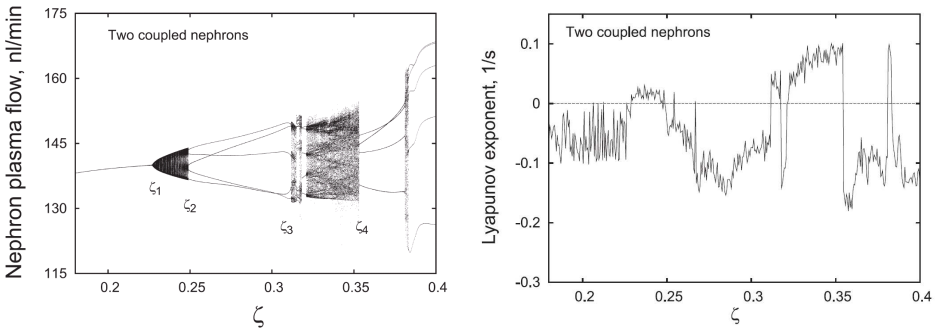

Figure 5.1 Two vascular coupled nephrons. a) Bifurcation diagram of the coupled nephrons with with TGF-myogenic coupling parameter ζ as bifurcation parameter and constant coupling between the two nephrons. b) Corresponding Lyapunov exponents.

the paper and section 3.3.2 the model is quite detailed and contains both the TGF and myogenic mechanisms which are accepted to be determinants for the oscillations in blood flow and regulatory processes of the blood pressure. Calculation of bifurcation diagrams and Lyapunov exponents with the TGF-myogenic coupling parameter as bifurcation parameter for both the uncoupled system show that the single nephron primary exhibits 1:5 mode-locking. There is a tendency for the single system to show chaotic behavior at increased TGF-myogenic coupling, but not very pronounced.

Figure 5.1(a) shows the bifurcation diagram for two vascular coupled nephrons. At low coupling, only the native myogenic oscillations are present, while the TGF system is at a stationary state. As the coupling is increased, the TGF mechanism is destabilized in a torus bifurcation, giving rise to quasiperiodic dynamics, followed by a 1:5 mode-locking between the two TGF and myogenic oscillations. A 1:5 locking is the most common behavior of cortical nephrons in the normotensive rat. Hence, the parameter range of the 1:5 mode-locking region may be considered as a normal coupling range for a normotensive rat. A very abrupt transition to chaos takes place at about ζ_3=0.31 and continues until ζ_4=0.35. Increased coupling have, together with irregular or chaotic dynamics, been shown experimentally to be characteristic for hypertension [31]. The Lyapunov exponents plotted in Fig. 5.1(b) guarantee that there actually is sensitivity on initial conditions in the chaotic range.

To conclude, the complexity increases in the more realistic case of coupled

nephron compared to the single nephron. Additional complexity of both the single and especially the coupled model, is induced as the TGF-myogenic coupling is increased.

As far as this detailed model concerns two interacting nephrons do behave chaotically at high coupling. If the model is correct and actually does include the responsible mechanisms, we can say that the model is a strong indicium for the kidney to behave chaotically under hypertensive conditions. It must be noted, that we actually only have made the calculation for two nephrons. Larger systems comprising a nephron tree or the to, be extreme, the whole kidney may, in principle, change the picture. But to this we can note that if a subset consisting of two nephrons show chaos, then the larger system of many pairs of chaotically oscillating systems most likely maintain the chaotic dynamics, or at least maintain the possibility for chaotic dynamics to reappear at slightly different parameter values.

Earlier studies by Marsh *et al.* [23], of 22 hemodynamically and vascularly coupled nephrons organized in a nephron tree also show that the complex chaotic dynamics depend on the vascular coupling. The individual nephron in this study was modelled by the simpler model described in section 3.1. The tendency is that increased vascular coupling leads to chaotic dynamics.

CHAPTER 6

Periodically forced spiral type system

This chapter is devoted to the study of periodically forced Rössler systems and the periodically forced nephron model. The motivation for studying a forced Rössler system is partly associated with a series of papers by Kuznetsov *et al.* [16, 19, 17]. Kuznetsov demonstrated that deviations from the usual Feigenbaum scaling of period-doubling cascades arise in quadratic maps and low-dimensional time-continuous systems. This deviation takes place at the border of a resonance tongue. The so called cyclic type (or C-type) criticality, is for instance found in the forced Rössler system. To understand the origin of this deviation and how it is connected to the transition between phase synchronized chaos and the desynchronization at the edge a number of studies was performed. Several results from these studies are either already published (or submitted for publication) in *Publication P1* and *Manuscripts M1* and *M2*. In this chapter the main results from these manuscripts are reviewed.

6.1 Periodically forced Rössler system

The synchronization region of an externally forced nonlinear system, is bounded by saddle-node bifurcations. If the system in its unforced version display period-doubling cascades under variation of a parameter it will also display period-doubling bifurcations within the Arnol'd tongue. In Fig. 6.1 a sketch of the typical structure of the strong 1:1 resonant Arnol'd tongue is shown together with its largest neighbor tongues 2:1 and 1:2. In the following studies a different cut in parameter space is considered for a fixed forcing amplitude or coupling.

The higher order resonant solutions produced in the period-doubling bifurcations must also be limited by a saddle-node bifurcation at the border of the resonance zone. However, these can not be the same as those limiting

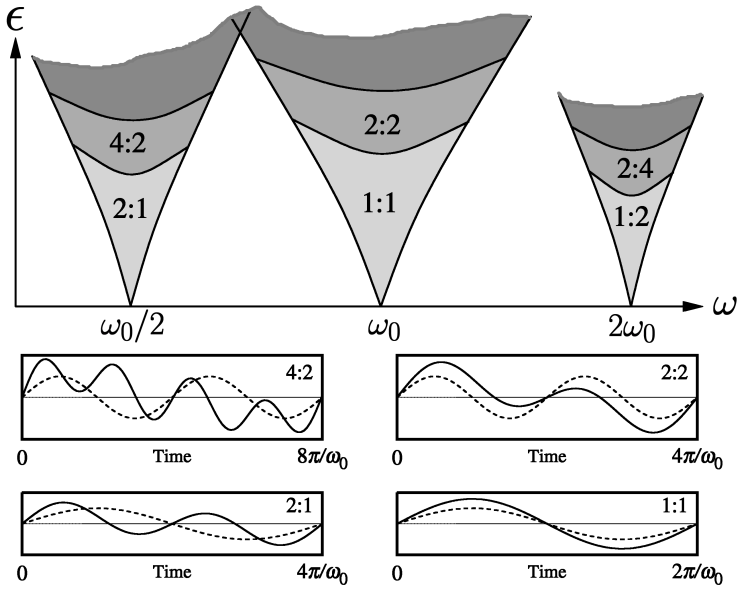

Figure 6.1 Arnol'd tongues in the forcing frequency and amplitude plane. Tongues are limited by saddle-node bifurcations on either side of the tongues. Within a tongue period-doubling bifurcations may take place taking the dynamics to higher order resonances. A resonant solution is located on a torus as shown in Fig. 6.2. Outside the tongues ergodic tori exist (quasi-periodicity). In the lower part of the figure the time evolutions corresponding to various phase-locked are depicted.

the 1:1 resonant solution, because 1:1 solution is limited by a saddle-node bifurcations taking place only on the 1:1 solution [2]. Thus, there must be one saddle-node bifurcation for each periodic solution and the question is from where they arise. Detailed bifurcation analyses in the form of continuation of both the stable resonant node and the corresponding resonant saddle solution is very powerful in explaining the origin and structure of such apparently hidden bifurcations.

Figure 6.3(a) show the 1:1 Arnol'd tongue for the forced Rössler system. Inside the tongue at low c values a stable period-1 node (N^1) is located on a torus. A co-existing unstable saddle S^1 is located on the same torus, see the sketch in Fig. 6.2.

As the angular frequency ω of the periodic forcing is increased or decreased the saddle and node approach each other and at some precise value

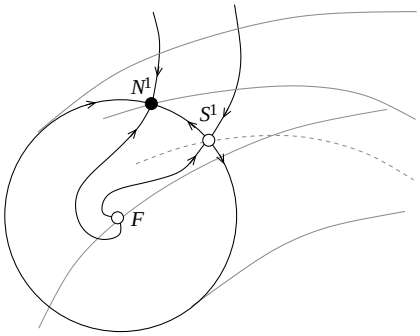

Figure 6.2 Period-1 cycles on a torus. One cycle is a stable node N^1 and the other is a saddle S^1. The torus is originally born in a torus bifurcation from the unstable focus point F.

of ω they collide in a saddle-node bifurcation. When this happens both the node and the saddle cease to exist. The torus, however, still exist and what is left is ergodic dynamics on this torus. For increasing values of c a period-doubling bifurcation take place, first on the stable node (PD_1^S) and, at larger values of c, also on the saddle solution (PD_1^U). The 1:1 resonant solutions still exist but now as a saddle and doubly unstable saddle. Close to the point where the two branches of period doublings meet at the left edge and are tangential to the saddle-node bifurcation a new saddle-node bifurcation SN_2^L is born in the point Q_2 on the unstable branch of the period-doubling bifurcation PD_1^U. It is this saddle-node bifurcation that becomes the border for both the stable node and unstable saddle on the 2:2 resonant torus. Since it is a topological violation to define a saddle-node-saddle-node bifurcation of co-dimension 2, i.e. birth of a saddle-node bifurcation on an existing saddle-node bifurcation, the new saddle-node bifurcation SN_2^L must be born on the period-doubling bifurcation, either on the stable branch, PD_1^S or the unstable branch PD_1^U. These two possibilities give rise to two topologically different cases, which are generally present in an alternating way in periodically forced period-doubling systems. Figure 6.3(b) show the enlargement at the region of tangency at the left edge. As mentioned above the saddle-node bifurcation for the next level emerge from the unstable branch PD_1^U. This leaves a gap where the 2:2 resonant torus is not limited by a saddle-node bifurcation. Therefore a bifurcation is needed to close the gap or rather give birth to the ergodic torus that exist in the grey region. It must be a bi-

furcation that can bridge between a period doubling and a saddle-node in order to fully close the gap. To our knowledge, the only local bifurcation, that meet these conditions is a torus bifurcation. In this particular case the torus bifurcation is subcritical and the ergodic torus torus is destroyed at a torus-fold bifurcation G_2.

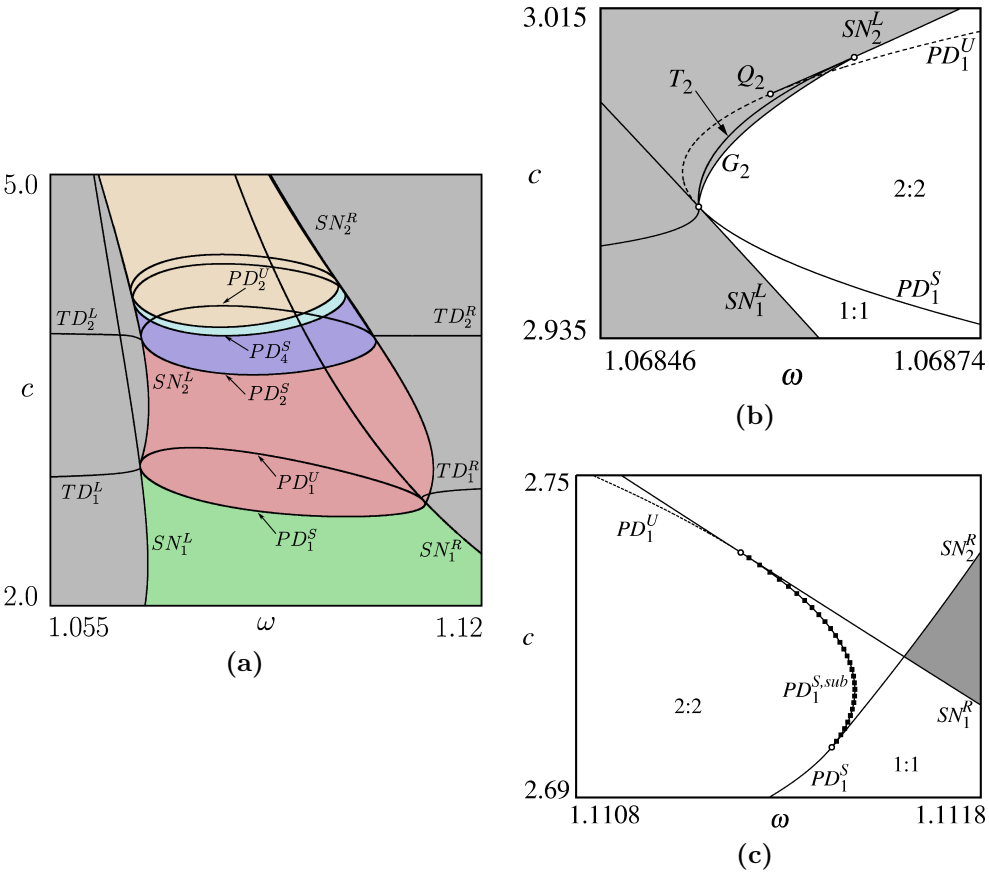

Figure 6.3 Bifurcation structure of the 1:1 Arnol'd tongue in the periodically forced Rössler system. a) Overview with the first four period doublings and saddle-node bifurcations. Only the first two sets of saddle-node bifurcations are distinguishable from the next levels at this scale. b) Enlargement of the region around the supercritical PD_1 and SN_1^L. The gap between the tangent point and birth of SN_2^L is closed by the subcritical torus bifurcation T_2. c) Enlargement of the region around PD_1 and SN_1^R. Here the period doubling is subcritical and SN_2^R is born on the stable branch PD_1^S.

The other situation where the saddle-node emerge from the stable branch PD_1^S, i.e. below the point of tangency is found at the opposite edge, see Fig. 6.3(c). In this case the birth of SN_2^R leaves no gap between resonant and ergodic dynamics. This can easily be checked by trying to find a path from the 2:2 resonant region to ergodicity without passing SN_2^R. Hence, there is no additional bifurcation reguired. However, the period doubling that run from the point where SN_2^R is born to the point of tangency must change its nature in order to include the part of SN_2^R that exist below PD_1^S. To do this it becomes subcritical. Consequently, SN_2^R must cross SN_1^R and at least locally run along the right side of SN_1^R. Similar bifurcation structures take place at the points of tangency at the next period-doubling bifurcation, except that here the subcritical case is found at the left edge and the supercritical (with implication of an additional torus bifurcation) appear at right edge. Actually, it appears that the two cases continue to shift, as sketched i Fig. 6.4, and has been confirmed numerically by Kuznetsov *et al.* [19] up to period-256 and upto period-128 in our own studies in *Manuscript M2*. Although the torus bifurcation is a minor phenomenon taking place only over a very small parameter range, its existence is highly intersting because for coupled almost identical systems this bifurcation assume a new, important role for the transition between phase synchronized and desynchronized dynamics. There is no bifurcational requirements for this alternation, since one could draw a bifurcation structure where all cases are either super- or subcritical at both edges and still maintain a structurally correct phase space. A possible cause of the alternation may be the lack of symmetry between the oscillations of the Rössler system and the perfectly harmonic forcing.

Kuznetsov *et al.* [19, 17, 18] have used renormalization group theory to study the scaling properties of forced period-doublings systems, and shown that the scaling properties along the edge of the resonance tongue deviate from the usual Feigenbaum scaling in quadratic maps and low dimensional time-continuous period-doubling systems. It is the alternating (or cyclic) behavior of the bifurcation structure near the edge that causes this deviation.

Transition between chaotic phase synchronization and desynchronization essentially takes place in the same way as the transition between the phase synchronized periodic (resonant) behavior and desynchronized quasiperiodic (ergodic) behavior. Since the period-doubling cascade is infinite, there must also be a infinite set of saddle-node bifurcations, all born on the infinitely many period doublings. In *Manuscript M2* we explain in high detail how the

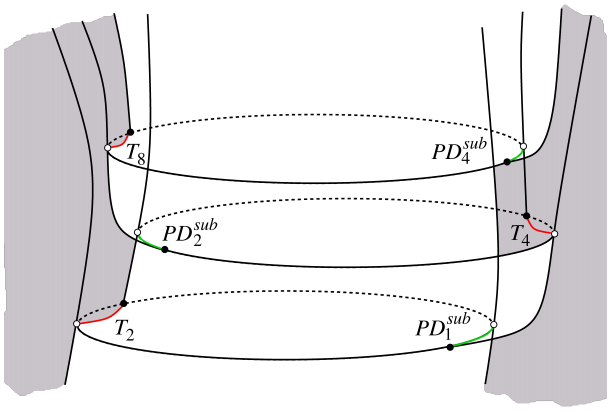

Figure 6.4 Sketch of the cyclic type criticality bifurcation structure found in the forced Rössler system. At the left edge start from the supercritical case that also involve a torus bifurcation, while at the right edge it starts from the subcritical case.

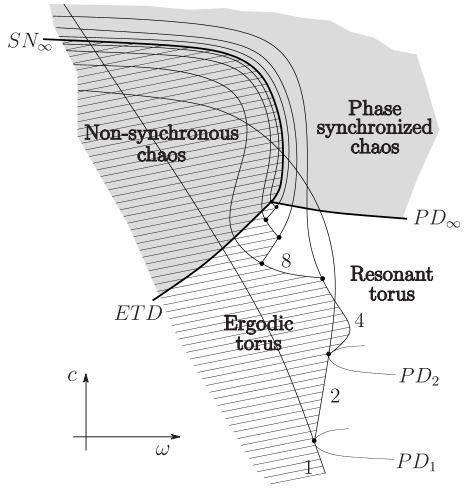

Figure 6.5 Sketch illustrating the accumulation of period doublings and saddle-node bifurcations that form the transition between phase-synchronized chaos to the right of SN_∞. The curve ETD denote the border between ergodic and non-synchronized chaos.

infinite set of saddle-node bifurcation is arranged. Especially it is interesting that the cyclic behavior of subcriticality and supercriticality give rise to a dense set of bifurcations. This means that the saddle-node bifurcation accumulate or converge to a single curve, much in the same way as the period-doubling cascade accumulate to a curve where the transition to chaos take place. Figure 6.5 illustrate the arrangement of period doubling and saddle-node bifurcations at the edge of a resonance tongue. Accumulation bifurcations PD_∞ and SN_∞ are displayed with thick curves. Note, that at some point the curves must join, in order to fulfill the condition that both cascade must converge and the saddle-node bifurcation must be born on the period doubling. In analogy with the resonant and ergodic situation the edge of synchronization is found at the accumulation curve for the alternating saddle-node bifurcation cascade.

Outside the resonance tongue and for small values of c an ergodic torus reside. Imagine for a moment the unforced Rössler system (or simply put $A = 0$) in a situation where it display a stable limit cycle, e.g. at $c = 2$. If we increase c a complete period-doubling cascade evolves, as shown with green (stable orbits) and red (unstable orbits) curves in Fig. 6.6(b). At zero amplitude a torus bifurcation takes place and an ergodic torus arises with a cross-section diameter depending on the amplitude and the now unstable limit cycle appear as the axis of evolution of the torus. In some sense the trajectory on the torus can be considered as the previously stable limit cycle modulated by the external forcing. In the same way a period-2 cycle of the unforced Rössler system should show a period-2 cycle modulated by the external forcing to create a period-2 torus, and if the diameter of the torus is small enough this appears as a two-band quasiperiodic attractor. This means that one can expect a torus doubling close to the parameter values where the unforced system undergoes period-doubling bifurcations. A possible method to detect a torus-doubling bifurcation is to locate the point where one of the negative Lyapunov exponents become zero and turn negative and immediately after turn negative. In Fig. 6.6(a) the third largest Lyapunov exponent region to the left of the resonance zone is visualized. The grey region is where the largest exponent is positive and the horizontal dark red stripes show where the exponent become zero. The region close to the accumulation of period-doubling bifurcations suggest seems to chaotic before the accumulation. However, with a higher resolution and more accurately calculated exponents more torus-doublings emerge to the left of these period doublings. Note, that the torus-doublings in Fig. 6.6(b) take place after the period doublings. This means that the forcing has some stabilizing effect on

the torus. Figures 6.6(c)-(d) shows the three largest exponents correspond-

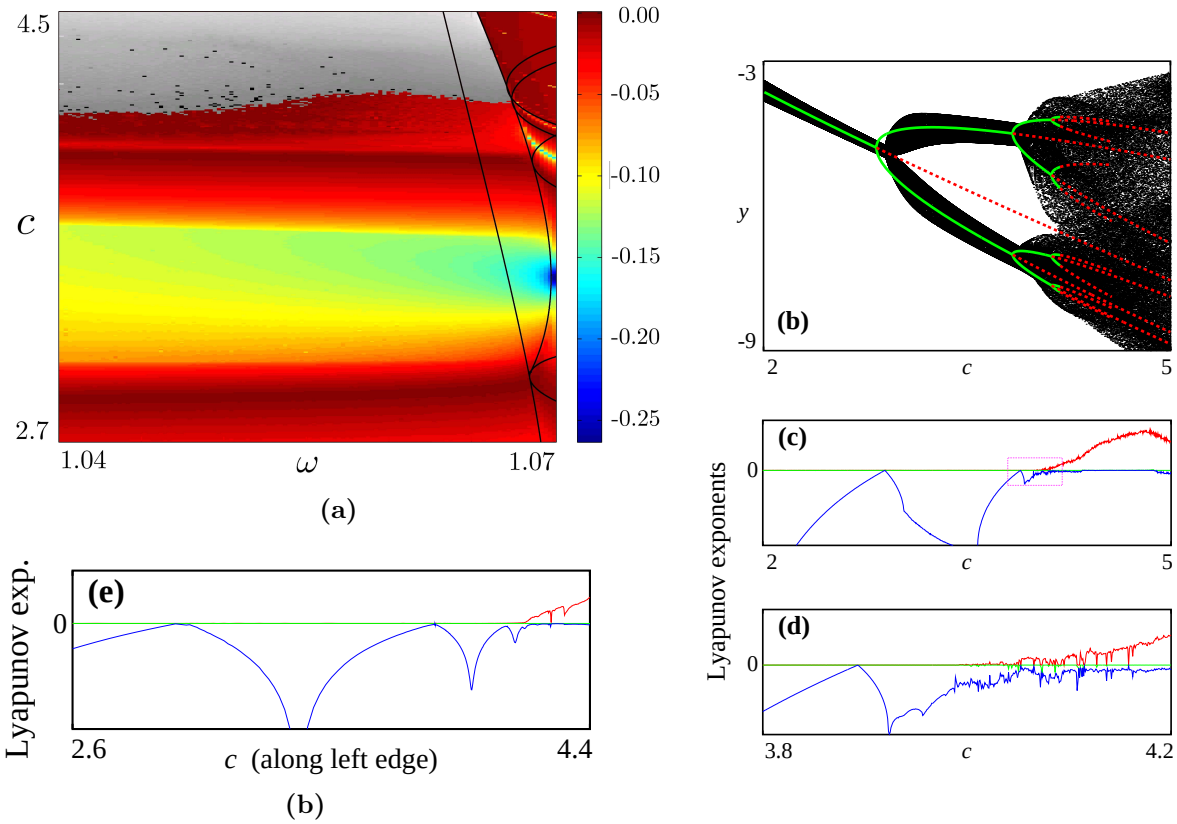

Figure 6.6 Lyapunov exponents and torus-doubling bifurcation at the edge between synchrony and ergodicity and the emergence of a torus doubling at a momentary zero Lyapunov exponent. a) Colored region show the second largest Lyapunov exponent and the grey region is where the largest exponent become positive. To the right the bifurcation structure at the left edge is superposed. b) Brute-force diagram showing the doubling and separation of the period-1 and period-2 ergodic tori as function of c and fixed ω=1.055. c) Lyapunov exponents along the scan in b). d) Enlargement of c). e) The exponents calculated on the left side of the left edge.

ing to Fig. 6.6(b). At this particular scan two successive torus doublings are detected, whereafter a transition to chaos take place. Some discussion has been conducted in the literature on whether such a torus-doubling cascade can be infinite in the same way as the period-doubling cascade is infinite. This appears to depend on the amplitude and on distance to the saddle-node

bifurcations of the resonance tongue. In the unforced Rössler system a homoclinic bifurcation takes place at the points where an unstable cycle touch the stable attractor. Possibly, the termination of the torus cascade is due to the same mechanism. The torus doublings create stable doubled tori and leave the original tori as unstable undoubled tori. Since the diameter of the unstable tori is larger than zero and depend on the forcing amplitude it is possible that this collision take place much earlier, so that the torus-doubling cascade fail to complete before the transition to chaos. This proposition is supported by numerical experiments showing that for large forcing amplitude fewer torus-doublings is observed, while smaller amplitudes reveal additional torus doublings. Figure 6.6(e) show the exponents at the left side of the left edge. Clearly, at least one more event of zero Lyapunov exponent take place before chaotic dynamics set in; supporting the hypothesis that an infinite cascade is possible. To find the next torus-doublings it is necessary to increase the accuracy of both the edge and the time over which exponents are calculated.

While doubled tori is related to the dynamics outside the resonance zone, multilayered tori is a term used for resonant tori, where the layers has arised through bifurcations transverse to the invariant cycle [32]. In our *Manuscript M1* and *Publication P1* we describe how a multilayered-torus is formed trough transverse period doublings of the node and saddle existing inside the tongue. At the edge of the tongue these cycles destroy in saddle-node bifurcations that form the edge and create a stable doubled ergodic torus and an unstable undoubled ergodic torus. In the intermediate state, where only one of the resonant states has terminated, an unstable ergodic torus exist together with a resonant solution, for which the stability depends on the sequence in which the saddle-node bifurcations take place. In order to clarify the numerical results presented in the publication a sketch of the mechanism for the creation multilayered tori is shown in Fig. 6.7. The situation corresponds to that of the right edge at the first period doubling in the cascade, Fig. 6.7(a). Following the circular direction around the point of tangency, five structurally different situations exist. At point b, we find the period-1 resonant node and saddle located on a torus. Trajectories escaping from the unstable focus point are attracted to the node. Point c illustrates the transverse period doubling of the node, creating a period-2 node and leaving a saddle. On crossing the period doubling of the saddle solution (PD_1^U) the point d is reached, the period-2 saddle is created and the period-1 saddle turn into an doubly unstable saddle. At point e, the first saddle-node bifurcation has destroyed the resonant period-1 solution, whereby an unstable ergodic torus is formed. The manifolds of the period-2 solution must be related to

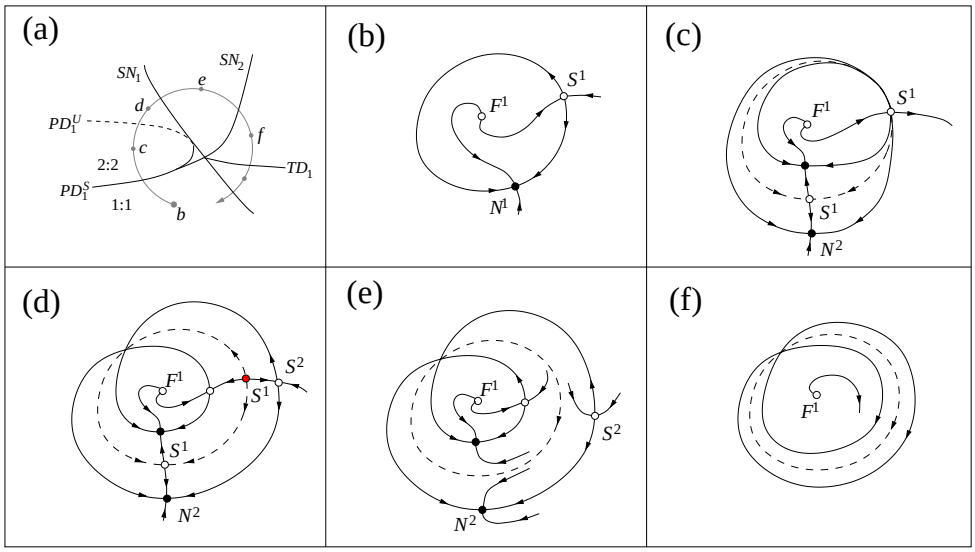

Figure 6.7 Sketch of the bifurcations that form a resonant multilayered torus (inside the tongue) and a doubled torus (outside the tongue) through transverse period doublings. Sub-figures (b)-(f) correspond to the points in (a).

the period-1 dynamics of the unstable torus, so the manifolds are asymptotically connected to the torus. At point f the saddle-node bifurcation of the period-2 resonance has destroyed as well. This leaves a stable period-2 torus surrounding the unstable torus. At the same time all manifolds are destroyed, and have become asymptotic trajectories between the two tori. If we follow the circle to the point g the torus-doubling is crossed, whereby the double-layered ergodic torus merges into a single layer ergodic torus.

6.2 Periodically forced nephron model

Realistic nephron models are obviously much more complex than the simple case of the forced Rössler system discussed in the previous section. Nevertheless, the periodically forced nephron model posses a bifurcation structure almost topologically identical to that of the Rössler system with respect to the evolution of a period-doubling cascade, formation of a dense set of saddle-node bifurcations and torus-doubling bifurcations residing in the non-resonant region. However, a few differences are present, regarding the

period-doubling structure and the birth of the saddle-node bifurcations. In the following a discussion of the main results from a study of the nephron model with a periodically oscillating arterial blood pressure is imposed to the model.

More specific, the intention in this study is to reproduce the simple situation of a nephron's response to an oscillation in the arterial blood pressure. This situation is an extension and improvement of the autoregulatory mechanism of the nephron. Without the external forcing the model corresponds to a nephron's autoregulation of pressure variations produced within the nephron it self. While the forced version correspond to response of the autoregulation to an externally generated periodic variation in the arterial pressure.

The nephron is fixed to work at a delay time equal to 16 sec, corresponding to a TGF period of 40 sec and a TGF gain of the value α=24, where the single nephron operate close to the border of 1:4 and 1:5 relationship between the TGF and myogenic oscillations. The TGF gain may appear unrealistic large compared to experimental values of a normotensive rat (and maybe even for a hypertensive rat), however, this is justified with reference to the fact that we only consider a single nephron. The simultaneous pressure of other nephrons is likely to shift the bifurcations in the individual nephron to lower values of α.

Consider the nephron model presented in section 3.1, with an externally applied variation in the blood pressure of the form

$$P_a(t) = P_{a,0}(1 + A\sin(\omega t)), \tag{6.1}$$

where $P_{a,0}$=13.3 kPa is the average blood pressure, $A = 0.0075$ is the relative amplitude, and ω is the angular frequency. By letting the nephron oscillate at a fixed period of 40 sec, the corresponding angular frequency takes a value in some range around $\omega = 0.155$ s^{-1}, the model is studied as function of ω and a second control parameter, which is chosen to be the afferent flow resistance in its unconstrained state.

In *Manuscript M4 and Manuscript M5* we first demonstrate that period-doubling bifurcations is a phenomenon that take place in the nephron of a normotensive living kidney and not just a mathematical phenomenon. However, the period-doubled time trace of the tubular pressure is only preserved for limited time, because the conditions of the nephron change constantly. We also show that a nephron in a hypertensive kidney display irregular time traces of the tubular pressure, with a power spectrum displaying several sub-

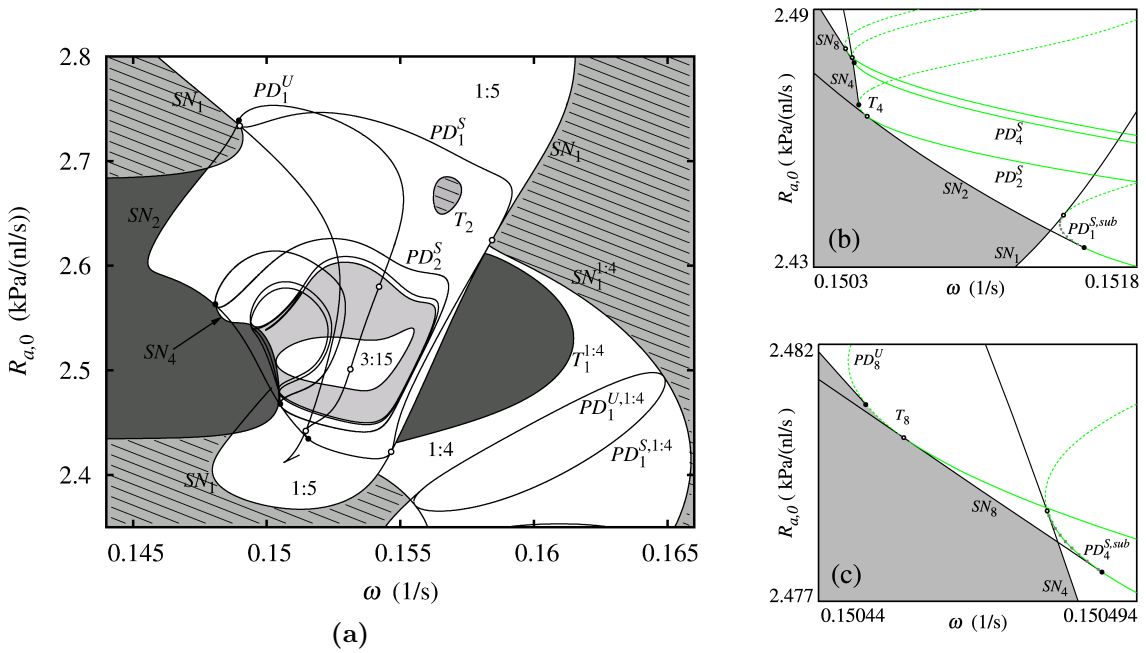

Figure 6.8 Main result from bifurcation analysis of the forced nephron system. a) Overview showing the regions of 1:5 (at center) and 1:4 (at bottom-right) mode-locking. Hatched region is desynchronized quasiperiodic (light grey) and chaotic (dark grey) dynamics. Note, that period doublings here share the same saddle-node bifurcation. b) Close up of the lower period-doubling structure, showing the alternation between super- and subcritical period doublings. c) Enlargement of the bifurcations at level 4 and 8.

harmonics of the TGF frequency. In this case the TGF frequency is not very well defined since there are also a faster mode with a frequency 1.5 of the TGF frequency, indicating that the irregular dynamics not only is in the amplitude but also in the phase.

The mathematical model that approach the experimental setup is subject to a detailed analysis in *Manuscript M4*. This analysis reveal practically all the same phenomena as found in the forced Rössler system:

- A complete period-doubling cascade of both the node and saddle resonant solutions.
- A cascade of saddle-node bifurcations emerging from points on the

period doublings that limit the resonance region.

- A torus bifurcation is in place to close the gap arising due to the supercritical period doublings.
- A cyclic behavior of super- and subcritical period doublings at the edges of the tongue.
- A torus-doubling bifurcation in the desynchronized regions. However, so far subsequent torus-doublings has not been observed.

Except from the torus-doubling, these findings are all presented in Fig. 6.8(a). Note, that the limit between phase-synchronized chaos and desynchronized chaos appear close to, but not exactly at the accumulation of saddle-node bifurcations. So, far there is no explanation to that. However, the coupled oscillators discussed in the next chapter may in future be part of the answer.

One difference compared to the overall structure of period doubling and saddle-node bifurcations is that period doublings are winded and twisted such that they share the same saddle-node bifurcation, and the twisting cause the unstable period doubling to appear before the stable one at the upper edge. From that it is reasonable to conjecture that in the more classical parameter plane for an Arnol'd tongue (frequency-amplitude plane) and other parameter planes, the saddle-node bifurcations of the left and right edge are related and possibly even connected. If they are not connected then there must be some bifurcation taking place on the smooth transformation from the $(\omega, R_{a,0})$ plane to the (ω, A)-plane, that cause a splitting of the saddle-node bifurcation curves.

A generic property of the bifurcations in this class of systems, is the alternation between super- and subcriticality of the period doublings. A confirmation of that is not clearly presented in our *Manuscript M4*. However, it is clearly demonstrated in Figs. 6.8(b)-(c) that at the lower edge this property actually is present. Also, not treated in the paper, is the possibilities of in-phase and out-of-phase synchronization. We just shortly mention that the chaotic region enclosed in the 1:5 regime is largely in-phase dynamics, while the quasiperiodic dynamics born at $T_1^{1:4}$ and chaotic area (further above $T_1^{1:4}$) in the 1:4 region, display out-of-phase synchronized between the externally oscillating pressure and the tubular pressure $P_t(t)$.

CHAPTER 7

Coupled almost identical systems

Having presented the main results from the study of two externally periodically forced period-doubling systems, this chapter extends the analysis to mutually coupled almost identical systems. Compared to unidirectional coupled systems (e.g. the externally forced systems), mutually coupled systems are often more appealing to biological problems, because a system that is influenced by an other similar system, would need some extra mechanism to prevent a similar coupling to that other system.

7.1 Coupled Rössler systems

7.1.1 Resource coupling

Two different coupling types for the Rössler system have been examined. The first version represents an attempt to make the coupling more physiological sound as a model for two coupled nephrons, with respect to the hemodynamic mechanism. Recall the variables of the Rössler system from section 3.3.3 and consider the coupling term

$$a_e y_1 = a[1 + \alpha_1(x_2 - c)]y_1, \tag{7.1}$$

where α_1 is the coupling parameter, x_2 is the afferent arteriolar radius of nephron 2 and y_1 is the rate by which the arteriolar radius of nephron 1 changes. When x_2 is small ($x_2 << c$) the radius x_1 increases, corresponding to a rising blood pressure in the shared arteriole. Thus, this mechanism conforms well with the hemodynamic coupling type.

In *Manuscript M3* an overview of the bifurcation structure is presented. The main purpose with this study was to obtain an idea of what to expect from studies of other almost identical systems and to see if the special type

of coupling may give some additional phenomena, that possibly could be generic and especially characteristic to such systems.

Our analysis clearly demonstrates that there is some changes in the bifurcational behavior compared to the more simple forced systems. Most remarkable is the existence of a phase-synchronized torus inside the resonant region. This quasiperiodic regime involve a pitchfork bifurcation giving rise to co-existing periodic attractors, that each undergoes period-doubling cascades to form co-existing chaotic attractors.

An interesting result from this analysis is that the internal torus gives rise to a pair of saddle-node bifurcations that run along with the saddle-node bifurcations that form the border between resonant and ergodic dynamics. Let us take a look at the bifurcations of the 1:1 resonant solution. Figure 7.1 (ignore the blue curves for a moment) shows the Arnol'd tongue in the more traditional projection with ω on the x-axis and coupling parameter α on the y-axis. The 1:1 resonant solution is found in the lower region of the tongue. At at coupling value of approximately 0.14 bifurcations of the 1:1 solutions set in. Closer to the edges a period doubling PD_1 take place, first on the stable node (point a) leaving a saddle solution, which at point b also period doubles and leaves a doubly unstable saddle. The original 1:1 saddle also bifurcates twice, first at point c and later at point d, whereafter the original 1:1 saddle solution is a triply unstable saddle.

In the figure a blue curve is drawn (by hand). This curve is a representation of the period-2 resonant solution and must not be confused with the bifurcation curves. The solid curve emanating from point h represent the 2:2 resonant stable node. It co-exist with another stable node that emanate from point k. Following either of the stable solutions horizontally, they turn back into the tongue at the saddle-node bifurcations. Starting as stable nodes they turn into saddles (dashed) and then doubly unstable saddles (dotted) at the opposite edge, from where they start to gain in stability until they finally connect. Note, that the solution drawn is a period-2 solution and therefore should not bifurcate at SN_1. There is another saddle-node bifurcation emanating from the second point of tangency (point M) that is practically coinciding with SN_1 and it is this bifurcation that is involved in the above description.

The fact that there are co-existing solutions that are connected through saddle-node bifurcations suggest that the co-existency is born in a pitchfork bifurcation. It takes place just a the point where the two SN_2 intersect (point

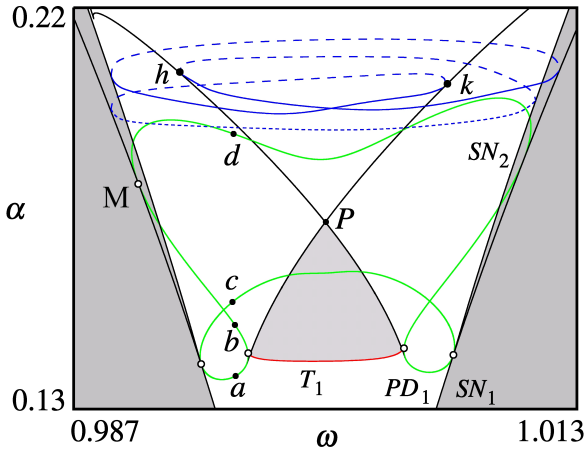

Figure 7.1 Resonance tongue in the frequency and coupling parameter plane for a pair of resource coupled Rössler oscillators. Black curves are saddle-node bifurcations, the green curve is a period doubling and the red curve is a torus bifurcation of the stable 1:1 node. Note, that the blue curves are projections of one-dimensional bifurcations curves, please see text for details.

P). In this parameter cut it appears as a point because the symmetry of the system is broken due to detuning of frequencies. To imagine the birth of two co-existing period-2 solutions, we now follow the original 1:1 saddle that comes from the saddle-node bifurcation SN_1 of the stable period-1 node. As this curve cross T_1 nothing happens, because it is only a bifurcation on the stable 1:1 node. As the point P is crossed the pitchfork bifurcation occurs, whereby the doubly unstable period-1 solution and two co-existing single unstable period-2 saddles are born. These are the dotted blue curve and the two dashed blue curves. The stable versions of the period-2 dynamics arise straight forward in the saddle-node bifurcations at the edge.

We also want to find out what happens further up in the Arnold tongue. However, the analysis of this simplified system appears to be much more complicated than one could expect. Since one of the purposes of studying Rössler systems is to keep things as simple as possible, before extending to the physiological model versions, there is a need to reconsider the coupling mechanism.

An alternative and simpler coupling is the diffusive or linear coupling. To keep the analogy with the physiology of the nephron we couple the system

through the z variable that correspond to the salt concentration at macula densa, so that a high salt concentrations at nephron 1 cause the beginning of a decreasing salt concentration of nephron 2. Note, that the diffusion does not directly involve any transfer of salt between the nephron, it is rather the effect of the existence of a salt concentration that is exchanged. As will be clear in the next section, the change of coupling is a good choice, because a much simpler behavior, without loss of phenomena, appear in this system.

7.1.2 Linear coupling

Rössler systems coupled through a linear relationship between a variable of each system, is one of the most studied system classes in the field of nonlinear dynamics and bifurcation theory. Nevertheless, it is still possible to find new and interesting phenomena and this underlines the enormous wealth of complex phenomena in nonlinear dynamics. With a coupling term previously studied by Rasmussen *et al.* [28], the system is studied in the (a_1, ω) parameter plane, where a_1 is the usual amplification parameter of system 1, and ω is the detuning parameter controlling the fundamental frequency of system 2. Note, that the choice of this plane deviates from earlier studies in this thesis.

In *Manuscript M5* it is demonstrated that the left and right edge of the resonance tongue behave differently. At the right edge the transition between resonant and quasiperiodic dynamics follow the same bifurcation structure with saddle-node bifurcation emerging from the period doublings, as was found in the forced Rössler system. This is also the case for the left edge, however, there is more to be added, before the description is complete. Firstly, the torus bifurcation, that also appeared in the resource coupled Rössler system inside the resonance zone, is terminated by saddle-node bifurcations and they both run along the left edge, such that there in total are three saddle-node bifurcations at that edge. These cause the period-doubling bifurcation to make an extra turn before running further into the resonance zone as the period doubling of the saddle cycle. Close to all of the three turning points three new saddle-node bifurcations are born, and therefore the next period doubling in the cascade take the same folded shape. As an infinite period-doubling cascade evolves, three dense sets of saddle-node bifurcations are formed. The transition from resonant to non-resonant dynamics is mainly associated with the inner saddle-node bifurcations, while the outer set limit a co-existing phase-synchronized quasiperiodic solution.

So far this behavior, except from the existence of three sets of saddle-node bifurcations, was to be expected. A phenomenon not observed in the previous models is that a second torus bifurcation of the period-2 node is present at the left edge giving rise to an additional degree of complexity close to the border of the tongue. It is suspected to be born on one of the three saddle-node bifurcations of the same period-2 node. However, at the moment of writing this has not been confirmed. As the torus bifurcation runs along the inner side of the left edge it intersects with the next period-doubling bifurcation and a torus bifurcation on the period-4 solution.

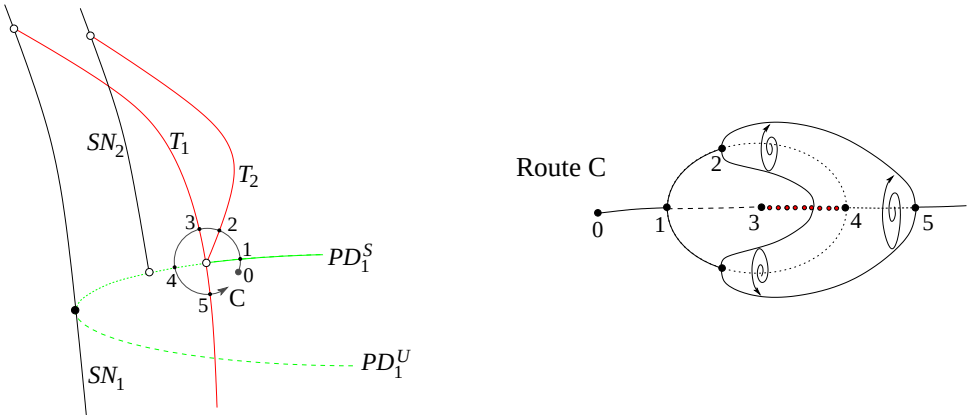

Figure 7.2 Left: Bifurcation structure with a torus bifurcation (with doubled periodicity) emerging from the intersection between a period doubling and torus bifurcation of the same periodicity. Right: Solutions and bifurcations along the circle C.

In the following we will present what can be concluded from the event of an intersecting period doubling and torus bifurcation of the same solution. For the numerically obtained bifurcation curves the reader is referred to figure 3 in *Manuscript M5*, however, here the following detailed explanation of the bifurcation structure. Figure 7.2 show a schematical representation of the situation at hand. To simplify, the extra turn of the period doubling is ignored and the first period doubling of an eventually infinite cascade is considered. The saddle-node bifurcation that limit the resonant 1:1 node and saddle is labelled SN_1, the period doublings of the node and saddle cycles are PD_1^S and PD_1^U, respectively, and SN_2 is the saddle-node bifurcation that limit the period-doubled node and saddle cycle. The dotted part of the period-doubling curve represents a period doubling of a doubly unstable saddle cycle. The red curve (T_1) marks the torus bifurcation taking place on

the period-1 node and runs from the 1:1 resonant region. From below, T_1 intersects with PD_1^U, but that does not change anything, because the torus bifurcation take place on the node, while the PD_1^U is a period doubling of the saddle solution. Next, the torus bifurcation T_1 intersect PD_1^S, thus, at that point both a torus and a period doubling take place at the same time. From the point of intersection a new torus bifurcation T_2 of the period-2 node emerge.

The question is now: how does the solutions organize in the phase space? To demonstrate that, a circle around the point of intersection is drawn, and to the right of the figure a sketch of the solutions and bifurcations taking place along that circle is shown. Beginning from the point 0, where a stable period-1 node exist, and following the circle counter clockwise, the first intersection is at point 1, where the period of the node is doubled and the node become a period-1 saddle. Then a torus bifurcation take place on the period-2 node (point 2) giving birth to a period-2 torus, whereby the period-2 become a doubly unstable saddle. The initial solution, now a saddle, then undergo a torus bifurcation at point 3, further destabilizing the period-1 to be triply unstable. To simplify the description, we now turn the direction to go clockwise from the end of the arrow, where we have the stable period-1 node. The first bifurcation we meet on this path is T_1 (point 5) giving rise to a period-1 torus, and a period-1 unstable focus (two unstable directions) that undergo a period doubling at point 4. The solutions emerging from point 4 and 5 must conform with the solutions born at points 2 and 3. For the cycles it is straight forward to connect the solutions at the point where we turned direction, because stabilities of the period-1 and period-2 cycles match perfectly. The torus must follow the cycles, such that it surround a focus point. Therefore it must separate into a double torus at the point where the focus undergoes a period-doubling bifurcation.

One could now wonder, if the birth of T_2 must take place exactly in the point of intersection between PD_1^S and T_1. To illustrate that it actually must be the case, the situation where they do not coincide is draw in Fig. 7.3(a). Two different routes are inserted, one around each of the two intersection points, and Fig. 7.3(b) illustrate the attempt to make the solutions match when following route A and B. As far as the period-1 solution is concerned stabilities along both route A and B fit well, while the period-2 along route B fail to conform both routes. This means that some extra bifurcations must be present to account for the lack of stabilization required to make the solutions conform. Thus, it can be concluded that, unless a pair of saddle-node

bifurcations taking the role of the torus bifurcation, the torus bifurcation must start from the point of intersection between SN_1 and T_1.

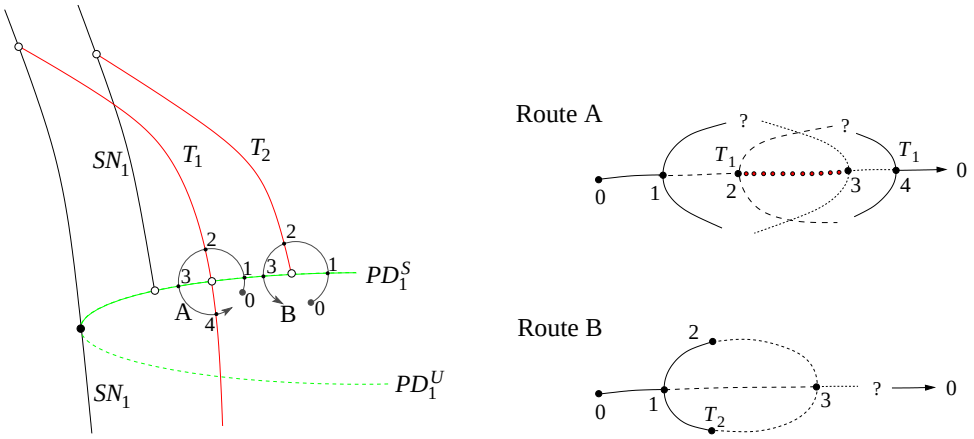

(a) Incorrect structure **(b)** Stability mismatch

Figure 7.3 Incorrect sketches of the bifurcation structures. a) An incorrect sketch in the two dimensional parameter plane, where the next torus bifurcation do not emerge from the intersection between PD_1 and T_1. b) sketches showing a mismatch (at the question marks) in stability on the period-2 and period-1 solution for route A and B, respectively.

Some very interesting consequences follow from this description. Suppose the period-doubling cascade is a complete Feigenbaum cascade and that the torus bifurcations all run along parallel with the evolution of the Feigenbaum cascade, then we can conclude that an infinite torus bifurcation cascade takes place as well. Actually, the numerical simulations published in *Manuscript M5* also indicate that the birth of torus bifurcations take place in an alternating way around the sequence of PD-T intersection points and, therefore, the torus bifurcations must converge to a dense set of curves. Furthermore, this also support that an infinite torus-doubling cascade can evolve along the edge. Here, an enlargement of the bifurcation structure with saddle-node, torus-, and period doublings up to period-32 is shown in Fig. 7.4, where the accumulation curves have been estimated.

It is usually said that the transition from phase-synchronized to desynchronized dynamics take place at the saddle-node bifurcations associated with the resonant nodes and saddles. In chapter 6 we demonstrated in all details that this is the responsible mechanism for the externally forced Rössler system. However, there is at least one alternative bifurcational mechanism

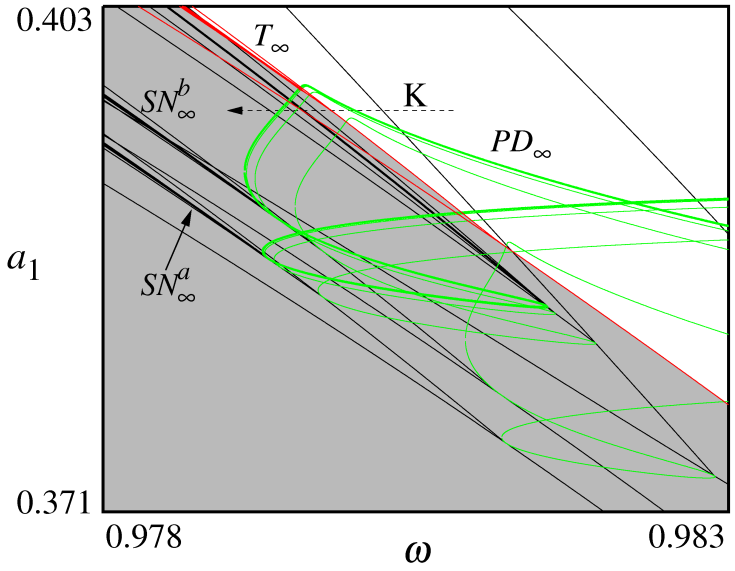

Figure 7.4 Evolution of period doubling (green), saddle-node (black) and torus (red) bifurcation cascades at the left edge. The first level of bifurcations, SN_2^a, SN_2^b, SN_2^c, PD_2 and T_2, are located at the lower right. Note, that the synchronization border is here indicated to be at the torus bifurcations, although the border actually is at homoclinic bifurcations close to the torus bifurcations.

that might be caused by the existence of multistability in the system. This second possibility takes place through a homoclinic bifurcation of tori. Existence of this desynchronization mechanism has previously been reported by Postnov *et al.* in a system of diffusively coupled modified van der Pol oscillators [26] and a externally forced predator-prey model [27].

Here only one example of the homoclinic transition is presented. From calculation of the phase in the two dimensional parameter plane it is known that a transition takes place close to the torus bifurcations. Figure 7.5 shows the stable attractors along the direction K in Fig. 7.4. The direction is just above PD_4 and cross the torus bifurcation and saddle-node bifurcations of the period-8 solution. The parameter range of Fig. 7.4 extends into both the resonant periodic and resonant chaotic region to the right and into the phase desynchronized (ergodic) region outside the tongue to the left. At the torus bifurcation T_8 the 8:8 resonant node bifurcates to a period-8 torus. This torus remains phase synchronized as it grows in size with decreasing ω. The apparent jump in size shortly after T_8 is due to the projection, it

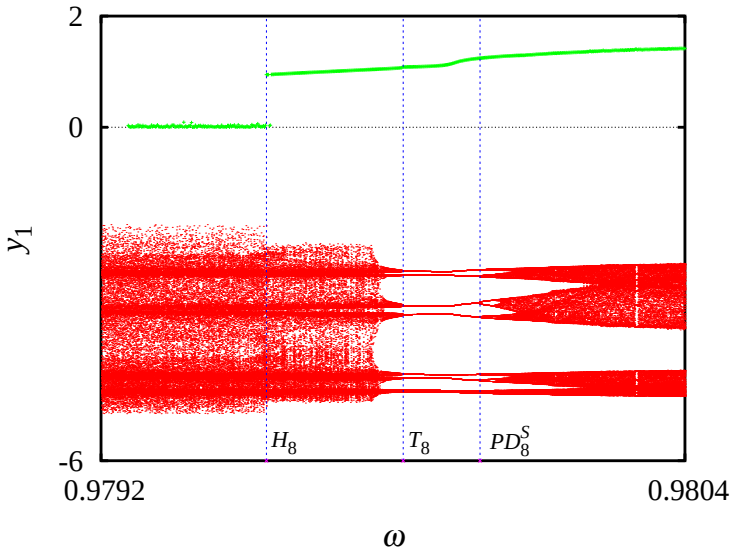

Figure 7.5 Transition to desynchronized chaos through a homoclinic bifurcation along direction K in Fig. 7.4. Brute-force bifurcation diagram showing the period-doubling cascade leading to phase synchronized chaos at increasing ω. For decreasing ω we first meet the torus bifurcation T_8 leading to a phase-synchronized torus, that desynchronizes at the homoclinic bifurcation H_8. The green curve show the phase between the two systems, where zeros phase means a drifting phase, i.e. asynchronous dynamics.

continues to grow in other variables. The jump at H_8, on the other hand is a true abrupt change in attractor size, caused by a homoclinic bifurcation. At this point the torus touches the homoclinic orbit of a saddle point located outside the torus and destroys while at the same time a larger torus is born.

7.2 Vascular coupled nephron models

The corresponding physiological case to the more abstract coupled Rössler system is a system of vascular coupled nephrons. In the externally forced nephron discussed in chapter 6 we found that the period-doubling bifurcation structure folded to meet at the same edge of the resonance tongue, such that the saddle-node bifurcation that limit the individual resonances are connected. We also found that the transition to phase desynchronized chaos

take place before the accumulation of saddle-node bifurcations, but we did not propose a reason for that. Here, we may find a possible answer to this problem, however, for the time being it is left as an open problem.

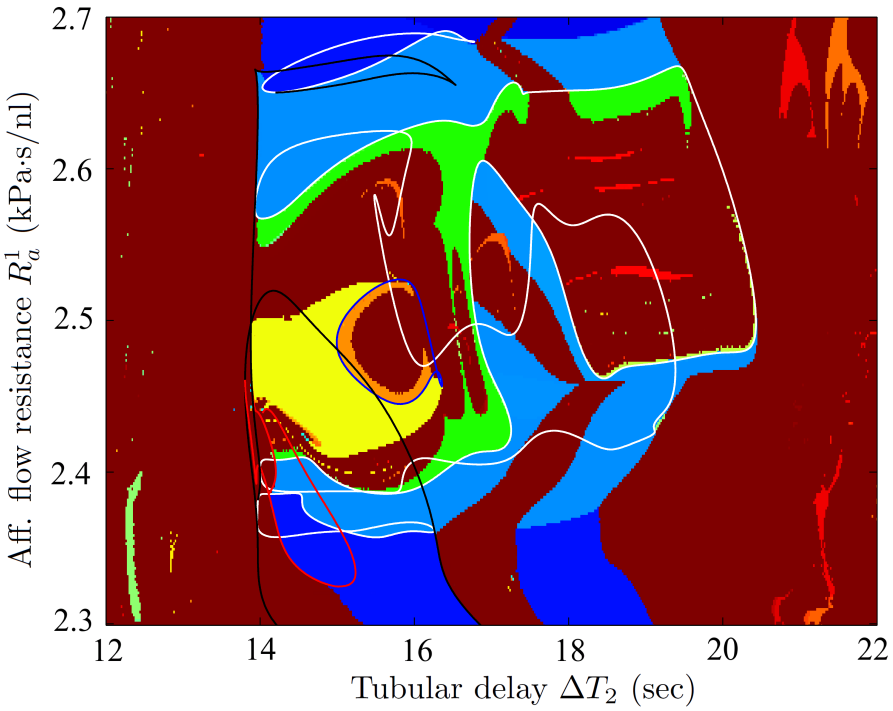

Figure 7.6 Overview of the stable attractors in the coupled nephron model. Blue regions represent 1:4 and 1:5 mode-locking and the brown regions represent quasiperiodic and chaotic dynamics. White curves are the first two period doublings. Black and red are the first pair of saddle-node and torus bifurcations, respectively.

The degree of interaction for vascular coupled of nephrons mainly depends on the distance between glomeruli, because the electric signal decrease exponentially with distance from where it is generated. Here, the coupling is a fixed relative small value, corresponding to a normotensive state. The purpose of this study is to see how the bifurcation structure change compared to the forced version of the model. In that respect it must be noted, that while the forced version was perturbed on the arterial pressure, the coupled version concerns the degree to which the TGF-regulation of one nephron affects the neighboring nephron. So, the intention is not to try to attribute the changes

to a perturbation of a specific variable or parameter. The purposes should rather be taken to be individual for each study. However, regarding the bifurcational changes comparisons can be made because the overall structure usually change mainly due extensions, for instance through couplings.

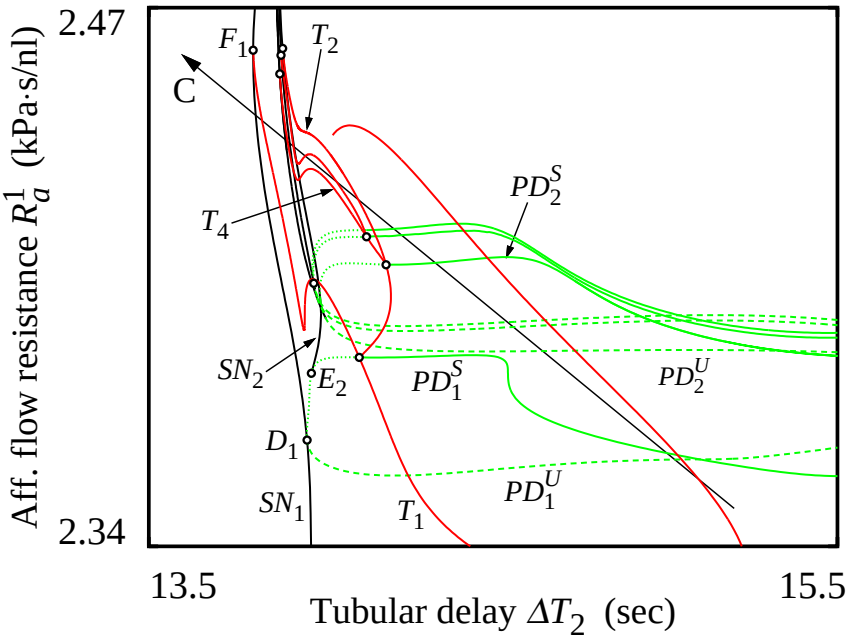

Figure 7.7 Bifurcation diagram of the coupled nephron model, showing the cascades of saddle-node, torus, and period-doubling bifurcations.

In Fig. 7.6 an overview of the stable attractors is displayed, with the first period doubling, saddle-node and torus bifurcation overlayed. The blue regions in the lower and upper parts are period-1 solutions in mode-locking ratios of 1:5 and 1:4 between the TGF and myogenic oscillations. The brown tongues dividing these regions into a right and left part are bordered by torus bifurcations. The brown regions at either side represent ergodic tori and chaotic dynamics. In the middle of the figure a yellow regions, with period-3 dynamics is found on which a period-doubling cascade leads to chaos to the right of the period-3 region. Light blue and green represent period-2 and period-4 solutions, respectively. The right half of the scan displays another period-doubling structure such that the first two period doubling are shared with the cascade in the left part, and the following period doublings are

then individual for each cascade. Clearly, there are many similarities with the corresponding bifurcation diagram for the forced nephron (see Fig. 3.2). Especially the folding of the period doubling, that makes them return to the same edge and the formation of the saddle-node bifurcations also on the same edge.

A main result from the analysis is the emergence of a more or less similar bifurcation structure as we found for the forced nephron model. Let us focus on the region where the period doublings are tangent to the corresponding saddle-node bifurcations at the lower part of the left edge. This region is shown in more detail in Fig. 7.7.

In the previous section we discussed the emergence of torus bifurcations from the period-doubling bifurcation and demonstrated the transition to phase-synchronization through a homoclinic bifurcation near these torus bifurcations. But, we did not attribute the birth of these bifurcations at the other end of the curve in the two-parameter plane, because the torus bifurcation seemed just to continue along with saddle-node bifurcations. In Fig. 7.7 the folded period-doubling structure limit the parameter region, such that the curves are more confined. This enables us to see that the torus bifurcations actually terminate on saddle-node bifurcations in Bogdanov-Takens (BT) bifurcations. It has been shown by Knudsen *et al.* [15] that BT bifurcation imply the existence of a homoclinic bifurcation emanating from that bifurcation point. This tell us that together with all the other cascades also a cascade of homoclinic bifurcations must exist. Recall that we were unable to determine the end point of the torus bifurcations in the bifurcation structure of the coupled Rössler system. The above finding support the idea that they are born on one of the three sets of saddle-node bifurcations.

CHAPTER 8

Conclusion

The first part of the study was devoted to the analysis of a detailed nephron model, that describe the spatial variation of flow, pressure and salt concentration in the tubular system, and model the myogenic process on a cellular level. By calculating the Lyapunov exponents from simulated time series of the model in versions representing a single nephron and two vascular coupled nephrons we have shown that increased TGF-myogenic coupling and increased vascular inter-nephron coupling induce chaotic behavior of the tubular flows. From that we can conclude that increased TGF-myogenic and inter-nephron couplings are possible reasons for the experimentally observed irregular blood pressures in hypertensive rats.

The remaining part of the study may be seen as two parallel directions. One of them intend to search for bifurcational phenomena in externally forced and mutually coupled simple models. The other direction intend to make similar studies of the physiological, mechanism based, and more complicated models. These models posses bifurcation structures that are much more complicated and messy. By using the knowledge from the simpler cases, parts of the complicated bifurcation structures can be filtered away whereby only the important parts, that explain the main bifurcations remain.

In the study of the periodically forced Rössler system, we demonstrated how the period-doubling cascade unfold in the resonant region and how the saddle-node bifurcations that is born on the period-doubling bifurcation close to the point where the two bifurcations are tangent to each other. These saddle-node bifurcations form the edges of the resonance zone is formed through the cyclic behavior of sub- and supercritical period-doubling bifurcations at the edges, where the supercritical case in general involve a torus bifurcation in order to close a gap which is not bordered by a saddle-node bifurcation. We also showed that the cyclic behavior cause the formation of a dense set of saddle-node bifurcations as the period-doubling cascade leads to chaos and that the accumulation curve of the saddle-node bifurcations form

the edge between phase-synchronized and desynchronized chaos. Finally, we explained how multilayered tori inside the resonance tongue is formed and how they are related to the torus-doubling bifurcations outside the resonance zone.

The forced nephron model was analyzed with the forcing frequency and resting value of the afferent flow resistance as parameters. We showed that in this parameter plane the period doublings fold, such that they share the same saddle-node bifurcations. This system also showed the cyclic behavior of the period-doubling bifurcations. However, the edge between phase synchronized and desynchronized dynamics against our expectations did not involve the saddle-node bifurcations. A conclusion on this problem remain for the time being.

To a large extend we found the same phenomena in the mutually coupled Rössler system. In the resource coupled version the existence of an internal torus bifurcation was found. The quasiperiodic and phase synchronized dynamics born in this bifurcation, terminate in saddle-node bifurcations that imply a pitchfork bifurcation giving rise to co-existing solutions, whos existence are symmetrical in the parameter plane considered. The linear coupled Rössler systems was studied in a different parameter plane. Still we found a structurally similar bifurcation structure compared to the resource coupled systems. Due to the folding of the period-doubling bifurcations at the left edge three dense sets of saddle-node bifurcations form. Unique for the mutually coupled system is the formation of a torus bifurcation cascade. We have described how the torus bifurcation cascade must emerge due to the intersection of torus bifurcations with the period-doubling cascade. The transition from phase synchronized dynamics to non-synchronous dynamics was show to take place through a homoclinic bifurcation on a torus.

Our study on vascular coupled nephron models coincided very well with the study on coupled Rössler systems and the forced nephron model. We found a similar folded period-doubling and saddle-node structure as in the forced nephron model. From the emergence of additional cascades of torus and homoclinic bifurcations we can suggest that these phenomena may be very common for coupled period-doubling systems. An interesting finding was that both ends of the torus bifurcations was located, one end starting from the period-doubling bifurcation, just like it was found in the Rössler system, the other end was found to connect to the saddle-node bifurcations (Bogdanov-Takens bifurcation) emerging from the same period doubling. We concluded that if the torus bifurcation cascade continue then the formation

of homoclinic bifurcations should also continue. A finding that we could not conclude from the Rössler, but it is natural to conjecture that homoclinic bifurcations in the Rössler system also evolve due to existence of Bogdanov-Takens bifurcations.

Our findings so far is of high relevance for future studies on larger systems of coupled nephrons. The next steps in the process is to study how the nephrons in a nephron tree behave and how nephron trees coupled through arcuate arteries behave. Such large systems are almost impossible to study by continuation techniques. Our studies can give some ideas of how such large systems can behave and how they can synchronize. For instance it is likely for large systems to show multistability. Therefore we might to a first guess expect torus bifurcation structures and homoclinic bifurcations to be involved in these kinds of studies.

References

[1] Ch. Aalkjaer and H. Nilsson. Vasomotion: cellular background for the oscillator and for the synchronizat ion of smooth muscle cells. *British Journal of Pharmacology*, 144(5):605, 2005.

[2] V.S. Anishchenko, T.E. Vadivasova, D.E. Postnov, and M.A. Safonova. Synchronization of chaos. *International Journal of Bifurcation and Chaos in Applied Sciences and Engineering*, 2(3):633–644, 1992.

[3] M. Barfred, E. Mosekilde, and N.-H. Holstein-Rathlou. Bifurcation analysis of nephron pressure and flow regulation. *Chaos*, 6(3):280–7, 1996.

[4] W. M. Deen, C. R. Robertson, and B. M. Brenner. A model of glomerular ultrafiltration in the rat. *Am. J. Physiol.*, 223:1178–1183, 1972.

[5] W. M. Deen, C. R. Robertson, and B. M. Brenner. Glomerular ultrafiltration. *Federation Proceedings*, 33(1):14–20, 1974.

[6] E. J. Doedel. *AUTO-07p: continuation and bifurcation software for ordinary differential equations*. Concordia University, Montreal, Canada, Februrary 2008.

[7] R. Feldberg and M. Colding-Jorgensen. Analysis of interaction between TGF and the myogenic response in renal blood flow autoregulation. *American Journal of Physiology*, 269(4):F581, 1995.

[8] A. Goldbeter. *Biochemical Oscillations and Cellular Rhythms*, chapter 9: Oscillations and waves of intracellular calcium. Cambridge Unviersity Press, 1996.

[9] J. M. Gonzalez-Fernandez and B. Ermentrout. On the origin and dynamics of the vasomotion of small arteries. *Mathematical Biosciences*, 119(2):127–167, 1994.

[10] N.-H. Holstein-Rathlou. Oscillations and chaos in renal blood flow control. *Journal of the American Society of Nephrology*, 4(6):1275–1287, 1993.

[11] N.-H. Holstein-Rathlou and D. J. Marsh. Oscillations of tubular pressure, flow, and distal chloride concentration in rats. *Am. J. Physiol.*, 256:F1007–F1014, 1989.

[12] N.-H. Holstein-Rathlou, K.-P. Yip, O. V. Sosnovtseva, and E. Mosekilde. Synchronization phenomena in nephron-nephron interaction. *Chaos*, 11(2):417–426, 2001.

[13] K. S. Jensen, N.-H. Holstein-Rathlou, P. P. Leyssac, E. Mosekilde, and D. R. Rasmussen. *Chaos in a system of interacting nephrons.* Chaos in Biological Systems. Plenum, 1987.

[14] K. S. Jensen, E. Mosekilde, and N.-H. Holstein-Rathlou. Self-sustained oscillations and chaotic behavior in kidney pressure regulation. *Mondes en Developpement*, 54/55:91–109, 1986.

[15] C. Knudsen, J. Sturis, and J. S. Thomsen. Generic bifurcation structures of arnold tongues in forced oscillators. *Physical Review A*, 44(6):3503–3510, 1991.

[16] A. P. Kuznetsov, S. P. Kuznetsov, and I. R. Sataev. A variety of period-doubling universality classes in multi-parameter analysis of transition to chaos. *Physica D*, 109(1-2):91–112, 1997.

[17] S. P. Kuznetsov, A. P. Kuznetsov, and I. R. Sataev. Multiparameter critical situations, universality and scaling in two-dimensional period-doubling maps. *Journal of Statistical Physics*, 121(5-6):697–748, 2005.

[18] S. P. Kuznetsov, A. A. Mailybaev, and I. R. Sataev. Birth of a new class of period-doubling scaling behavior as a result of bifurcation in the renormalization equation. *Journal of Statistical Physics*, 130(3):599–616, 2008.

[19] S. P. Kuznetsov and I. R. Sataev. Universality and scaling for the breakup of phase synchronization at the onset of chaos in a periodically driven Rössler oscillator. *Physical Review E*, 64(4):046214/1–7, 2001.

[20] Y. A. Kuznetsov. *Applied Mathematical Sciences: Elements of Applied Bifurcation Theory.* Springer Verlag NY, 2004.

[21] P. P. Leyssac and N.-H. Holstein-Rathlou. Tubulo-glomerular feedback response: Enhancement in adult spontaneously hypertensive rats and effects of anaesthetics. *Pflügers Archive*, 413:267–272, 1989.

[22] D. J. Marsh, O. V. Sosnovtseva, Ki. H. Chon, and N.-H. Holstein-Rathlou. Nonlinear interactions in renal blood flow regulation. *American Journal of Physiology - Regulatory Integrative Comparative Physiology*, 57(5):R1143, 2005.

[23] D. J. Marsh, O. V. Sosnovtseva, E. Mosekilde, and N.-H. Holstein-Rathlou. Vascular coupling induces synchronization, quasiperiodicity, and chaos in a nephron tree. *Chaos*, 17(1):15114–1–10, 2007.

[24] D. J. Marsh, I. Toma, O. V. Sosnovtseva, J. Peti-Peterdi, and N.-H. Holstein-Rathlou. Electrotonic vascular signal conduction and nephron synchronization. *Am.J.Physiol.Renal.Physiol*, 296:F751–F761, 2009.

[25] R. J. Paul. *Physiology in Gastrointestinal Tract*, chapter Smooth muscle mechanochemical energy conversion relations between metabolism and contractility, pages 269–288. Raven, NY, 1981.

[26] D. Postnov, S. K. Han, and H. Kook. Synchronization of diffusively coupled oscillators near the homoclinic bifurcation. *Physical Review E*, 60(3):2799–2807, 1999.

[27] D. E. Postnov, A. G. Balanov, N. B. Janson, and E. Mosekilde. Homoclinic bifurcation as a mechanism of chaotic phase synchronization. *Physical Review Letters*, 83(10):1942–1945, 1999.

[28] J. Rasmussen, E. Mosekilde, and C. Reick. Bifurcations in two coupled Rössler systems. *Mathematics and Computers in Simulation*, 40(3-4):247–270, 1996.

[29] O.E. Rössler. An equation for continuous chaos. *Physics Letters A*, 57(5):397–398, 1976.

[30] F. Takens. Detecting strange attractors in turbulence. *Lecture Notes in Mathematics*, pages 366–381, 1981.

[31] K-P Yip, N H H Rathlou, and D J Marsh. Chaos in blood flow control in genetic and renovascular hypertensive rats. *American Journal of Physiology*, 261(3 PART 2):F400–F408, 1991.

[32] Zh. T. Zhusubaliyev and E. Mosekilde. Formation and destruction of multilayered tori in coupled map systems. *Chaos - Woodbury*, 18(3):37124, 2008.

Note: In this introductory text, only the most important references has been included. Please, note the more complete reference lists in the publications and manuscripts that follow.

Manuscript M1:

Bifurcation structure of the C-type period-doubling transition

---

Submitted to *Physica D*.

Bifurcation structure of the C-type period-doubling transition

Jakob L. Laugesen

Department of Physics,
The Technical University of Denmark, 2800 Lyngby, Denmark

Erik Mosekilde*

Department of Physics,
The Technical University of Denmark, 2800 Lyngby, Denmark

Zhanybai T. Zhusubaliyev*

Kursk State Technical University, Department of Computer Science
50 Years of October Str., 94, Kursk 305040, Russia

Abstract

The period-doubling transition to chaos along the edge of an Arnold tongue is known to display unusual organization and scaling behavior [Kuznetsov *et al.*, 2005]. It is also known that forced period-doubling systems may be associated with the appearance of so-called period-doubled tori [Arneodo *et al.*, 1983]. Using the Rössler system as an example, we present a detailed analysis of the bifurcation structure associated the forcing of a three-dimensional period-doubling system. We explain how this structure is related to the recently discovered phenomenon of multi-layered tori and discuss a sequence of bifurcations that transform a resonance torus into a period-2 ergodic torus. A similar bifurcation structure has recently been observed in a biologically relevant model of kidney blood flow regulation in response to arterial pressure fluctuations.

Keywords: Forced period-doubling systems, Bifurcation structure, Transverse period-doubling cascades, Multi-layered tori, Torus doubling bifurcations, Multi-dimensional dynamics
PACS: 05.45.-a, 05.45.Gg, 05.45.Pq

1. Introduction

It is well-known that deviations from classical Feigenbaum scaling are observed in one-dimensional maps that display a non-quadratic extremum [1]. A related situation arises if an essentially one-dimensional system operates in the neighborhood of a point in parameter space where two quadratic extrema are mapped one into the

*Corresponding author
Email addresses: Laugesen@fysik.dtu.dk (Jakob L. Laugesen), Erik.Mosekilde@fysik.dtu.dk (Erik Mosekilde), zhanybai@hotmail.com (Zhanybai T. Zhusubaliyev)

other by a so-called doubly superstable orbit [2]. This situation, which occurs for instance for the classic sine-circle map [3], underlies the formation of the characteristic crossroad (or swallow tail) structure that has been used to describe the substructure of the resonance tongues for a variety of different low dimensional systems [4, 5, 6].

Deviations from classical Feigenbaum scaling also occur in a number of situations that involve specific symmetries [7]. However, a more generic and apparently less studied phenomenon, denoted cyclic (or C-type) criticality [7, 8], takes place when a period-doubling transition to chaos unfolds along the edge of a resonance tongue. The scaling relations that apply to this situation have been worked out by Kuznetsov *et al.* [8, 9] who considered both a periodically forced Rössler system and a two-dimensional map constructed originally to illustrate the different ways in which a periodic orbit can be destabilized. However, the associated bifurcation structure, particularly the formation of multi-layered resonance tori through cascades of period-doubling bifurcations of the stable and unstable resonance cycles transversally to the torus manifold, was not considered. A similar structure, involving interconnected cascades of period-doubling bifurcations for symmetric and antisymmetric orbits, has been described for two coupled Rössler systems [10]. However, again, the observed bifurcations were not related to the formation of multi-layered resonance tori.

The purpose of the present paper is to develop a more complete description of the bifurcation structure associated with the cyclic (or C-type) period-doubling transition in multi-dimensional, time-continuous systems. We first demonstrate how the $1:1$ resonant node and saddle cycles in the periodically forced Rössler system undergo interconnected cascades of period-doubling bifurcations. Near the edges of the Arnold tongue, node and saddle cycles with the same periodicity approach one another, and at the very edge their period-doubling bifurcations occur simultaneously. Away from the tongue edges, however, the node solution in the forced Rössler system tends to bifurcate first, i.e. for lower values of the parameter that controls the nonlinearity in the system.

Each pair of period-doubling bifurcations gives rise to a new set of saddle-node bifurcation curves along the sides of the resonance tongue. As the period-doubling cascade unfolds, the edges of the resonance tongue thus accumulate more and more almost parallel saddle-node bifurcation curves, each defining the boundaries for the resonance zone at a particular level of the period-doubling cascade. For low values of the forcing amplitude, the new saddle-node bifurcation curves are generally formed away from the existing edges of the tongue, and additional bifurcations are required to complete the boundary of the resonance zone. This involves the interplay of a couple of local and global bifurcations that transform a multi-layered resonance torus into a stable period-doubled ergodic torus. We have recently observed that a similar bifurcation structure arises in a biologically relevant model of the kidney blood flow regulation in response to variations in the arterial pressure [11, 12] and suggest that this structure is generic for a class of multi-dimensional, forced period-doubling systems.

Outside the resonance region, the ergodic period-2 torus disappears in an inverse torus doubling bifurcation, i.e., a transition in which the period-2 torus transforms into an ordinary (period-1) ergodic torus. For higher values of the forcing amplitude, the gap between the saddle-node bifurcation curves at the edge of the resonance

domain tends to disappear, and the transition from multi-layered resonance torus to period-doubled ergodic torus now occurs through the saddle-node bifurcation along the edge of the resonance tongue [13].

Torus doubling was first described by Arneodo *et al.* [14] and by by Kaneko [15] who examined the phenomenon both for multi-dimensional maps and for time-continuous systems. These authors observed, for instance, how a finite sequence of torus doubling bifurcations can lead to chaotic dynamics. More recently, Sekikawa *et al.* [16] have demonstrated the transition to chaos through a series of successive torus doubling bifurcations in an electronic circuit and Sekikawa *et al.* [17] have shown how coupled logistic or sine-circle maps can produce a sequence of torus-doubling bifurcations. To our knowledge, however, a more detailed explanation of the phenomenon of torus doubling has never been provided. Kuznetsov *et al.* [18] have determined the scaling relations at the terminal points of the torus doubling bifurcation curve where the regimes of torus and doubled torus dynamics meet with regions of strange-non-chaotic behavior and chaos, and Kuznetsov [19] has examined the effects of noise on the dynamics of the torus doubling termination point.

The present paper provides a detailed analysis of the transitions that occur near the edge of the resonance zone. We show how the recently discovered phenomenon of multi-layered resonance tori is linked with the phenomenon of ergodic torus doubling and demonstrate how a multi-layered resonance torus can be transformed into a period-doubled ergodic torus through a sequence of bifurcations.

We have previously described the formation of multi-layered closed invariant curves (referred to as tori) both for a number of two-dimensional maps [20, 21] and for a model of a pulse modulated power electronic DC/DC converter [22]. For a system of two symmetrically coupled logistic maps, for instance, we have demonstrated how a three-layered torus can arise from an ordinary (i.e., single-layered) resonance torus either through a period-doubling or a pitchfork bifurcation of the saddle cycle transverse to the torus manifold. The phenomena considered in the present paper are somewhat different in that they involve interconnected cascades of transverse period-doubling bifurcations of both the resonant node and saddle cycles and thus produce tori with a continuously increasing number of layers.

2. Main bifurcation structure for the periodically forced Rössler system

Let us consider the periodically forced Rössler system:

$$\dot{x} = -y - z + A\sin(\omega t); \quad \dot{y} = x + ay; \qquad (1)$$
$$\dot{z} = b + z(x - c),$$

where x, y and z are the dynamical variables of the Rössler oscillator and $A\sin(\omega t)$ represents the externally applied forcing. The parameters a and b and the forcing amplitude A are assumed to remain constant and attain the values $a = 0.2$, $b = 0.2$ and $A = 0.1$. The nonlinearity parameter c and the forcing frequency ω are used as bifurcation parameters, and a few calculations will also be performed with other values of the forcing amplitude. The unforced Rössler system ($A = 0$) undergoes a Hopf bifurcation at $c = 0.4$ and for increasing values of c, the system hereafter exhibits a Feigenbaum cascade of period-doubling bifurcations to chaos. On the

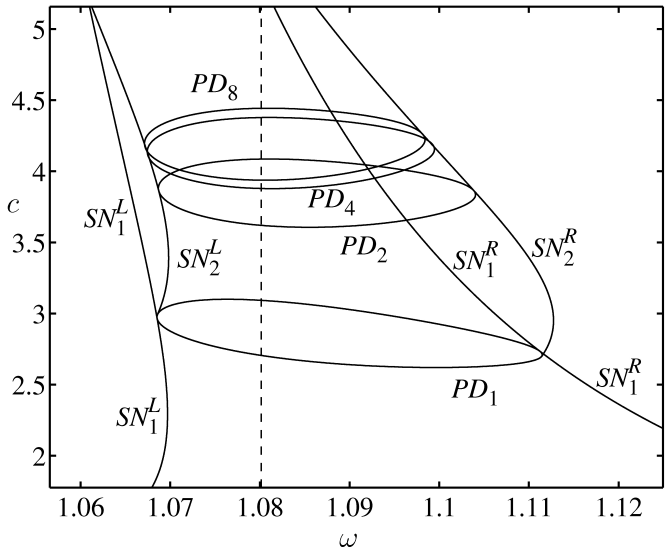

Figure 1: Overview of the main bifurcation curves associated with the first four period-doubling bifurcations in the forced Rössler system. At the edges of the tongue, defined by the saddle-node bifurcation curves, period doubling of corresponding node and saddle cycles occurs simultaneously. Away from the zone boundary, period doubling of the stable cycles occurs before period doubling of the saddle cycles. Each pair of period-doubling bifurcations generates a new pair of saddle-node bifurcation curves to delineate the resonance zone for the cycles at the next level in the cascade (for detail see Fig. 3).

other hand, as long as we consider the regime of periodic oscillations, the forced system might be expected to display quasiperiodic dynamics on a two-dimensional torus, interrupted by an infinite set of resonance zones in which the internal dynamics of the Rössler system synchronizes with the external forcing signal. The purpose of the present section is to examine the main structures arising from the interplay between these two processes in multi-dimensional systems. Details of this structure and the involved bifurcations will be described in the following sections.

Figure 1 provides an overview of the main bifurcations associated with the first four period-doubling transitions. Below the first period-doubling curve PD_1, the $1:1$ resonance zone is delineated to the left and right by the saddle-node bifurcation curves SN_1^L and SN_1^R, respectively. In this area, the system displays a stable node and a saddle solution, both situated on the closed invariant curve that represents our two-dimensional torus. The period-doubling curve PD_1 has two branches. Along the lower branch, the $1:1$ node solution undergoes its first period-doubling bifurcation, while the corresponding saddle solution doubles its period along the upper branch. At the edge of the tongue, the two solutions coincide and the system displays both an eigenvalue (Floquet multiplier) of $+1$ and an eigenvalue of -1. The two eigenvalues correspond to different directions in phase space. Hence, we conclude that the period doubling bifurcation involves a direction transverse to the invariant curve.

A pair of new saddle-node bifurcation curves, SN_2^L and SN_2^R, emanate from the period-doubling curve close to the two edges of the tongue. They delineate the synchronization region for the stable and unstable $2:2$ solutions and are, therefore, tangents to the next period-doubling curve PD_2. Like PD_1, PD_2 has two branches such that the stable $2:2$ solution undergoes a second period doubling along the lower

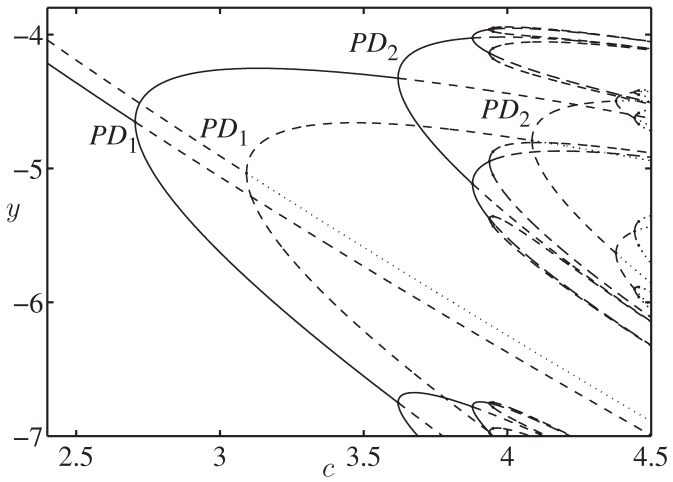

Figure 2: Interconnected period-doubling cascades in the 1:1 resonance tongue for $\omega = 1.08$. Full curves represent stable node solutions, dashed curves are saddle solutions and dotted curves are doubly unstable saddle solutions. The period-doubling cascade for the stable node cycles accumulates in a transition to chaos approximately at $c_\infty = 3.95381$. Note that these period-doubling bifurcations take place in a direction transverse to the original torus manifold.

branch and the saddle $2:2$ solution period doubles along the upper branch. These period doublings again take place in a direction transverse to the closed invariant curve, and again a pair of new saddle-node bifurcation curves is born to delineate the synchronization range for the $4:4$ solutions (see Fig. 3).

As the value of parameter c increases, the same process is found to repeat itself until the system undergoes a transition to chaos. Close to the tongue edges, corresponding node and saddle solutions period double almost simultaneously. However, as we move deeper into the resonance zone, the period-doubling of the node cycles occurs earlier and earlier in comparison with the period doubling of the corresponding saddle cycles. For this reason, the accumulation points for the two cascades are different, and the structure of the multi-layered tori produced in the transition will depend on the forcing frequency ω [13]. For $\omega = 1.08$, the two interconnected period-doubling cascades are illustrated in Fig. 2. Starting with the first period-doubling bifurcation of the $1:1$ node cycle near $c = 2.70551$, the cascade of period-doubling bifurcations for the node cycles accumulates approximately at $c_\infty = 3.95381$.

Figure 3 provides a blow-up of the bifurcation structure along the left tongue edge. The two-dimensional bifurcation diagram to the left in the figure presents the actual structure, and the sketch to the right shows a somewhat distorted version of the same structure, drawn with the intention of clarifying the formation of new saddle node bifurcation curves in connection with each pair of period-doubling bifurcations. Note how the new saddle-node bifurcation curves are born in points of the period-doubling curves slightly away from the existing tongue edge, how they proceed in a manner that is not strictly parallel to this edge, and how they become tangent to the next period-doubling bifurcation curve. As a result of this process, an increasing number of nearly parallel saddle-node bifurcation curves accumulate along the tongue edges, each curve representing the border of the resonance zone for a specific pair of node and saddle cycles in the bifurcation cascade. This structure is

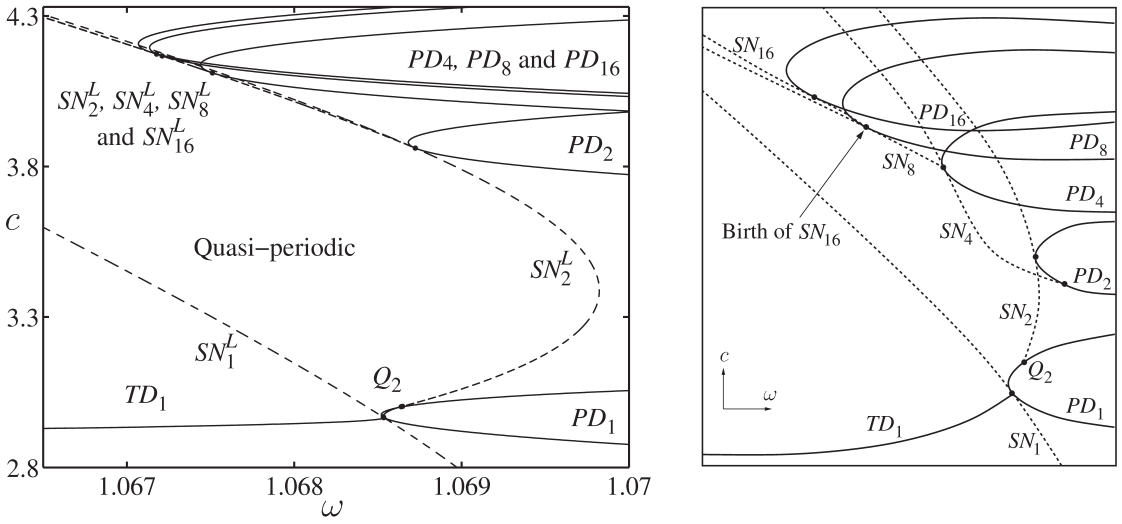

Figure 3: Left: Main structure of the first five period-doubling bifurcations close to the left edge of the $1:1$ resonance tongue. The figure illustrates how new saddle-node bifurcation curves are born close to the points where the period-doubling curves are tangent to the existing tongue edges. Right: Sketch of the bifurcation structure showing how the newly born saddle-node bifurcation curves define the edges of the resonance tongue until the next period-doubling occurs. The curve TD_1 represents the torus doubling bifurcation. Superscripts L on the saddle-node curves have been omitted.

obviously required to avoid that any of the cycles generated in the period-doubling cascades escapes the resonance domain.

3. Details of the bifurcation structure for the forced Rössler system

Let us consider the above bifurcation structure in a little more detail, focusing particularly on the formation of new saddle-node bifurcation curves in connection with each pair of period-doubling bifurcations. Figure 3 shows how the saddle-node bifurcation curve SN_2^L emanates from a point Q_2 to the right of the point where PD_1 is tangent to the tongue edge. This seems to leave a hole in the boundary of the resonance zone. However, as illustrated in the blow-up of the region around the formation of SN_2^L shown in Fig. 4, additional local and global bifurcations are in place to ensure that the $2:2$ cycles do not escape the resonance area through the gap between the two saddle-node bifurcation curves. Inspecting this figure, we immediately locate the two branches of the period-doubling curve PD_1, the saddle-node bifurcation curves SN_1^L and SN_2^L , and the point Q_2 where SN_2^L is born. At T_2 the $2:2$ stable node cycle produced at the lower branch of the period-doubling curve PD_1 (and now transformed into a stable focus) loses its stability in a subcritical torus bifurcation. G_2 represents a sequence of closely situated local and global bifurcations that give birth to the large period-2 ergodic torus observed in Fig. 5, and TD_1 represents the torus doubling curve at which the period-2 torus is transformed into an ordinary (period-1) ergodic torus that exists outside the resonance tongue and below TD_1. The sequence of bifurcations in which the period-2 torus is born will be discussed in significant detail in Sec. 4.

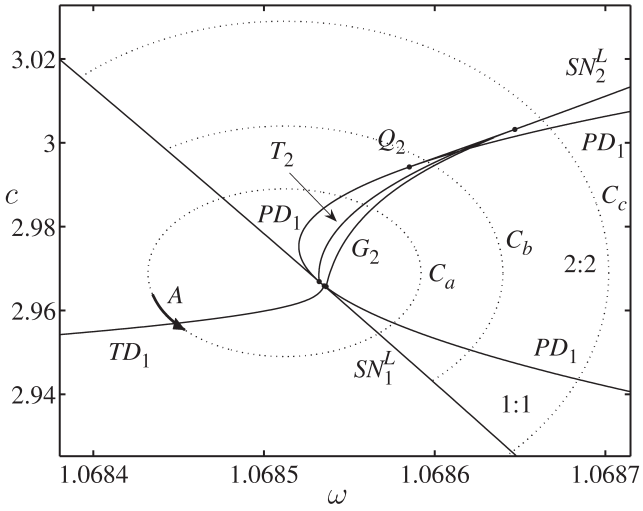

Figure 4: Magnification of part of the bifurcation diagram near the edge of the resonance tongue. PD_1 is the period-doubling bifurcation curve and Q_2 denotes the point in which the saddle-node bifurcation curve SN_2^L starts. G_2 represents the sequence of bifurcations that give rise to the large period-2 ergodic torus seen in Fig. 5, and TD_1 is the torus doubling bifurcation in which this torus is transformed into an ordinary period-1 ergodic torus. Note that some of the substructure disappears when the forcing amplitude becomes sufficiently large.

In the presence of these additional bifurcations, the brute force bifurcation diagram calculated along the elliptic curve denoted C_a in Fig. 4 takes the form illustrated in Fig. 5. In both ends of this diagram we observe the ergodic period 1 torus that exists below TD_1 and to the left of the resonance zone. As we follow the transitions from left to right in the intermediate range we first meet the saddle node bifurcation SN_1^L at the edge of the resonance tongue where the $1:1$ node cycle is born. This is followed by the period-doubling bifurcation in which the $1:1$ node is transformed into a $1:1$ saddle cycle while producing a stable $2:2$ cycle transverse to the torus surface. Hereafter follows the sequence G_2 of closely situated local and global bifurcations that give birth to both the large period-2 torus that dominates most of the right hand side of the diagram and to an unstable two-branch torus around the 2:2 focus cycle. The unstable two-branch torus again disappears in the subcritical Hopf bifurcation T_2 while the large period-2 torus continues to exist until it undergoes the aforementioned reverse torus doubling bifurcation at the point TD_1. As shown in Fig. 4, this last transition takes place outside of the resonance tongue.

The sketches in Fig. 6 give a clearer account of the structure of local bifurcations observed in the region around the birth of the saddle node bifurcation curve SN_2^L. The curves along which these bifurcation diagrams are thought to be drawn are indicated in Fig. 4 by the letters C_a, C_b, and C_c. Starting from the bottom, panel (a) first shows the saddle-node bifurcation through which the $1:1$ node and saddle cycles are born as the system enters the resonance domain. Hereafter follows the period-doubling bifurcation PD_1 on the $1:1$ node. At T_2, the $2:2$ cycle generated in this bifurcation (now a stable focus) undergoes a subcritical torus bifurcation and turns into an unstable focus. In accordance with the brute force diagram in Fig. 5,

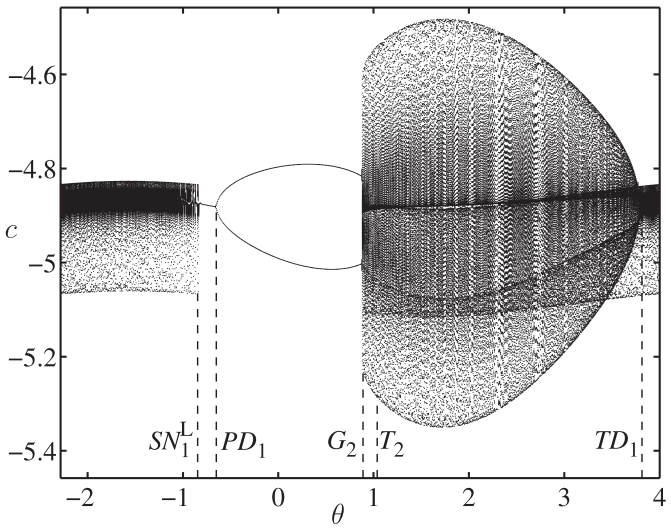

Figure 5: Brute force bifurcation diagram calculated along the elliptic curve C_a in Fig. 4. θ is a measure of the position along C_a with 0 (and 2π) representing the outmost right point and π the outmost left point. For increasing values of θ the diagram first shows the saddle-node bifurcation SN_1^L that occurs when the system enters the $1:1$ resonance zone. Hereafter follows the period-doubling PD_1 that produces the stable $2:2$ resonant node and the subcritical torus bifurcation T_2 in which the $2:2$ cycle loses its stability. G_2 represents the sequence of bifurcations that give birth to the large ergodic period-2 torus and TD_1 denotes the torus doubling bifurcation in which this torus transforms into an ordinary period-1 ergodic torus.

the unstable two-branch torus produced in this bifurcation disappears in a global bifurcation close to the point G_2. As we continue the scan, the unstable $2:2$ focus cycle (now a doubly unstable saddle) undergoes a reverse period doubling bifurcation in PD_1 while the $1:1$ saddle destabilizes into a doubly unstable cycle. This latter cycle finally disappears in a saddle node bifurcation at the tongue edge SN_1^L.

If we denote the period-doubling bifurcation that ends the life of the $2:2$ cycle in panel (a) as subcritical, the corresponding period-doubling bifurcation in panel (b) has become supercritical as the saddle node bifurcation curve SN_2^L has transformed the doubly unstable $2:2$ saddle into a $2:2$ saddle cycle with a single unstable direction. In this way the torus bifurcation T_2 serves to degrade the stability of the stable $2:2$ cycle so that it can annihilate with the $2:2$ saddle cycle at the upper branch of the period doubling curve. Finally, in panel (c) the torus bifurcation on the $2:2$ cycle no longer occurs, and the SN_2^L saddle node bifurcation has overtaken the full role of delineating the edge of the resonance tongue for the $2:2$ cycles.

In order to provide a clear impression of the structure of the period-2 torus and of the torus doubling bifurcation that occurs along TD_1, Fig. 7 presents a series of Poincaré sections of the ergodic torus observed in the one-dimensional brute force bifurcation diagram. As defined in the caption to Fig. 5, the parameter θ is the angle along the curve C_a in Fig. 4. For $\theta = 3.8$, the Poincaré section shows an ordinary (i.e. period-1) ergodic torus. Note, however, that there is an uneven distribution of points along the periphery, indicating a 'hesitation' of the system near the top of the section. This is the well-known sign that the system is approaching a resonance zone, in this case the $1:1$ resonance.

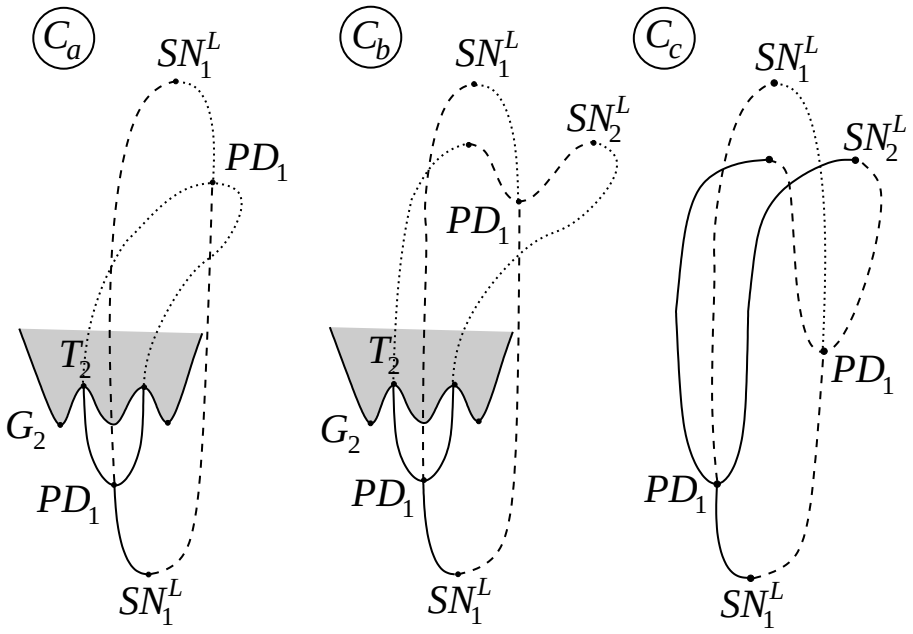

Figure 6: Bifurcation diagrams drawn along parts of the curves C_a, C_b, and C_c in Fig. 4 and extended in both ends to the saddle-node bifurcation curve SN_1^L. Note how the $2:2$ cycles in all cases are captured before they can escape from the resonance zone. Full lines represent stable node or focus solutions, dashed lines saddle solutions, and dotted lines doubly unstable node or unstable focus solutions. The transformations that occur at the point G_2 will be discussed in detail in Sec. 4.

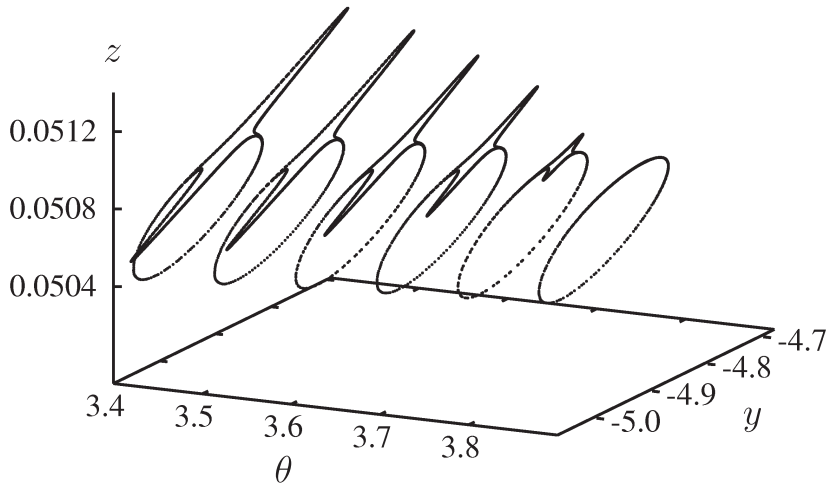

Figure 7: Illustration of the transition that occurs as the forced Rössler system crosses the torus doubling bifurcation curve TD_1 in the direction indicated by the arrow A in Fig. 4. The figure presents a series of Poincaré sections of the ergodic torus for different positions along the curve C_a. Compare with the bifurcation diagram in Fig. 5.

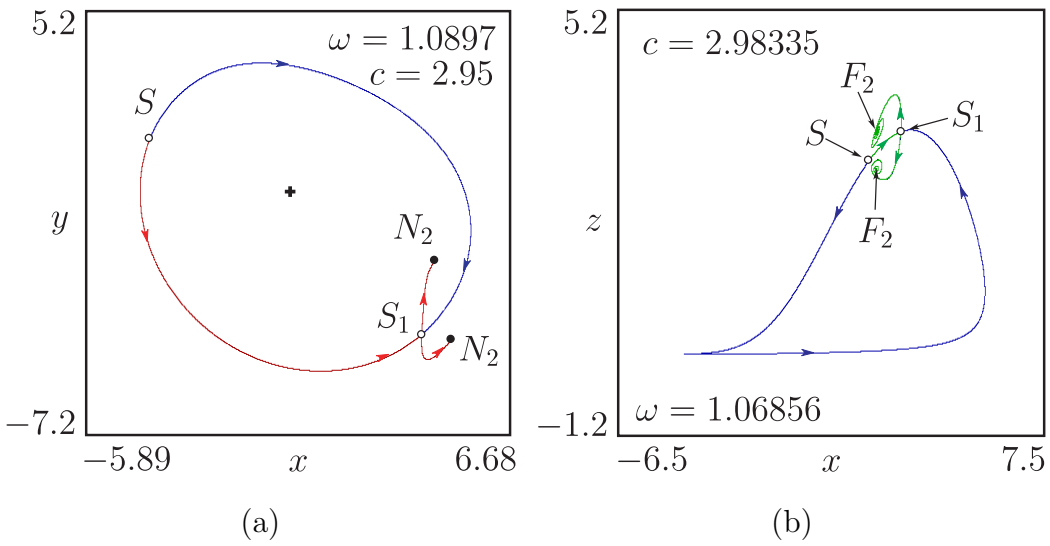

Figure 8: (a) Phase portrait after the period-doubling bifurcation transversal to the $1:1$ resonance torus. (b) The structure after the period-2 node N_2 has turned into a stable period-2 focus F_2. Note that two different projections have been used to draw these figures.

As θ is reduced one can observe how the invariant curve starts to split into two different windings, as the quasiperiodic oscillator alternatively chooses one route over the other. This is another indication of the fact that the resonance mode from which the torus originates has undergone a period-doubling transition in the direction transverse to the periphery of the closed invariant curve. As θ is further reduced, the separation between the two windings is seen to continue to grow and for larger values of the parameter c, one can observe how the two windings of the period-2 torus move completely apart.

4. From 1 : 1 resonance torus to ergodic period-2 torus

After the above discussion of the main bifurcation structures in the periodically forced Rössler oscillator (1) let us turn the attention towards the processes by which the $1:1$ resonance torus is transformed into a period-2 ergodic torus.

Let us start in a point in the middle of the resonance tongue in Fig. 1 and well below the period-doubling curve PD_1. Here, the system displays an ordinary resonance torus with a stable $1:1$ node and corresponding saddle cycle. As the system crosses the lower branch of the bifurcation curve PD_1, the $1:1$ node undergoes a period-doubling bifurcation. As illustrated by the phase portrait in Fig. 8(a), this period-doubling takes place in a direction transverse to the torus manifold. This implies that whereas the original saddle cycle S is stable transversely to the torus manifold and unstable along this manifold, the saddle S_1, arising in the period-doubling bifurcation is stable in the direction along the torus manifold and unstable in the transverse direction. N_2 denotes the points of the $2:2$ resonance node.

As we more upwards in the resonance tongue and closer to the left edge, the two saddle cycles approach one another. At the same time, the $2:2$ node turns into a stable $2:2$ focus cycle as two of its eigenvalues become complex conjugate. This situation is illustrated in Fig. 8(b) which also shows how the $2:2$ focus cycle moves

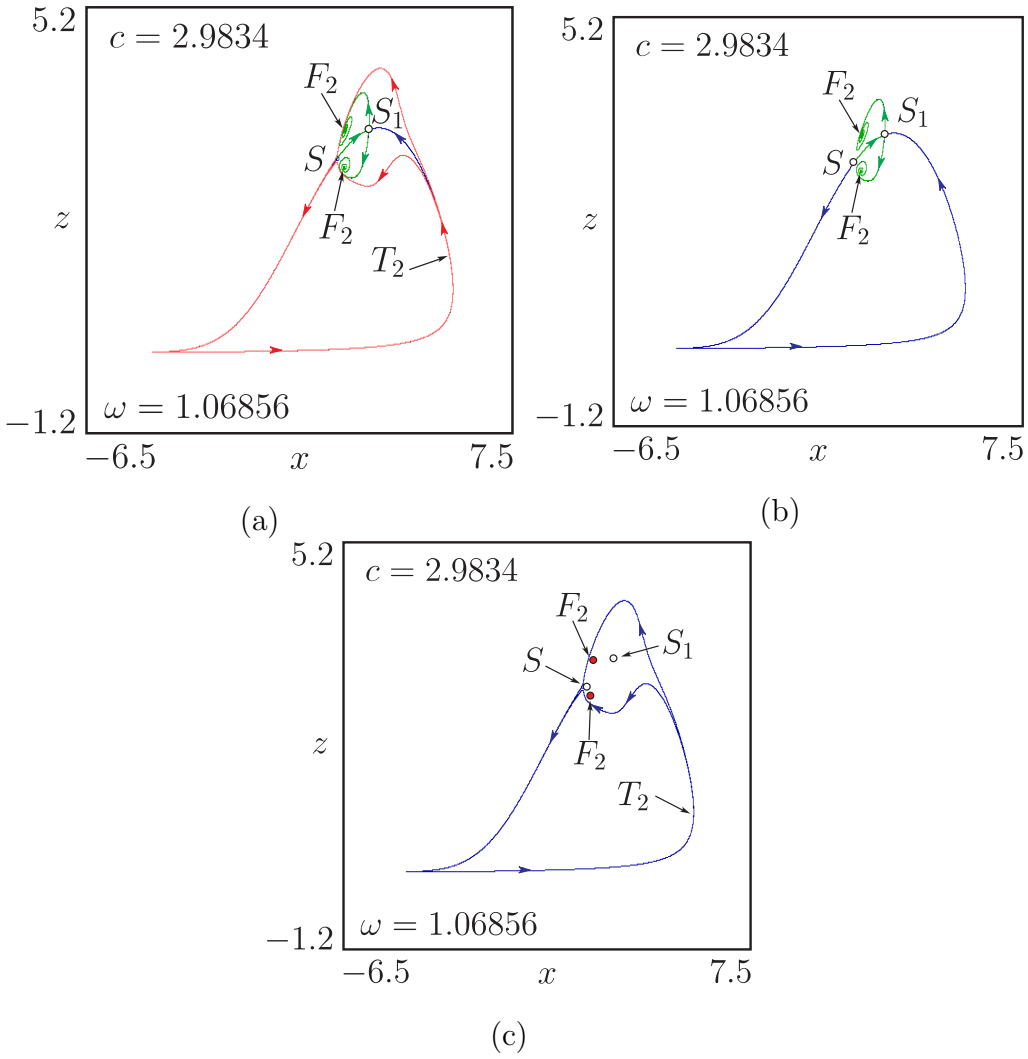

Figure 9: (a) Phase portrait after the torus fold bifurcation that occurs when the system crosses the curve G_2. In this bifurcation a stable period-2 ergodic torus T_2 appears together with an unstable period-2 torus of a similar shape. (b) resonance torus with the stable period-2 focus cycle F_2. (c) period-2 ergodic torus. The stable period-2 ergodic torus T_2 now coexists with the stable period-2 cycle F_2. The basins of attractions of these states are separated by the repelling period-2 torus. All figures are drawn for the same parameters.

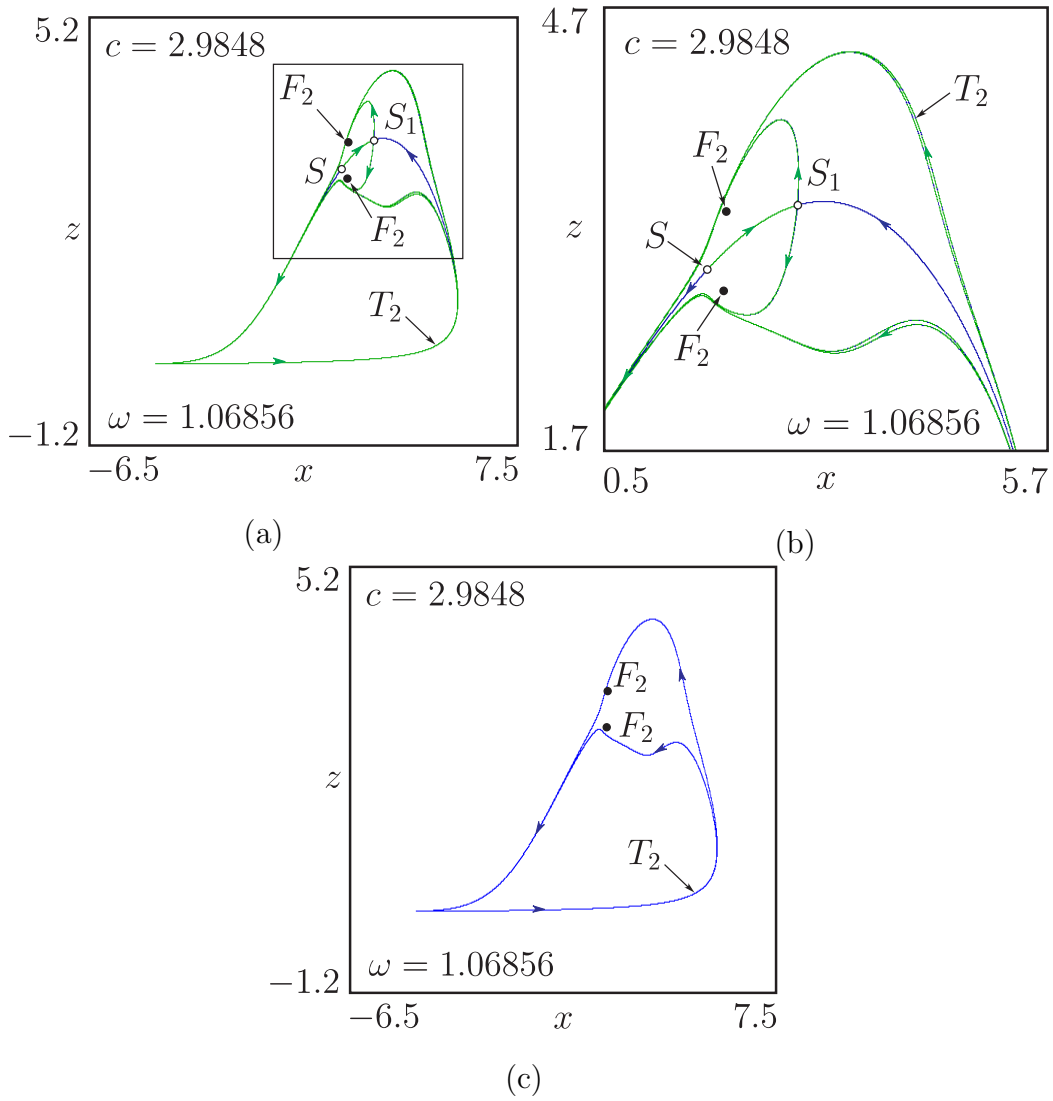

Figure 10: Phase portrait after the heteroclinic bifurcation. (a) Existing structures. The focus cycle F_2 is still stable, but is now isolated from the saddle cycles by a double-branched unstable torus. (b) Magnified part of the phase portrait that is outlined by the rectangle in (a). (c) Ergodic period-2 torus T_2. The curves that follow T_2 closely are the unstable manifolds of the saddle cycles S and S_1.

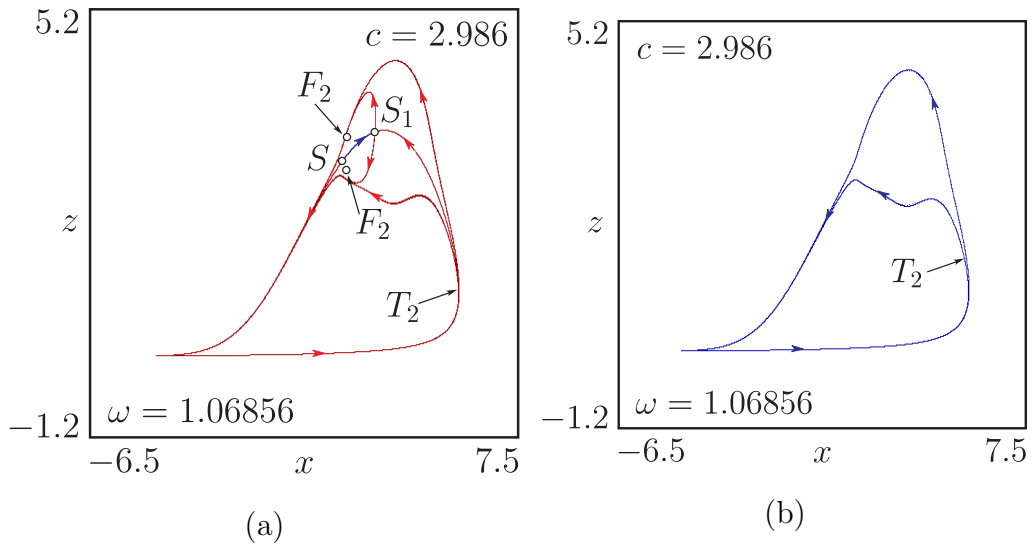

Figure 11: Situation after the period-2 focus F_2 has lost its stability in the subcritical torus bifurcation. (a) Existing structures. F_2 is now a repelling focus period-2 cycle. (b) Ergodic period-2 torus. This torus is the only remaining attracting state.

towards the saddle cycle S. Note that two different projections have been used to illustrate the situations in (a) and (b).

When the system crosses the curve G_2 for increasing values of the nonlinearity parameter c, a stable period-2 ergodic torus arises together with a repelling period-2 torus in a torus fold bifurcation. As illustrated in Fig. 9, both the $1:1$ resonance torus and the stable period-2 focus cycle continue to exist. Figure 9(b) shows the structure of the $1:1$ resonance torus together with the two saddle cycles S and S_1 and with the stable period-2 focus cycle F_2. Figure 9(c) illustrates the stable period-2 ergodic torus, and Fig. 9(a) shows a superposition of (b) and (c) to illustrate the overall structure. The unstable period-2 ergodic torus produced in the torus fold bifurcation (but not shown in the figure) delineates the basin boundary for the coexisting attracting states: F_2 and T_2.

With further increase of c, one can observe a couple of global bifurcations that lead to the disappearance of the unstable period-2 ergodic torus and to the formation of a two-branched unstable torus around the stable focus cycle F_2. In this way the focus cycle is isolated from the saddle cycles S and S_1, and the unstable two-branched torus becomes the basin boundary between the regions of attraction to the focus cycle F_2 and to the ergodic period-2 torus T_2. This situation is illustrated in Figs. 10(a) and (b). We note how the unstable manifold from the saddle cycle S_1 no longer connects to the period-2 focus cycle F_2.

Finally, with further increase c, the period-2 focus cycle F_2 loses its stability in a subcritical Hopf bifurcation. This is illustrated in Fig. 11. Figure 11(a) shows the position of the $1:1$ and $2:2$ resonance cycles. However, none of these cycles an attracting, and the ergodic period-2 torus shown in (b) is the only remaining attracting structure.

5. Bifurcation structure in the period-3 window

Let us complete our study of the forced Rössler system by demonstrating that similar bifurcation phenomena take place in the periodic windows that exist in the chaotic regime. Figure 12 shows the main bifurcation structure of the period-3 window. Here, SN_3^B denotes the saddle-node bifurcation in which the $3:3$ resonant node and saddle cycles are born. This curve continues up along the two sides of the resonance tongue, now denoted SN_3^L and SN_3^R, respectively. The closed curve PD_3 represents the first period-doubling bifurcation. The resonant $3:3$ node cycle period doubles along the lower branch of this curve, and the $3:3$ saddle cycle doubles its period along the upper branch. Similarly, the closed curve PD_6 represents the second period doubling with the node cycle period doubling at the lower branch and the saddle cycle at the upper branch. With its pronounced cusp structure, the bifurcation curve SN_3^C represents a couple of saddle-node bifurcations in which the $3:3$ saddle cycle generated in the period doubling bifurcation PD_3 first loses and subsequently regains stability in a secondary direction. Finally, T_3 is a torus bifurcation curve that serves a purpose similar to that of the torus bifurcation curve T_2 in Fig. 4. This curve closes a hole in the edge of the resonance tongue between SN_3^L and the saddle node bifurcation curve that delineates the sides of the resonance zone for the $6:6$ cycles.

In close accordance with the bifurcation structure observed for the $1:1$ resonance regime, examination of the bifurcation structure in the $3:3$ region confirms that:

(i) The period-doubling cascades for the node and saddle solutions are interconnected. At the edge of the synchronization tongue, the two bifurcations are simultaneous, but away from the tongue edge the node solution bifurcates before the saddle solution.

(ii) Each pair of period-doubling bifurcations generates a new pair of saddle node bifurcations that define the edges of the resonance zone at the next level in the cascade.

(iii) Additional torus and global bifurcations serve to close the gap between the new and the previous boarders of the resonance zone.

6. Conclusions

Periodically forced Rössler systems of the form (1) have previously been examined by a large number of authors [23, 24], mostly with the aim of studying the synchronization of the internally generated chaotic dynamics by the external periodic forcing. In the chaotic regime, the power spectrum of the Rössler oscillator displays a clearly distinguishable maximum around an angular frequency of 1.0 and, depending on the parameter values considered, the external forcing will lock the internal dynamics into a $1:1$ ratio over a smaller or larger interval of ω. Vadivasova *et al.* [25] have provided a relatively detailed chart of the distribution of stable modes in the two-dimensional parameter plane around the $1:1$ resonance tongue. This diagram clearly shows the unusual structure of period-doubling bifurcations that emanate directly from the edges of the resonance tongue. This distinguishes the structure from the commonly observed swallow tail structure that describes the substructure of the resonance tongues for low-dimensional systems [5]. Vadivasova

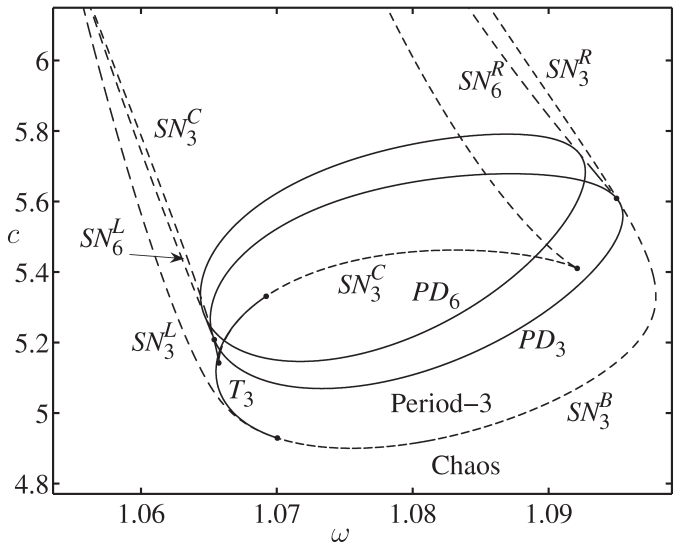

Figure 12: Main bifurcation structure in the period-3 window. The lower saddle-node bifurcation curve marks the onset of the period-3 resonance solutions. For increasing values of the nonlinearity parameter c, the same saddle-node curve extends up along both tongue edges. PD_3 and PD_6 represent the first and second period doubling with the node solution bifurcating at the lower branch and the saddle solution at the upper branch.

et al. [25] also delineated the regions of existence for a couple of period doubled ergodic tori. However, the unusual period-doubling structure was not examined in detail.

The swallow tail structure involves a complex interplay between period-doubling and saddle-node bifurcations. However, the presence of a superstable $1:1$ cycle that extends all the way to infinity along the tongue edges [5] ensures that none of these bifurcations can connect to the edges of the resonance zone. The one-dimensional sine-circle map [3], which explains the organization of the swallow tail structure, only deals with the phase (and periodicity) of the resonance modes. Hence it follows that the period-doubling bifurcations in the swallow tail structure take place along the invariant closed curve described by the map and that no bifurcation can occur in the direction transverse to this curve. Moreover, a saddle cycle on the closed invariant curve cannot undergo a period-doubling bifurcation.

Using the periodically forced Rössler system as an example the present paper reported on the results of a detailed study of the bifurcation phenomena that can arise in multi-dimensional systems through the interaction of a period-doubling process with the mechanisms of synchronization. We showed how this interaction can give rise to interconnected cascades of period-doubling bifurcations for the node and saddle cycles on the original $1:1$ resonance torus. By contrast to the phenomena described by the swallow tail structure [4, 5], however, these bifurcations took place in a direction transversal to the original resonance torus, hence creating resonance tori with an increasing number of layers of interconnected manifolds. Multi-layered resonance tori of this type have recently been observed in variety of map systems [20, 21], but have not previously been described for time-continuous systems.

Each pair of period-doubling bifurcations of corresponding node and saddle cy-

cles was found to produce a new set of saddle-node bifurcation curves to delineate the resonance tongues. For high forcing amplitudes, these new saddle-node bifurcation curves initiate from points at the existing zone edge. However, for lower values of the forcing amplitude a gap tends to arise between the existing edge of the resonance zone and the new saddle-node bifurcation curves. Hence, a couple of additional bifurcations are called upon to complete the edge of the resonance tongue. These bifurcations include a subcritical Hopf bifurcation in which a period-doubled focus cycle loses its stability. However, the bifurcations also include a heteroclinic bifurcation capable of transforming the structure of the resonance torus into a so-called period-doubled ergodic torus. Period-doubled ergodic tori have been known since the early 1980's [15, 14], but they appear never to have been examined in much detail. The heteroclinic bifurcation we have described represents a general mechanism that can relate multi-layered resonance tori to period-doubled ergodic tori.

In order to examine the generic nature of the observed mechanisms we showed that a similar bifurcation structure arises in the period-3 window that exists in the chaotic regime. In parallel with the present study we have also examined both a two dimensional nonlinear map subjected to a periodic forcing and a model of kidney blood flow regulation. The map system has the advantage of being significantly simpler to handle computationally. The biological model represents an attempt to describe how the individual functional units in the kidney regulate the incoming blood flow to compensate for variations in the arterial blood pressure [11, 12].

Acknowledgments

The work was supported by the EU Life Sciences for Health Program through the BioSim Network of Excellence (Contract No. LSHB-CT-2004-005137).

References

[1] B. Hu, I. I. Satija, A spectrum of universality classes in period doubling and period tripling, Phys. Lett A 98 (1983) 143–146.

[2] S.-J. Chang, M. Wortis, J. A. Wright, Iterative properties of a one-dimensional quartic map: Critical lines and tricritical behavior, Phys. Rev. A 24 (1981) 2669–2684.

[3] V. I. Arnold, Small denominators I. Mappings of the circumference onto itself, AMS Trans. Series 2 46 (1965) 213-284.

[4] J. P. Carcasses, C. Mira, M. Bosch, C. Simo, J. C. Tatjer, Crossroad area-Spring area transition (I) parameter plane representation, Int. J. Bifur. Chaos 1 (1991) 183-196.

[5] L. Glass, R. Perez, Fine structure of phase locking, Phys. Rev. Lett. 48 (1982) 1772–1775.

[6] A. P. Kuznetsov, S. P. Kuznetsov, E. Mosekilde, L. V. Turukina, Two-parameter analysis of the scaling behavior at the onset of chaos: tricritical and pseudo-tricritical points, Physica A 300 (2001) 367–385.

[7] S. P. Kuznetsov, A. P. Kuznetsov, I. R. Sataev, Multiparameter critical situations, universality and scaling in two-dimensional period-doubling maps, J. Stat. Phys. 121 (2005) 697–748.

[8] A. P. Kuznetsov, S. P. Kuznetsov, I.R. Sataev, A variety of period-doubling universality classes in multi-parameter analysis of transition to chaos, Physica D 109 (1997) 91–112.

[9] S. P. Kuznetsov, I. R. Sataev, Universality and scaling for the breakup of phase synchronization at the onset of chaos in a periodically driven Rössler oscillator, Phys. Rev. E 64 (2001) 046214.

[10] J. Rasmussen, E. Mosekilde, C. Reick, Bifurcations in two coupled Rössler systems, Math. Comp. Sim. 40 (1996) 247–270.

[11] M. Barfred, E. Mosekilde, N.-H. Holstein-Rathlou, Bifurcation analysis of nephron pressure and flow regulation, Chaos 6 (1996) 280–287.

[12] N.-H. Holstein-Rathlou, K.-P. Yip, O. V. Sosnovtseva, E. Mosekilde, Synchronization phenomena in nephron-nephron interaction, Chaos 11 (2001) 417–426.

[13] Zh. T. Zhusubaliyev, O.O. Yanochkina, E. Mosekilde, J. L. Laugesen, Formation of multilayered tori through repeated period-doubling, to be submitted for publication.

[14] A. Arneodo, P. H. Coullet, E. A. Spiegel, Cascade of period doublings of tori, Phys. Lett. 94A (1983) 1–6.

[15] K. Kaneko, Doubling of torus, Prog. Theor. Phys. 69 (1983) 1806–1810.

[16] M. Sekikawa, T. Miyoshy, N. Inaba, Successive torus doubling, IEEE Trans. Circuits Systems I 48 (2001) 28–34.

[17] M. Sekikawa, N. Inaba, T. Yoshinaga, T. Tsubouchi, Bifurcation structure of successive torus doubling, Phys. Lett. A 348 (2006) 187–194.

[18] S. P. Kuznetsov, U. Feudel, A. Pikovsky, Renormalization group for scaling at the torus-doubling terminal point, Phys. Rev. E 57 (1998) 1585–1590.

[19] S. P. Kuznetsov, Effect of noise on the dynamics at the torus-doubling terminal point in a quadratic map under quasiperiodic driving, Phys. Rev. E 72 (2005) 026205.

[20] Zh. T. Zhusubaliyev, E. Mosekilde, Multilayered tori in a system of two coupled logistic maps, Phys. Lett. A 373 (2009) 946–951.

[21] Zh. T. Zhusubaliyev, E. Mosekilde, Novel routes to chaos through torus breakdown in non-invertible maps, Physica D 238 (2009) 589–602.

[22] Zh. T. Zhusubaliyev, E. Mosekilde, Birth of bilayered torus and torus breakdown in a piecewise-smooth dynamical system, Phys. Lett. A 351 (2006) 167–174.

[23] M. G. Rosenblum, A. Pikovsky, J. Kurths, Phase Synchronization of Chaotic Oscillators, Phys. Rev. Lett. 76 (1996) 1804–1807.

[24] A. S. Pikovsky, M. G. Rosenblum, G. V. Osipov, J. Kurths, Phase synchronization of chaotic oscillators by external driving, Physica D 104 (1997) 219–238.

[25] T. E. Vadivasova, A. G. Balanov, O. V. Sosnovtseva, D. E. Postnov, E. Mosekilde, Synchronization in driven chaotic systems: Diagnostics and bifurcations, Phys. Lett. A 253 (1999) 66–74.

Publication P1:

From multi-layered resonance tori to period-doubled ergodic tori

---

Published in *Physics Letters A*.

Physics Letters A 374 (2010) 2534–2538

Contents lists available at ScienceDirect

Physics Letters A

www.elsevier.com/locate/pla

From multi-layered resonance tori to period-doubled ergodic tori

Zhanybai T. Zhusubaliyev [a,*], Jakob L. Laugesen [b], Erik Mosekilde [b]

[a] Kursk State Technical University, Department of Computer Science, 50 Years of October Str. 94, Kursk 305040, Russia
[b] Department of Physics, The Technical University of Denmark, 2800 Lyngby, Denmark

ARTICLE INFO

Article history:
Received 29 March 2010
Accepted 8 April 2010
Available online 10 April 2010
Communicated by A.R. Bishop

Keywords:
Forced period-doubling systems
Bifurcation structure
Transverse period-doubling cascades
Multi-layered tori
Torus-doubling bifurcations
Multi-dimensional dynamics

ABSTRACT

The Letter presents a number of new bifurcation structures that can be observed when a multi-dimensional period-doubling system is subjected to a periodic forcing. We show how multi-layered tori arise through transverse period-doubling bifurcations of the resonant saddle and node cycles, and how these multi-layered tori transform into period-doubled ergodic tori through sets of saddle–node bifurcations.

1. Introduction

The periodically forced Rössler system has been investigated by many authors, in recent years often with the aim of studying synchronization of the internally generated chaotic dynamics with the external forcing [1–5]. In the chaotic regime, the power spectrum of the Rössler oscillator displays a clearly distinguishable maximum and, depending on the parameters of the Rössler system and the forcing amplitude, chaotic phase synchronization may be achieved over a smaller or larger range of forcing frequencies.

Vadivasova et al. [6] have obtained a relatively detailed chart of the distribution of stable modes in the two-dimensional parameter plane spanned by the forcing frequency and one of the parameters of the Rössler system. An interesting aspect of this chart is the unusual structure of period-doubling bifurcation curves that are observed to emanate directly from the edges of the resonance tongue. This clearly distinguishes the structure from the classic swallow-tail structure [7,8] that can be used to describe the substructure of the resonance tongues for many low-dimensional systems. Vadivasova et al. [6] also determined a couple of bifurcation curves in which the ergodic torus that exists outside of the resonance tongue doubles its period.

Observing the same unusual bifurcation structure both in a two-dimensional map and in the forced Rössler system, Kuznetsov et al. [9,10] determined the scaling properties that characterize a period-doubling cascade that unfolds along the edge of a resonance tongue (denoted as cyclic or C-type criticality). More recently, Kuznetsov et al. [11] have determined the scaling relations for the terminal points of the torus doubling bifurcation curves for a related problem in which a low-dimensional period-doubling system is driven by quasiperiodic forcing.

The purpose of the present Letter is to examine the bifurcation structure associated with the interaction between the processes of period-doubling and synchronization in greater detail. In particular we show how complex structures of multi-layered resonance tori arise through period-doubling bifurcations of resonant node and saddle cycles in a direction transverse to the torus manifold. We also show how these multi-layered tori transform into period-doubled ergodic tori through a set of saddle–node bifurcations delineating the edge of the synchronization regime.

Torus doubling was first investigated by Arneodo et al. [12] and by Kaneko [13] who described the phenomenon both for three- and four-dimensional maps and for time-continuous systems. More recently, Sekikawa et al. [14] have demonstrated the formation of period-doubled tori in an electronic oscillator system and Postnov et al. [15] have used a double Poincaré-section technique to illustrate torus doubling in a van der Pol oscillator driven by a strong chaotic forcing. However, to our knowledge, a description of how these ergodic tori interact with the resonance structure in the synchronization tongues has not been presented.

We have previously observed the formation of multi-layered tori both for a variety of two-dimensional maps [16,17] and for a model of a pulse modulated power electronic DC/DC con-

* Corresponding author.
E-mail addresses: zhanybai@hotmail.com (Z.T. Zhusubaliyev), Laugesen@fysik.dtu.dk (J.L. Laugesen), Erik.Mosekilde@fysik.dtu.dk (E. Mosekilde).

0375-9601/$ – see front matter
doi:10.1016/j.physleta.2010.04.022

verter [18]. In a recent Letter [19] we have described the transition from double-layered resonance torus to period-doubled ergodic torus through a series of local and global bifurcations that occur at relatively low forcing amplitudes. The present Letter presents a more generic mechanism that involves sets of saddle–node bifurcations.

2. Main bifurcation structure for the periodically forced Rössler system

Let us consider the periodically forced Rössler system:

$$\dot{x} = -y - z + A\sin(\omega t); \qquad \dot{y} = x + ay;$$
$$\dot{z} = b + z(x - c), \tag{1}$$

where x, y and z are the dynamical variables of the Rössler oscillator and $A\sin(\omega t)$ represents the externally applied forcing. The nonlinearity parameter c and the forcing frequency ω are used as bifurcation parameters while the parameters a and b and the forcing amplitude A are kept constant at the values $a = 0.2$, $b = 0.2$ and $A = 0.1$. The unforced Rössler system ($A = 0$) undergoes a Hopf bifurcation at $c = 0.4$ and for increasing values of c, the system hereafter exhibits a Feigenbaum cascade of period-doubling bifurcations to chaos. When an external forcing is applied in the regime of periodic oscillations, the Rössler system displays regions of quasiperiodic dynamics interrupted by an infinite set of resonance zones where the internally generated periodic oscillations synchronize with the external forcing. Our aim is to examine the structures that arise from the interplay between these two processes in multi-dimensional systems.

Fig. 1 provides an overview of the main bifurcations associated with the first four period-doubling transitions. Below the first period-doubling curve PD_1^S, the 1 : 1 resonance zone is delineated to the left and right by the saddle–node bifurcation curves SN_1^L and SN_1^R, respectively. In this area, the system displays a stable node and a saddle solution, both situated on the closed invariant curve that represents the two-dimensional resonance torus. Along the lower curve PD_1^S, the 1 : 1 node solution undergoes its first period-doubling bifurcation, while the corresponding saddle solution doubles its period along the upper curve PD_1^U. At the edge of the tongue, the two solutions merge and, as our calculations show, the system displays both an eigenvalue (Floquet multiplier) of $+1$ and an eigenvalue of -1. The two eigenvalues correspond to different directions in phase space. Hence, we conclude that the period-doubling bifurcation occurs in a direction transverse to the torus manifold.

A pair of new saddle–node bifurcation curves, SN_2^L and SN_2^R, emanate from the period-doubling curve close to the two edges of the tongue. They delineate the synchronization region for the stable and unstable 2 : 2 solutions and are, therefore, tangents to the next period-doubling curve. The stable 2 : 2 solution undergoes a second period doubling along the lower branch PD_2^S and the saddle 2 : 2 solution period doubles along the upper PD_2^U. These period doublings again take place in a direction transverse to the closed invariant curve, and again a pair of new saddle–node bifurcation curves is born to delineate the synchronization range for the 4 : 4 solutions.

As the value of parameter c increases, the same process is found to repeat itself until the system undergoes a transition to chaos. Close to the tongue edges, corresponding node and saddle solutions period double almost simultaneously. However, as we move deeper into the resonance zone, the period-doubling of the node cycles occurs earlier and earlier in comparison with the period doubling of the corresponding saddle cycles. For this reason, the accumulation points for the two cascades are different and the structure of the multi-layered tori produced in the transition will depend on the forcing frequency ω. A similar bifurcation structure, involving interconnected cascades of period-doubling bifurcations for symmetric and antisymmetric orbits, has been discussed for two coupled Rössler systems [20]. However, the observed bifurcations were not related to the formation of multi-layered tori.

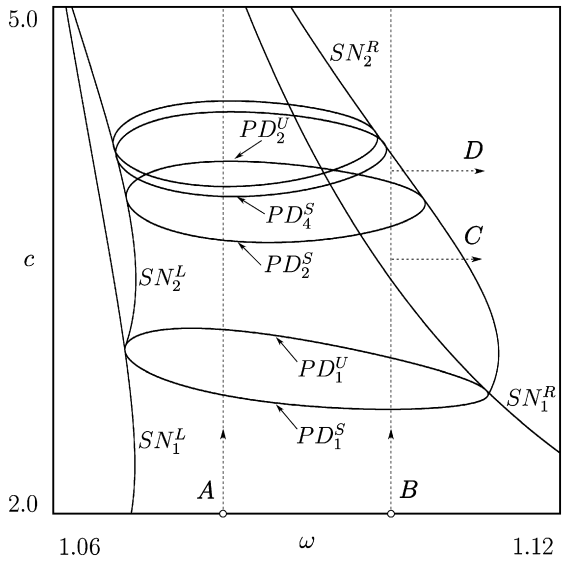

Fig. 1. Bifurcation structure associated with the first four period-doubling bifurcations of the 1 : 1 resonance cycles in the periodically forced Rössler oscillator. At the edges of the resonance tongue, defined by the saddle–node bifurcation curves SN_i^L and SN_i^R, $i = 1, 2$, period doubling of corresponding node and saddle cycles occurs simultaneously. Inside the zone, the stable cycles are found to period double at lower values of c than the saddle cycles. Note that each period-doubling gives rise to a new pair of saddle–node bifurcation curves to delineate the resonance zone for the period-doubled cycles. Arrows A, B, C and D denote scanning directions to be examined in the following figures.

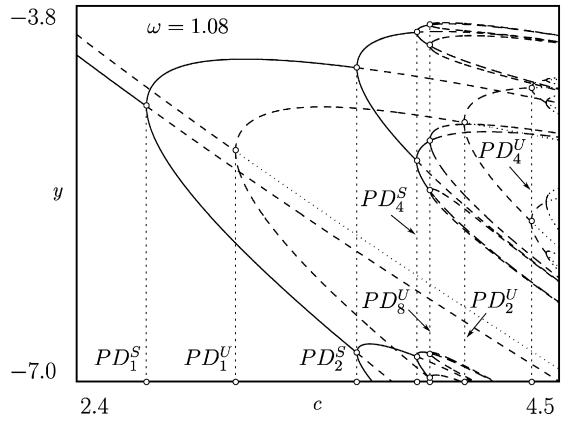

Fig. 2. One-dimensional bifurcation diagram along the direction A in Fig. 1. Full curves represent stable node solutions, dashed curves are saddle solutions, and dotted curves are doubly unstable saddle solutions. The period-doubling cascade for the stable node cycles accumulates in a transition to chaos approximately at $c_\infty = 3.95381$.

Fig. 2 shows a one-dimensional bifurcation diagram along the line A in Fig. 1. Here, $\omega = 1.08$. Full curves represent stable node solutions, dashed curves are saddle solutions, and dotted curves are doubly unstable saddle solutions. In accordance with the notation used in Fig. 1, a superscript S denotes a bifurcation of a stable node, and a superscript U indicates that the bifurcation occurs for a saddle cycle. Subscripts 1, 2, 4, etc., denote period-doubling bifurcations of period-1, period-2, etc., solutions. For the stable node cycles the transition to chaos occurs at $c \approx 3.95381$.

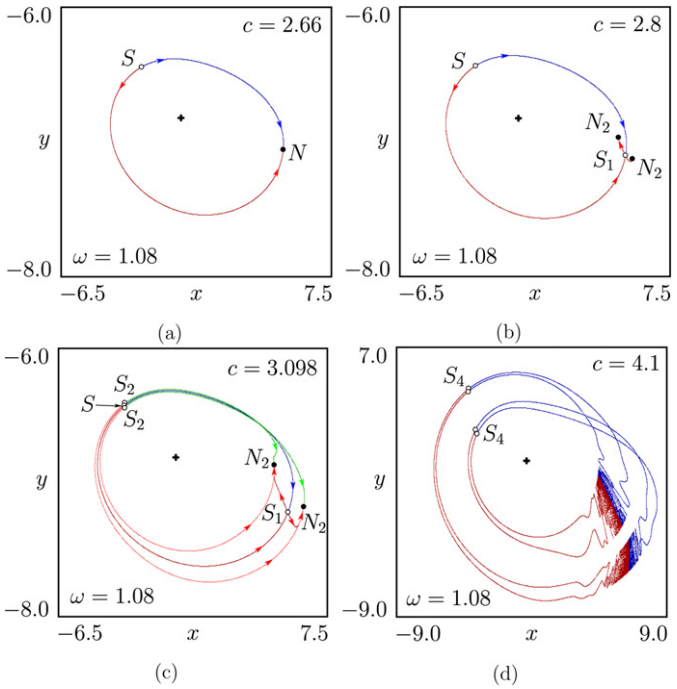

Fig. 3. Phase portraits of the resonance torus along the scan line A in Fig. 1. (a) Original 1 : 1 resonance torus with its node N and saddle cycle S. (b) The node cycle has undergone a period-doubling bifurcation transversely to the torus manifold. (c) Formation of a double-layered torus after the saddle cycle has also undergone a transverse period doubling transition. (d) Multi-layered chaotic structure after the saddle cycle has undergone a second period doubling and the original node cycle a complete transverse period-doubling cascade to chaos.

3. Formation of double-layered resonance tori and torus doubling

Below the period-doubling curve PD_1^S the system displays an ordinary 1 : 1 resonance torus with a stable period-1 node N and corresponding saddle cycle S (see Fig. 3(a)). As the system crosses the bifurcation curve PD_1^S, the 1 : 1 node undergoes a period-doubling bifurcation. As illustrated by the phase portrait in Fig. 3(b), this period-doubling takes place in a direction transverse to the torus manifold. This implies that whereas the original saddle cycle S is stable transversely to the torus manifold and unstable along this manifold, the saddle S_1, arising in the period-doubling bifurcation, is stable in the direction along the torus manifold and unstable in the transverse direction. N_2 denotes the points of the 2 : 2 resonance node. As c is further increased, the saddle cycle S undergoes a first period-doubling bifurcation when the system crosses the bifurcation curve PD_1^U. As the result, a multi-layered torus structure softly arises from the 1 : 1 resonance torus. Note how the now repelling 1 : 1 resonance torus is surrounded by the stable period-2 resonance torus (Fig. 3(c)).

As illustrated in Fig. 2, with further increase of the value of parameter c, one can observe a cascade of period-doubling bifurcations transverse to the 2 : 2 resonance torus, leading finally to a transition to chaos. Starting with the first period-doubling bifurcation of the 1 : 1 node cycle near $c = 2.70551$, the cascade of period-doubling bifurcations for the node cycles accumulates approximately at $c_\infty = 3.95381$. Fig. 3(d) shows the phase portrait in the region of chaotic dynamics for the original node cycle and after the second period-doubling bifurcation of the saddle cycle S_2.

Let us now examine the transition that occurs as we move out of the resonance tongue in the direction B (see Fig. 1), i.e., as we increase the parameter c from 2.4 to 4.3 while maintaining the forcing frequency constant at $\omega = 1.1$. This transition is shown in Fig. 4.

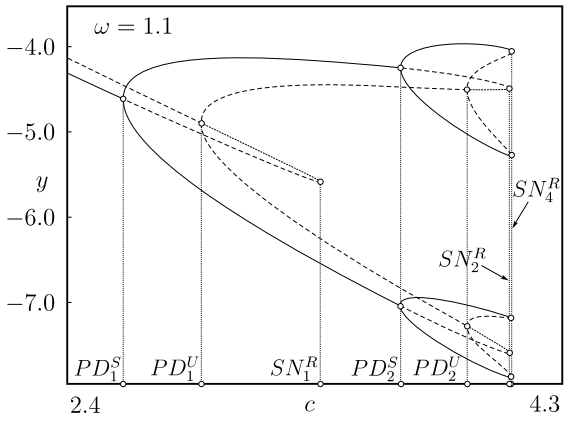

Fig. 4. One-dimensional bifurcation diagrams along the scan B in Fig. 1. After the period-doubling transitions at PD_1^S and PD_1^U, the 1 : 1 node and saddle cycles disappear in a saddle–node bifurcation on SN_1^R. The 2 : 2 node and saddle cycles undergo new period doublings at PD_2^S and PD_2^U, respectively, and then disappear in the saddle–node bifurcation SN_2^R. Finally, the 4 : 4 node and saddle cycles disappear in a saddle–node bifurcation at SN_4^R. Note how each level in the period-doubling cascade requires a saddle–node bifurcation of its own to demarcate the resonance zone.

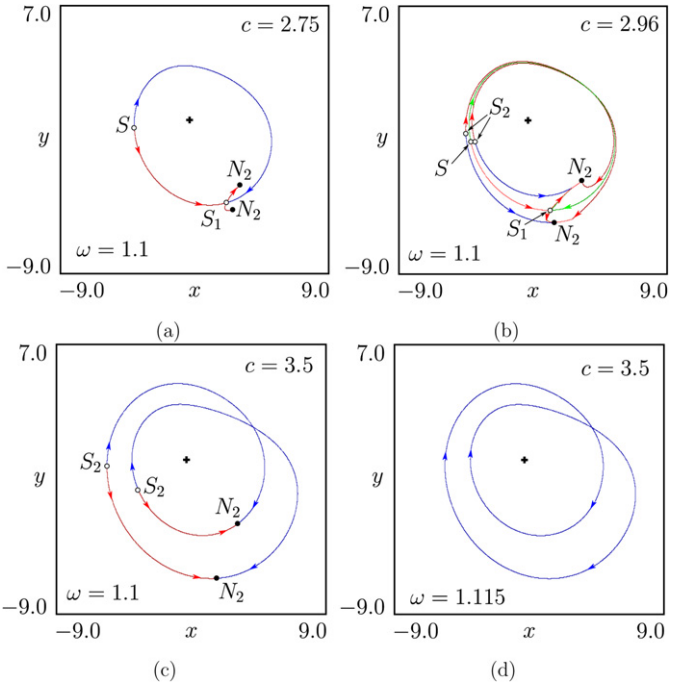

Fig. 5. Transition from double-layered resonance torus to period-doubled ergodic torus. (a) Phase portrait after the period-doubling bifurcation of the stable node transversely to the 1 : 1 resonance torus. As the parameter c is increased the saddle period-1 cycle S undergoes a period-doubling bifurcation. This leads to the formation of the period-2 resonance torus with a double-layered structure (b). (c) Phase portrait after the saddle–node bifurcation in which the saddle cycles S and S_1 merge and disappear. (d) Period-2 ergodic torus that arises when we leave the resonance tongue along the direction C in Fig. 1.

At the starting point the system displays a period-1 resonance torus. As the value of parameter c is increased, the stable node N undergoes a period-doubling bifurcation transverse the 1 : 1 resonance torus when the system crosses the curve PD_1^S. This is illustrated in the phase portrait in Fig. 5(a). When the system crosses the bifurcation curve PD_1^U the saddle period-1 cycle S undergoes a period-doubling bifurcation. As a result, a double-layered torus structure softly arises from the original resonance torus. Fig. 5(b) presents the phase portrait for the double-layered torus. As illustrated in Figs. 1 and 4, with further increase of the parameter c the saddle cycles S and S_1 merge and disappear in a saddle–node

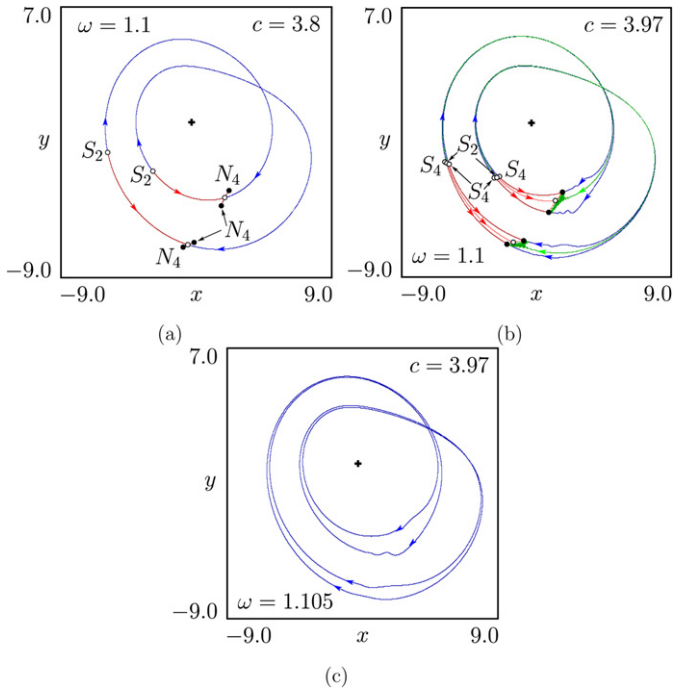

Fig. 6. Transition from a period-4 resonance torus to period-4 ergodic torus. (a) Period-doubling bifurcation of the stable period-2 cycle transversely to the 2:2 resonance torus. (b) Period-4 resonance torus after the period-doubling bifurcation of the saddle period-2 cycle S_2. S_4 and N_4 are the points of the period-4 saddle and stable cycles, respectively. (c) Period-4 ergodic torus. This torus appears when the system leaves the resonance tongue along the direction D in Fig. 1.

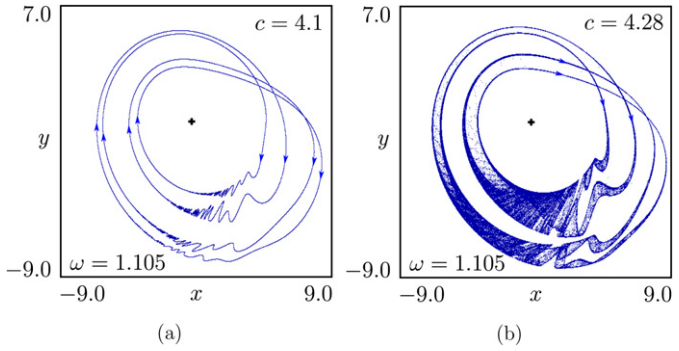

Fig. 7. (a) Folded structure for the period-4 ergodic torus. (b) Phase portrait for the chaotic dynamics.

bifurcation on the bifurcation curve SN_1^R, and the repelling layer of the original period-1 resonance torus disappears (Fig. 5(c)). Finally, when we leave the resonance tongue through the second saddle–node bifurcation curve SN_2^R along the direction C in Fig. 1, the period-2 resonance torus transforms into the period-2 ergodic torus through a saddle–node bifurcation. Fig. 5(d) shows the phase portrait for the period-2 ergodic torus after the saddle–node bifurcation.

When crossing the period-doubling bifurcation curves PD_2^S and PD_2^U with increasing parameter c along the direction B (see Figs. 1 and 4), we again observe the doubling of the resonance torus. Fig. 6(a) presents the phase portrait of system (1) after the second period-doubling bifurcation for the stable period-2 node N_2 transverse to the period-2 resonance torus. Fig. 6(b) shows the phase portrait of the system (1) after the second period-doubling bifurcation of the saddle period-2 cycle S_2 in which the double-layered period-4 resonance torus appears. When we leave the resonance tongue along the direction D in Fig. 1, the period-4 resonance torus transforms into a period-4 ergodic torus in a similar manner (Fig. 6(c)).

With further increase the value of the c, the invariant set of the ergodic period-4 torus first starts to fold. Further change of the parameter c leads to the appearance of the chaotic oscillations. This transition is illustrated for $\omega = 1.105$ in the Fig. 7.

4. Conclusions

The Letter established a more complete picture of the bifurcation phenomena that occur when a multi-dimensional period-doubling system is subjected to an external forcing and showed how the recently discovered phenomena of multi-layered resonance tori is linked to the phenomenon of period-doubled ergodic tori.

We first demonstrated how multi-layered resonance tori are formed through cascades of period doubling bifurcations of the resonant saddle and node cycles transversely to the torus manifold. Close to the edge of synchronization zone, where the bifurcations occur more and less simultaneously for the node and saddle cycles, one can follow a relatively high number of interconnected period doublings. In the interior of the resonance zone, where period doubling of the node cycle proceeds faster then period doubling of the saddle cycle, one can observe multi-layered chaotic structures produced through a complete period-doubling cascade of the original node cycle.

Each pair of period-doubling bifurcations generates a new set of saddle–node bifurcation curves along the sides of resonance tongue. As the period-doubling process proceeds, the edges of the tongue, therefore, accumulate more and more saddle–node bifurcation curves, each delineating the boundaries for the resonance modes at a particular level of the period-doubling cascade. Similarly to what one observes in the case of phase multistability [21] it appears that there is no specific ordering of the saddle–node bifurcation curves, and the ordering differs between the two sides of the tongue. This ordering influences the detailed transition by which a resonance torus is transformed into an ergodic torus. At low forcing amplitudes, one can observe that additional local and global bifurcation are involved in this transition [19].

Acknowledgements

The work was supported by the EU Life Sciences for Health Program through the BioSim Network of Excellence (Contract No. LSHB-CT-2004-005137).

References

[1] E.F. Stone, Phys. Lett. A 163 (1992) 367.
[2] M.G. Rosenblum, A. Pikovsky, J. Kurths, Phys. Rev. Lett. 76 (1996) 1804.
[3] A.S. Pikovsky, M.G. Rosenblum, G.V. Osipov, J. Kurths, Physica D 104 (1997) 219.
[4] E. Rosa Jr., E. Ott, M.H. Hess, Phys. Rev. Lett. 80 (1998) 1642.
[5] E. Rosa Jr., W.B. Pardo, C.M. Ticos, J.A. Walkenstein, M. Monti, Int. J. Bifur. Chaos 10 (2000) 2551.
[6] T.E. Vadivasova, A.G. Balanov, O.V. Sosnovtseva, D.E. Postnov, E. Mosekilde, Phys. Lett. A 253 (1999) 66.
[7] J.P. Carcasses, C. Mira, M. Bosch, C. Simo, J.C. Tatjer, Int. J. Bifur. Chaos 1 (1991) 183–196.
[8] L. Glass, R. Perez, Phys. Rev. Lett. 48 (1982) 1772.
[9] A.P. Kuznetsov, S.P. Kuznetsov, I.R. Sataev, Physica D 109 (1997) 91.
[10] S.P. Kuznetsov, I.R. Sataev, Phys. Rev. E 64 (2001) 046214.
[11] S.P. Kuznetsov, U. Feudel, A. Pikovsky, Phys. Rev. E 57 (1998) 1585.
[12] A. Arneodo, P.H. Coullet, E.A. Spiegel, Phys. Lett. 94A (1983) 1.
[13] K. Kaneko, Prog. Theor. Phys. 69 (1983) 1806.
[14] M. Sekikawa, T. Miyoshy, N. Inaba, IEEE Trans. Circuits Syst. I 48 (2001) 28.

[15] D.E. Postnov, A.G. Balanov, O.V. Sosnovtseva, E. Mosekilde, Phys. Lett. A 283 (2001) 195.
[16] Zh.T. Zhusubaliyev, E. Mosekilde, Phys. Lett. A 373 (2009) 946.
[17] Zh.T. Zhusubaliyev, E. Mosekilde, Physica D 238 (2009) 589.
[18] Zh.T. Zhusubaliyev, E. Mosekilde, Phys. Lett. A 351 (2006) 167.
[19] J.L. Laugesen, E. Mosekilde, Zh.T. Zhusubaliyev, Physica D, submitted for publication.
[20] J. Rasmussen, E. Mosekilde, C. Reick, Math. Comput. Simulation 40 (1996) 247.
[21] E. Mosekilde, D.E. Postnov, O.V. Sosnovtseva, Prog. Theor. Phys. Suppl. 150 (2003) 147.

Manuscript M2:

The edge of chaotic phase synchronization

Submitted to *European Physics Letters*.

The edge of chaotic phase synchronization

E. Mosekilde[1], J. L. Laugesen[1] and Zh. T. Zhusubaliyev[2]

[1] *Department of Physics, The Technical University of Denmark, 2800 Lyngby, Denmark*
[2] *Department of Computer Science, South West State University, 50 Years of October Str., 94, Kursk 305040, Russia*

PACS 05.45.-a – Nonlinear dynamics and chaos
PACS 05.45.Gg – Control of chaos, applications of chaos
PACS 05.45.Pq – Numerical simulations of chaotic systems
PACS 05.45.Xt – Synchronization; coupled oscillators

Abstract. - The edge of chaotic phase synchronization is known to consist of a dense set of saddle-node bifurcation curves. By following the synchronization transition through the cascade of period-doubling bifurcations in a forced Rössler system, this Letter describes how these saddle-node bifurcations arise and explains how they are organized. We identify the cycles that are involved in the saddle-node bifurcations and describe how the transitions that take place at the edge of the synchronization domain are related to the torus doubling bifurcations that occur outside this domain.

Chaotic phase synchronization [1–4] denotes an interesting form of synchronization in which a chaotic oscillator adjusts the frequencies of its internal dynamics to the rhythm of an external forcing, or to the dynamics of another chaotic oscillator, while the amplitudes continue to vary in an irregular fashion. In a numerical experiment one can observe [1–4] how the average frequency of a periodically driven chaotic oscillator varies with a control parameter until the system enters a region of synchronization where the average frequency remains constant and equal to the forcing frequency. The width of the mode-locking interval typically increases with the forcing amplitude and, as the system leaves this interval, its average frequency again starts to change.

Chaotic phase synchronization has been observed in a broad range of different physical, technical and biological systems, including a plasma discharge tube paced with a low amplitude wave generator [5], an array of coupled electronic oscillators [6], and a system of interacting functional units of the kidney [7]. The transition between phase-locked and un-locked states represents a significant change in behavior, and we have previously suggested that transitions between different synchronization states among the functional units of the kidney may be an important component in the normal physiological regulation of the blood flow to this organ [7].

Over the years, chaotic phase synchronization has been the focus of considerable theoretical interest [1–4, 8–10], and concepts and methods developed through this work have been used to interpret mode-locking phenomena in data from many different sources.

Along with changes in the variation of the average frequency, the transition between phase-locked and un-locked chaos is also reflected in a specific variation of the Lyapunov exponents, in characteristic changes of the spectrum of the forced chaotic oscillator, and through changes in the shape and size of the Poincaré section [11, 12]. It is generally established that the edge of the synchronization domain is made up by a dense set of saddle-node bifurcations [1–4, 8–12]. However, the details of how this set arises, how it is organized, and how the transition to the ergodic torus that exists outside the resonance zone take place appear not yet to have been worked out.

We have recently illustrated the detailed scaling theory developed by Kuznetsov *et al.* [13] by showing how the bifurcation structure of the periodically forced Rössler system develops through continued period-doubling bifurcations of both the node and the saddle cycles in a direction transverse to the original resonance torus, thus producing a system of so-called multi-layered resonance tori [14]. By following the synchronization transition for the forced Rössler system from the region where the oscillator displays simple periodic dynamics and all the way up through the cascades of period-doubling bifurcations to the regime of chaos, the present Letter describes how the saddle-node bifurcations arise and how they are arranged. We explain how the bifurcating modes are organized and determine at which of the many saddle-node bifurcation curves, the

ergodic torus that exists outside the resonance domain is born. This leads to a discussion of how the torus doubling bifurcations that take place outside of the resonance zone are related to the transitions that occur in the synchronization domain.

Let us consider the periodically forced Rössler system

$$\dot{x} = -y - z + A\sin(\omega t); \quad \dot{y} = x + ay; \quad \dot{z} = b + z(x - c) \quad (1)$$

that has also formed the basis for many earlier investigations of chaotic phase synchronization [3, 4, 12]. Here x, y and z are the dynamical variables of the unforced oscillator and $A\sin(\omega t)$ represents the externally applied forcing. The parameters a and b and the forcing amplitude A are kept constant at the values $a = b = 0.2$ and $A = 0.1$ while the nonlinearity parameter c and the forcing frequency ω are used as bifurcation parameters. With the above parameter values, the unforced Rössler system undergoes a Hopf bifurcation at $c = 0.4$ and for increasing values of c, the system hereafter exhibits a Feigenbaum cascade of period-doubling bifurcations. When an external periodic forcing is applied in the regime of periodic oscillations, the Rössler system displays regions of quasiperiodic (two-mode) dynamics interrupted by a dense set of resonance zones where the internally generated periodic oscillations synchronize with the external forcing. The 1:1 resonance domain is by far the most prominent, and the purpose of the present Letter is to examine the structures that arise in and near this tongue as a result of the interplay between synchronization and period doubling.

Figure 1 provides an overview of the first four period-doubling bifurcations in the 1:1 resonance tongue. Below the first period-doubling bifurcation PD_1^S, the resonance zone is delineated to the left and the right by the saddle-node bifurcation curves SN_1^L and SN_1^R, respectively. In this region the system displays a stable, synchronized period-1 cycle and a corresponding saddle solution, both situated on the closed invariant curve that represents the resonance torus. Along the lower curve PD_1^S, the stable period-1 cycle undergoes its first period-doubling bifurcation, while the saddle solution period doubles at the curve PD_1^U. At the edge of the resonance zone the two solutions merge, and period doubling occurs simultaneously. We notice, however, that the period-doubling transitions take place in a direction transverse to the invariant curve [14]. The repeated period-doubling process of both the node and saddle resonant cycles in this way gives rise to the formation of multi-layered resonance tori, i.e., nested structures of interconnected resonance tori [15].

Above the curve PD_1^U, the system displays a pair of period-1 saddle and doubly unstable node cycles together with a pair of period-2 saddle and stable node cycles. The region of synchronization for the period-2 cycles is not identical to that of the period-1 cycles. Hence, while the saddle-node bifurcation curves SN_1^L and SN_1^R continue up along the tongue edge to delineate the region of resonant period-1 dynamics, a new set of saddle-node

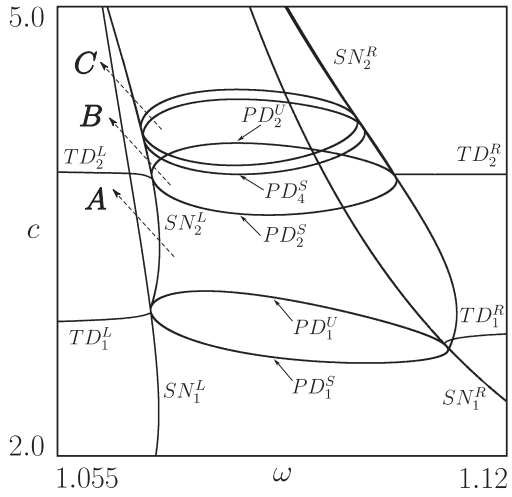

Fig. 1: Two-dimensional bifurcation diagram for the 1:1 resonance zone of the periodically forced Rössler oscillator (1). PD^S and PD^U denote period-doubling bifurcation curves for stable (node) and unstable (saddle) cycles, respectively. SN denotes saddle-node bifurcation curves, and TD torus doubling bifurcations. The arrows A, B and C define scan lines to be examined below.

bifurcation curves SN_2^L and SN_2^R are born to delineate the range of synchronized period-2 dynamics. These new saddle-node bifurcation curves originate from the period-doubling curve in which the corresponding mode is born, typically from a point close to where the period-doubling curve is tangent to the former set of saddle-node bifurcation curves. However, there is generally a gap between the two saddle-node bifurcation curves, and a number of local and global bifurcations are in place to close the hole and complete the border of the resonance zone [16].

The saddle-node bifurcation curves SN_2^L and SN_2^R are tangent to the next pair of period doubling curves. The stable period-2 solution undergoes a second period-doubling at PD_2^S, and the saddle period-2 solution period doubles at PD_2^U. As the value of c continues to increase, the same process repeats itself until the system undergoes a transition to phase synchronized chaos. This explains the build-up of a dense set of saddle-node bifurcation curves along the edges of the synchronization domain: A new pair of saddle-node bifurcation curves is generated for each pair of period-doubling bifurcations in order to delineate the region of existence for the newborn cycles. After the next pair of period-doubling bifurcations, the saddle-node bifurcation curves become curves at which the produced saddle and doubly unstable node cycles merge and disappear.

As first observed by Arnéodo *et al.* [17], the ergodic torus undergoes a series of torus-doubling bifurcations along the edge of the resonance zone [1, 18]. Moreover, as illustrated in Fig. 1, where the first two torus-doubling bifurcations are denoted TD_1 and TD_2, the torus-doubling bifurcations are coupled directly to the period-doubling

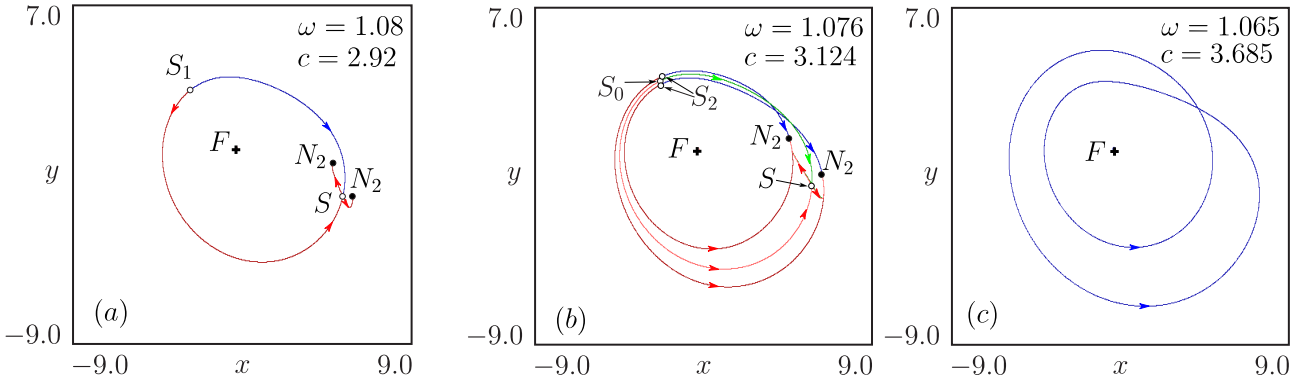

Fig. 2: Transition from double-layered resonance torus to period-doubled ergodic torus along the scan A in Fig. 1 ($c = -51\omega + 58$). (a) Phase portrait after the period-doubling bifurcation of the stable node transversely to the 1:1 resonance torus. Here S_1 and S are resonant period-1 saddle solutions with multipliers $\rho_1 = -0.8827$, $\rho_2 = 1.1055$, $\rho_3 = -2.95 \cdot 10^{-7}$ and $\rho_1 = 0.899$, $\rho_2 = -1.1598$, $\rho_3 = -3.12 \cdot 10^{-7}$, respectively. N_2 is a stable period-2 node cycle. (b) Double-layered structure that arises through a period-doubling bifurcation of the original period-1 saddle cycle S_1. Here S_0 is a doubly unstable period-1 cycle with multipliers $\rho_1 = -1.015$, $\rho_2 = 1.089$, $\rho_3 = -7.61 \cdot 10^{-8}$. (c) Period-2 ergodic torus that arises when the system leaves the resonance tongue along the direction A in Fig. 1.

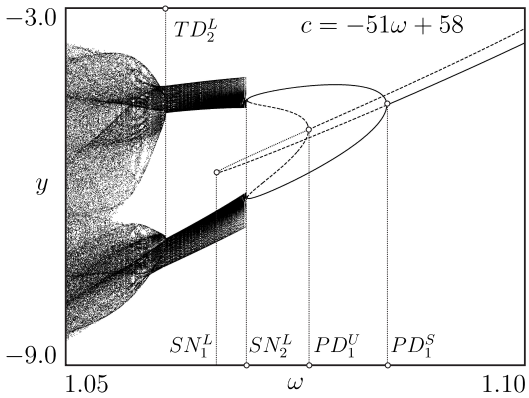

Fig. 3: One-dimensional scan along the direction A in Fig.1. The pair of saddle and doubly unstable 1:1 resonance cycles merge and disappear in SN_1^L. The pair of saddle and stable 2:2 cycles merge in SN_2^L, leading to a period-doubled ergodic torus. The ergodic torus undergoes a new period-doubling at TD_2^L.

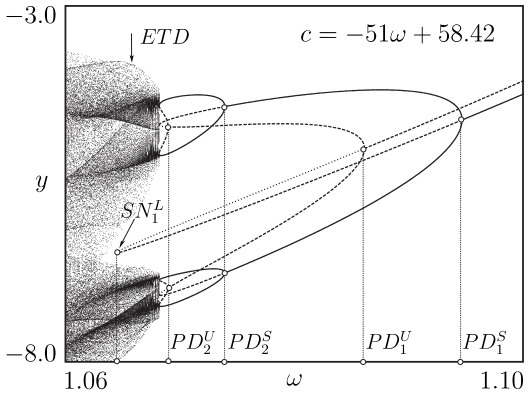

Fig. 4: One-dimensional scan along the direction B in Fig. 1. As the forcing frequency ω is reduced, the resonant period-4 torus ends in a saddle-node bifurcation that gives birth to a period-4 ergodic torus. At the point ETD, this ergodic torus is destroyed, and to the left of ETD the system displays non-synchronous chaos.

bifurcations in the resonance zone. Hence, the ergodic torus always displays the same periodicity as the resonance torus it couples to across the synchronization edge. Below the first period-doubling bifurcation, the period-1 ergodic torus ends in a bifurcation (SN_1^L or SN_1^R) that creates by a pair of period-1 node and saddle cycles. Between the first and the second period-doubling bifurcation, the period-2 ergodic torus ends in by a pair of period-2 node and saddle cycles along SN_2^L (or SN_2^R).

As an illustration to this point, Fig. 2 shows the transition through which the period-doubled ergodic torus arises if the parameters are scanned along the direction A in Fig. 1. Starting at a point after the first period-doubling curve PD_1^S, Fig. 2(a) shows how the originally stable 1:1 resonance cycle has undergone a period-doubling bifurcation in a direction transverse to the synchronization manifold, i.e., the unstable manifold of the 1:1 resonance saddle S_1. While giving birth to the stable 2:2 resonance cycle N_2, the period-doubling bifurcation has left the original 1:1 node as a saddle cycle with its unstable direction transverse to the synchronization manifold. When crossing the period-doubling bifurcation curve PD_1^U, the original 1:1 resonance saddle also undergoes a transverse period-doubling bifurcation, leading to the 2:2 resonance saddle S_2 and the doubly unstable resonance cycle S_0 (Fig. 2(b)). This latter transition gives birth to a so-called double-layered torus [14–16], i.e. a structure of interconnected layers of stable and unstable tori. As the scan continues through the saddle-node bifurcation curves SN_2^L and SN_1^L we observe first how the 2:2 saddle and stable node cycles merge and disappear through the birth of a period-doubled

ergodic torus at SN_2^L and, thereafter, how the pair of 1:1 saddle and doubly unstable node cycles merge and disappear in the saddle-node bifurcation SN_1^L (Fig. 2(c)).

If the scan is continued one can observe how the ergodic torus undergoes a second torus doubling at the bifurcation curve TD_2^L in Fig. 1. This is illustrated in the one-dimensional bifurcation diagram of Fig. 3 which again shows the transitions that take place along the direction A. Full curves represent stable periodic cycles, dashed curves saddle cycles, and dotted curves doubly unstable node solutions. Notice how the stable 1:1 solution that exists in the upper right corner of the figure undergoes a period-doubling at PD_1^S while the corresponding 1:1 saddle solution suffers its first period doubling at PD_1^U. From here we can follow the two solutions (now as a saddle cycle and a doubly unstable node) to the saddle-node bifurcation SN_1^L to the left in the figure. This saddle-node bifurcation defines the zone edge for the period-1 cycles. The saddle and stable node 2:2 resonance cycles merge at SN_2^L to give birth to a period-doubled ergodic torus. Finally, when crossing the torus doubling bifurcation point TD_2^L, the ergodic torus undergoes a new period-doubling transition.

Fig. 4 shows a similar one-dimensional bifurcation diagram for the direction B in Fig. 1. After the first period-doubling bifurcations for the 1:1 resonance node and saddle cycles at PD_1^S and PD_1^U, the interconnected period-doubling processes continue to the left in the figure. Here we can locate the period-doubling bifurcation PD_2^S for the stable period-2 cycle and the bifurcation PD_2^U for the corresponding saddle cycle. Each pair of saddle and doubly unstable node cycles born in these bifurcations can subsequently be followed to the saddle-node bifurcation that demarcates their synchronization zone.

In Fig. 4, the boundary of the resonance zone consists of saddle-node bifurcations for the period-1, period-2, and period-4 cycles, but only the period-4 node is stable. Hence, we observe that the period-4 resonance torus ends in a saddle-node bifurcation in which an ergodic period-4 torus is born. The repelling period-1 resonance torus continues to exist into the region of the stable period-4 ergodic torus. As the system moves further away from the resonance zone, the ergodic torus starts to fold and it finally undergoes torus destruction at the point ETD where its different layers begin to mix.

Figs. 5 (a) and (b) provide an illustration to the ergodic torus destruction process. Here we have plotted a Poincaré section of the period-4 ergodic torus that exists to the right of the point ETD in Fig. 4 together with a similar section and of the non-synchronized chaotic attractor that arises when threshold of torus destruction is crossed. The transition from ergodic torus dynamics to non-synchronous chaos is accompanied by one of the Lyapunov exponents turning positive.

Figure 6 shows a one-dimensional bifurcation diagram along the scan line C in Fig. 1. Here, $c = -51\omega + 58.75$, and the scan takes the system from the region of period-1 resonance all the way through the regime of phase chaos and out across the edge of the resonance zone. With decreasing values of ω, the state of phase-synchronized chaos is reached when the stable resonance cycles have completed their period-doubling cascade. In Fig. 6 this region is indicated by means of dots as obtained in a normal brute-force bifurcation scan. In this way we can also illustrate the appearance of periodic windows in the region of phase-synchronized chaos. With further decrease of ω, the doubly unstable modes arising through period-doubling of the saddle cycles also start to contribute to the chaotic state. Finally, a transition to non-synchronous chaos occurs at SN_∞^L. This transition is associated with the abrupt change of one of the Lyapunov exponents from being negative to becoming zero, hence resembling a normal saddle-node bifurcation between a resonant and an ergodic torus.

After this description we are left with one main question: Is there a specific organization of the saddle-node bifurcation curves along the edge of the resonance zone?

The sketch in Fig. 7 addresses this question and also illustrates some of the results of the above discussion. Here, we have plotted the saddle-node bifurcations that occur along the left hand side of the resonance tongue. While distorting the scales, this sketch strictly maintains the systematic of the variation. The curves denoted 1, 2, 4, 8, etc., represent the saddle-node bifurcation curves SN_1^L, SN_2^L, SN_4^L, etc. As mentioned above, each saddle-node bifurcation curve is tangent to the period-doubling curve at the next level of the period-doubling cascade. The following saddle-node bifurcation curve is then born at a point of this period-doubling curve close to the point of tangency but not in that point. Hence, there is a small gap between the saddle-node bifurcation curves where other (local and global) bifurcations are in place [16]. This gap is not of direct significance to the present discussion, and in the figure the gap is neglected.

Inspection of Fig. 7 shows that while the first few saddle-node bifurcation curves follow individual courses, a systematic arrangement is gradually established in which the saddle-node bifurcation curves alternate between the two sides of what at the end becomes the accumulation curve SN_∞ for the saddle-node bifurcation curves. In the periodic region, i.e., the region below the transition to chaos, the ergodic torus is found to penetrate the cascade of saddle-node bifurcations along the edge of the resonance zone until it meets a stable periodic cycle. As illustrated in Fig. 7, where the region of non-synchronized dynamics to the left of the resonance domain is hatched, this implies that the transition from non-resonant to resonant dynamics at a given value of c always occurs along the saddle-node bifurcation curve that produces cycles with the highest periodicity.

Alternation of the saddle-node bifurcation curves delineating the ranges of existence for different levels of a period-doubling cascade has also been observed in a system of coupled Rössler oscillators [20]. Closer examination

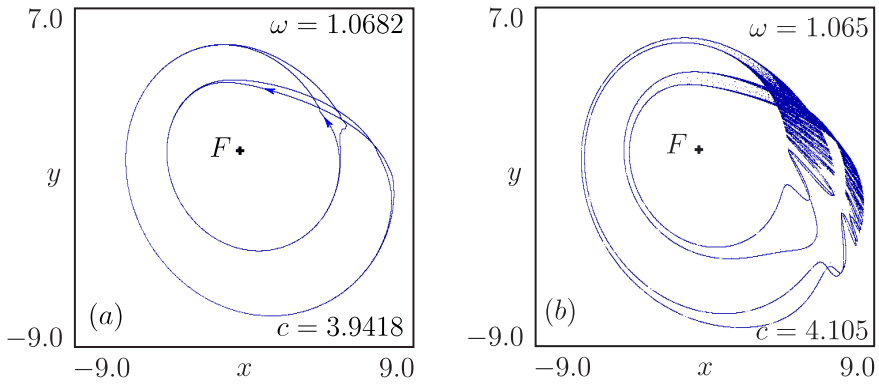

Fig. 5: The process of ergodic torus destruction. (a) Cross section of the period-4 ergodic torus that exists to the right of the threshold ETD in Fig. 4. (b) Non-synchronous chaotic attractor to the left of ETD.

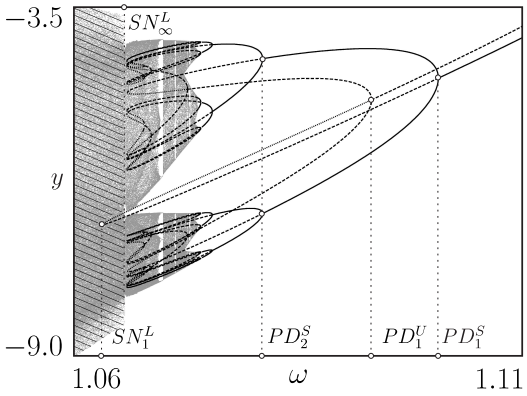

Fig. 6: Bifurcation diagram along the scan line C in Fig. 1. Each pair of saddle and doubly unstable node cycles generated in the period-doubling bifurcations merges in a specific saddle-node bifurcation along the edge of the resonance zone. The figure also illustrates the transition from phase-locked chaos (dotted) to non-synchronous chaos (hatched) at the point SN_∞^L.

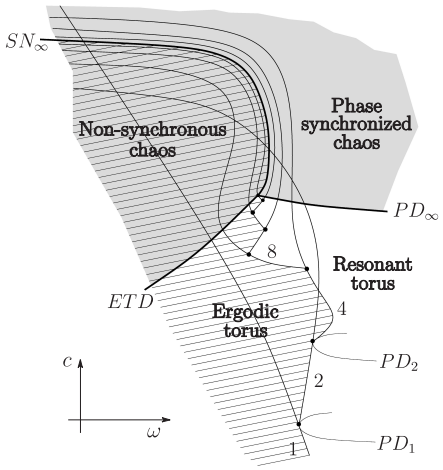

Fig. 7: Sketch to illustrate the cascade of saddle-node bifurcation curves along the edge of the resonance zone. The curves denoted 1, 2 ,4, etc., represent the saddle-node bifurcation curves SN_1^L, SN_2^L, SN_4^L, etc. Note how the curves after an initial lack of organization begin to converge in an alternating fashion towards the final accumulation curve SN_∞. The hatched area represents the region of non-synchronous dynamics outside the resonance zone. PD_∞ represents the accumulation curve for the period-doubling cascade and ETD is the curve of ergodic torus destruction.

shows that the emergence of a new saddle-node bifurcation curve along a given zone boundary tends to alternate between points on the stable and on the unstable branch of the period-doubling curve. Moreover, if the saddle-node bifurcation curve along one zone boundary emerges from the stable branch of the period-doubling bifurcation curve, then the saddle-node bifurcation along the other boundary will emerge from the unstable branch.

Based on a detailed analysis of the bifurcation structure for the periodically forced Rössler system, the Letter has established a coherent picture of the many different phenomena and processes associated with chaotic phase synchronization for systems with spiral-type chaos. In particular, we have demonstrated how period-doubling bifurcations develop in a direction transverse to the synchronization manifold, how the period-doubling processes in the resonant and non-resonant regimes work together, and how the saddle-node bifurcations along the zone boundary produce an alternating structure that finally accumulates in a well-defined curve. The transition from phase-locked chaos to non-synchronous chaos takes place along the curve SN_∞ which at one and the same time is the accumulation curve for the saddle-node bifurcations and threshold for the ergodic torus destruction ETD. Let us finally note that deviations from the above picture may arise for chaotic systems that display a broader distribution of their internal frequencies such as, for instance the Lorenz attractor where the presence of an equilibrium point of saddle type allows the return times to diverge [19].

REFERENCES

[1] Anishchenko V. S. *et al.*, *Int. J. Bifur. Chaos*, **2** (1992)

633.
[2] Dykman G. S., Landa P. S. and Neymark Yu. I., *Chaos, Solitons and Fractals*, **1** (1992) 339; Landa P. S., Rosenblum M. G., *Appl. Mech. Rev.*, **46** (1993) 414.
[3] Rosenblum M. G., Pikovsky A. S. and Kurths J., *Phys. Rev. Lett.*, **76** (1996) 1804; Rulkov N. F., *Chaos*, **6** (1996) 262.
[4] Pikovsky A. S. *et al.*, *Physica D*, **104** (1997) 209; Osipov G. V. *et al.*, *Phys. Rev. E*, **55** (1997) 2353.
[5] Rosa Jr. E. *et al.*, *Int. J. Bifur. Chaos*, **10** (1997) 2551.
[6] Dabrowski A., Galias Z. and Ogorzalek M., *Int. J. Bifur. Chaos*, **10** (2000) 2391.
[7] Holstein-Rathlou N.-H. *et al.*, *Chaos*, **11** (2001) 417.
[8] Pikovsky A. S. *et al.*, *Chaos*, **7** (1997) 680; Rosa Jr. E., Ott E. and Hess M. H., *Phys. Rev. Lett.*, **80** (1998) 1642.
[9] Rosenblum M. G., Pikovsky A. S. and Kurths J., *IEEE Trans. CAS-I*, **44** (1997) 874; Vadivasova T. E. *et al.*, *Phys. Lett. A*, **253** (1999) 66.
[10] Postnov D. E. *et al.*, *Chaos*, **9** (1999) 227.
[11] Pikovsky A., Rosenblum M. and Kurths J., *Synchronization: A Universal Concept in Nonlinear Science* (Cambridge University Press, UK) 2001.
[12] Mosekilde E., Maistrenko Yu. and Postnov D., *Chaotic Synchronization: Applications to Living Systems* (World Scientific, Singapore) 2002.
[13] Kuznetsov S. P., Kuznetsov A. P. and Sataev I. R., *J. Stat. Phys.*, **121** (2005) 697; Kuznetsov S. P., Kuznetsov A. P. and Sataev I. R., *Physica D*, **109** (1997) 91.
[14] Zhusubaliyev Zh. T., Laugesen J. L. and Mosekilde E., *Phys. Lett. A*, **374** (2010) 2534.
[15] Zhusubaliyev Zh. T. and Mosekilde E., *Phys. Lett. A*, **373** (2009) 946; Zhusubaliyev Zh. T. and Mosekilde E., *Physica D*, **238** (2009) 589.
[16] Laugesen J. L., Mosekilde E. and Zhusubaliyev Zh. T., *Physica D*, (submitted for publication) .
[17] Arnéodo A., Coullet P. H. and Spiegel E. A., *Phys. Lett. A*, **94** (1983) 1; Kaneko K., *Prog. Theor. Phys.*, **69** (1983) 1806.
[18] Sekikawa M., Miyoshy T. and Inaba N., *IEEE Trans. Circuits Syst. I*, **48** (2001) 28; Sekikawa M.*et al.*, *Phys. Lett. A*, **374** (2006) 2534.
[19] Zaks M. A., Park E.-H. and Kurths J., *Int. J. Bifur. Chaos*, **10** (2000) 2649; Osipov G. V. *et al.*, *Phys. Rev. Lett.*, **91** (2000) 024101.
[20] Rasmussen J., Mosekilde E. and Reick C., *Math. Comput. Simul.*, **40** (1996) 247.

Manuscript M3:

Bifurcation analysis of resource coupled Rössler systems

Accepted for publication in *Journal of Applied Functional Analysis*.

Bifurcation analysis of resource coupled Rössler systems

J. L. Laugesen and E. Mosekilde
Complex Systems Group and
Department of Physics, The Technical University of Denmark

March 8, 2010

Abstract

Nephrons in the kidney interact via different mechanisms that involve mutual readjustments in the distribution of the blood flow. At the same time, the flow of blood controls the dynamics of the individual nephron, including its ability to produce complex nonlinear oscillations, synchronization of various internal modes, and deterministic chaos. In order to better understand a variety of phenomena that are specific to this type of coupling we have studied a system of two interacting Rössler oscillators with a coupling that reproduces essential aspects of the biological mechanism. We have performed detailed one- and two-dimensional bifurcation analyses of the 1:1 resonance tongue in this system. These analyses have disclosed an unusual substructure with cascades of period-doubling bifurcations unfolding along the edges of the tongue. This structure is typical of interacting period-doubling systems. However, while associated with the so-called C-type critical behavior, it appears that the bifurcation structure has not previously been examined in detail.

Keywords: Nephron, resource coupling, Rössler system, resonance, synchronization, bifurcation analysis.

1 Introduction

The human kidney contains approximately 1.2 million functional units, called nephrons. Each of these units possesses a certain ability to protect its own function against fluctuations in the arterial blood pressure by regulating the flow resistance of the incoming arteriole. As experiments on anesthetized rats have shown [2, 1], this regulation tends to be unstable and produce interacting oscillatory modes, period-doubling bifurcations, and other complicated dynamic phenomena in the tubular pressures and flows. The nephrons interact with one another through different mechanisms of which the so-called vascular propagated coupling involves waves of muscular contractions that travel along the common

structure of blood vessels. This coupling tends to produce in-phase synchronization among the interacting nephrons. An alternative mechanism, denoted hemodynamic coupling, arises from the simple fact that as one nephron reduces its incoming blood flow, more blood will flow to its neighbors. This mechanism generally causes the interacting nephrons to show out-of-phase oscillations in their pressures and flows. Both in-phase and anti-phase synchronization of neighboring nephrons have been observed experimentally [3].

Figure 1 shows a sketch of two nephrons with their afferent arterioles branching off from a common larger arteriole. Under the control of a variety of regulatory feedback mechanisms, water and salt filtered out from the capillary system in the glomerulus is processed as the fluid flows through the tubular system. As mentioned above, interaction between the nephrons arises from the influence that contraction of the afferent arteriole of one nephron has on the blood flow to neighboring nephrons.

Despite its simplicity, the hemodynamic coupling is of significant interest both from a theoretical point of view and in view of its relevance to a range of other systems, including coupled electronic oscillators [12] and coupled population dynamic systems [13]. The peculiar aspect of this interaction is that it is mediated directly through variations in the supply (or distribution) of those resources that cause the individual subsystem to oscillate or, in other words, the coupling takes place through a main bifurcation parameter rather than through the system variables as for the more commonly studied diffusive coupling.

The purpose of the present paper is to examine some of the bifurcation phenomena that are characteristic for the resource distributed type of coupling. The hemodynamic interaction between neighboring nephrons is almost immediate such that the, displacement of the blood flow away from one nephron immediately leads to an increasing blood flow to its neighbors. Besides involving regulation of a main bifurcation parameter, the coupling between our two Rössler oscillators should therefore be designed such that growing oscillations in one system leads to declining amplitudes in the other.

To better understand the generic aspects of this type of coupling, we have performed detailed one-and two-dimensional bifurcation analyses of a pair of coupled Rössler systems with resource mediated coupling. These analyses have revealed an unusual structure with cascades of period-doubling bifurcations that unfold along the edges of the resonance tongues. This structure is related to the so-called C-type criticality [5, 6]. It appears, however, that a detailed bifurcation analysis of the structures has not previously been performed [8].

2 Coupled Rössler systems

Detailed mechanism-based modeling is often possible for physiological systems, and over the years we have developed increasingly advanced models of the blood flow regulation for the individual nephron [1, 7]. We have used these models to study both the synchronization of neighboring nephrons [3] and the interaction of a large number of nephrons in a so-called nephron tree [10]. This physiology-based modeling approach has the advantage of providing significant insight into the biological processes and their mutual interaction. However to shed light on some of the more generic phenomena it is obviously preferable to choose a simpler system, even if it has no direct physiological interpretation. Hence we shall

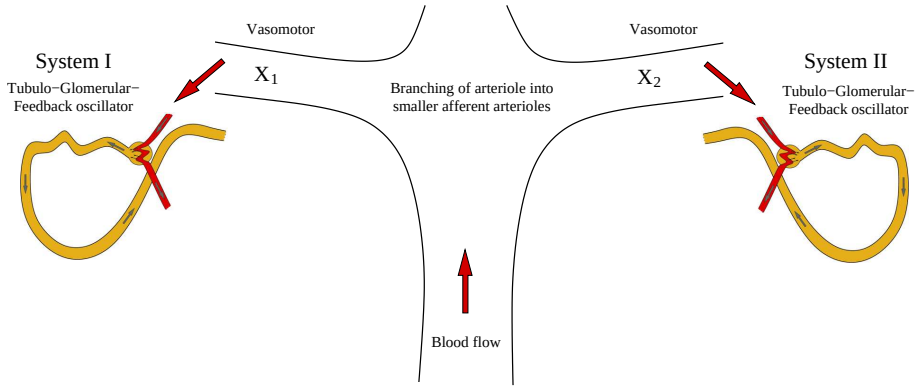

Figure 1: Sketch of two interaction nephrons with their afferent arterioles branching off from a common larger arteriole. Coupling between the nephrons arises from phenomena that play out via the vascular system that connect them. At the same time this system provides the individual nephron with the flow of blood it needs to maintain its complicated dynamics.

consider a system of two coupled Rössler oscillators where the coupling is introduced via the parameter a that can be considered as a main control of the dissipation of the individual oscillator. To a certain extent the Rössler system displays a dynamics similar to the dynamics of our more detailed physiological models: For part of the time the Rössler system exhibits a relatively fast expanding oscillatory dynamics close to the (x, y)-plane. This may be interpreted as representing the relatively fast so-called myogenic oscillations that arise in the blood flow regulation from periodic contractions of the smooth muscle cells surrounding the afferent arteriole. When the amplitude of these oscillations becomes sufficiently large, the trajectories are folded back towards the unstable equilibrium point to start a new outwards spiral. This may be interpreted as representing the slower component of nephron oscillations that arise through a feedback from variations in the sodium concentration in the tubular fluid [9, 2]. Our system thus takes the form:

$$I: \quad \begin{cases} \dot{x}_1 &= -y_1 - z_1 \\ \dot{y}_1 &= x_1 + a[1 - \alpha(x_2 - x_1 - c)]y_1 \\ \dot{z}_1 &= b + z_1(x_1 - c) \end{cases} \tag{1}$$

$$II: \quad \begin{cases} \dot{x}_2 &= -\omega y_2 - z_2 \\ \dot{y}_2 &= \omega x_2 + a[1 - \alpha(x_1 - x_2 - c)]y_2 \\ \dot{z}_2 &= b + z_2(x_2 - c) \end{cases} \tag{2}$$

where the parameter values throughout this paper are taken to be $a = 0.057258$, $b = 0.2$ and $c = 5.7$. ω is a bifurcation parameter that controls the frequency of system II. The value of a is defined as the mean value between the Hopf bifurcation point and the first period-doubling. As described above the coupling takes place via the variable y, and the coupling term for system I take the form

$$a_{eff} y_1 = a[1 - \alpha(x_2 - x_1 - c)]y_1, \tag{3}$$

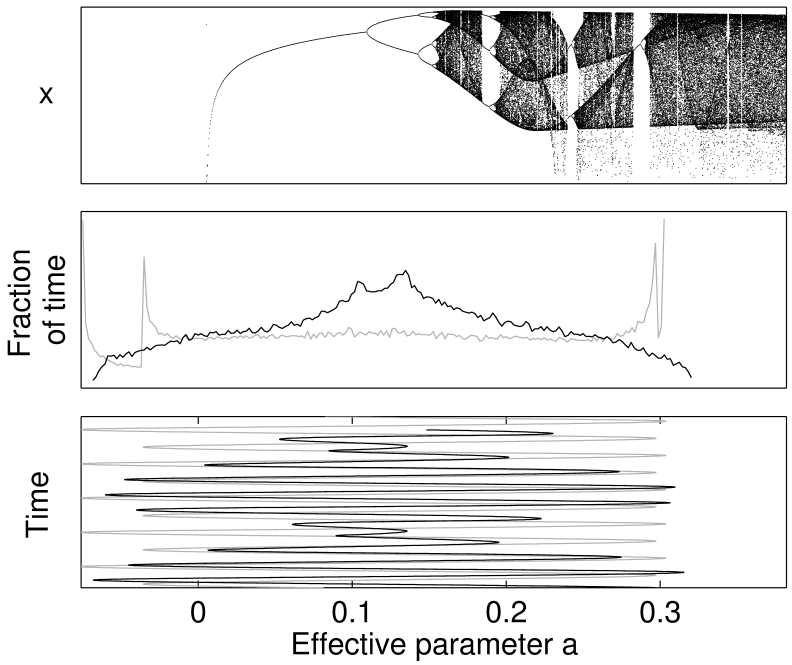

Figure 2: The period-doubling cascade to chaos in two coupled Rössler systems together with the fraction of time spent at different values of a_{eff} and the time evolution of a_{eff} at two different situations: $(\omega, \alpha) = (1.001, 0.2)$ (gray) and $(\omega, \alpha) = (1.2, 0.2)$ (black).

where α is a coupling parameter and a_{eff} may be considered as an effective, time-dependent value of parameter a. When $\Delta x = x_2 - x_1 > c$ the effective a in system I reduces linearly and thus the rate of change in y due to the coupling change non-linearly by $a_{eff}y_1$. In accordance with our previous comments, this type of coupling may be called a resource mediated coupling [11], since parameter a may be considered to describe the flow of resources that maintain the dynamics of the system. The system may be interpreted as a single Rössler system, where a is oscillating over the period-doubling cascade and eventually into the chaotic region. This is illustrated in Figure 2. The top panel of this figure shows a one-dimensional bifurcation diagram for the single Rössler system with a as parameter. The middle panel shows two examples of the fraction of time that the effective a on average spend at specific values for a period two orbit at $(\omega, \alpha) = (1.001, 0.2)$ and for an ergodic torus at $(\omega, \alpha) = (1.2, 0.2)$. Note, that the period two orbit shows four spikes, two at the maxima and two at the minima, where the rate of change of a_{eff} is slow. The lower panel shows the time evolution of a_{eff} for the two cases.

3 Bifurcation analysis

Continuation methods represent a unique tool to follow bifurcations and thus to understand how the two systems interact. We have applied this method to study

the resonnance and synchronization mechanisms in the 1:1 Arnold' tongue. Figure 3 shows the main bifurcations with the coupling parameter α and the forcing frequency ω as bifurcation parameters. For low values of α the system is in a 1:1 resonant state and saddle-node bifurcation (labelled SN_1^L and SN_1^R) form the borders of the tongue. As α increases two different bifurcations occur, depending on ω. At the borders of the resonance zone, period-doubling bifurcations take

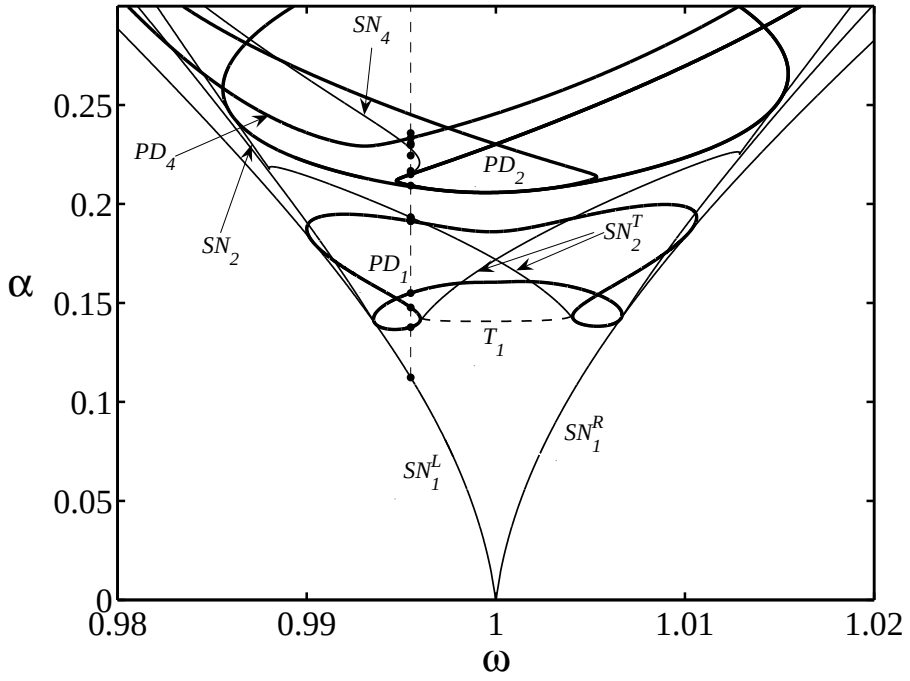

Figure 3: Main Arnold' tongue (1:1) with part of the bifurcation structure. The torus bifurcation inside the tongue give rise to quasi-periodic dynamics. It is terminated by saddle node bifurcations (SN_2^T) of a period-2 cycle, which exist only in the region above $SN_{2,T}$. Period-doubling bifurcations are drawn with thick lines.

place, while around the center a torus bifurcation (T_1) leads to the formation of an ergodic torus. The torus is later destroyed by the birth of a period-2 cycle in the saddle-node bifurcations ($SN_{2,T}^L$ and $SN_{2,T}^R$). The saddle-node bifurcations extend towards the borders of the resonant region and become the new borders for the 2:2 resonant region. At the point of contact between PD_1 and SN_1^L a new saddle-node bifurcation is born, which becomes the border for the period-2 cycle that co-exist with the period-2 cycle emerging at $SN_{2,T}$. Figure 4 shows the bifurcations along the dashed line at $\omega = 0.9955$. Starting from the period-1 cycle a period-doubling bifurcation (PD_1) takes place, and the period-2 subsequently undergoes a second period-doubling at (PD_2). The period-4 then suffers a cusp bifurcation (SN_4) and leaves the cascade to follow a second period-doubling cascade (labelled with superscript 2). The new attractor undergoes a full period-doubling cascade to chaos (not shown). A third attractor co-exist in the range $\alpha > 0.19$. This is the cycle that terminated the torus mentioned

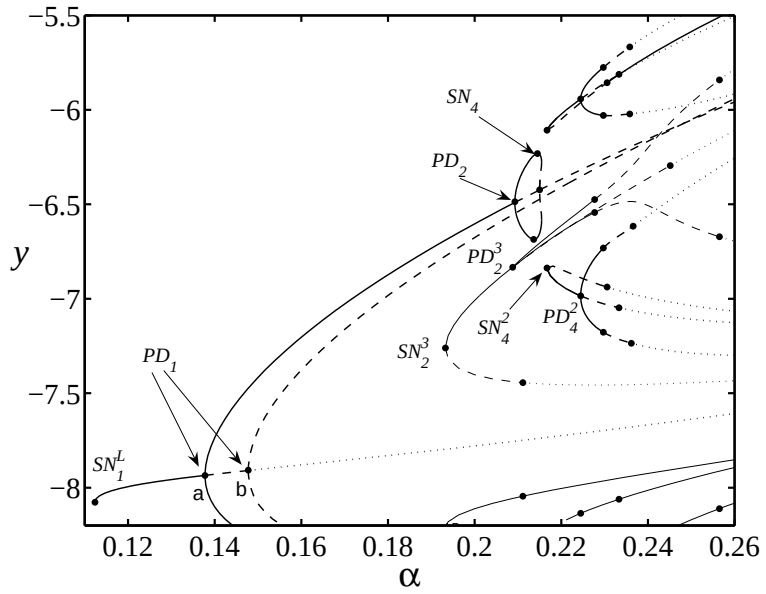

Figure 4: Bifurcations on the **stable** branch of the 1:1 resonance cycle along the dashed line at $\omega = 0.9955$ in Figure 3.

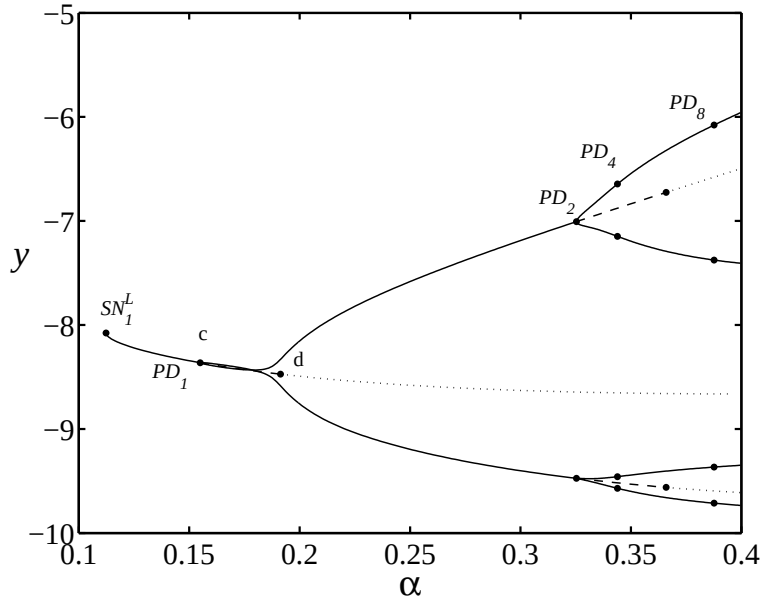

Figure 5: Bifurcations on the **unstable** branch of the 1:1 resonance cycle along the dashed line at $\omega = 0.9955$ in Figure 3. Note, that in this figure saddles are drawn with solid lines, doubly unstable nodes are dashed lines and triply unstable nodes are dotted lines.

above. It is born as a period-2 cycle. The first period-doubling (PD_2^3) taking place on this 2-cycle behaves in an unusual way, but this is likely to be due the Poincaré section chosen, i.e. the projection of the orbit. The further evolution shows a period-doubling cascade to chaos.

The looping of the period-doubling PD_1 is typical for systems, where a parameter is replace by a variable that span over a period-doubling cascade and similar loops of other higher period-doublings exist. As we follow the stable period-1 cycle it undergoes a period-doubling at (a) and turns into a saddle. The saddle then undergoes a period-doubling at (b) and turns into an unstable node. The remaining two intersections with PD_1 take place on the unstable branch of the period-1 cycle. Figure 5 shows the bifurcations on the unstable branch. Similar, as for the stable branch, the 1-cycle undergoes two succesive period-doublings at (c) and (d).

4 Conclusion

The coupling used here is a first attemp to approach the mechanisms involved in the coupling between nephrons. Although the study is preliminary it has brought valuable information on the bifurcation structure. This may be useful in interpreting a larger study of a complete nephron tree with physiologically more correct models. The dynamics of the two Rössler systems with the special resource coupling are out of phase for all parameter ranges explored, because of the symmetry of the coupling. The bifurcation structure show a termination of a period-doubling cascade followed by a second period-doubling cascade, due to a cusp bifurcation. A co-existing period-doubling structure was also found.

5 Acknowledgement

This work was supported by the European Union through the Network of Excellence BioSim (LSHB-CT-2004 005137). We acknowledge inspiring discussions with Zh. T. Zhusubaliyev.

References

[1] M. Barfred, E. Mosekilde and N.-H. Holstein-Rathlou, Bifurcation analysis of nephron pressure and flow regulation, *Chaos*, 6, 280-287, 1996.

[2] N.-H. Holstein-Rathlou, Oscillations and Chaos in Renal Blood Flow Control, *Journal of the American Society of Nephrology*, 4, 1275-1287, 1993.

[3] N.-H. Holstein-Rathlou, K.-P. Yip, O. V. Sosnovtseva and E. Mosekilde, Synchronization phenomena in nephron-nephron interaction, *Chaos*, 11, 417-426, 2001.

[4] K. S. Jensen, E. Mosekilde and N.-H. Holstein-Rathlou, Self-sustained oscillations and chaotic behavior in kidney pressure regulation, *Mondes en Developpement*, 54/55, 91-109, 1986.

[5] S. P. Kuznetsov, A. P. Kuznetsov and I. R. Sataev, Multiparameter Critical Situations, Universality and Scaling in Two-Dimensional Period-Doubling Maps, *Journal of Statistical Physics*, 121, 697-748, 2005.

[6] S. P. Kuznetsov and I. R. Sataev, Universality and scaling for the breakup of phase synchronization at the onset of chaos in a periodically driven Rössler oscillator,*Physical Review E (Statistical, Nonlinear, and Soft Matter Physics)*, 64, 046214/1-7, 2001.

[7] J. L. Laugesen, O. V. Sosnovtseva, E. Mosekilde, N.-H. Holstein-Rathlou and D. J. Marsh,Coupling induced complexity in nephron models of renal blood flow regulation, *Am J Physiol Regul Integr Comp Physiol*, 2010.

[8] J. L. Laugesen, E. Mosekilde and Zh. Zhusubaliyev, Bifurcation structure of the C-type period-doubling transition, *Submitted to Physica D*, 2010.

[9] P. P. Leyssac and N.-H. Holstein-Rathlou, Tubulo-glomerular feedback response: Enhancement in adult spontaneously hypertensive rats and effects of anaesthetics, *Pflügers Archive*, 413, 267-272, 1989.

[10] D. J. Marsh, O. V. Sosnovtseva, E. Mosekilde and N.-H. Holstein-Rathlou, Vascular coupling induces synchronization, quasiperiodicity, and chaos in a nephron tree, *Chaos*, 17, 15114-1-10, 2007.

[11] D. E. Postnov, O. V. Sosnovtseva and E. Mosekilde, Oscillator clustering in a resource distribution chain, *Chaos*, 15, 13704-1-12, 2005.

[12] D. E. Postnov, O. V. Sosnovtseva, P. Scherbakov and E. Mosekilde, Multimode dynamics in a network with resource mediated coupling, *Chaos*, 18, 015114-1-9, 2008.

[13] D. E. Postnov, A. G. Balanov and E. Mosekilde, Synchronization phenomena in an array of population dynamic systems, *Advances in Complex Systems*, 1, 181-202, 1998.

[14] O. E. Rössler, An equation for continuous chaos, *Physics Letters A*, 57, 397-398, 1976.

Manuscript M4:

C-type period-doubled transition in nephron autoregulation

Accepted for publication in the *Journal of Royal Society Interface Focus*.

Interface Focus

FirstCite® e-publishing

Interface Focus
doi:10.1098/rsfs.2010.0004
Published online

C-type period-doubling transition in nephron autoregulation

Jakob L. Laugesen[1,*], Erik Mosekilde[1] and Niels-Henrik Holstein-Rathlou[2]

[1]*Department of Physics, The Technical University of Denmark, 2800 Lyngby, Denmark*
[2]*Department of Biomedical Sciences, University of Copenhagen, 2200 Copenhagen N, Denmark*

The functional units of the kidney, called nephrons, utilize mechanisms that allow the individual nephron to regulate the incoming blood flow in response to fluctuations in the arterial pressure. This regulation tends to be unstable and to generate self-sustained oscillations, period-doubling bifurcations, mode-locking and other nonlinear dynamic phenomena in the tubular pressures and flows. Using a simplified nephron model, the paper examines how the regulatory mechanisms react to an external periodic variation in arterial pressure near a region of resonance with one of the internally generated mode-locked cycles. We show how the stable and unstable resonance cycles generated in this response undergo interconnected cascades of period-doubling bifurcations and how each period doubling leads to the formation of a new pair of saddle-node bifurcation curves along the edges of the resonance zone. We also show how period doubling of the resonance cycles is accompanied by a torus-doubling process in the quasiperiodic regime that exists outside of the resonance zone.

Keywords: nephron autoregulation; multi-mode dynamics; forced period-doubling system; C-type criticality; bifurcation analysis; torus doubling

1. INTRODUCTION

Living organisms operate under far-from-equilibrium conditions [1]. This implies that many of the feedback regulations that control the biological processes at different time and space scales are unstable and produce self-sustained oscillations and other complex nonlinear dynamic phenomena.

The regulation of the incoming blood flow to the individual functional unit of the kidney, for instance, involves at least two different mechanisms that tend to produce oscillatory dynamics [2,3]. The tubuloglomerular feedback (TGF) mechanism produces self-sustained oscillations in the 40 mHz regime because of a delay associated with the flow of fluid through the loop of Henle, and the myogenic mechanism produces vasomotoric oscillations in the 200 mHz regime in connection with the synchronized activation of the smooth muscle cells in the arteriolar wall in response to increasing transmural pressures. Detailed statistical analyses [4,5] have clearly shown how the oscillatory mechanisms interact to produce different forms of synchronization between the two modes. Similar analyses have revealed episodes of period-doubling dynamics in nearly 50 per cent of the available time series for normotensive rats. In rats with 2-kidney, 1-clip Goldblatt hypertension and in spontaneously hypertensive rats, one observes chaotic dynamics caused, presumably, by the combination of an increased sensitivity in the myogenic response and a stronger feedback gain for the TGF mechanism.

We have recently examined the bifurcation structure associated with the C-type period-doubling transition to chaos in a periodically forced Rössler oscillator [6,7]. This transition is characteristic of multi-dimensional systems where the period-doubling bifurcations take place in the presence of transitions between states of synchronized and non-synchronized dynamics. We have demonstrated how the stable (node) and unstable (saddle) cycles in the forced Rössler system undergo interconnected cascades of period-doubling bifurcations. Near the edge of the synchronization zone, node and saddle cycles with the same periodicity approach one another and at the very edge, the period-doubling bifurcations occur simultaneously. Away from the edge of synchronization, the node solution in the forced Rössler system tends to bifurcate first, i.e. for lower values of the parameter that controls the nonlinearity of the system. More importantly, however, these period doublings take place in a direction transverse to the unstable manifold of the saddle cycle that connects the resonance modes, and period-doubling transitions of the periodic modes are accompanied by a torus-doubling process in the quasiperiodic region outside the resonance zone.

Each pair of period-doubling bifurcations gives rise to a new set of saddle-node bifurcation curves along the sides of the resonance zone. As the period-doubling cascade unfolds, the edges of the resonance zone thus

*Author for correspondence (laugesen@fysik.dtu.dk).

One contribution to a Theme Issue 'Advancing systems medicine and therapeutics through biosimulation'.

Received 3 September 2010
Accepted 10 November 2010

accumulate more and more of almost parallel saddle-node bifurcation curves, each defining the boundaries of the resonance zone for a particular level of the interconnected period-doubling cascades. The new saddle-node bifurcation curves are supported by the corresponding period-doubling curves, but are formed a little away from the existing zone edge. This produces a gap between the saddle-node bifurcation curves, and additional local and global bifurcations are required to complete the zone boundary [7]. We have also demonstrated how the saddle-node bifurcations along the edge of the resonance zone accumulate and, in an alternating manner, approach a well-defined threshold curve for the transition between phase-synchronized chaos and non-synchronous chaos.

The purpose of the present paper is to demonstrate how a similar structure arises in a model of the physiological mechanisms by which the individual functional unit (nephron) of the kidney regulates the incoming blood flow to compensate for variations in arterial pressure arising, for instance, from changing levels of physical activity. As mentioned above, the individual nephron generates two different and clearly recognizable internal modes of oscillation. Interaction between these modes leads to a variety of additional nonlinear dynamic phenomena, including mode-locking, multistability, period doubling and transitions to deterministic chaos. Over the years, these phenomena have been extensively studied both in experiments on anaesthetized rats [2,8] and through model simulations [9,10]. In the frequency regime of interest for the present discussion, the nephron autoregulation functions as a mechanical high-pass filter: rapid fluctuations in arterial pressure are allowed to propagate into the tubular system, but the delicate regulatory processes that take place in the distal tubule are protected from more lasting variations.

After a short introduction to the considered nephron model [10,11] and a discussion of a few of the underlying experiments, the paper first presents a two-dimensional bifurcation diagram in order to clarify the organization of the internal modes in the physiologically relevant regime. We then apply an external periodic forcing and determine the resulting bifurcation structure as a function of the afferent arteriolar resistance and the frequency of the applied forcing. Although the details of the organization are somewhat different, we rediscover many of the characteristic features associated with the C-type criticality in the forced Rössler system: the interconnected cascades of period-doubling bifurcations for the resonant node and saddle cycles, the accumulation of saddle-node bifurcation curves along the edges of the resonance tongue, the gaps that open up between the saddle-node bifurcation curves and the torus-doubling process that takes place outside of the resonance zone.

2. NEPHRON PRESSURE AND FLOW REGULATION

It is well known that the kidneys function as a filter to remove metabolic end products and regulate the excretion of water and salts so as to maintain a proper volume and osmolality of the blood and appropriate conditions for the cells in general. The kidneys also play a part in the regulation of the blood pressure, both directly by controlling the extracellular fluid volume and through the production of hormones that, together with hormones from other organs, regulate the peripheral flow resistance of the vascular system. At the same time, to protect their own function, the individual nephrons in the kidney utilize two different mechanisms that can compensate for variations in the arterial blood pressure and maintain a relatively constant filtration rate.

The myogenic mechanism depends on the inherent propensity of the smooth muscle cells in the afferent arteriolar wall to contract in response to an increasing pressure difference across the arteriolar wall [3,12]. This contraction causes the flow resistance to increase and, hence, leads to lower glomerular pressure and reduced filtration. The TGF mechanism, on the other hand, depends on a signal from specialized cells (the macula densa cells) near the end of the loop of Henle. These cells respond to changes in the salt concentration in the fluid leaving the loop of Henle. A high rate of glomerular filtration will lead to a faster flow through the loop of Henle, to incomplete reabsorption of salt from the tubular fluid, and to increasing concentrations of salt at the macula densa. This produces a signal to the smooth muscle cells in the arteriolar wall to contract, thus causing the filtration to go down.

As mentioned above, experiments on rats [2,8] have demonstrated that the TGF mechanism is unstable and produces clearly detectable self-sustained oscillations in the tubular pressures and flows with periods in the 30–40 s range. This relatively long periodicity is directly related to the time of approximately 15 s that it takes for the tubular fluid to flow through the loop of Henle. The myogenic (or vasomotoric) mechanism is also capable of producing self-sustained oscillations through synchronization of the cytoplasmic Ca^{2+} dynamics among the smooth muscle cells in the arteriolar wall as the muscular activation increases [3,13]. As the entire signalling pathway for the myogenic mechanism is present with the individual smooth muscle cell, its response time is faster than that of the TGF mechanism. As a consequence, the corresponding myogenic oscillations have a period of only 5–10 s [14,15]. The two oscillatory modes both work through activation of the smooth muscle cells in the arteriolar wall. This allows the oscillations to interact and to produce mode-locking and other nonlinear dynamic phenomena [4,5]. The frequency ratios most commonly observed between the two modes are 1 :4, 1 : 5 and 1 : 6 [16].

The autoregulatory system involves a number of nonlinear relations. A main nonlinearity acting to constrain the amplitudes of the oscillatory modes is associated with the limited dynamic range for the arteriolar contraction. This range, which differs between normotensive and spontaneously hypertensive rats [14,15], can be determined through open-loop experiments where the rate of glomerular filtration is measured as a function of the rate of infusion of

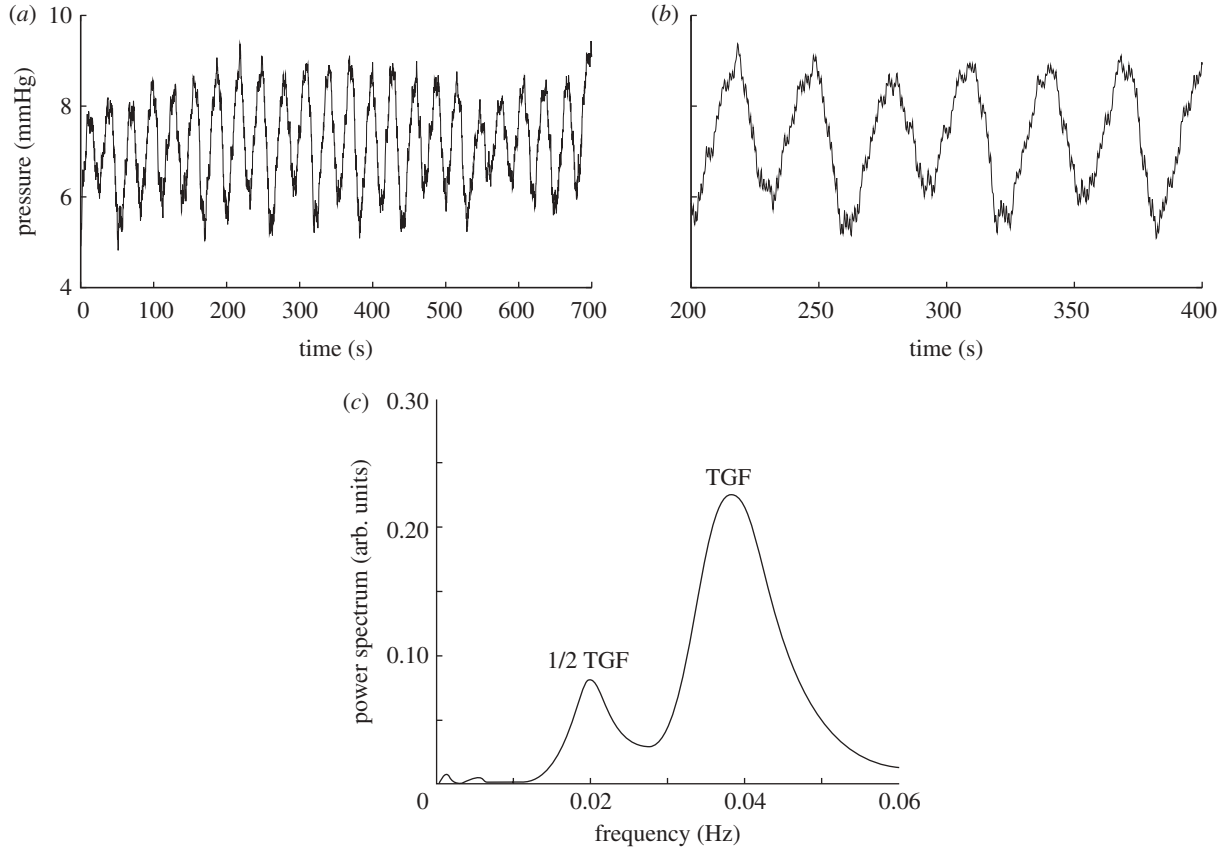

Figure 1. Experimental time series for the proximal tubular pressure in a normotensive rat. (*a*) Large amplitude oscillations caused by an instability in the tubuloglomerular feedback (TGF). (*b*) Alternating deep and shallow minima signalling that a period doubling has occurred. (*c*) Besides a strong peak at 40 mHz associated with the TGF frequency, the power spectrum also demonstrates the presence of a pronounced subharmonic component at 20 mHz.

artificial tubular fluid into the loop of Henle, while preventing flow through the proximal tubule by means of a wax seal [14,17]. The slope of this relation determines the feedback gain factor α for the TGF mode. This gain factor is typically 30–50% larger for spontaneously hypertensive rats than for rats with normal blood pressure [14,15]. Interaction between the two regulatory mechanisms is also found to be significantly stronger in hypertensive than in normotensive rats [5,18].

Figure 1 shows a typical example of the pressure oscillations observed in the proximal tubule of a normotensive rat. The mean tubular pressure in this experiment is about 7 mmHg. However, this pressure is modulated by relatively slow TGF-mediated oscillations with amplitudes of the order of 1–2 mmHg. The faster myogenic oscillations reveal themselves as a ripple on top of the TGF oscillations. Wavelet analysis clearly confirms their existence and can also detect how their amplitudes and frequencies are modified by the amplitude of the TGF oscillations [5]. Closer inspection of the time trace in figure 1*a* reveals an episode of period-2 dynamics, extending approximately from time 200 s to 500 s, where the tubular pressure alternates between shallow and deep minima. This part of the time trace is magnified in figure 1*b*. The spectral distribution shown in figure 1*c* also provides clear evidence for the presence of subharmonic components corresponding to half the frequency (or twice the period) of the TGF signal. Approximately 50 per cent of our time series for normotensive rats show evidence of period doubling.

The tubular pressure variations in hypertensive rats are much more irregular, even though the amplitudes are often smaller. This is illustrated for a spontaneously hypertensive rat in figure 2. The differences between the two types of dynamics can probably not be related to a single factor. We have already indicated that both the feedback gain and the interaction between the two regulatory modes are higher for hypertensive than for normotensive rats. It is also likely that the higher arterial pressure has shifted the working point on the TGF feedback curve and enhanced the sensitivity of the myogenic response. The main conclusions that can be drawn from the time series for hypertensive rats are that the myogenic component plays a stronger role, that synchronization between the two modes is less common, and that the experimentally observed pressure variations for most practical purposes can be considered as chaotic [18,19]. The spectral distribution in figure 2*c* demonstrates the presence of three to four subharmonic components to the TGF-mediated oscillation.

Over the years, a range of different experiments have been performed to determine the precise mechanisms underlying the two modes of oscillation [8,15,17] and to explicitly measure the different parameters and nonlinear relations. The proximal and distal tubule of superficial nephrons can be detected on the surface of

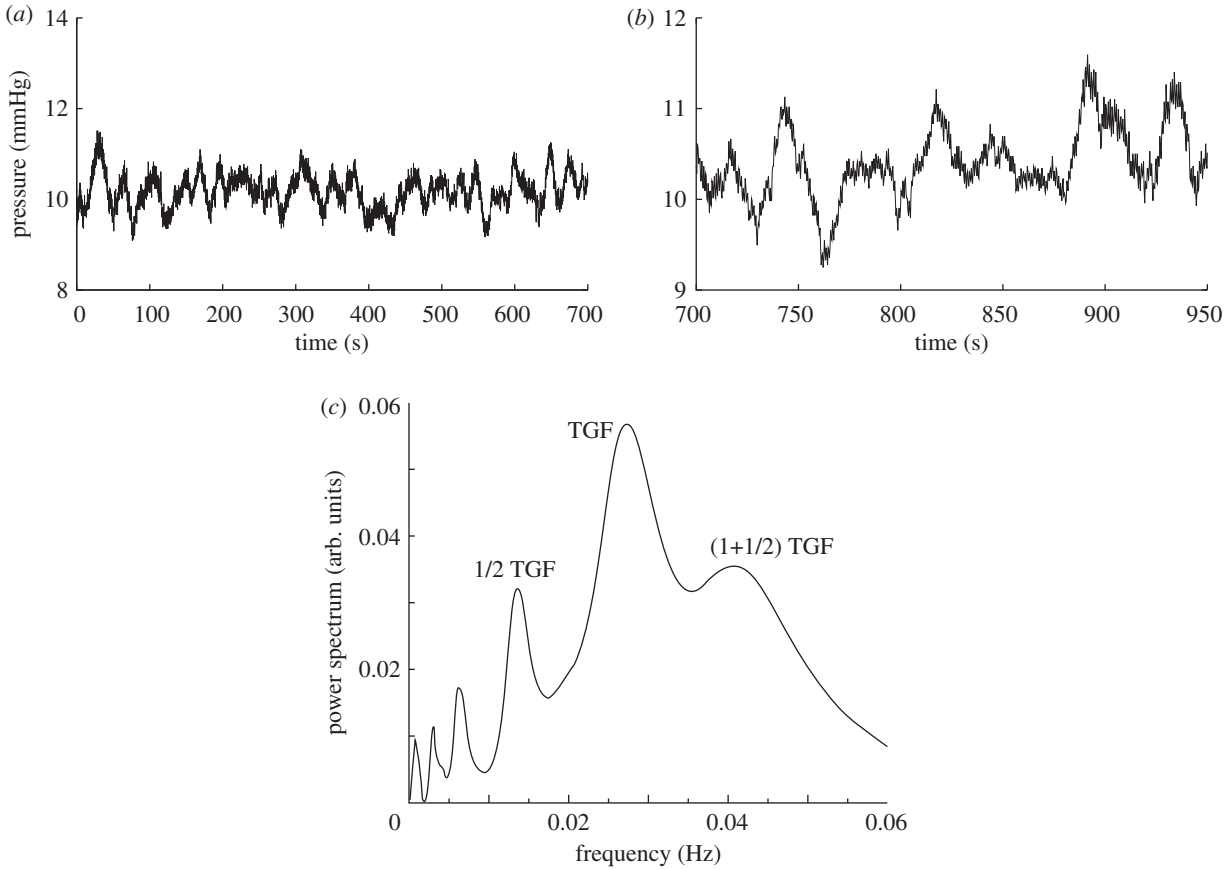

Figure 2. Experimental time series for the proximal tubular pressure in a spontaneously hypertensive rat. (*a*) The fast myogenic oscillations are strongly excited. (*b*) Magnified continuation of the time series in (*a*). Synchronization between the fast myogenic and slow TGF-mediated oscillations often does not occur. (*c*) The power spectrum shows a cascade of subharmonic components. Similar results are obtained for 2-kidney, 1-clip Goldblatt hypertensive rats [15,16].

the kidney and the tubular pressures can be measured by means of a small glass pipette [2]. It is also possible to examine the effect of a perturbation to the system by infusing artificial tubular fluid into the loop of Henle at rates of 5–10 nl min^{-1}. Besides open-loop experiments to measure the feedback relation, experiments have been performed to determine the tubular flow resistance, the damping of the pressure oscillations along the loop of Henle and the delay in the fluid flow [20]. Experiments have also been made to determine the amplitude and phase of the NaCl concentration oscillations near the macula densa and to determine the degree of cross-talk between neighbouring nephrons [21].

The ability of the renal autoregulation to handle external pressure fluctuations can be tested by applying a forcing signal to the arterial pressure while simultaneously recording the spectral distributions of the variations observed in this pressure and in the renal blood flow. In practice, the experiment can be performed [15] by connecting a computer-operated pump that generates broadband fluctuations at the distal end of the abdominal aorta through a blood-filled cannula.

Figure 3 shows an example of the frequency characteristics observed in such an experiment and covering the range from 1 mHz to 1 Hz. This characteristic clearly shows the damping of the pressure oscillations in the nephron blood flow at frequencies lower than 30 mHz. Also revealed are the resonances characteristic of the autoregulatory system: the relatively slow TGF mode at about 40 mHz and the faster myogenic mode around 200 mHz. We conclude that the nephron autoregulation functions as a high-pass filter that protects the nephron against more long-term variations in the arterial pressure. Fluctuations above the range of the myogenic oscillations are likely to be damped out by the dissipative processes associated with the fluid flow

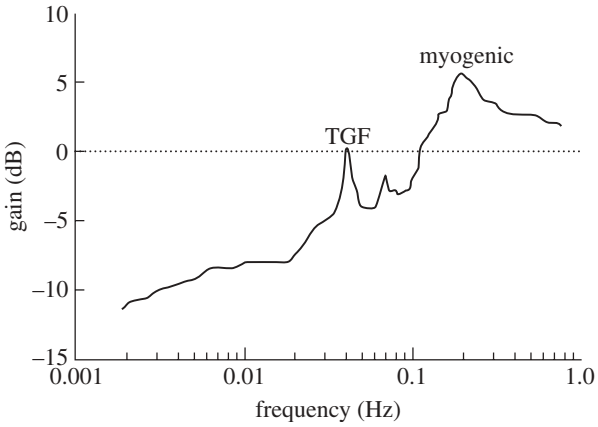

Figure 3. Frequency characteristic for the nephron autoregulation. This characteristic represents a high-pass filter with a low-frequency cut-off immediately below the frequency of the TGF-mediated oscillations. The high-frequency peak in the nephron autoregulation represents the myogenic oscillations.

through the loop of Henle. The TGF mechanism is unique to the nephrons. By virtue of the enormous blood flow that the kidneys have to handle, the TGF mechanism is required as a reinforcement of the myogenic mechanism. The frequency response of the TGF mechanism is restricted, though, by the delay in the Henle flow and, while reduced in amplitude by a factor of the order of two, the TGF oscillations are still present in the distal tubular pressure and salt concentration. By allowing the feedback to be oscillatory, the system presumably achieves the fastest possible reaction with the given delay.

3. SIMPLIFIED SINGLE NEPHRON MODEL

Together with the experimental work we have constructed a number of different models of the autoregulatory system [10,14,19,22]. These models each emphasize particular aspects of the problem such as, for instance, the absorption processes in the loop of Henle [2] or the mechanisms involved in the feedback from the macula densa cells to the smooth muscle cells in the arteriolar wall [22]. In the present paper, we shall use the simplified model described by Mosekilde *et al.* [11]. This model is particularly useful for more detailed bifurcation studies. The model integrates the most essential aspects of nephron autoregulation into a consistent picture and, over the years, it has been able to predict several phenomena that have subsequently been detected in the experimental data. The model has also been used to examine different types of nephron–nephron interaction [23–25].

The first component in the model is a simple conservation equation that relates changes in the proximal tubular pressure to the rate of glomerular filtration, the absorption in the proximal tubule and the flow into the loop of Henle. This is combined with a number of algebraic equations that determine the rate of glomerular filtration in terms of the arterial pressure and the afferent arteriolar resistance and determine the rate of flow into the loop of Henle in terms of the proximal tubular pressure, the distal pressure and the tubular flow resistance. Calculation of the rate of glomerular filtration also involves an equation that relates the protein osmotic pressure to the protein concentration in the arteriolar blood. The TGF-mediated variation in the afferent arteriolar resistance is determined from the measured open-loop feedback relation, but also includes a smooth delay to represent the time it takes for the fluid to pass the loop of Henle. Finally, we have applied a couple of first-order differential equations to simulate the myogenic mechanism that generates the fast oscillatory component. In the form we use the model here, these equations describe a damped oscillator, but the myogenic oscillations are continuously excited through the variation in the arteriolar resistance caused by the TGF mechanism.

Figure 4 shows a two-dimensional bifurcation diagram for the unforced nephron model in a parameter plane spanned by the delay time T in the loop of Henle and the gain factor α for the TGF mechanism.

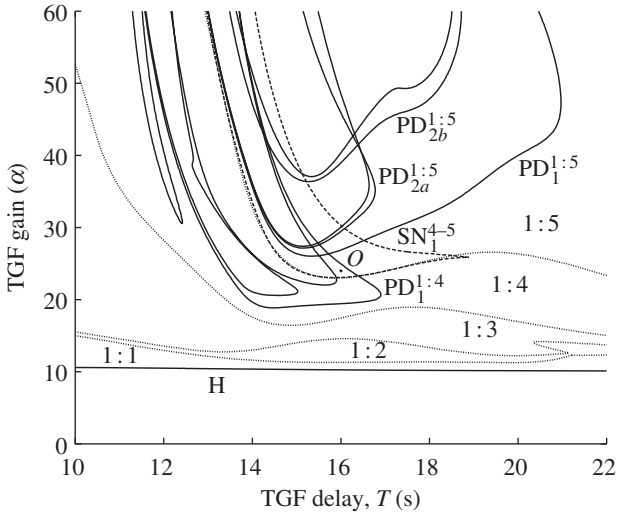

Figure 4. Two-dimensional bifurcation diagram for the unforced nephron model. The control parameters are the delay T and gain α in the TGF. The dotted curves delineate the regions of existence for different modes of synchronization between the fast myogenic and slower TGF-mediated oscillations. Fully drawn curves are period-doubling bifurcation curves and dashed curves are saddle-node bifurcation curves. The horizontal curve at $\alpha \approx 10$ is the Hopf bifurcation in which the TGF oscillations are born. The point O is the point of operation considered in the following numerical study.

Normal values for the feedback delay are about $T = 15$ s and, as defined in the model, the feedback gain factor is typically $\alpha = 10–15$ for normotensive rats and some 30–50% larger for spontaneously hypertensive rats. However, as explained above, other parameters also differ between the two strains of rats and it is, therefore, of interest to consider higher values of α where excitation of the myogenic oscillations becomes stronger.

The horizontal curve H at $\alpha \approx 10$ represents the Hopf bifurcation at which the onset of the TGF-mediated oscillations takes place. Below this curve, the nephron autoregulation displays a stable equilibrium point, and TGF-mediated oscillations do not occur. Experimentally, nephrons in normotensive rats are found to operate above, but relatively close to this threshold in most cases. As previously mentioned, the myogenic oscillations are assumed to be damped, but to be continuously excited by the TGF-mediated oscillations. The regions delineated by the dotted curves and denoted as 1 : 1, 1 : 2, 1 : 3, 1 : 4 and 1 : 5 represent the different regions of synchronization between the myogenic and the TGF-mediated oscillations. For small values of α, the myogenic oscillations lock directly into a 1 : 1 mode as one expects for a periodically driven oscillator at low amplitudes. As the gain factor increases, the excitation of the myogenic oscillator becomes stronger, and a shift to higher and higher excitation frequencies occurs. Double-wavelet analysis of the experimental data has confirmed that the most common frequency ratios under realistic conditions are 1 : 4 and 1 : 5 [4], i.e. the myogenic mode completes four or five oscillations each time the slower TGF-mediated mode completes one full period.

The fully drawn curves represent period-doubling bifurcations. In the middle of the figure, for instance, we observe two cascades of period-doubling bifurcations denoted $PD_1^{1:5}$, $PD_{2a}^{1:5}$, $PD_{2b}^{1:5}$, etc., for the 1 : 5 mode-locked solution. In a period-doubling bifurcation, an existing stable periodic motion loses its stability and is replaced by a stable motion that oscillates alternatingly between two different amplitudes (see, e.g. the experimental pressure trace in figure 1). At the curve $PD_1^{1:5}$, for instance, the synchronized 1 : 5 mode is replaced by a 2 : 10 mode in which the oscillation repeats itself only after two full TGF oscillations and 10 myogenic oscillations. This type of transition is common for nonlinear dynamic systems and often leads to a complete cascade of period-doubling bifurcations to deterministic chaos. We notice that mode-locking is maintained between the two oscillatory components during the period-doubling process.

A little to the left, the 1 : 4 mode-locked solution is found to undergo similar cascades of period-doubling bifurcations. The dashed curve denoted SN_1^{4-5} is a saddle-node (or fold) bifurcation curve that delineates the region of coexistence between the 1 : 4 and 1 : 5 mode-locked solutions. In this region, depending on the initial conditions, the model will approach a dynamics with either four myogenic oscillations per TGF oscillation or five myogenic oscillations per full cycle of the TGF oscillation. A saddle-node bifurcation in general denotes a transition in which a stable periodic motion (the node) appears or disappears through collision with an unstable cycle (the saddle) of the same periodicity. In the present case, the region of 1 : 5 dynamics extends all the way to the left-hand branch of SN_1^{4-5}, where the stable 1 : 5 cycle collides with an unstable 1 : 5 cycle. Similarly, the region of 1 : 4 dynamics extends all the way to the right-hand branch of SN_1^{4-5}.

4. PERIODICALLY FORCED NEPHRON

Let us now start to examine the response of the single nephron model to an externally applied periodic variation in the arterial pressure of the form

$$P_a(t) = P_{a,0}(1 + A\sin(\omega t)), \qquad (4.1)$$

where $P_{a,0} = 13.3$ kPa is the average arterial pressure. $A = 0.0075$ is the relative amplitude of the sinusoidal pressure variation and ω the angular frequency. This frequency is chosen to be close to the TGF frequency of the unforced system.

To be specific, we have chosen a point of operation O corresponding to a delay $T = 16$ s for the Henle flow and a gain factor $\alpha = 24$ in the TGF feedback (figure 4). With these parameters, the TGF-mediated oscillation has a period of about 40 s, corresponding to an angular frequency $\omega_0 = 0.155\ s^{-1}$. Moreover, the model operates in a regime where the 1 : 5 mode-locked solution for the two internally generated oscillations coexists with the 2 : 8 solution (i.e. with the 1:4 solution after its first period doubling). The forcing amplitudes that we can apply must, obviously, be fairly small both to avoid breaking up the mode-locking between the internally generated modes and to reduce the effect of mixing between the coexisting modes.

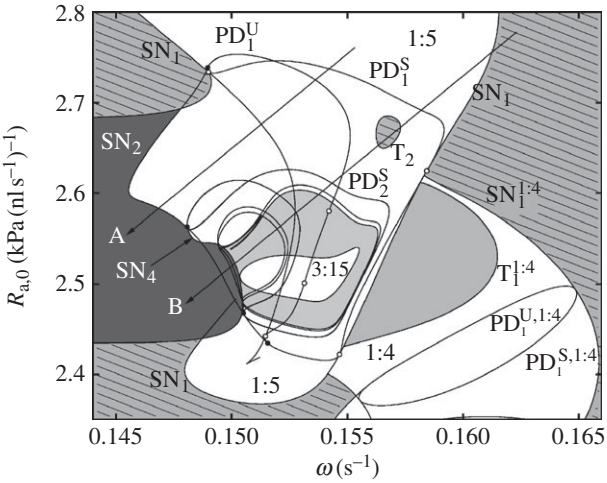

Figure 5. Two-dimensional bifurcation diagram for the forced nephron. Control parameters are the angular frequency ω of the forcing signal and the equilibrium value of the afferent arteriolar resistance $R_{a,0}$. White regions denote synchronized periodic dynamics, light grey regions mark phase-synchronized chaos and dark grey regions represent non-synchronous chaos. The region where quasiperiodic dynamics occurs is hatched.

Figure 5 provides an overview of the two-dimensional bifurcation diagram for the forced nephron model using the angular forcing frequency ω and the equilibrium value of the afferent arteriolar resistance $R_{a,0}$ as control parameters. We recall that the instantaneous value of the afferent resistance is the variable through which both the myogenic and the TGF-mediated regulations are effectuated.

The first thing to notice when inspecting figure 5 is the different shading we have applied to distinguish among different types of dynamics. White denotes synchronized periodic dynamics, i.e. in the white regions the internally generated mode-locked solutions synchronize with the externally applied forcing signal. This synchronization involves either the internally generated 1 : 5 periodic solution (in the middle of the figure) or the internally generated 1 : 4 solution (in the lower right corner of the figure). Hatched light grey areas are regions with ergodic two-mode dynamics (quasiperiodicity), while the light grey regions represent phase-synchronized chaos. In the region of ergodic two-mode dynamics (quasiperiodicity), the internally generated 1 : 4 (or 1 : 5) mode fails to synchronize with the external forcing signal. The result is a type of motion that never repeats itself but gradually fills out a two-dimensional torus surface in phase space. In the region of phase-synchronized chaos, the system displays dense sets of unstable periodic solutions, but in such a manner that all of these solutions are synchronized with the external forcing [11,26,27]. Finally, the dark grey areas to both sides of the 1 : 5 synchronization zone represent non-synchronous chaos. The curves denoted T are torus bifurcation curves where the periodic solution loses stability as two complex conjugated eigenvalues cross out of the unit circle, and quasiperiodic dynamics results.

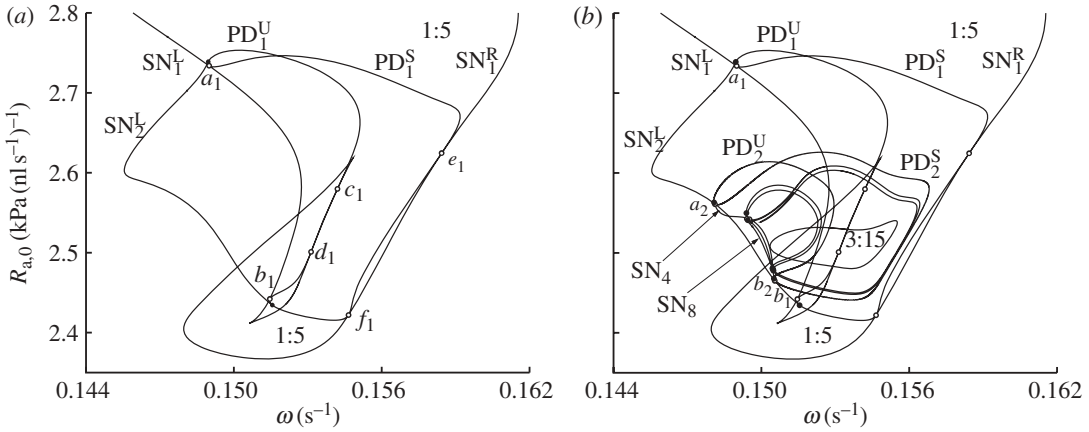

Figure 6. Basic bifurcation structure for the 1 : 5 resonance region. (*a*) The first few bifurcation curves. (*b*) The period-doubling cascade along the edge of the synchronization zone. SN_1^L and SN_1^R are the saddle-node bifurcation curves that delineate the region of existence for the 1 : 5 synchronized modes. PD_1^S and PD_1^U are period-doubling curves at which the stable 1 : 5 node solution, respectively, the 1 : 5 saddle solution, undergo their first period-doubling bifurcation. The saddle-node bifurcation curve SN_2 delineates the range of existence for the 2 : 10 solutions.

The following discussion will focus on the bifurcations observed for the internally synchronized 1 : 5 mode. Hence, we have dropped the superscript 1 : 5 on the bifurcation curves that relate to this mode and retained only the subscripts 1, 2, 4, etc., to denote the periodicity of the bifurcating mode relative to the forcing signal. For the period-doubling curves, superscript S denotes a period doubling of a stable cycle (node) and superscript U denotes period doubling of an unstable cycle (saddle).

Before we leave the 1 : 4 mode, let us note that the region in figure 5 where this mode synchronizes with the external forcing continues to exist in the part of the region of resonance with the 1 : 5 mode. We also notice that the torus arising in the torus bifurcation $T_1^{1:4}$ destroys almost immediately and gives rise to synchronized chaotic dynamics. Besides, by this torus bifurcation, the visible part of the 1 : 4 synchronization regime is primarily delineated by the saddle-node bifurcation curve $SN_1^{1:4}$. At this saddle-node bifurcation, a pair of 1 : 4 saddle and stable node cycles is born. The saddle cycle undergoes a period-doubling bifurcation at $PD_1^{U,1:4}$, and the node doubles its period when crossing the curve $PD_1^{S,1:4}$ in the downward direction. Together, these two curves form a closed period-doubling curve that is tangent to the edge of the resonance zone on both sides. Below $PD_1^{S,1:4}$, period doubling of the 1 : 4 stable node and saddle solution continues (not shown) in a manner similar to the development described below for the 1 : 5 modes.

To better understand the bifurcation structure for the region in parameter space where the internally generated 1 : 5 mode-locked solution synchronizes with the external forcing, we have drawn the simplified bifurcation diagrams reproduced as figure 6*a*,*b*. Along its left-, respectively, right-hand side, the 1 : 5 synchronization regime is primarily delineated by the two branches SN_1^L and SN_1^R of the saddle-node bifurcation curve SN_1. In the projection shown in the figure, this curve displays an extra fold structure, causing some added complexity to the variation of the stability of the 1 : 5 synchronized mode.

At the boundary of the resonance zone, a pair of saddle and stable node 1 : 5 mode-locked solutions arises. If we follow the development along the main diagonal starting in the upper right corner, the stable 1 : 5 solution undergoes its first period doubling at the curve PD_1^S, and the saddle solution doubles its period at PD_1^U. The two branches of the period-doubling curve meet at the points a_1 and b_1, where the curve is tangent to the saddle-node bifurcation curve SN_1^L. Close to the saddle-node bifurcation curve, the 1 : 5 node and saddle cycles approach one another, and at the very edge of the synchronization regime, the period-doubling bifurcations of the node and saddle solutions occur simultaneously. The points denoted a_1 and b_1 (open circles) are thus so-called codimension-2 points in which two Floquet multipliers simultaneously cross the unit circle, one through +1 and one through −1. (The Floquet multipliers measure the rates at which neighbouring trajectories approach or move away from a given periodic orbit. A Floquet multipler that exceeds 1 in numerical value signals instability. A Floquet multipler of +1 indicates a saddle-node bifurcation and a multiplier of −1 indicates a period-doubling bifurcation.)

To the left of the period-doubling curves PD_1^S and PD_1^U, the system, besides a saddle and a doubly unstable 1 : 5 node solution, displays a pair of saddle and stable node 2 : 10 solutions. The region of existence for the 1 : 5 cycles continues to be delineated by SN_1^L and SN_1^R. To bound the range of existence for the two 2 : 10 cycles, a new saddle-node bifurcation curve SN_2^L is born. This saddle-node bifurcation curve is supported by the period-doubling curves PD_2^S and PD_2^U in points (full circles) close to, but not coinciding with a_1 and b_1. We shall return to the detailed bifurcation structure around these points in §5.

Closer inspection of figure 6*a* shows that the period-doubling curves PD_1^S and PD_1^U together have four additional points of tangency with the saddle-node bifurcation curve SN_1, denoted c_1, d_1, e_1 and f_1. The presence of these points gives rise to further complexity in the bifurcation structure. However, this complexity is

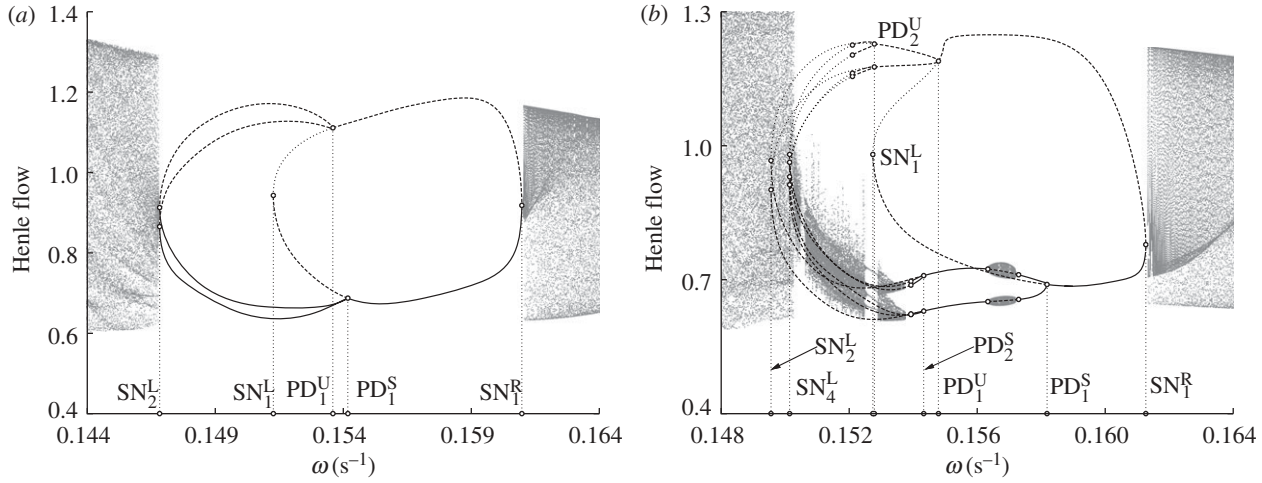

Figure 7. One-dimensional bifurcation scans along the directions A and B shown in figure 5*a*. (*a*) Direction A: the node and saddle $1:5$ resonance cycles arising in SN_1^R undergo period-doubling bifurcations at PD_1^S and PD_1^U, respectively, to subsequently disappear in the saddle-node bifurcation SN_1^L. The $2:10$ resonance cycles produced in the period-doubling bifurcations disappear in the saddle-node bifurcation SN_2^L, producing a period-2 ergodic torus. (*b*) Direction B: both cycles undergo a complete period-doubling cascade first leading to phase-synchronized chaos and subsequently to non-synchronous chaos. Only the first three period-doubling bifurcations of the infinite cascades are shown.

not directly in the focus of the present study. Hence, we shall not discuss the bifurcations here, but only mention that the full analysis includes various torus birth bifurcations in which the number of unstable directions for the involved cycles is adjusted up or down by two. These processes are similar in several respects to the processes we shall discuss in §5.

As illustrated in figure 6*b*, the stable $2:10$ cycle undergoes a new period doubling at PD_2^S, and the $2:10$ saddle solution period doubles at PD_2^U. The two branches of the second period-doubling curve meet at the points a_2 and b_2 on the saddle-node bifurcation curve SN_2^L, where the node and saddle $2:10$ cycles simultaneously period-double, merge and disappear. We can hereafter follow the repetition of the same process through a complete period-doubling cascade and via a region of phase-synchronized chaos (figure 5) to the large period-3 window (denoted $3:15$) in the middle of the figure. Each time a pair of saddle and stable node cycles period-double, a new saddle-node bifurcation curve arises to delineate the range of existence for the period-doubled cycles.

To illustrate the results of the above discussion, figure 7*a*,*b* shows a couple of one-dimensional bifurcation diagrams obtained by scanning across the $1:5$ synchronization regime along the lines A and B in figure 5. Following the transitions observed in figure 7*a* from right to left, we first observe the formation of a pair of saddle (dashed curve) and stable node (solid curve) $1:5$ cycles from the ergodic torus that exists to the right of the saddle-node bifurcation curve SN_1^R. At PD_1^S, the stable node cycle undergoes a period-doubling bifurcation, and at PD_1^U, the $1:5$ saddle cycle suffers a similar bifurcation. At SN_1^L, the two $1:5$ modes (now a saddle and a doubly unstable node) merge and disappear. The $2:10$ saddle and stable node cycles continue to the saddle-node bifurcation SN_2^L where they merge and disappear. It is interesting to note that the ergodic torus formed in this process is a period-doubled torus [28,29]. As discussed below, we generally expect the merger and disappearance of a pair of period-2^n ($n = 0,1,2\ldots$) saddle and stable node cycles to produce an ergodic torus that has the same periodicity. In many cases, the range of existence for these period-doubled tori is very narrow. They tend to disintegrate into non-synchronous chaos a little away from the resonance zone.

The processes observed along scan line B in figure 7*b* initially follow the same pattern as those along scan line A. After period doubling of the stable $1:5$ node at PD_1^S, there is a small interval with ergodic torus dynamics (quasiperiodicity) before the stable period $2:10$ node proceeds through a complete period-doubling cascade to phase-synchronized chaos. The resonant $1:5$ saddle cycle undergoes its first period doubling at PD_1^U and thereafter completes a period-doubling cascade leading to a dense set of doubly unstable nodes. In the mean time, the doubly unstable $1:5$ node and the $1:5$ saddle cycle produced in the period-doubling processes PD_1^U and PD_1^S merge and disappear in the saddle-node bifurcation SN_1^L, and the doubly unstable $2:10$ node and the $2:10$ saddle cycle produced in PD_2^U and PD_2^S have merged and disappeared in the saddle-node bifurcation SN_2^L. Similarly, as we approach the left edge of the synchronization regime, many of the other solutions produced in the interconnected period-doubling cascades gradually merge and disappear, leading the system into a state of non-synchronous chaos.

Figure 8 illustrates the phenomenon of torus doubling [28,29]. Here we have plotted simultaneous values of the Henle flow and the proximal tubular pressure as determined from a sequence of Poincaré sections of the ergodic torus that exists along the outside edge of the resonance zone a little to the left of the point b_1 where the first period-doubling curve PD_1 is tangent to the saddle-node bifurcation curve SN_1^L. The equilibrium value of the afferent arteriolar flow resistance $R_{a,0}$ is used as a bifurcation parameter, and

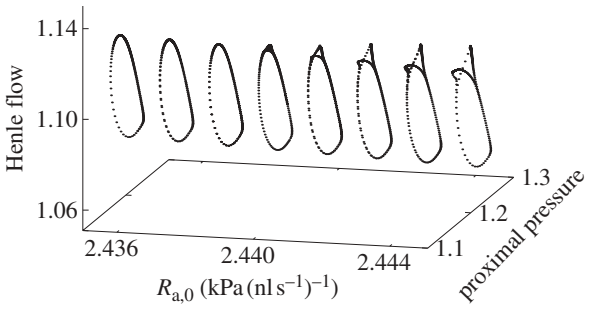

Figure 8. Torus doubling along the outside edge of the resonance zone. Using the equilibrium value of the afferent arteriolar resistance $R_{a,0}$ as a parameter, the figure shows a set of Poincaré sections in the quasiperiodic regime immediately to the left of the point b_1 in figure 5. The two variables—the proximal tubular pressure and the rate of flow into the distal tubule—are both in relative units ($\omega = 0.1505 \text{s}^{-1}$).

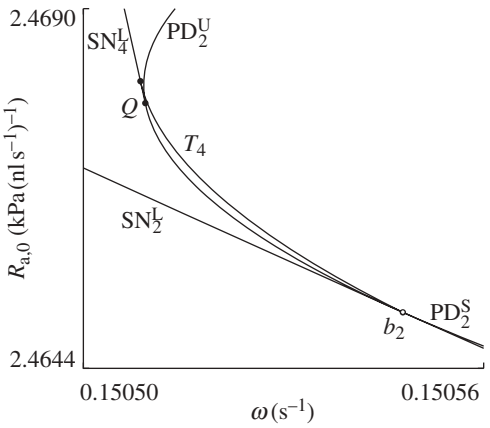

Figure 9. Two-dimensional bifurcation diagram near the point of tangency b_2 between PD_2 and SN_2^L. The diagram illustrates how the new saddle-node bifurcation curve SN_4^L emerges from a point Q away from b_2. Also shown is the torus bifurcation curve T_4 that covers the gap between the two saddle-node bifurcation curves.

the angular frequency of the forcing signal is kept constant at $\omega = 0.1505\ \text{s}^{-1}$. To the left in the figure, i.e. for $R_{a,0} < 2.44$ kPa (nl s^{-1})$^{-1}$, we observe the cross-section of a normal ergodic torus with points distributed along a closed invariant curve. As we increase the arterial resistance $R_{a,0}$, the return points of the trajectory alternatingly follow two different loops of a period-doubled invariant curve.

5. DETAILS OF THE BIFURCATION STRUCTURE

The bifurcation diagram in figure 5 includes a considerable number of additional details, some of which are generic for the C-type period-doubling transition while others are specific for the considered model. Among the generic aspect is the fact that the new saddle-node bifurcation curves that emerge after a period-doubling bifurcation of a pair of saddle and stable node cycles emanate in points of the period-doubling curves close to, but not in the points of tangency with the previous saddle-node bifurcation curves. To illustrate this, figure 9 shows an enlargement of a part of the bifurcation diagram around the point b_2 in figure 6*b*. We notice how the saddle-node bifurcation curve SN_4^L emerges from a point Q on the unstable branch of the period-doubling curve PD_2 different from the point of tangency b_2 with SN_2^L. A little above Q we observe another point (closed circle). This is the point in which the torus bifurcation curve T_4 that bridges between SN_2^L and SN_4^L is supported by SN_4^L.

As described above, the saddle-node bifurcation curve SN_2^L delineates the range of existence for cycles with 2:10 mode-locking. Below b_2, a pair of 2:10 saddle and stable node cycles are born as the system crosses through SN_2^L from left to right. Above b_2, the pair of 2:10 saddle and doubly unstable node cycles arising from the period-doubling bifurcations PD_2^S and PD_2^U merge and disappear as the system passes through SN_2^L from right to left. SN_4^L similarly delineates the range of existence for solutions with 4:20 mode-locking. The gap between the two saddle-node bifurcation curves would allow 4:20 mode-locked solutions to escape from the synchronization regime had it not been for the presence of the supercritical torus bifurcation curve T_4. At this curve, the stable 4 : 20 cycle (now of focus type) looses its stability as two complex conjugated eigenvalues cross out of the unit circle and a period-4 ergodic torus is formed. The doubly unstable 4 : 20 cycle (now again a node) subsequently undergoes a reverse period-doubling bifurcation at PD_2^U, and the doubly unstable 2 : 10 node produced disappears in the saddle-node bifurcation SN_2^L.

Similar phenomena take place in the neighbourhood of other codimension-2 points. In some cases, the torus bifurcation is subcritical and accompanied by a torus fold bifurcation. The saddle-node bifurcation curve SN_4 that delineates the region of stable period-4 dynamics arises from a point on the stable branch of PD_2. The saddle-node bifurcation curve SN_8 hereafter emerges from a point on the unstable branch of PD_4, and the saddle-node bifurcation curve SN_{16} emerges from a point on the stable branch of PD_8. In general, we find that the point of emergence for a new saddle-node bifurcation curve tends to alternate through the period-doubling cascade between the stable and unstable branches of the period-doubling curves. Moreover, if the saddle-node bifurcation curve in one side of the period-doubling curves emanates from the stable branch, the saddle-node bifurcation curve at the other side emanates from the unstable branch. As the cascade of period-doubling bifurcations unfold, more and more saddle-node bifurcation curves accumulate along the edge of the resonance zone. Except for the first few saddle-node bifurcation curves, this accumulation process takes place in an alternating manner and leads to a limiting curve that delineates the existence of phase-synchronized chaos.

6. DISCUSSION

The formulation of dynamic and mechanism-based descriptions of living systems represent an enormous

challenge, not only to the biological sciences, but also to mathematics, physics and computer science. Part of this challenge arises from the fantastic number of different processes and feedback mechanisms involved in the regulation of the biological functions and the extraordinary ranges of time and space over which this regulation is maintained. Another contribution derives from the heterogeneity of biological tissues and structures. In the years to come, the biological sciences are likely to become an important test bed for the development of new advanced concepts and approaches in mathematics as well as in physics.

However, as emphasized in §1, an additional source of complexity derives from the fact that living systems operate under far-from-equilibrium conditions. This implies that many feedback regulations are unstable and produce self-sustained oscillatory dynamics. Nonlinearity in the feedback and interaction between the oscillatory processes give rise to even more complicated dynamics in the form, for instance, of period-doubling transitions or transitions between different forms of resonance dynamics. The cells and organs make use of these complex phenomena both to regulate their internal processes and as a means to communicate with other cells and organs.

Nephron autoregulation can be viewed as a set of mechanisms that serve to protect the delicate processes in the distal tubule from fluctuations in the arterial pressure. Experimental studies applying broadband random perturbations to the arterial pressure have shown [15] that the regulation works as a high-pass filter that provides damping for arterial pressure variations slower than the response time of the TGF regulation. However, experimental studies also show that the two mechanisms involved in nephron autoregulation—the myogenic and the TGF mechanism—both produce oscillatory dynamics and that coupling between these oscillations and nonlinearity in the systems produce both mode-locking and period-doubling transitions.

Recent theoretical analyses have shown that the period-doubling transition to chaos along the edge of a resonance zone displays an unusual organization and scaling behaviour, denoted as cyclic or C-type criticality [30]. It is also known that forced period-doubling systems may be associated with the appearance of period-doubled ergodic tori along the outside edge of the resonance zone. This phenomenon was first observed by Arnéodo *et al.* [28] and by Kaneko [29] who found torus doubling both for multi-dimensional maps and for time-continuous systems and described, for instance, how a finite number of torus-doubling bifurcations can lead to chaotic dynamics. More recently, Sekikawa *et al.* [31] have demonstrated the transition to chaos through a series of subsequent torus-doubling bifurcations in an electronic circuit, and Sekikawa *et al.* [32] have illustrated the occurrence of torus-doubling bifurcations in coupled logistic and sine-circle maps.

Kuznetsov and co-workers [30,33,34] determined the scaling relations for the period-doubling process along the edge of an Arnold tongue, and Kuznetsov [35] examined a number of related problems, including the effect of noise on the dynamics near the torus-doubling terminal point for a quadratic map subjected to quasiperiodic forcing. To our knowledge, however, no realistic example of this type of behaviour has so far been described, and the associated bifurcation structure still remains largely unexplored.

Using a simplified nephron model, we have performed a detailed analysis of the response of the regulatory system to variations of the arterial pressure with periods close to the period of the TGF-mediated oscillations. To our knowledge, this analysis also represents the first study of a C-type period-doubling transition in a realistic system. This transition, which is generic for forced period-doubling systems [30], is characterized both by a particular bifurcation structure and by specific scaling relations.

The bifurcation structure involves a cascade of simultaneously occurring saddle-node and period-doubling bifurcations on the edge of the synchronization zone. At the same time, one can observe the process of torus doubling along the outside boundary of this zone. Each pair of period-doubling bifurcations of the resonant saddle and stable node solutions leads to the formation of a new pair of saddle-node bifurcations along the zone edge. These saddle-node bifurcation curves arise from points on the period-doubling curves away from the points of tangency with the previously formed saddle-node bifurcation curves. This leaves a gap in the zone edge, a gap that is closed by either a sub- or a supercritical torus bifurcation curve. In the case of a subcritical torus bifurcation, this will in general be accompanied by a global (torus fold) bifurcation. In this way, the stable resonance node and the corresponding saddle cycle always communicate with an ergodic torus of the same periodicity across the edge of the resonance zone.

As the period-doubling cascade unfolds, more and more saddle-node bifurcations accumulate along the zone boundary. In accordance with the scaling theory [30], our detailed simulations indicate that this accumulation takes place in an alternating manner and in the limit leads to a well-defined curve that delineates the region of phase-synchronized chaos from that of non-synchronous chaos.

The presence of noise in the biological system will obviously wash out some of the finer details in the bifurcation structure. However, double-wavelet analysis and other effective statistical methods have allowed us to clearly demonstrate the existence both of episodes of period-doubling behaviour and of intra-nephron synchronization in the temporal variation of the proximal tubular pressure [5]. Transitions between different states of dynamics may represent elements in the normal physiological regulation or they may signal the development of a disease. Some types of hypertensive rats, for instance, are clearly distinct in their tubular pressure dynamics as well as in their intra- and inter-nephron synchronization behaviours.

We thank A. N. Pavlov for performing the wavelet analyses of the tubular pressure variations. The project was sponsored by the European Union through the Network of Excellence BioSim (contract no. LSHB-CT-2004-005137).

REFERENCES

1 Nicolis, G. & Prigogine, I. 1977 *Self-organization in nonequilibrium systems*. New York, NY: Wiley.
2 Holstein-Rathlou, N.-H. & Leyssac, P. P. 1986 TGF-mediated oscillations in the proximal intratubular pressure: differences between spontaneously hypertensive rats and Wistar-Kyoto rats. *Acta Physiol. Scand.* **126**, 333–339. (doi:10.1111/j.1748-1716.1986.tb07824.x)
3 Gustafsson, H., Bulow, A. & Nilsson, H. 1994 Rhythmic contractions of isolated, pressurized small arteries from rat. *Acta Physiol. Scand.* **152**, 145–152. (doi:10.1111/j.1748-1716.1994.tb09794.x)
4 Sosnovtseva, O. V., Pavlov, A. N., Mosekilde, E. & Holstein-Rathlou, N.-H. 2002 Bimodal oscillations in nephron autoregulation. *Phys. Rev. E* **66**, 061909. (doi:10.1103/PhysRevE.66.061909)
5 Sosnovtseva, O. V., Pavlov, A. N., Mosekilde, E., Holstein-Rathlou, N.-H. & Marsh, D. J. 2004 Double-wavelet approach to study frequency and amplitude modulation in renal autoregulation. *Phys. Rev. E* **70**, 031915. (doi:10.1103/PhysRevE.70.031915)
6 Zhusubaliyev, Zh. T., Laugesen, J. L. & Mosekilde, E. 2010 From multi-layered resonance tori to period-doubled ergodic tori. *Phys. Lett. A* **374**, 2534–2538. (doi:10.1016/j.physleta.2010.04.022)
7 Laugesen, J. K., Mosekilde, E. & Zhcusubaliyev, Zh. T. 2010 Bifurcation structure of the C-type period-doubling transition. *Physica D.*
8 Holstein-Rathlou, N.-H., Wagner, A. J. & Marsh, D. J. 1991 TGF dynamics and renal blood flow autoregulation in rats. *Am. J. Physiol.* **260**, F53–F68.
9 Holstein-Rathlou, N.-H. & Marsh, D. J. 1990 A dynamic model of tubuloglomerular feedback mechanism. *Am. J. Physiol.* **258**, F1448–F1459.
10 Barfred, M., Mosekilde, E. & Holstein-Rathlou, N.-H. 1996 Bifurcation analysis of nephron pressure and flow regulation. *Chaos* **6**, 280–287. (doi:10.1063/1.166175)
11 Mosekilde, E., Maistrenko, Yu. & Postnov, D. 2002 *Chaotic synchronization: applications to living systems*. Singapore: World Scientific.
12 Davis, M. J. & Hill, M. A. 1999 Signalling mechanisms underlying the vascular myogenic response. *Physiol. Rev.* **79**, 387–423.
13 Jacobsen, J. C. B., Aalkjær, C., Matchkov, V. V., Nilsson, H., Freiberg, J. J. & Holstein-Rathlou, N.-H. 2008 Heterogeneity and weak coupling may explain the synchronization characteristics of cells in the arterial wall. *Phil. Trans. R. Soc. A* **366**, 3483–3502. (doi:10.1098/rsta.2008.0105)
14 Holstein-Rathlou, N.-H. 1993 Oscillations and chaos in renal blood flow control. *J. Am. Soc. Nephrol.* **4**, 1275–1287.
15 Holstein-Rathlou, N.-H. & Marsh, D. J. 1994 Renal blood flow regulation and arterial pressure fluctuations: a case study in nonlinear dynamics. *Physiol. Rev.* **74**, 637–681.
16 Pavlov, A. N., Sosnovtseva, O. V., Pavlova, O. N., Mosekilde, E. & Holstein-Rathlou, N.-H. 2008 Characterizing multimode interaction in renal autoregulation. *Physiol. Meas.* **29**, 945–958. (doi:10.1088/0967-3334/29/8/007)
17 Moore, L. C. 1984 Tubuloglomerular feedback and SNGFR autoregulation in the rat. *Am. J. Physiol. Renal Physiol.* **247**, F267–F276.
18 Sosnovtseva, O. V., Pavlov, A. N., Mosekilde, E., Yip, K.-P., Holstein-Rathlou, N.-H. & Marsh, D. J. 2007 Synchronization among mechanisms of renal autoregulation is reduced in hypertensive rats. *Am. J. Physiol. (Renal Physiol.)* **293**, F1545–F1555. (doi:10.1152/ajprenal.00054.2007)
19 Jensen, K. S., Mosekilde, E. & Holstein-Rathlou, N.-H. 1986 Self-sustained oscillations and chaotic behaviour in kidney pressure regulation. *Mondes Dev.* **54**, 91–109.
20 Holstein-Rathlou, N.-H. & Marsh, D. J. 1989 Oscillations in tubular pressure, flow and distal chloride concentration in rats. *Am. J. Physiol.* **256**, F1007–F1014.
21 Holstein-Rathlou, N.-H. 1987 Synchronization of proximal intratubular pressure oscillations: evidence for interactions between nephron. *Pflügers Arch.* **408**, 438–443. (doi:10.1007/BF00585066)
22 Laugesen, J. K., Sosnovtseva, O. V., Mosekilde, E., Holstein-Rathlou, N.-H. & Marsh, D. J. 2010 Coupling induced complexity in nephron models of renal blood flow regulation. *Am. J. Physiol.* **298**, R997–R1006.
23 Holstein-Rathlou, N.-H., Yip, K.-P., Sosnovtseva, O. V. & Mosekilde, E. 2001 Synchronization phenomena in nephron-nephron interaction. *Chaos* **11**, 417–426. (doi:10.1063/1.1376398)
24 Postnov, D. E., Sosnovtseva, O. V. & Mosekilde, E. 2005 Oscillator clustering in a resource distribution chain. *Chaos* **15**, 013704. (doi:10.1063/1.1852151)
25 Marsh, D. J., Sosnovtseva, O. V., Mosekilde, E. & Holstein-Rathlou, N.-H. 2007 Vascular coupling induces synchronization, quasiperiodicity and chaos in nephron tree. *Chaos* **17**, 15114. (doi:10.1063/1.2404774)
26 Rosenblum, M. G., Pikovsky, A. S. & Kurths, J. 1996 Phase synchronization of chaotic oscillators. *Phys. Rev. Lett.* **76**, 1804–1807. (doi:10.1103/PhysRevLett.76.1804)
27 Rosa, E., Ott, E. & Hess, M. H. 1998 Transition to phase synchronization of chaos. *Phys. Rev. Lett.* **80**, 1642–1645. (doi:10.1103/PhysRevLett.80.1642)
28 Arnéodo, A., Coullet, P. H. & Spiegel, E. A. 1983 Cascade of period doublings of tori. *Phys. Lett. A* **94**, 1–6. (doi:10.1016/0375-9601(83)90272-4)
29 Kaneko, K. 1983 Doubling of torus. *Progr. Theor. Phys.* **69**, 1806–1810. (doi:10.1143/PTP.69.1806)
30 Kuznetsov, S. P., Kuznetsov, A. P. & Sataev, I. R. 2005 Multiparameter critical situations, universality and scaling in two-dimensional period-doubling maps. *J. Stat. Phys.* **121**, 697–748. (doi:10.1007/s10955-005-6973-6)
31 Sekikawa, M., Miyoshi, T. & Inaba, N. 2001 Successive torus doubling. *IEEE Trans. Circ. Syst. I* (*Fundam. Theory Appl.*) **48**, 28–34. (doi:10.1109/81.903185)
32 Sekikawa, M., Inaba, N., Yoshinaga, T. & Tsubouchi, T. 2006 Bifurcation structure of successive torus doubling. *Phys. Lett. A* **348**, 187–194. (doi:10.1016/j.physleta.2005.08.089)
33 Kuznetsov, A. P., Kuznetsov, S. P. & Sataev, I. R. 1997 A variety of period-doubling universality classes in multi-parameter analysis of transition to chaos. *Physica D* **109**, 91–112. (doi:10.1016/S0167-2789(97)00162-0)
34 Kuznetsov, S. P. & Sataev, I. R. 2001 Universality and scaling for the breakup of phase synchronization at the onset of chaos in periodically driven Rössler oscillator. *Phys. Rev. E* **64**, 046214. (doi:10.1103/PhysRevE.64.046214)
35 Kuznetsov, S. P. 2005 Effect of noise on the dynamics of the torus-doubling terminal point in a quadratic map under quasiperiodic driving. *Phys. Rev. E* **72**, 026205. (doi:10.1103/PhysRevE.72.026205)

Manuscript M5:

Synchronization of period-doubling oscillations in multi-dimensional systems

---

Submitted to *Chaos*.

Synchronization of period-doubling oscillations in vascular coupled nephrons

J. L. Laugesen,[1, a)] E. Mosekilde,[1, b)] and Niels-Henrik Holstein-Rathlou[2, c)]
[1)] *Department of Physics, The Technical University of Denmark, 2800 Lyngby, Denmark*
[2)] *Department of Biomedical Sciences, University of Copenhagen, 2200 Copenhagen N, Denmark*

(Dated: 29 November 2010)

The mechanisms by which the individual functional unit (nephron) of the kidney regulates the incoming blood flow give rise to a number of nonlinear dynamic phenomena, including period-doubling bifurcations and intra-nephron synchronization between two different oscillatory modes. Interaction between the nephrons produces complicated and time-dependent inter-nephron synchronization patterns. In order to understand the processes by which a pair of vascular coupled nephrons synchronize we have performed a detailed analysis of the bifurcations that occur at the threshold of synchronization. We have shown that these transitions involve infinite cascades of mutually connected saddle-node, torus and homoclinic bifurcations. To demonstrate the universality of this bifurcation structure for coupled period-doubling systems we have shown that the same structure arises in a system of two coupled Rössler oscillators.

PACS numbers: Valid PACS appear here
Keywords: Suggested keywords

RESUME

Besides their system's nature, by which we refer to the enormous number of interacting feedback regulations that control the biological processes, living organisms are characterized by their sustained and self-generated activity. This activity, ranging from genetic clocks over the complex bursting of spiking dynamics by which the cells organize their internal processes and communicate with their neighbors, to the pacemaker activities and rythms of the brain, arises through instabilities and nonlinear dynamic phenomena.

Regulation of the blood flow to the individual functional unit (nephron) of the kidney likewise involves mechanisms that produce self-sustained oscillations, synchronization of different oscillatory modes in the individual nephron and period-doubling transitions. Moreover, adjacent nephrons interact with one another through signals that propagate along their connecting blood vessels. This interaction causes the nephrons to synchronize their blood flow regulation in a complex spatial pattern that reflects the underlying structure of blood vessels but also show temporal variations, indicating that they play an integrated part in overall kidney regulation.

The purpose of the present paper is to examine the processes involved in the synchronization and desynchronization of neighboring nephrons. We show that these transitions involve an interesting new structure of interconnected bifurcations. More precisely, we find that the transition from non-synchronized chaos to synchronized periodic dynamics besides a saddle-node bifurcation involves the combination of a torus bifurcation and a homoclinic bifurcation. Moreover, these bifurcations are organized in a characteristic structure such that a new sets of bifurcation curves arise for each period-doubling bifurcation of the individual nephron. We show that this structure is common to a class of interacting period-doubling systems by demonstrating its occurence in a pair of coupled Rössler systems.

I. INTRODUCTION

Synchronization and other nonlinear dynamic phenomena play an essential role in the regulation of normal physiological systems[1]. Activation of a tissue of smooth muscle cells, for instance, typically involves the gradual recruitment of the cells into a state of synchronization where incoherent cytoplasmic calcium fluctuations in the individual cells interact to produce an overall oscillatory dynamics[2]. In other cases, such as Parkinson's tremor, the development of the disease may be ascribed to the transition of a cluster of brain cells from a state of relatively independent spiking into a state of strong synchronization. Patients who cannot be treated through medication may often be helped by deep brain electrical stimulation designed to de-synchronize the cellular dynamics[3] or through selective modulation of brain rhythms by means of multi-electrode arrays[4].

As part of an effort to understand the relation between hypertension and kidney function we have long been engaged with a study of nephron autoregulation, i.e., of the mechanisms by which the individual functional unit of the kidney regulates the incoming blood flow in response to variations in the arterial pressure[5–7]. This regulation involves two different mechanisms: A myogenic mechanism that reacts directly to changes in the arterial pressure, and a so-called tubuloglomerular feedback

[a)] Electronic mail: laugesen@fysik.dtu.dk
[b)] Electronic mail: erik.mosekilde@fysik.dtu.dk
[c)] Electronic mail: nhhr@sund.ku.dk

(TGF) mechanism that responds to signals from specialized cells (the macula densa cells) near the terminal part of the loop of Henle.

The myogenic mechanism depends on an inherent propensity of the smooth muscle cells in the arteriolar wall to contract in response to an increasing pressure difference across the vascular wall[8,9]. This contraction causes the flow resistance to increase and, thereby, leads to a lower glomerular pressure and a reduced rate of filtration. The TGF mechanism, on the other hand, depends on a response from the macula densa cells to changes in the salt concentration of the tubular fluid. A high rate of glomerular filtration leads to a faster flow through the loop of Henle, to incomplete reabsorption of salt from the tubular fluid, rising salt concentrations at the macula densa, and a signal to the smooth muscle cells in the arteriolar wall to contract, thus causing the rate of filtration to decline.

The TGF mechanism is a negative feedback. However, as demonstrated in experiments on rats[5,6], this mechanism tends to be unstable and to produce large amplitude self-sustained oscillations in the tubular pressures and flows with periods in the 30-40 sec range. The instability in the feedback regulation and the relatively long periodicity of the oscillations are directly related to the time of 12-15 sec that it takes for the tubular fluid to pass the loop of Henle[10].

The myogenic (or vasomotoric) mechanism also produces oscillations in the afferent arteriolar resistance as the muscular activation increases. In this case, the transition to self-sustained oscillations takes place through synchronization of the cytoplasmic Ca^{+2} waves in the individual cells as discussed above[2,8]. The period of the vasomotoric oscillations in the afferent arterioles of the kidney is typically 6-8 sec, or approximately a factor 5 shorter than the period of the TGF oscillations.

The two regulatory mechanisms both work through activation of the smooth muscle cells in the arteriolar wall. This allows the modes to interact and to produce frequency-locking with typical locking ratios of 1:4, 1:5 and 1:6[11,12]. Nephron pressure and flow regulation involves a number of additional nonlinear relations, including the nonlinear feedback characteristic for the TGF mechanism[13], the nonlinear static strain-stress relation for the arteriolar wall[14], and the nonlinear relation between the concentration and osmotic pressure of protein in the efferent blood. As a result, episodes of period-2 dynamics can be observed in about 50% of the experimental time traces for the proximal tubular pressure in normotensive rats[15].

Figure 1 shows an example of such a time series. The mean tubular pressure in this experiment is about 7 mmHg. But this pressure is strongly modulated by relatively slow TGF-mediated oscillations with an amplitude of about 1-2 mmHg. The faster myogenic oscillations manifest themselves as a ripple on top of the TGF oscillations. Closer examination of the time trace in Fig. 1(a) reveals an episode of period-2 dynamics lasting approximately from time 200 sec to time 500 sec. This part of the time trace is amplified in Fig. 1(b) where the tubular pressure oscillation is seen to alternate between shallow and deep minima. The corresponding power spectrum, shown in Fig. 1(c), also provides evidence for the presence of subharmonic components in the pressure variation.

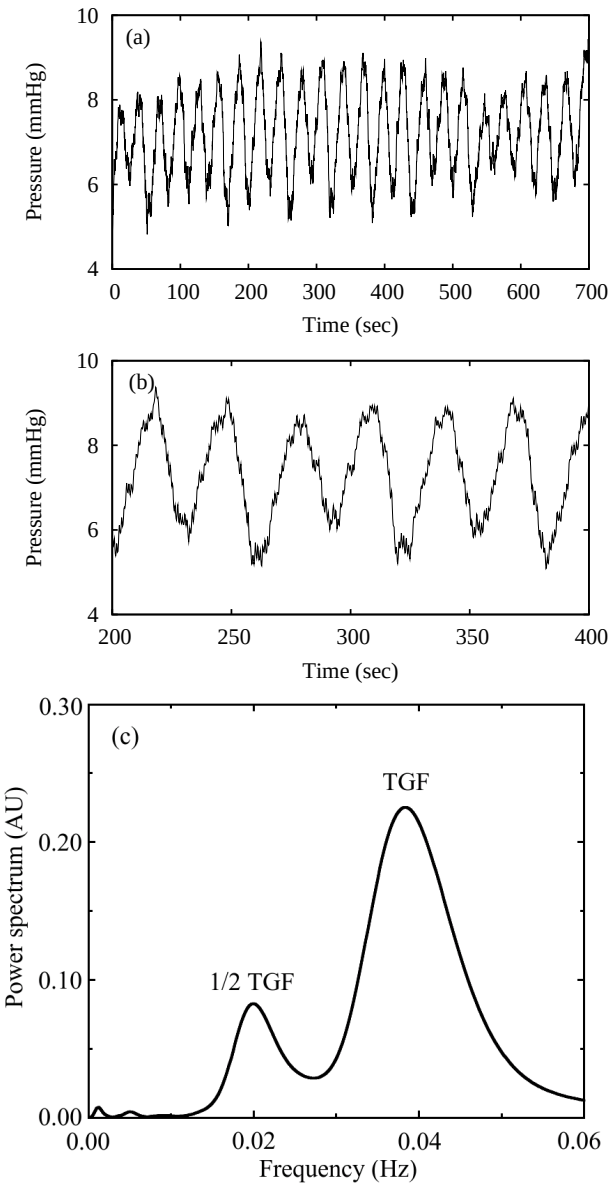

FIG. 1. Experimentally observed time series for the proximal tubular pressure in a normotensive rat. (a) Large amplitude oscillations produced by instability in the tubuloglomerular feedback (TGF). (b) Alternating deep and shallow minima signaling period-2 dynamics. (c) Power spectrum showing the main TGF peak at 40 mHz together with a subharmonic component at 20 mHz. For hypertensive rats, the tubular pressure oscillations are chaotic.

The nephrons are organized in a tree structure around a common blood supply[18]. This allows the functional units to interact with one another[6] both via a simple

displacement of blood from one nephron to its neighbors as the first nephron reduces its incoming blood flow (hemodynamic coupling) and via signals of muscular activation that travel from nephron to nephron along the blood vessels (vascular propagated coupling)[19]. These two mechanisms tend to synchronize the pressure oscillations of the interacting nephrons, typically such that the hemodynamic coupling favors anti-phase synchronization, and the vascular propagated mechanism causes in-phase synchronization[20,21].

The purpose of the present paper is to examine the transitions in and out of synchrony that occur through interaction between neighboring nephrons. It is well-known that a period-doubling cascade that unfolds along the edge of a resonance zone may display an unusual organization and a specific scaling behavior, referred to as cyclic (or C-type) criticality[22,23]. In such systems, one observes that the stable and unstable resonance cycles generated at the edge of the synchronization regime undergo interconnected cascades of period-doubling bifurcations and that each period doubling leads to the formation of a new pair of saddle-node bifurcation curves along the edges of the resonance zone. Moreover, these saddle-node bifurcations accumulate to finally define the transition between phase synchronized chaos and non-synchronous chaos. Our analysis shows that a different structure arises in connection with the synchronization of two vascular coupled nephrons. In particular we find that the transition from synchronized periodic dynamics to asynchronous chaotic dynamics involves the combination of a torus and a homoclinic bifurcation. To illustrate the universal character of this transition we shall use the last section to demonstrate that the same structure arises in a system of two coupled Rössler oscillators.

II. MODEL STRUCTURE

Over the years we have developed a number of different models of the regulation of the afferent blood flow to the individual nephron[24–26], each emphasizing a specific aspect of the problem such as the absorption of water and salts along the loop of Henle[24] or the interaction between the macula densa cells and the smooth muscle cells in the arteriolar wall[26]. In the present paper we will use the model developed by Barfred *et al.*[25]. This model integrates the most essential aspects of nephron autoregulation into a consistent picture and is, due to its relatively simple structure, particularly useful for detailed bifurcation studies. The same model has been applied in a number of earlier studies of nephron-nephron interaction[20,27].

The first component in the model is a conservation equation

$$\frac{dP_t}{dt} = \frac{1}{C_{tub}}[F_{filt} - F_{reab} - F_{Hen}] \tag{1}$$

that relates the changes in the proximal tubular pressure P_t to the rate of glomerular filtration F_{filt}, the absorption that takes place in the proximal tubule F_{reab}, and the flow into the loop of Henle F_{Hen}. C_{tub} denotes the elastic compliance of the proximal tubule. This equation is supported by a number of algebraic equations that determine first the rate of glomerular filtration

$$F_{filt} = (1 - H_a)\left(1 - \frac{C_a}{C_e}\right)\left(\frac{P_a - P_g}{R_a}\right) \tag{2}$$

in terms of the arterial pressure P_a, the glomerular pressure P_g and the flow resistance R_a of the afferent arteriole, and secondly the flow into the loop of Henle

$$F_{Hen} = \frac{P_t - P_d}{R_{Hen}} \tag{3}$$

in terms of the distal tubular pressure P_d and the tubular resistance R_{Hen}. Here, H_a is the afferent hematocrit (i.e. the fraction of the blood volume that the blood cells occupy), and C_a and C_e are the concentrations of protein in the afferent and the efferent blood, respectively. The factor involving the two protein concentrations expresses the fact that protein is retained in the blood and does not filter out in the glomerulus.

To determine the efferent protein concentration C_e we make use of the assumption that before the blood leaves the glomerulus its protein osmotic pressure balances the hydrostatic pressure difference $(P_g - P_t)$ between the glomerulus and the proximal tubule. This gives

$$C_e = \frac{1}{2b}[\sqrt{a^2 + 4b(P_g - P_t)} - a] \tag{4}$$

where a and b are experimentally determined parameters that relate protein osmotic pressure P_{osm} and concentration C

$$P_{osm} = aC + bC^2. \tag{5}$$

The TGF mediated modulation of the glomerular filtration rate is modeled in terms of the experimentally determined open-loop feedback characteristic

$$F_{filt,open} = F_{filt}\{F_{Hen,inf}\} \tag{6}$$

i.e. the relation between the rate of filtration $F_{filt,open}$ and the artificially infused flow of tubular fluid $F_{Hen,inf}$ into the loop of Henle in an experiment where the feedback has been opened by inserting a wax seal into the proximal tubule[28]. In the dynamic model we replace $F_{Hen,inf}$ in the feedback characteristic by a delayed version X_3 of the Henle flow (3) as obtained by the delay equations

$$\begin{aligned}
\frac{dX_1}{dt} &= F_{Hen} - \frac{3}{T}X_1 \\
\frac{dX_2}{dt} &= \frac{3}{T}(X_1 - X_2) \\
\frac{dX_3}{dt} &= \frac{3}{T}(X_2 - X_3).
\end{aligned} \tag{7}$$

T is the delay time.

Finally, the myogenic modulation of the afferent arteriolar resistance is modelled by a form of Poisson's equation

$$R_a = (\beta + (1-\beta)r^{-4})R_{a,0} \tag{8}$$

in combination with a second order differential equation

$$\frac{d^2r}{dr^2} + d\frac{dr}{dt} + \Omega(P_{av} - P_{eq}) = 0 \tag{9}$$

to describe the dynamics of the normalized arteriolar radius r. Here, $(1-\beta)$ represents the fraction of the arterial length that is modulated by the myogenic activity, $R_{a,0}$ is the equilibrium value of the afferent arteriolar resistance, d is the damping constant for the myogenic oscillations, and Ω determines the frequency of these oscillations. P_{av} is the average arteriolar pressure and P_{eq} is the pressure at which the arteriolar radius would be at equilibrium with the existing level of muscular activation. The relation between P_{eq} and the muscular activation represents the static stress-strain relationship for the arteriolar radius[14]. The second order differential equation (9) allows for an oscillatory myogenic response. In the form we use the equation here, the myogenic oscillations are damped ($d > 0$) but they are continuously excited by the TGF activity.

III. BIFURCATION STRUCTURE FOR VASCULAR COUPLED NEPHRONS

The regulatory mechanisms of the individual nephron act as a mechanical high-pass filter to protect the delicate processes that take place in the distal tubule from more lasting variations in the arterial blood pressure. While the myogenic mechanism is active in most tissues, the TGF mechanism is an additional mechanism required for the nephrons to handle the enormous blood flow that the kidneys receive. The response time of the TGF mechanism is restricted by the time it takes the tubular fluid to flow through the loop of Henle, and the system presumably achieves the fastest possible response by adopting an oscillatory mode of regulation. As described in the previous section, interaction between adjacent nephrons leads to synchronization of their pressure oscillations. One typically observes that the tubular pressures in a pair of neighboring nephrons oscillate in synchrony for a period of 20-40 min, lose synchrony for a while and then synchronize again.

In order to describe the transitions that occur as a couple of nephrons move in and out of synchrony we shall make use of standard continuation methods. Continuation[29] is a numerical technique developed to locate and follow periodic solutions as a parameter is changed, to determine bifurcation points and to follow bifurcation curves in phase space under variation of one (or more) parameters. In this way one can obtain a complete survey of the dynamics of a given system, the bifurcations it undergoes as a parameter is changed, and the overall structure of interconnected bifurcations. In this study we have applied the free software available from Doedel *et al.*[30].

As described above, the vascular propagated mechanism makes use of signals that travel from one nephron to its neighbors along the smooth muscle cells in the vascular wall. The amplitude of these signals decay more or less exponentially with distance, but their rate of propagation is quite fast as compared with the distance between the nephrons in terms of the period of the TGF oscillations. The vascular propagated coupling therefore tends to produce in-phase synchronization among the interacting nephrons. The relative contribution of this coupling depends on the structure of the connecting vascular system, primarily the involved distances and flow resistances[20,27]. In the model to be examined here, the coupling is considered to be symmetric, and it is assumed that 5% of the muscular activation of one arteriole reaches the active region of the other nephron.

As determined by the continuation approach, Fig. 2 provides a survey of the regions of existence for different behavioral modes in and around the main 1:1 synchronization zone. Parameters of the phase diagram are the delay $T^{(2)}$ in the loop of Henle for nephron-2 and the afferent arteriolar resistance $R^{(1)}_{a,0}$ for nephron-1. Base case values for these parameters are $T = 16$ sec and $R_{a,0} = 2.4$ kPa·s/nl. Other parameter values may be found in the above cited literature[25].

Different shades of blue and green are used to designate the regions of existence of stable low periodic orbits associated with the initial steps in the period-doubling cascade. Dark blue denotes regions of synchronized period-1 TGF oscillations. Light blue denotes regions of synchronized period-2 TGF oscillations, i.e., in these regions both nephrons have undergone a period-doubling bifurcation, but remain synchronized. Green denotes regions of synchronized period-4. The yellow area to the left in the diagram is a regions of synchronized period-3 dynamics. In the orange region we observe synchronized period-6 dynamics, and the red regions to the right in the synchronization zone are regions with synchronized period-5 dynamics. Finally, brown denotes regions with synchronous or non-synchronous quasiperiodic and chaotic dynamics.

The resonance zone is bounded to the left by black curves representing saddle-node bifurcations. The yellow closed curves (parts of which delinates the transition between the dark and light blue regions) are period-doubling curves where the stable (node) and unstable (saddle) period-1 cycles undergo their first period-doubling bifurcation. At the left hand edge of the resonance zone (at $T^{(2)} \approx 14$ sec), the two branches of the period-doubling curves approach one another, and at the zone boundary the stable and unstable period-1 cycles undergo simultaneous period-doubling bifurcations. The white closed curves similary represents the period-

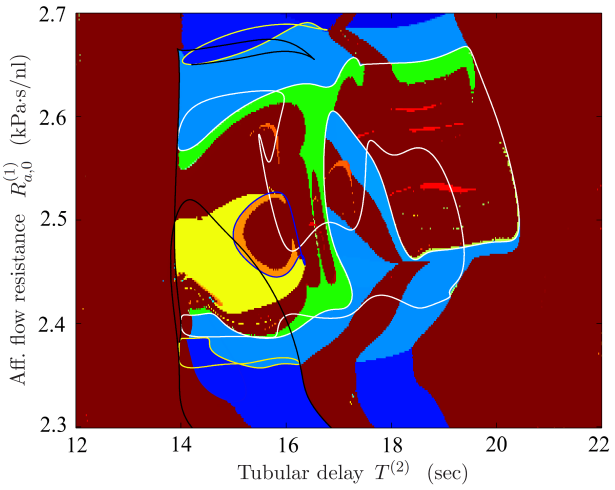

FIG. 2. Survey of the bifurcation structure in the main synchronization regime for a model of two coupled nephrons. Parameters in the figure are the resting value of the afferent arteriolar flow resistance for one of the nephrons and the delay of the fluid flow through the loop of Henle for the other nephron. The color code refers to the periodicity of the various cycles. The yellow region represents the region of period-3 dynamics. Reference values for the two parameters are $R_{a,0}^{(2)} = 2.4$ kPa·s/nl and $T^{(1)} = 16.0$ sec.

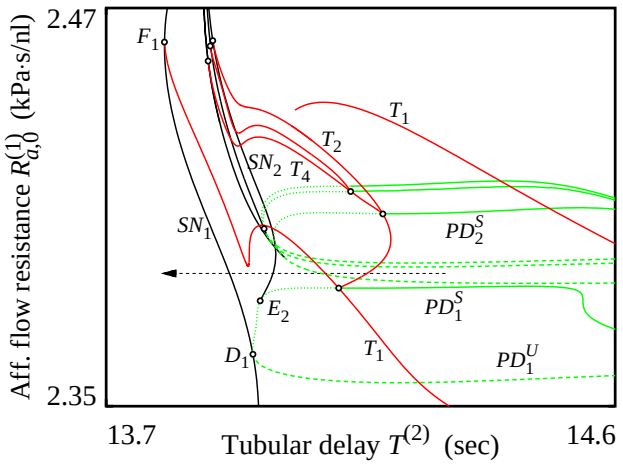

FIG. 3. Blow-up of the bifurcation structure in the lower left corner of Fig. 2. Saddle-node bifurcation curves are black, period-doubling curves green, and torus bifurcation curves red. Note the torus bifurcation curves that accumulate along the edge of the resonance tongue. This process displays a structure in which new torus bifurcation curves are formed alternatingly to the right and the left of the former torus bifurcation curve.

doubling curves at which the transition to period-4 dynamics take place for the stable and unstable period-2 cycles.

Inspection of the figure allows us to identify a main period-doubling structure connecting as a horseshoe from top to bottom in the resonance zone and accumulating in a (brown) region of the phase synchronized chaos around the large yellow window of synchronized period-3 dynamics. This is the structure we shall be concerned with in the present analysis. Our aim is to understand how the breakdown of the synchronization between two nephrons takes place as the system crosses out of the resonance region and into the large brown area of non-synchronized dynamics to the left in the figure. In the region of chaotic phase synchronization mentioned above, both nephrons display chaotic dynamics but their phases move in near synchrony[31,32]

In the upper part of the diagram the period-doubling cascade follows the typical transition associated with C-type criticality[33]. However, the structure associated with the lower side of the same cascade is somewhat more complicated in that each pair of period-doubling bifurcations generates not only a new saddle-node bifurcation curve to delineate the range of existence of the period-doubled modes, but also a torus bifurcation curve that continues up along the edge of the synchronization regime. Moreover, it appears that these torus bifurcation curves play an important role in delineating the range of synchronized periodic dynamics from that of quasiperiodicity and non-synchronous chaos.

Figure 3 shows a more detailed representation of the unusual bifurcation structure in the lower left corner of the bifurcation diagram in Fig. 2. Here, torus bifurcation curves are red, period-doubling curves are green, and saddle-node bifurcation curves are black. We immediately identify the saddle-node bifurcation curve SN_1 to the left in the figure. SN_1 is tangent to the first period-doubling curve PD_1 at the point D_1, and this saddle-node bifurcation serves to delineate the range of existence of period-1 resonant cycles. However, when the point of operation crosses the saddle-node bifurcation curve into the resonance region below the point D_1 it is found to give birth to a pair of doubly and a triply unstable saddle solutions rather than, as expected, to a saddle and a stable node cycle. A second saddle-node bifurcation curve SN_2, delineating the range of existence for period-2 resonance cycles, emerges from the point E_2 on the unstable branch of the first period-doubling bifurcation curve. And again, a pair of doubly and triply unstable period-2 saddle cycles is produced when the point of operation crosses this saddle-node bifurcation. As well as we can follow the structure, the same picture repeats itself all the way up along the bifurcation cascade.

The first torus bifurcation curve T_1 is supported by the point F_1 on the saddle-node bifurcation curve SN_1. From here it proceeds down along the saddle-node bifurcation curve, performs a couple of turns and returns to the upper part of the bifurcation diagram. At the point where T_1 intersects the stable branch PD_1^S of the first period-doubling curve, a new torus bifurcation curve T_2 emerges, and at the point where this torus bifurcation curve intersects the stable branch PD_2^S of the second period-doubling curve a third torus bifurcation curve T_4

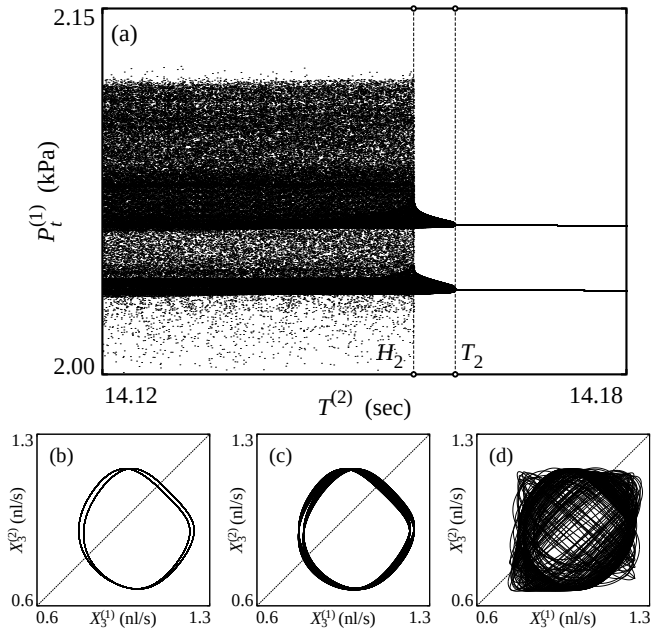

FIG. 4. (a) One-dimensional scan through the boundary of the resonance zone for $R_{a,0}^{(1)} = 2.39$ kPa·s/nl illustrates the transition from stable periodic dynamics to non-synchronized chaos through a pair of torus and homoclinic bifurcation. (b), (c) and (d) show phase portraits of the stable period-2 solution, the period-2 torus, and the non-synchronous chaotic attractor, respectively.

arises. In accordance with our numerical calculations, this cascade of torus bifurcations continues along with the cascade of period-doubling transitions, and all the torus bifurcation curves attach to points on the saddle-node bifurcations that accumulate along the edge of the resonance zone.

Figure 4(a) shows a scan through the boundary of the synchronization regime in Fig. 3 for $R_{a,0}^{(1)} = 2.39$ kPa·s/nl. If we read the scan from right to left we start in a situation where the coupled nephrons displays a stable (and a singly unstable) synchronized period-2 solution. These solutions correspond to the resonance modes one would normally expect to find in the synchronization region. However, as we move to the left, rather than undergoing a saddle-node bifurcation at the edge of synchronization, the stable period-2 cycle undergoes a torus bifurcation at T_2, producing a synchronized period-2 torus and a doubly unstable period-2 cycle. As the point of operation moves further to the left, the period-doubled torus undergoes a homoclinic bifurcation at H_2, and the synchronization is lost. Figures 4(b),(c) and (d) show phase portraits of the stable period-2 solution, the synchronized period-2 torus and the non-synchronous chaotic attractor, respectively. The saddle-node bifurcation SN_2 falls far to the left of the scan and is not directly involved in the transition from synchronous periodic dynamics to non-synchronous chaos.

IV. COUPLED, NON-IDENTICAL RÖSSLER OSCILLATORS

Systems of two interacting period-doubling oscillators have been investigated by a significant number of authors, often with a focus on the stability problems associated with chaos-chaos synchronization and the application of chaotic oscillators for secure communication[34,35]. Rasmussen *et al.*[36] have performed a detailed bifurcation analysis for a system of two identical and symmetrically coupled Rössler oscillators. They have demonstrated the appearance of a cascade of new saddle-node bifurcation curves along the edge of the synchronization zone. Kuznetsov *et al.*[37] have considered the synchronization of a pair of bi-modal oscillators constructed by driving a Duffing oscillator by a Van der Pol oscillator. Particular emphasis was given to the transition between mode-locked and unlocked chaos, but the authors also demonstrated the presence of separate synchronization regimes for the fast and the slow dynamics. Finally, Postnov *et al.*[38] have studied the process of synchronization for a Van der Pol oscillator driven by the chaotic forcing from a Rössler system. They have identified the underlying mechanisms as a set of inverse torus bifurcations of saddle orbits embedded in the synchronized chaotic state.

Multi-dimensional systems that display period-doubling cascades along the edge of a synchronization tongue typically exhibit the special scaling behavior known as C-type criticality[22,23]. The bifurcation structure observed for such systems differs essentially from the structures we know from low-dimensional systems. Until now, however, few examples of this transition, if any, have been worked out for realistic systems. We have recently studied the C-type transition for a single-nephron model subjected to a periodic variation of the arterial pressure[39]. This has confirmed the theoretical predictions for this kind of system, but has also lead to a more detailed picture of the involved bifurcation structure. However, the structure we observed in the coupled nephron model is different in that the transition to synchronization occurs through the combination of a homoclinic and a torus bifurcation.

In order to examine the generic character of these results and establish the role of the different bifurcations, let us consider the much simpler system of two coupled, non-identical Rössler oscillators:

$$\dot{x}_1 = -y_1 - z_1 \tag{10}$$
$$\dot{y}_1 = x_1 + a_1 y_1 \tag{11}$$
$$\dot{z}_1 = b + z_1(x_1 - c_1) + d(z_2 - z_1) \tag{12}$$
$$\dot{x}_2 = -\omega y_2 - z_2 \tag{13}$$
$$\dot{y}_2 = \omega x_2 + a_2 y_2 \tag{14}$$
$$\dot{z}_2 = b + z_2(x_2 - c_2) + d(z_1 - z_2), \tag{15}$$

where $a_2 = 0.345$, $b = 2$, $c_1 = 4$, $c_2 = 3.9$, and the coupling parameter $d = 0.1$. The value of a_2 is chosen

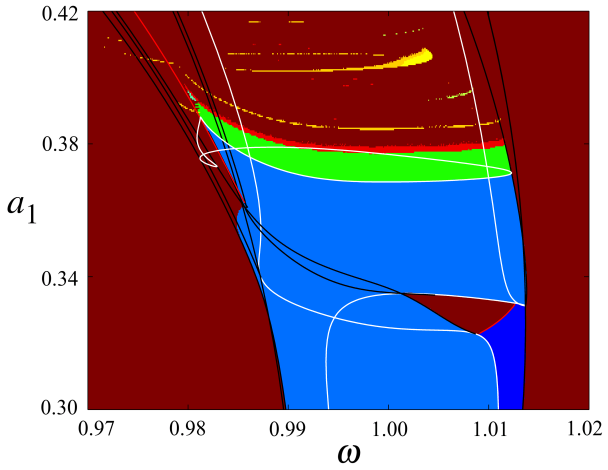

FIG. 5. Overview of the bifurcation structure of the 1:1 resonance zone for a pair of coupled, non-identical Rössler oscillators. Blue and green denote low-periodic cycles in the period-doubling cascade, yellow represents period-3 dynamics, and brown represents quasiperiodic or chaotic dynamics. Note the large number of saddle-node bifurcation curves that accumulate along the left hand side of the resonance region.

such that the second oscillator in the uncoupled state operates near the point of its first period-doubling. The gain parameter a_1 of the first oscillator and the mistuning (relative frequency) ω are used as control parameters.

Figure 5 provides a survey of the region of existence of different stable modes in and around the main resonance zone for the coupled Rössler oscillators. Different shades of blue and green are again used to distinguish the low-periodic stable cycles that arise in the initial steps of the period-doubling cascade. Brown denotes chaotic or quasiperiodic dynamics, and yellow identifies the region of existence for the period-3 mode. Black curves represent saddle-node bifurcations, red curves denote torus bifurcations, and white curves are curves where a period-doubling bifurcation takes place. Several of the period-doubling bifurcations relate to transitions that involve unstable cycles. In that case there is no change in the stable mode, and the color of the chart remains unchanged.

The first period-doubling bifurcation is a little unusual in that it is connected with a triangular region of torus dynamics within the resonance zone[36]. However, like the subsequent period-doubling bifurcations along the right hand side of the resonance regime it follows the general structure for C-type criticality. In particular, we note the formation of a new saddle-node bifurcation curve along the edge of the resonance zone to delineate the regime in which saddle and stable node period-2 cycles exist.

Similar saddle-node bifurcation curves are generated at each level in the period-doubling cascade. As previously noted they serve to delineate the ranges of existence for the saddle and node cycles born in the period-doubling bifurcations. Previously generated saddle-node bifurcation curves continue to exist to delineate the range of existence for the now unstable resonance cycles of lower periodicity. The new saddle-node bifurcation curves emerge from a point on the corresponding period-doubling curve a little away from the point at which the former saddle-node bifurcation curve is tangent to the period-doubling curve, and a torus bifurcation or a subcritical period-doubling bifurcation is generally in place to complete the zone boundary.

From the triangular region of torus dynamics associated with the first period-doubling transition two extra saddle-node bifurcation curves emerge and proceed all the way to the left hand edge of the resonance tongue. This phenomenon is accompanied by the generation of three saddle-node bifurcation curves for each pair of period-doubling bifurcations in the left hand side of the resonance zone.

More interesting, however, is the observation that each pair of period-doubling bifurcations give rise to the generation of a torus bifurcation curve that extends along the boundary of the resonance zone. In this way, the bifurcation structure for the the right hand side of the coupled Rössler systems corresponds to that of the upper part of the resonance zone for our coupled nephron model, and the bifurcation structure of the left hand side of the resonance zone for the coupled Rössler systems corresponds to the structure observed in the lower part of the resonance zone for the coupled nephrons.

To pursue this observation a little further, Fig. 6(a) shows a more detailed bifurcation diagram for the first pair of interconnected period-doubling bifurcations near the left hand side of the resonance zone. The period-doubling curves are green, the saddle-node bifurcation curves black, and the torus bifurcation curves red. For the period-doubling curves we distinguish between fully drawn curves, dashed curves and dotted curves depending on whether a stable node cycle, respectively a saddle cycle with one or two unstable directions is involved in the period-doubling transition.

When inspecting Fig. 6(a), we can follow the period-doubling curve PD_2^S for the stable period-2 cycle from the right hand side of the figure to the point C_2 where the torus bifurcation curve T_2 intersects with PD_2^S and the next torus bifurcation T_4 is born. From this point PD_2 continues as a curve of period-doubling for doubly-unstable period-2 saddles until it reaches the intermediate saddle-node bifurcation curve SN_2^b. From here the curve continues first to the innermost saddle-node bifurcation curve SN_2^c as a period-doubling curve for singly unstable saddle cycles and thereafter to the outmost saddle-node bifurcation curve SN_2^a as a period-doubling curve for stable node period-2 resonant cycles.

Below the point of tangency with the period-doubling bifurcation curve, the outermost saddle-node bifurcation curve in this way limits the range of existence for a pair of saddle and stable node period-2 solutions. The innermost saddle-node bifurcation curve serves a similar purpose, whereas the intermediate saddle-node bifurca-

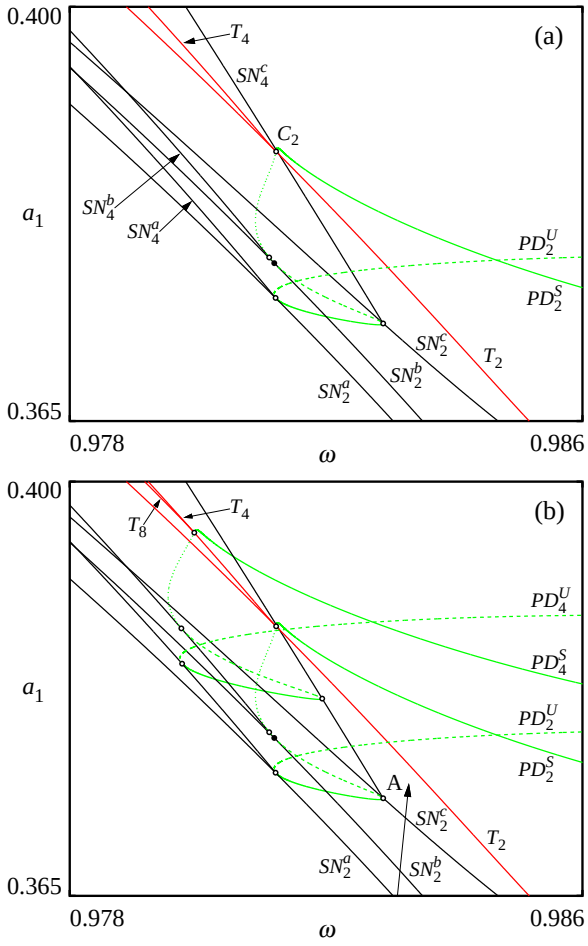

FIG. 6. Detail of the bifurcation diagram in Fig. 5 illustrating the bifurcations that take place close to the lower left zone boundary. (a) Bifurcation structure for the period-2 cycles. (b) Bifurcation structure for the period-2 and period-4 cycles. Note the birth of three new saddle-node bifurcation curves and one new torus bifurcation curve for each level in the period-doubling cascade.

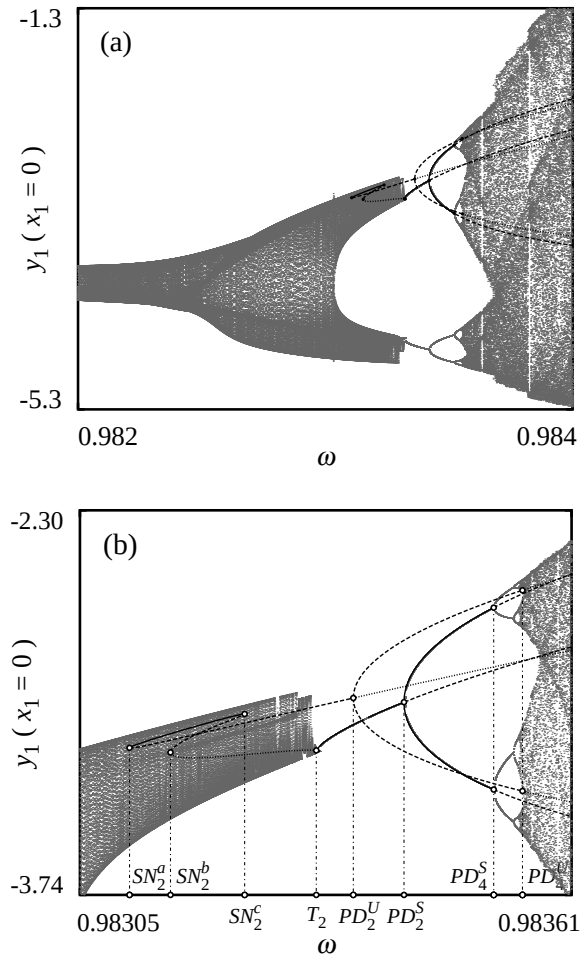

FIG. 7. (a) One-dimensional bifurcation diagram along the direction A in Fig. 6(b). Note the period-doubling of the ergodic torus in the left hand side of the figure. (b) Close-up on the upper branch of (a). The stable resonant mode arises in an reverse torus bifurcation rather than in a saddle-node bifurcation.

tion curve delineates the range of existence for a pair of saddle and doubly-unstable saddle period-2 cycles below the period-doubling point and for a pair of doubly and triply unstable saddle solutions above this point. The torus bifurcation curve T_2 is required to close the hole between the point C_2 and the innermost saddle-node bifurcation curve SN_2^c. Below C_2 and to the right of T_2, a stable period-2 node loses its stability in two dimensions at the supercritical torus bifurcation T_2.

The period-4 cycles produced at the period-doubling curves require their own system of saddle-node and torus bifurcation curves to restrict their ranges of existence. Hence, close to (but not in) each of the points where the period-doubling bifurcation curve is tangent to one of the saddle-node bifurcation curves SN_2^a, SN_2^b and SN_2^c delineating the ranges of existence for the various resonant period-2 cycles, new saddle-node bifurcation curves are born to delineate the range of existence for the period-4 node, saddle, and doubly-unstable saddle cycles. Similarly, at the point C_2 where the period-doubling curve PD_2^S intersects the torus bifurcation curve T_2, a new torus bifurcation curve T_4 is born.

As shown in Fig. 6(b), precisely the same picture applies to the period-doubling curves for the period-4 cycles and to the following curves in the period-doubling transitions as well. We conclude that the system generates a set of three saddle-node bifurcation curves for each pair of period-doublings along the edge of the resonant domain. More importantly, the system at the same time gives birth to a new torus bifurcation curve and, as our preliminary investigation shows, this set of torus bifurcation curves accumulate in an alternating manner along the boundary of the resonance zone.

To provide a clearer picture of the different steps in the transition from ergodic (quasiperiodic) dynamics to

synchronous periodic dynamics, Fig. 7(a) shows a one-dimensional bifurcation diagram obtained along the direction A in Fig. 6(b). To the left in this diagram we observe the ergodic torus that exists outside of the resonance zone. As this torus approaches the resonance zone, it first undergoes a torus doubling bifurcation[16,17]. The close-up of the upper branch of the torus displayed in Fig. 7(b) shows that the saddle-node bifurcations at SN_2^a, SN_2^b, and SN_2^c all take place in the regime of the torus dynamics. We conclude that the saddle-node bifurcations are not directly involved in the transition from ergodic to stable periodic dynamics.

At T_2, a stable, phase-synchronized period-2 torus undergoes a reverse torus bifurcation and produces a stable period-2 (focus) cycle. Finally, to the right in the bifurcation diagram we can follow how the stable period-2 cycle together with a saddle period-2 cycle originating in the above saddle-node bifurcations undergo interconnected cascades of period-doubling bifurcations. The transition from quasiperiodicity to synchronized periodic dynamics thus takes place via a torus bifurcation.

V. CONCLUSIONS

We have examined the mechanisms involved in the transition of a pair of interacting nephrons between states of synchronized and non-synchronized behavior. This problem is of interest in connection with the description of larger systems of interacting nephrons in the form, for instance, of a nephron tree, i.e., a group of 15-20 nephrons organized around a common blood vessel[18]. We are also involved in the study of synchronized patterns generated by larger populations of superficial nephrons observed simultaneously by means of laser speckle microscopy.

The classical theory of synchronization of nonlinear oscillators leads to the concept of an Arnol'd tongue of synchronized states delineated by a set of saddle-node bifurcations. This description applies to systems that are essentially one-dimensional.

The bifurcation structure associated with the synchronization of a period-doubling system in the presence of an external periodic forcing proceeds in a different manner[33]. Here, one can observe that each pair of period-doubling bifurcations of the node and saddle resonance cycles leads to the formations of a new pair of saddle-node bifurcation curves to delineate the range of existence for the period-doubled cycles. The saddle-node bifurcations are found to be supported by points on the period-doubling curves close to but a little away from the points of tangency between the period-doubling curve and the last pair of saddle-node bifurcation curve.

However, our investigation of two interacting nephrons has lead to a number of new phenomena. First of all we observe that a cascade of torus bifurcation curves are generated along the border of the resonance zone. Moreover, these torus bifurcation curves control the transition from synchronized periodic dynamics to quasiperiodic dynamics. We also observe the formation of a cascade of homoclinic bifurcations, with each homoclinic bifurcation supported by the point in which the torus bifurcation curve attach to the corresponding saddle-node curve. The homoclinic bifurcations are responsible for the transition from synchronized torus dynamics to non-synchronous behavior.

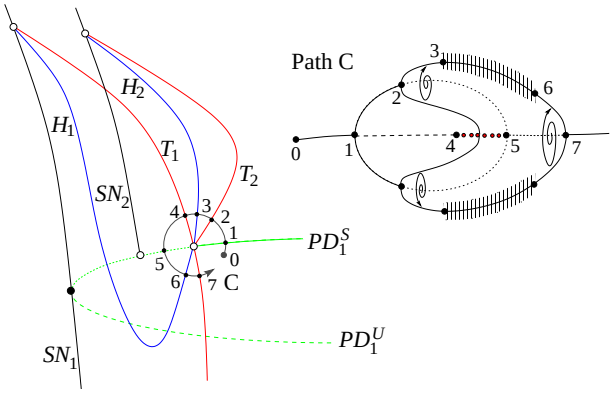

FIG. 8. Sketch illustrating the observed bifurcation structure for the transition from synchronized periodic dynamics to non-synchronous chaotic dynamics. At each level of the period-doubling cascade this involves a new set of saddle-node, torus and homoclinic bifurcations. The inset illustrates the bifurcations that occur along the circular path C.

Figure 8 illustrates the basic elements of the proposed bifurcation structure. We note how the saddle-node bifurcation curve SN_1 is tangent to the period-doubling curve PD_1. However, the stable period-1 cycle that exists below PD_1^S does not proceed all the way out to the saddle-node bifurcation curve. Instead this cycle undergoes a torus bifurcation at T_1 (red curve) followed by a homoclinic bifurcation at H_1 (blue curve). The torus bifurcation produces quasiperiodic dynamics while non-synchronous chaotic dynamics takes over after the homoclinic bifurcation. We note that the torus bifurcation curve T_1 and the homoclinic bifurcation curve H_1 both arise from the same point on the saddle-node bifurcation curve SN_1.

A new saddle-node bifurcation curve SN_2 emerges from a point on the period-doubling curve PD_1^S. Moreover, at the point where the torus bifurcation curve T_1 intersects PD_1^S, a new torus bifurcation T_2 is born together with the corresponding homoclinic bifurcation curve H_2. These bifurcation curves again connect to a common point on the saddle-node bifurcation curve SN_2. It is interesting to note that, at least for the models we have considered in the present paper, the homoclinic bifurcation curve H_1 also connects to the point on PD_1^S, where H_2 and T_2 originate.

At the next period-doubling curve PD_2^S (not shown) almost the same picture repeats. A new torus bifurcation T_4 is born at the intersection between T_2 and PD_2^S, and T_4 runs along the edge of synchronization and attaches to SN_4. However, the homoclinic bifurcation born in this

point does not connect to the intersection point of T_2 and PD_2^S. Instead, it connects to the next intersection in the cascade, i.e. the intersection between T_4 and PD_4^S. In this way only every second intersection point between period-doubling and torus bifurcation curves involves homoclinic bifurcations.

The insert in Fig. 8 describes the bifurcations that occur along the circular path C, thus supporting the consistency of the above description. Starting at point 0 the system displays a stable period-1 cycle. As we move around C, this cycle undergoes a period-doubling bifurcation at 1. At point 2 the stable period-2 cycle undergoes a torus bifurcation. This leaves us with a singly unstable period-1 cycle and a doubly unstable period-2 cycle. In 4 the period-1 cycle undergoes a torus bifurcation, producing a triply unstable cycle. In point 5, this cycle undergoes a inverse period-doubling bifurcation with the doubly unstable period-2 and, finally, at point 7 the now doubly unstable period-1 undergoes an inverse torus bifurcation, re-establishing its position as a stable node. At points 3 and 6 the torus undergo homoclinic bifurcations H_2 and H_1, respectively, leading to the birth and subsequent disasppearance of non-synchronous chaotic dynamics.

We conclude that the two examined systems of coupled period-doubling oscillators display the same bifurcation structure. This illustrates the universal character of the proposed structure.

[1] J. Belair, L. Glass, U. an der Heiden, J. Milton, Chaos **5**, 1, (1995).
[2] J. C. B. Jacobsen, C. Aalkjaer, V. V. Matchkov, H. Nilsson, J. J. Freiberg, N.-H. Holstein-Rathlou, Phil. Trans. Roy. Soc. A **366**, 3483, (2008).
[3] U. B. Barnikol, O. V. Popovych, C. Hauptmann, V. Sturm, H.-J. Freund, P. A. Tass, Phil. Trans. Roy. Soc. A **366**, 3545, (2008).
[4] J. Modolo, B. Bhattacharya, R. Edwards, J. Campagnaud, A. Legros, A. Beuter, Front. Neuro. Sci. **4**, 1, (2010).
[5] N.-H. Holstein-Rathlou, P. P. Leyssac, Acta Physiol. Scand. **126**, 333, (1986).
[6] N.-H. Holstein-Rathlou, Pflügers Arch. **408**, 438, (1987).
[7] N.-H. Holstein-Rathlou, D. J. Marsh, Physiol. Rev. **74**, 637-681, (1994).
[8] H. Gustafsson, A. Bulow, H. Nilsson, Acta Physiol. Scand. **152**, 145, (1994).
[9] M. J. Davis, M. A. Hill, Physiol. Rev. **79**, 387, (1999).
[10] N.-H. Holstein-Rathlou, A. J. Wagner, D. J. Marsh, Am. J. Physiol. **260**, F53, (1991).
[11] O. V. Sosnovtseva, A. N. Pavlov, E. Mosekilde, N.-H. Holstein-Rathlou, Phys. Rev. E **66**, 61909-1-7, (2002).
[12] O. V. Sosnovtseva, E. Mosekilde, A. N. Pavlov, N.-H. Holstein-Rathlou, D. J. Marsh, Phys. Rev. E **70**, 031915-1-8, (2004).
[13] L. C. Moore, Am. J. Physiol. **247**, F267, (1984).
[14] R. Feldberg, M. Colding-Jorgensen, N.-H. Holstein-Rathlou, Am. J. Physiol. **269**, F581, (1995).
[15] A. N. Pavlov, O. V. Sosnovtseva, O. N. Pavlova, E. Mosekilde, N.-H. Holstein-Rathlou, Chaos, Solitons and Fractals **41**, 930, (2009).
[16] A. Arnéodo, P. H. Coullet, E. A. Spiegel, Phys. Lett. A **94**, 1, (1983).
[17] M. Sekikawa, N. Inaba, T. Yoshinaga, T. Tsubouchi, Phys. Lett. A **348**, 187, (2006).
[18] D. Casellas, M. Dupont, Am. J. Physiol. **267**, F931, (1994).
[19] A. J. Wagner, N.-H. Holstein-Rathlou, D. J. Marsh, Am. J. Physiol. **272**, F372, (1997).
[20] N.-H. Holstein-Rathlou, K.-P. Yip, O. V. Sosnovtseva, E. Mosekilde, Chaos **11**, 417, (2001).
[21] D. J. Marsh, O. V. Sosnovtseva, E. Mosekilde, N.-H. Holstein-Rathlou, Chaos **17**, 15114-1-10, (2007).
[22] S. P. Kuznetsov, Phys. Rev. E **72**, 026205, (2005).
[23] S. P. Kuznetsov, A. P. Kuznetsov, I. R. Sataev, J. Stat. Phys. **121**, 697, (2005).
[24] N.-H. Holstein-Rathlou, J. Am. Soc. Nephrol. **4**, 1275, (1993).
[25] M. Barfred, E. Mosekilde, N.-H. Holstein-Rathlou, Chaos **6**, 280, (1996).
[26] J. L. Laugesen, O. V. Sosnovtseva, E. Mosekilde, N.-H. Holstein-Rathlou, D. J. Marsh, Am. J. Physiol. **298**, R997, (2010).
[27] D. E. Postnov, O. V. Sosnovtseva, E. Mosekilde, Chaos **15**, 013704-1-12, (2005).
[28] P. P. Leyssac and N.-H. Holstein-Rathlou, Pflügers Archive **413**, 267, (1989).
[29] Y. A. Kuznetsov, *Applied Mathematical Sciences: Elements of Applied Bifurcation Theory*, (Springer Verlag, NY, 2004).
[30] E. J. Doedel, R. C. Paffenroth, A. R. Champneys, T. F. Fairgrieve, Y. A. Kuznetsov, B. E. Oldeman, B. Sandstede, X. J. Wang, Technical report (Available via ftp from ftp.cs.concordia.ca/pub/doedel/auto.), California Institute of Technology, Pasadena CA91125, (2000).
[31] M. Rosenblum, A. Pikovsky, and J. Kurths, Phys. Rev. Lett. **76**, 1804, (1996).
[32] A. Pikovsky, M. Rosenblum, and J. Kurths, *Synchronization*, (Cambridge University Press, Cambridge, 2001).
[33] S. P. Kuznetsov and I. R. Sataev, Physical Review E **64**, 046214/1-7, (2001).
[34] N. F. Rulkov, M. M. Sushchik, Int. J. Bif. Chaos **7**, 625, (1997).
[35] S. Yanchuk, Yu. Maistrenko, E. Mosekilde, Physica D **154**, 26, (2001).
[36] J. Rasmussen, E. Mosekilde, C. Reick, Math. Comp. Sim. **40**, 247, (1996).
[37] A. P. Kuznetsov, E. Mosekilde, and L. V. Turukina, Physica A **371**, 280, (2006).
[38] D. E. Postnov, A. G. Balanov, O. V. Sosnovtseva, and E. Mosekilde, Physics Letters A **283**, 195, (2001).
[39] J. L. Laugesen, E. Mosekilde, N.-H. Holstein-Rathlou, J. Roy. Soc. Interface, to appear.

Publication P2:

Coupling-induced complexity in nephron models of renal blood flow regulation

---

Published in *The American Journal of Physiology*.

Am J Physiol Regul Integr Comp Physiol 298: R997–R1006, 2010.
First published February 10, 2010; doi:10.1152/ajpregu.00714.2009.

Coupling-induced complexity in nephron models of renal blood flow regulation

Jakob L. Laugesen,[1] Olga V. Sosnovtseva,[1] Erik Mosekilde,[1] Niels-Henrik Holstein-Rathlou,[2] and Donald J. Marsh[3]

[1]*Department of Physics, Technical University of Denmark, Kgs.Lyngby, Denmark;* [2]*Department of Biomedical Sciences, Panum Institute, University of Copenhagen, Copenhagen N, Denmark; and* [3]*Department of Molecular Pharmacology, Physiology, and Biotechnology, Brown University, Providence, Rhode Island*

Submitted 2 November 2009; accepted in final form 8 February 2010

Laugesen JL, Sosnovtseva OV, Mosekilde E, Holstein-Rathlou N, Marsh DJ. Coupling-induced complexity in nephron models of renal blood flow regulation. *Am J Physiol Regul Integr Comp Physiol* 298: R997–R1006, 2010. First published February 10, 2010; doi:10.1152/ajpregu.00714.2009.— Tubular pressure and nephron blood flow time series display two interacting oscillations in rats with normal blood pressure. Tubuloglomerular feedback (TGF) senses NaCl concentration in tubular fluid at the macula densa, adjusts vascular resistance of the nephron's afferent arteriole, and generates the slower, larger-amplitude oscillations (0.02–0.04 Hz). The faster smaller oscillations (0.1–0.2 Hz) result from spontaneous contractions of vascular smooth muscle triggered by cyclic variations in membrane electrical potential. The two mechanisms interact in each nephron and combine to act as a high-pass filter, adjusting diameter of the afferent arteriole to limit changes of glomerular pressure caused by fluctuations of blood pressure. The oscillations become irregular in animals with chronic high blood pressure. TGF feedback gain is increased in hypertensive rats, leading to a stronger interaction between the two mechanisms. With a mathematical model that simulates tubular and arteriolar dynamics, we tested whether an increase in the interaction between TGF and the myogenic mechanism can cause the transition from periodic to irregular dynamics. A one-dimensional bifurcation analysis, using the coefficient that couples TGF and the myogenic mechanism as a bifurcation parameter, shows some regions with chaotic dynamics. With two nephrons coupled electrotonically, the chaotic regions become larger. The results support the hypothesis that increased oscillator interactions contribute to the transition to irregular fluctuations, especially when neighboring nephrons are coupled, which is the case in vivo.

renal autoregulation; nonlinear dynamics; tubuloglomerular feedback; myogenic mechanism; chaos

TWO MECHANISMS, TUBULOGLOMERULAR feedback (TGF) and the myogenic mechanism, operate in each nephron of mammalian kidneys to regulate blood flow when arterial blood pressure changes (14–16, 22, 44). Each mechanism is potentially unstable and operates in a nonlinear regime: TGF oscillates at 0.02–0.04 Hz and the myogenic mechanism at 0.1–0.2 Hz. The TGF oscillation is the more pronounced. These mechanisms interact because they operate simultaneously on the contractile machinery of vascular smooth muscle cells. The interaction leads to modulation of the amplitude and frequency of the myogenic oscillation by TGF, a finding predicted by a mathematical model (26) and confirmed in experimental measurements (28).

Address for reprint requests and other correspondence: D. J. Marsh, Dept. of Molecular Pharmacology, Physiology, & Biotechnology, Brown Univ., Biomedical Center B-3, Providence, RI 02912 (e-mail: marsh@ash.biomed.brown.edu).

The dynamics of the TGF-myogenic ensemble undergo a transition in rats with either a genetic or a renovascular form of hypertension to a state with characteristics of deterministic chaos (51). Lyapunov exponents are positive; the phase space attractor constructed from the data is low dimensional and has a noninteger correlation dimension (51); surrogate data analysis confirms the nonlinearity of the system (52).

The question at issue is the cause of the transition. Dilley and Arendshorst (8) and Leyssac and Holstein-Rathlou (23) reported that the feedback gain of TGF, a component of the coupling of TGF to the inherent dynamics of the afferent arteriole, is greater in hypertensive rats than in rats with normal blood pressure. In our model, an increase in TGF gain or in the parameter expressing the coupling, or both, will increase the strength of the interaction. In this study, we test the hypothesis that the strength of the TGF-myogenic interaction functions as a bifurcation parameter and, when increased, can cause a bifurcation to chaos. For the test, we use a mathematical model of a single nephron and its afferent arterioles (26), and of two such nephrons coupled by electrotonic vascular signal conduction (29). With an increase in the strength of the interaction, the single nephron model succeeds in predicting transitions to chaotic dynamics, but the regions with these dynamics in a one-dimensional parameter scan appear to be small and therefore inadequate to account for the experimental observations. The simulation of two nephrons coupled electrically, which is closer to the natural state than is the single nephron model, generates larger domains of chaos than the model of one nephron alone. The results obtained with the coupled nephron model therefore support the hypothesis that increased coupling between TGF and the myogenic mechanism can cause a change in the dynamics of nephron blood flow regulation similar to that found in rats with chronic high blood pressure.

METHODS

Model

The essential elements and mechanisms of the model are summarized in the causal loop diagram in Fig. 1. Signs at the arrowhead indicate the direction of change of a given variable in response to a change in the variable at the arrow's tail. The elements of the feedback loop that generate TGF and its oscillation comprise glomerular filtration (GFR), the axial mass transport of NaCl and water, and the epithelial transport of NaCl and water in various tubular segments. These elements are shown in Fig. 1, *right*. Epithelial transport of NaCl is dependent on axial flow rate in several of these segments, so that the concentration of NaCl in tubular fluid at the macula densa is strongly dependent on the axial flow rate of tubular fluid. The apical membranes of macula densa cells have transporters sensitive to ionic

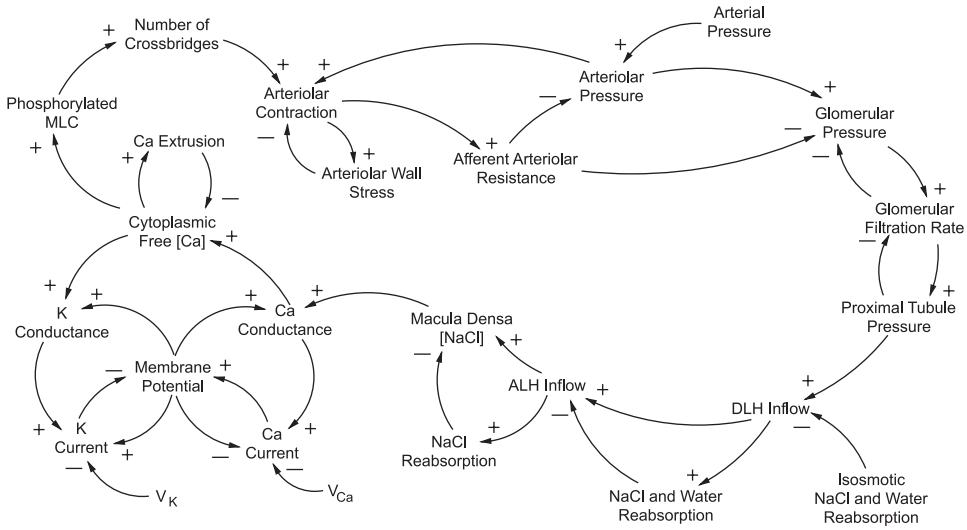

Fig. 1. Causal loop diagram representing the model of a single nephron. Signs in parentheses denote negative feedback loops. Increases in the Ca^{2+} current and the K^+ current produce changes in membrane potential difference of opposite sign because the difference between their reversal potentials, V_K and V_{Ca}, respectively, and the membrane potential have opposite signs. MLC, myosin light chain; DLH, descending limb of Henle's loop; ALH, ascending limb of Henle's loop. Brackets denote concentration.

concentrations, chiefly Cl^-. The signal from the macula densa produced in response to variation of the NaCl concentration in tubular fluid propagates through a number of cells and finally affects the Ca^{2+} conductance of vascular smooth muscle cells. The change in Ca^{2+} conductance alters intracellular Ca^{2+} and modifies the length of the contractile mechanism, altering the arteriolar vascular resistance. The change in vascular resistance affects GFR, closing the loop and providing negative feedback.

The myogenic mechanism is represented by the loops in Fig. 1, *left*. The period of the oscillation is determined by instability in membrane potential caused by an interaction between Ca^{2+} and K^+ currents. The magnitude of the oscillation in vascular diameter is determined by the level of intracellular Ca^{2+}. TGF affects the membrane Ca^{2+} conductance that is part of the myogenic mechanism in the model, allowing TGF to modulate both the amplitude and frequency of the myogenic mechanism. The magnitude of the TGF stimulus decreases with distance from the glomerulus, proceeding along the afferent arteriole toward the nearest branch point of the artery supplying blood to the nephron. A two-point approximation to this continuous decline gives the arteriolar model two distinct segments, each modeled separately and the one closer to the glomerulus receiving the greater TGF input. The arteriolar segments are coupled electrically. Details of the mathematical model of a single nephron and of a nephron pair were presented in previous work (26, 28). We used the same models in this study.

In the first of these papers, tubular pressure, flow, and NaCl concentration were modeled as functions of time and distance in a single nephron with a compliant epithelial wall that reabsorbs water and NaCl. The nephron consisted of a proximal tubule, a descending limb of Henle's loop, a thick ascending limb of Henle's loop, and an early distal tubule. Appropriate parameters were used for each tubular segment. The boundary conditions were GFR as the initial flow rate, a nonlinear expression for pressure at the end of the early distal tubule, reflecting the compliance of later segments of the tubule (24), and NaCl concentration in the glomerular ultrafiltrate. NaCl is the only tubular solute represented in the model, and its concentration is assumed to remain unchanged in the proximal tubule.

Each of two segments of the afferent arteriole was modeled with six ordinary differential equations whose dependent variables were membrane K^+ conductance, intracellular Ca^{2+} concentration, membrane electrical potential difference, myosin light chain phosphorylation, length of the contractile mechanism, and length of two different sets of elastic elements, one in series with the contractile mechanism forming an ensemble, which is in parallel with the second elastic component. The length of the parallel elastic element was equal to the sum of the lengths of the series element and of the contractile mechanism; the circumference of the vascular lumen was calculated from this length. This cellular model of arteriolar dynamics is based on the work of Gonzalez-Fernandez and Ermentrout (9) which was designed to simulate vasomotion in cerebral arterioles.

The TGF signal was calculated from the tubular NaCl concentration at the end of the thick ascending limb with a logistic equation in a form used to fit experimental data; TGF output was used to modify membrane Ca^{2+} conductance to cause changes in smooth muscle contraction and to simulate the interaction between TGF and the myogenic mechanism. Both segments of the afferent arteriole generated spontaneous self-sustained oscillations because of the interaction between voltage-gated Ca^{2+} channels and Ca^{2+}- and voltage-dependent K^+ channels. TGF stimulation of the arteriole produces maximal contraction at the point closest to the glomerulus; the vasoconstriction declines with distance from the glomerulus (29, 47); the fractional decrease data can be fitted with a single exponential. Two arteriolar segments were used as a two-point approximation to this decline; the TGF effect was greater in the segment close to the glomerulus and smaller in the farther segment. The two segments were coupled electrically with an ohmic conductance.

The interaction between TGF and the myogenic mechanism was expressed as: $g_{Ca,j,c} = (1 + \zeta_j \cdot \theta_j) \cdot g_{Ca}$, where g_{Ca} is the native Ca^{2+} conductance, $g_{Ca,j,c}$ is the Ca^{2+} conductance of the jth arteriolar segment when coupled to TGF, θ_j is TGF input to the jth arteriolar segment, and ζ is the parameter coupling the two mechanisms. We varied ζ to change the strength of the connection between TGF and the myogenic mechanism to test the hypothesis that ζ can act as a bifurcation parameter and explain the different dynamics observed in normal and hypertensive rats.

The two-nephron model consists of two versions of the single nephron model, each solved separately, but with the arteriolar segments farther from the glomerulus coupled electrically (29). These arteriolar segments were coupled to each other through an electrical node in the wall of the artery supplying the two nephrons with blood. In this study, cortical nephrons were simulated, and both nephrons of the pair were assigned the same length. Additional parameters needed for the two-nephron model were the conductance coupling the two nephrons through an electrical node, and a conductance of the node to ground. The model was otherwise used unmodified from the single nephron form.

Numerical methods. The partial differential equations describing pressure, flow, and NaCl concentration in each renal tubule were solved using centered difference approximations and are second-order correct (40). The spatial step was 0.125 mm and the time step 1 ms.

Reducing either the spatial step or the time step by a factor of 10 had no effect on the values of ζ required to produce bifurcations in the model results. The auxiliary equations, including the boundary conditions, were solved with the Newton Raphson method. All calculations were performed in double precision.

The solutions of the ordinary differential equations were obtained with Gear's variable step size method, using backward differentiation and numerically generated Jacobians. Because the solution of the partial differential equations required iterations at each time step, the time steps for the solution of the ordinary differential equations were synchronized with those used for the partial differential equations.

For each time step, the glomerular model was solved by using the afferent resistance and the tubular inlet pressure from the preceding time step as initial estimates. With the use of the calculated value for GFR for the inflow rate to the tubular system, the pressure, flow, and NaCl equations were solved iteratively at each time step of the whole system. Convergence was assumed when the fractional change of the Euclidian norm of the combined pressure and flow vectors was $<10^{-3}$ and $<10^{-5}$ for the NaCl concentration vector. The new calculated value for the NaCl concentration at the macula densa was applied to estimate the afferent arteriolar resistance. The procedure was repeated, using the new value for the afferent resistance and the tubular inlet pressure, until the system of equations converged. Convergence was assumed when the change in the Euclidean norm of the afferent resistance was $<10^{-6}$ in successive iterations. Three or four iterations were typically needed to achieve convergence.

Analytic approach. The model generates time series corresponding to solutions for tubular pressure, volume flow rate, and NaCl concentration at each spatial and time step and for each of the 12 ordinary differential equations used to simulate the afferent arteriole. We will present only nephron plasma flow rate, NaCl concentration in tubular fluid at the macula densa, and intracellular Ca^{2+} concentration in afferent arteriolar smooth muscle cells. These variables were chosen because, when combined, they form a phase space attractor with one variable, NaCl concentration at the macula densa, showing primarily TGF dynamics; a second, intracellular Ca^{2+} concentration in smooth muscle cells, representing dynamics mainly of the myogenic mechanism; and a third, nephron plasma flow rate, with the dynamics of both mechanisms.

The results of our simulations show limit cycle oscillations, quasiperiodicity, and chaos for different values of ζ, the parameter that couples TGF with the myogenic mechanism in the nephron model. In the phase space, each of these kinds of dynamics represents a specific type of attractor, i.e., invariant (steady) state for the system. A bifurcation diagram provides an overview of the different kinds of dynamics generated in the system. In such a diagram, the coordinates of the intersection between the trajectory of the system and a plane (a Poincaré section) in the space of state variables is mapped on the *y*-axis as a function of a parameter, in this case ζ.

The bifurcation diagrams are calculated by the following procedure. *1*) A Poincaré section is defined, which in our case is chosen to be $I_K - 0.1 = 0$, $dI_K/dt > 0$, where I_K is the K^+ current in the vascular smooth muscle cell. *2*) Starting with a value of $\zeta = 0.18$, the state variables are initialized. *3*) The system is simulated for 3,000 s to allow the solution of the system to converge to a stationary state. *4*) During an extension of the simulation by 3,000 s, the intersections with the Poincaré section are calculated by using a linear interpolation between the states just before and after the intersection. *5*) The parameter ζ is increased by 1.8×10^{-4}, and the state variables are maintained at their current state (adiabatic initial conditions). *6*) The procedure is repeated from *step 3* until ζ reaches its final value of 0.4.

The model generated four main types of dynamics as ζ changed: a state in which only the myogenic oscillation is present in the blood flow time series and states with periodic, quasiperiodic, or chaotic dynamics. Chaotic systems have the property that they are sensitive to initial conditions of the state variables. This means that the evolution in time of two sets of initial conditions, differing initially by an arbitrarily small amount, on average diverge exponentially. For nonlinear periodic systems, in contrast, the orbits will approach and relax onto a single limit cycle. A system in a quasiperiodic state is nonperiodic but does not show sensitivity to initial conditions. In fact, the two orbits remain different by a value that at most grows proportionally with time, and not exponentially.

Lyapunov exponents are often used to classify dynamics. In the present case, however, the system is too complicated to calculate a complete spectrum of exponents by the first principle approach. Instead, we used the method that calculates the largest exponent from a time series (48). This method is based on the idea of attractor reconstruction by embedding the time series together with past versions of the same time series into a multidimensional space. Relative divergence of nearby points on the trajectory is averaged along the trajectory. The embedding dimension may be chosen arbitrarily large, since the estimated exponent will converge to a fixed value. However, the drawback is that the larger the embedding dimension the slower the convergence. For the present case, the time series is represented by nephron plasma flow, and embedding dimension was set to 12. The time series was 1,500 s long. A positive Lyapunov exponent is an indication of the sensitivity to initial conditions, which is a fundamental characteristic of chaotic dynamics, whereas periodic and quasiperiodic dynamics show a negative and zero-valued exponent, respectively.

RESULTS

We wish to test whether systematic variation in ζ causes changes in the dynamics of the nephron. No changes were made in other parameters, or in the arterial pressure, which was 100 mmHg in all simulations reported here.

For different values of ζ, the model developed one of four different kinds of time-dependent behavior. At very low values, there was no TGF oscillation, and only the myogenic oscillation remained active. The three other patterns are shown in Fig. 2. At relatively low values of ζ, there was quasiperiodic behavior, which is characterized by the presence of two or more noncommensurate frequencies. Quasiperiodic motion has marginal stability, as indicated by the vanishing of the first two Lyapunov exponents. Figure 2, *top*, with $\zeta = 0.24$, shows quasiperiodicity. The two oscillations synchronize at higher values of ζ, shown in Fig. 2, *middle*, for which $\zeta = 0.275$. The larger oscillations are because of TGF. For each TGF cycle, there are five smaller peaks, each resulting from the self-sustained oscillation of the myogenic mechanism. The five peaks are not equally spaced, nor are they of equal magnitude in each TGF cycle. These variations among the myogenic peaks are the result of frequency and amplitude modulation (26, 28). The fluctuation pattern becomes irregular at higher values of ζ, shown in Fig. 2, *bottom*, which was generated using $\zeta = 0.35$. The TGF fluctuations persist, but the magnitude varies from cycle to cycle and in no apparent order. There were three to five myogenic peaks for each TGF cycle, and the number of myogenic peaks per TGF cycle varied in no apparent order in successive cycles. The time series in Fig. 2 are taken from the output of one of the nephrons in the two-nephron model. The two nephrons in that model had identical properties and parameters, and the time series of the two were identical. The time series from the one-nephron model showed minimal differences from those shown in Fig. 2 and are therefore not shown here.

Each type of motion shown in Fig. 2 forms a characteristic attractor in phase space. A later analysis of the results makes use of a Poincaré section, which is the intersection of a phase

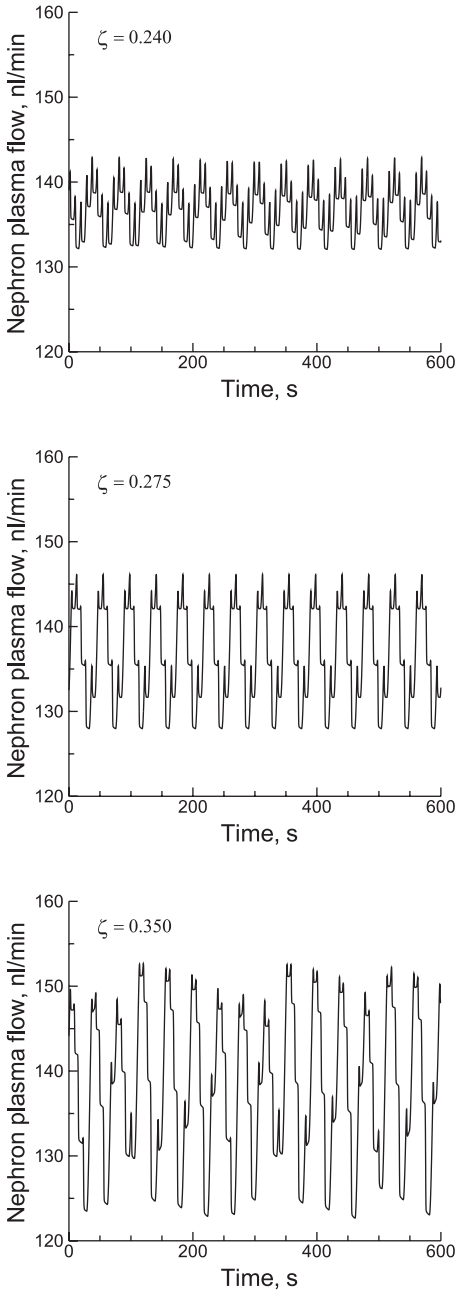

Fig. 2. Time series of renal plasma flow rate generated by one nephron of the two-nephron model, using 1 of 3 different values for the coupling parameter ζ.

space trajectory with a plane in phase space, and the phase space diagrams of the model results are therefore shown in Fig. 3. In each case, the phase space diagram is formed from the simulation results shown in the corresponding panels of Fig. 2, using the predicted time series of single nephron blood flow rate, NaCl concentration in tubular fluid at the macula densa, and intracellular Ca^{2+} in an arteriolar smooth muscle cell. Figure 3, *top*, shows the results with $\zeta = 0.24$. The pattern is that of a two-dimensional torus, with the large motion resulting from TGF and the smaller motions attributable to the myogenic oscillation dispersed around the TGF trajectory. If simulated to infinity, the orbit will densely fill the torus, without repeating itself. The quasiperiodic behavior may appear periodic in Fig. 2,

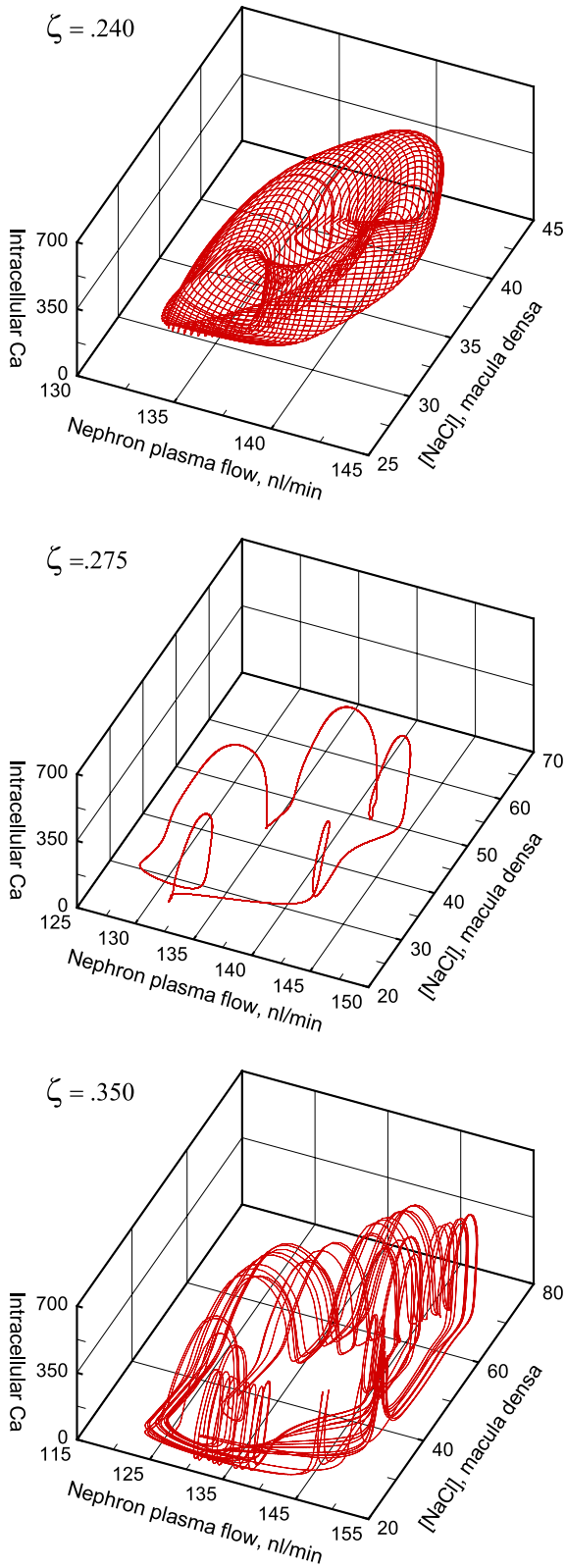

Fig. 3. Phase space diagrams generated by one nephron of the two-nephron model, using 1 of 3 different values for ζ. Each diagram was constructed from the time series of nephron plasma flow rate, NaCl concentration in tubular fluid from the macula densa, and intracellular Ca^{2+} concentration in an arteriolar smooth muscle cell. Each diagram used time series of 600 s duration. The scales differ among the 3 panels.

top, but the phase space attractor in Fig. 3 shows that the orbit runs on a torus. A closer look at the time series in Fig. 2, *top*, also confirms the aperiodic nature of the dynamics.

Figure 3, *middle*, shows the trajectory formed by a system with a stable oscillation. This tracing represents 600 s of simulated time, the same as in Fig. 3, *top* and *bottom*. The combined motion of the two oscillations retraces itself more than 14 times during this simulation without change from one repetition to the next, which is typical of phase-locked limit-cycle oscillations. Such oscillations are specific modes on the torus surface in which there is a rational ratio of the two periodicities. In our case, five myogenic oscillations are completed during each TGF cycle. The ability to synchronize different oscillatory modes is a characteristic feature of nonlinear systems. The myogenic trajectories are not equally spaced around the TGF loop because of frequency modulation by TGF, and they are not of equal amplitude because of amplitude modulation by TGF (26, 45).

Figure 3, *bottom*, shows the phase space diagram formed by the system at a higher value of ζ. The attractor no longer lies on the surface of a torus, and it does not retrace itself during the 600-s duration of the simulation. A chaotic attractor cannot run on a two-dimensional torus because two-dimensional dynamics are insufficient for chaos to occur and its attractor is therefore more complicated. The myogenic oscillations appear to differ in magnitude at different locations in phase space, suggesting that amplitude modulation persists in this chaos-like state. The time series in Fig. 2, *bottom*, also shows amplitude modulation of the myogenic oscillation by TGF.

To provide a quantitative description of the bifurcations shown by the model, we calculated one-dimensional bifurcation diagrams, which show the bifurcations through which chaos-like dynamics are developed as ζ is increased. The bifurcations taking place on the route from limit cycle to chaos-like behavior involve a torus bifurcation followed by saddle-node and homoclinic bifurcations. A torus birth bifurcation is a transition in which a periodic orbit loses its stability as two complex eigenvalues (called Floquet multipliers) cross out of the unit circle in the complex plane. In the present case, this happens when the newly born cycle (TGF in this case) modulates the existing cycle (from the myogenic mechanism) to form a torus in phase space. A saddle-node bifurcation is characterized by the collision of a stable and an unstable limit cycle during which both limit cycles cease to exist and the system seeks other attractors in the phase space. Bifurcations of this type are involved in the transitions between quasiperiodic and phase-locked periodic dynamics on the surface of the torus.

Homoclinic bifurcations, on the other hand, are involved in the destruction of the torus and the transition to chaos as the interaction between the two modes becomes too strong (1). A homoclinic bifurcation occurs, for instance, when a periodic orbit expands to touch the unstable manifold of an unstable equilibrium point. After the bifurcation, the periodic orbit no longer exists.

At low ζ values, only the myogenic mechanism oscillates. In the bifurcation diagram for the single nephron model (Fig. 4*A*), this mode is represented by a single curve. The TGF mechanism does not oscillate at this value of ζ because the signal from the macula densa is too weak. At $\zeta_1 = 0.221$, destabilization of the myogenic limit cycle takes place through a torus

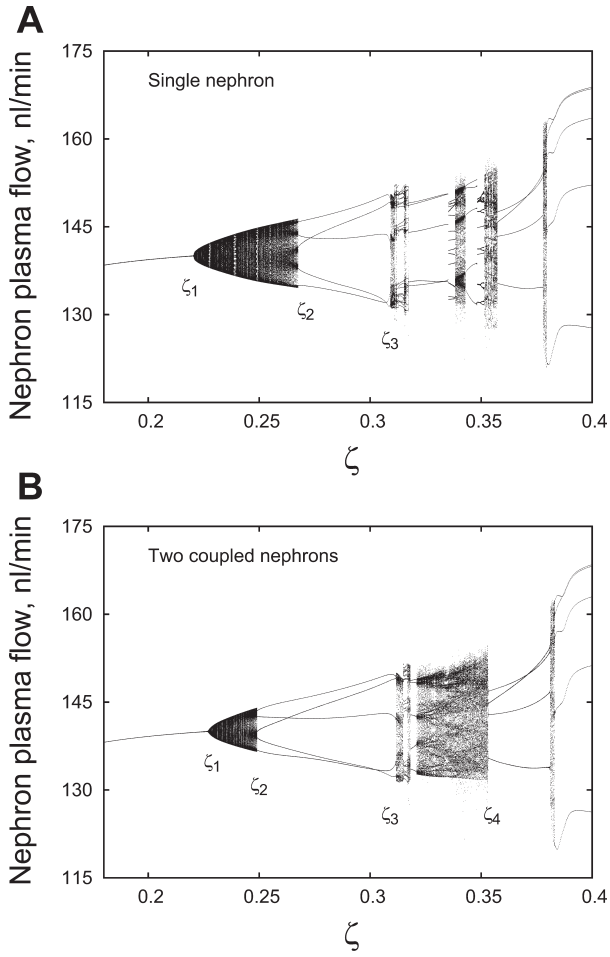

Fig. 4. One-dimensional bifurcation diagrams from the single and two-nephron models.

birth bifurcation. Oscillations are now present in both mechanisms.

In the region after ζ_1, there is an infinitely dense sequence of intervals, called windows or resonance tongues, with various mode lockings between the TGF and myogenic oscillations. Windows are terminated on both sides by saddle-node bifurcations and the transition to quasiperiodic dynamics. At $\zeta_2 = 0.267$, a wide window with 5:1 mode locking is born through a saddle-node bifurcation. The 5:1 mode locking is represented as five simultaneous curves, since the orbit makes five windings (myogenic oscillations) for each TGF cycle. This mode is present in the normotensive state. It is terminated at $\zeta_3 = 0.309$ through another saddle-node bifurcation, where the regular dynamics transform into chaos-like dynamics. For increasing ζ from this point, alternating regions show chaos-like and 5:1 and 4:1 dynamics.

The bifurcations in the two-nephron model (Fig. 4*B*) take place in much the same way as the single nephron model, but at different values of ζ. The torus bifurcations take place at $\zeta_1 = 0.221$, which as before leads to narrow windows with mode lockings and quasiperiodicity. The saddle-node bifurcation at ζ_2 leading to 5:1 mode locking takes place at $\zeta = 0.249$, a lower value than for the single nephron model, and is terminated at higher values, yielding a broader region with 5:1 dynamics. Most of the periodic windows that appear at larger

ζ in the single nephron model are absent, and the chaos-like motion is present over the interval $\zeta = [0.31, 0.355]$. At $\zeta_4 = 0.355$, a homoclinic bifurcation cause the emergence of 4:1 mode locking, which at higher ζ bifurcates to 5:1 mode locking through homoclinic bifurcations.

Figure 5 shows the Lyapunov exponent as a function of ζ. With the single nephron results (Fig. 5*A*), the exponent has negative values at the mode-locked regions and negative or almost zero exponents at ζ values where quasiperiodic dynamics occur. The narrow regions with positive exponents are chaotic. The values of the Lyapunov exponent with the two-nephron model (Fig. 5*B*) present a similar pattern but reflect the different values of ζ at which bifurcations occur.

DISCUSSION

Arterial blood pressure, the major input to the systems regulating renal blood flow, fluctuates irregularly (13, 25). The pattern of fluctuations in the ultradian frequency band is 1/*f*, signifying that the logarithm of the spectral power varies inversely with the logarithm of the frequency; small fluctuations are more frequent and large ones less so. The fluctuations are large enough to alter distal tubule flow rate, and therefore to disturb the epithelial transport mechanisms responsible for regulation of the composition and volume of body fluids. Renal autoregulation serves as a filter to reduce the impact of pressure fluctuations at frequencies <100 mHz (21, 41). Because the blood pressure is not steady, analysis of the time-dependent behavior of autoregulation is essential; steady-state constructs cannot, in principle, produce an adequate understanding of how autoregulation protects flow-dependent transport processes so that they can respond appropriately to hormonal control important for regulation of the body fluids. Moreover, the kidney develops in an environment with time varying arterial pressure, hormones, and other factors that affect it. The organization of renal structure and function must therefore reflect a response to these ongoing challenges, responses that cannot be understood with knowledge only of steady-state function. Oscillations, modulation effects, nephron synchronization, and bifurcations to chaos, all of which have been observed experimentally, arise out of time-dependent processes.

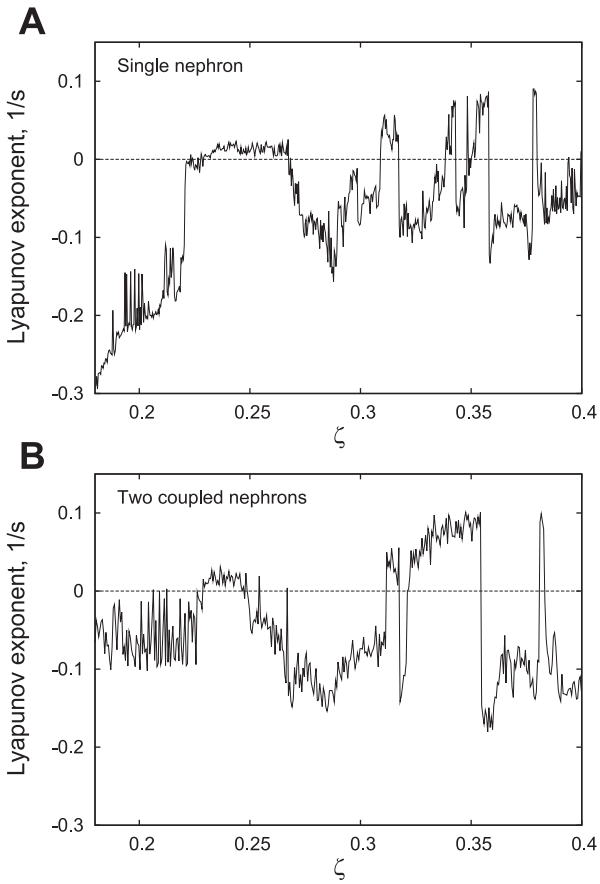

Fig. 5. Estimated first Lyapunov exponents from the one-nephron and coupled two-nephron models.

The delayed negative feedback control associated with TGF is responsible for periodic oscillations of tubular flow rate, GFR, and of tubular fluid NaCl concentration at the macula densa in time series of tubular pressure from rats with normal blood pressure (16). The arterioles supplying blood to these nephrons undergo periodic vasomotion and cause another, higher-frequency oscillation in tubular pressure and nephron blood flow (50). The periodic oscillations become irregular in rats with chronic high blood pressure, and the time series have properties of chaos (15, 51).

In this study, we tested whether changes in the strength of coupling between the TGF and myogenic mechanisms change the dynamics of blood flow control. We used a spatially extended model of tubular pressure, tubular flow rate, and tubular NaCl concentration in a compliant tubule to address the question. Boundary conditions for the system equations were GFR as the initial flow rate, the tubular pressure at the furthest extent of the distal tubule we simulated, and the concentration of NaCl in the glomerular filtrate. Because NaCl is the only solute whose epithelial transport is simulated in the model, its concentration is assumed invariant through the proximal tubule. The differential equation describing the change in NaCl concentration is therefore solved only from the transition between these tubular segments to the end of the model's tubular system.

GFR is heavily dependent on hydrostatic pressure in glomerular capillaries, and this pressure is dependent on the vascular resistance of the afferent arteriole that supplies blood to the glomerulus. The vascular resistance is affected by several factors: the length dependence of the contractile mechanism, the operation of a self-sustained oscillation in arteriolar radius caused by an instability in membrane electrical potential difference, input from TGF, and interactions among these factors. These components of the system act to maintain GFR constant over the range of arterial blood pressures occurring during a day (13, 25), and they have nonlinear properties. Finally, both the simulated tubule segments and those beyond the simulation show a significant mechanical compliance in response to changes in the tubular pressure (24). Hydraulic resistance to fluid outflow from the tubule therefore declines as flow increases. These boundary conditions provide nonlinearities to the system that contribute to the bifurcations we have simulated.

The model succeeds in simulating a number of measures of renal blood flow performance (26). Time-averaged results of GFR, of filtration fraction, of tubular flow rate, of tubular hydrostatic pressure, and of NaCl concentration in tubular fluid at the macula densa correspond to those found in experimental

measurements. The model also autoregulates GFR and renal plasma flow in response to changes in mean arterial pressure at flow rates characteristic of experimental responses (26). The dynamic predictions of the model include the presence of two oscillations at measured amplitudes and frequencies, sustained oscillations over a large range of arterial blood pressures and consistent with experimental studies of renal blood flow regulation, and modulation of the amplitude and frequency of the myogenic mechanism by TGF (26). Nonlinear interactions are found in measurements of whole kidney blood flow (6) and tubular pressure (28) and predicted in simulations with this model (26).

In this study, both the single nephron and two-nephron simulations undergo torus, saddle-node, and homoclinic bifurcations as the value of the coupling coefficient ζ is increased. This result is consistent with experimental findings (14, 15, 51). For the single nephron model, chaotic dynamics appear only for a small set of discontinuous values of the coupling parameter, whereas the two-nephron model behaves chaotically over a larger and more connected region. Nephrons are normally coupled to each other because of electrotonic signal propagation over the wall of the afferent arteriole (12, 29, 45), and the behavior of the two-nephron model is therefore more relevant to the kidney in vivo. The model also predicts that the bifurcation from quasiperiodicity to the 1:5 resonant oscillation in TGF occurs at lower values of ζ in the two-nephron model. Nephron coupling therefore increases the range of values over which both limit cycle oscillations and chaotic dynamics operate. Previously, we showed that nephron coupling improves the stability of the model with respect to the range of a parameter used to maintain the myogenic-to-TGF frequency ratio at 5:1 (29). Beach et al. (4) concluded that the TGF oscillation is more stable if nephrons interact than it is in single nephrons. The renal vascular structure is an example of a resource distribution network that can be a source of complex dynamics from both signaling and cardiovascular sources (27, 38, 39).

The model results suggest that an increased interaction between the TGF and myogenic oscillators can cause the bifurcation to the chaotic state. When the TGF oscillation is a limit cycle oscillator, there is synchronization between the two mechanisms at a 5:1 ratio, both in experimental results (45) and in the model. Increasing the value of ζ to produce chaos interferes with the synchronization between the mechanisms. We have shown previously that the interaction leads to synchronization and modulation effects (28). Clamping TGF input at a fixed value eliminated the time-varying modulation and allowed the myogenic mechanism to oscillate at a single frequency (26).

Using a simple nephron model lacking a representation of the myogenic mechanism (3), we have modeled transitions to chaos (18, 44). These earlier results showed period-doubling cascades as the bifurcation pathway from limit cycle oscillation to chaos. In this study, the pathway was through torus bifurcations. Period-doubling cascades have not been observed experimentally; tubules in the kidney are either oscillating or in a chaotic mode (15, 45, 49). The transition between the two states in vivo is therefore likely to be abrupt, which is characteristic of torus bifurcations. Abrupt transitions between dynamic states were found consistently in this study, as seen in Fig. 4. This distinction reinforces the conclusion that increased interaction between TGF and the myogenic mechanism can cause the bifurcation to chaos that occurs in animals with chronic hypertension.

TGF gain is increased in spontaneously hypertensive rats (8, 14). In our model, the gain is the product of the TGF output and the coupling parameter ζ. The coupling is assumed to act through the voltage-dependent Ca^{2+} conductance in the membrane of arteriolar smooth muscle cells. Strong experimental evidence suggests that the myogenic mechanism acts though membrane depolarization followed by Ca^{2+} influx through voltage-activated channels (7). Substantial evidence has accrued that TGF acts through activation of adenosine-sensitive A_1 receptors (43, 46). The adenosine appears to be derived from interstitial dephosphorylation of ATP released from the macula densa cells (42). The exact localization of the adenosine A_1 receptors mediating the TGF response is not known, but recent data suggest that adenosine receptors on vascular smooth muscle cells are critical for the TGF response (35). Activation of adenosine A_1 receptors on the vascular smooth muscle cells of afferent arterioles activates phospholipase C, leading to increased inositol trisphosphate production with subsequent release of intracellular Ca^{2+} (10). The major effect of this initial and transient increase in intracellular Ca^{2+} seems to be an activation of a Ca^{2+}-dependent Cl^- channel that results in membrane depolarization followed by influx of extracellular Ca^{2+} through the voltage-activated Ca^{2+} channels, causing contraction of the smooth muscle cells (11). The central role of voltage-activated Ca^{2+} channels is further emphasized by the fact that the TGF response, the myogenic response, and autoregulation of renal blood flow all are abolished by blockers of voltage-activated Ca^{2+} channels (7, 30, 33, 34). Because entry of extracellular Ca^{2+} through voltage-activated Ca^{2+} channels seems to be a shared mechanism in both TGF and the myogenic mechanism, we chose to model the effect of TGF as a direct activation of voltage-activated Ca^{2+} channels. We used a single parameter to represent the entirety of the signaling process from the macula densa to the vascular smooth muscle cells. This is in effect equivalent to linearizing it, which appears to be justified because a more detailed description introduces a level of complexity inconsistent with all other aspects of the model, and also because no dynamic data are available to justify anything more.

The effects of TGF output and coupling parameter cannot be separated in our model because they multiply each other. One may therefore imagine that the predicted action of TGF represents signaling from the macula densa to receptors on smooth muscle cells, whereas the coupling coefficient expresses the sensitivity of intracellular coupling mechanisms to input to those receptors.

We have earlier used a form of the spatially extended model with a linear coupling of TGF to the diameter of the afferent arteriole rather than an explicit representation of the myogenic mechanism (17). This simplified model simulates the TGF oscillation but could not be made to bifurcate to chaos over a larger range of TGF gain values than has been observed experimentally, a finding consistent with the idea that interactions between the two oscillators are required in single nephron simulations.

We have also observed that nephrons communicate with each other using vascular signals initiated by TGF (29). The strength of this coupling is increased in hypertension (5, 47).

We simulated a group of nephrons of different lengths, coupled by vascular signals (27). The nephron model (3) was much simpler than any we have used in this study and lacked a myogenic mechanism. Using parameter values that support a limit cycle oscillation with a single nephron version of this model, we found that many of the nephrons in this multinephron model operated in a chaos-like mode even at normal blood pressures. Increasing the coupling between nephrons increased the number of nephrons behaving chaotically. Layton et al. (20) and Pitman et al. (37), using their nephron model as the basis for a two-nephron configuration, found a range of values for a coupling term that generated chaos-like activity. Layton et al. (19) subsequently studied the effects of coupling two nephrons of different lengths on system dynamics, using their model of the thick ascending limb and TGF; nephron models were coupled linearly. They found that the two-nephron model exhibited limit cycle oscillations but could produce more complex dynamics under some combinations of nephron lengths. This result is quite similar to our finding with a multinephron model using a simpler nephron model than the one in this paper (27). Each of the simpler nephron models had a linear representation of vascular coupling between the macula densa and the afferent arteriole. The results of the current study show that the bifurcations of interest can also be caused in a single nephron model by an increase in value of the coefficient coupling TGF and the myogenic mechanism. All nephrons in this study were of identical lengths, a condition that, by itself, could not cause any of the bifurcations. The effects of the interplay between intranephron synchronization of TGF and the myogenic mechanisms, and internephron synchronization, remain to be studied.

Experimental results in two forms of experimental hypertension show irregular fluctuations in tubular and vascular dynamics (14, 15, 23, 51). The phase space attractor has been found to be low dimensional and to have a noninteger value, and the first Lyapunov exponent was positive (51). These are characteristics of datasets from chaotic systems. Surrogate data analysis confirmed the nonlinearity of the attractor (52). The ability to detect and measure chaos with these measures may be reduced when they are applied to experimental data. The principal reason for this uncertainty is that time series from real systems are affected by random processes, making it impossible to eliminate system and measurement noise. The animals used in those studies constitute complex systems from which it is technically impossible to eliminate all variation. Thus the experimental results can only be regarded as suggestive of chaos, and not a definitive demonstration.

An alternative to defining the dynamics generated by an experimental system is to simulate it, so that all sources of noise are eliminated and the results are strictly deterministic, the approach we used in this study. The models necessarily contain a number of approximations to the live kidney, however, and we know of no way to validate them completely. Moreover, the classic work on chaotic systems in the physics and mathematics literature generally uses third-order systems, whereas our models are much higher order, and the real kidney still higher. These considerations make it unlikely that a completely convincing case can be made that the observations of this study are due to chaos as rigorously defined.

The value of the approach we have followed, however, lies in the fact that chaotic systems have characteristic behaviors that differ from those of limit cycle oscillators, and in particular from those of linear systems, and these behaviors provide the basis for predictions about the performance of the real kidney. The task at hand then becomes one of predicting effects of nonlinear behavior in the kidney, and mapping these effects on to problems of physiological interest. The TGF and myogenic oscillations occur because those systems are nonlinear, at least second order, and contain dissipative terms, which are necessary conditions for a self-sustained oscillation to occur (2, 31, 32, 36). Whether systems with such properties oscillate is a matter of parameter values, and it would appear that the parameters in the kidney support these oscillatory dynamics. Because both TGF and the myogenic mechanism converge on a single contractile mechanism in arteriolar smooth muscle cells, an interaction is inevitable and synchronization is a likely outcome of that interaction.

Nephron synchronization is another effect of nonlinear interactions. This effect is well established in experimental measurements (12, 45, 49) and has been simulated with the same two-nephron model as used in this study (29) and with other simpler nephron models (4, 27, 37).

Nephron synchronization is impaired in hypertension (45). This effect may be a consequence of the bifurcation to the chaos-like state we have simulated in this study, or it may be a result of increased vascular signal coupling (5, 47), as we have also suggested (27), or both, and one change may be a response to the other.

Perspectives and Significance

We simulated tubular pressure, flow, and NaCl concentration in spatially extended mathematical models of one and two nephrons. Each nephron model included an active myogenic mechanism and an interaction between TGF and the myogenic mechanism operating at the Ca^{2+} conductance of afferent arteriolar smooth muscle cells. Nephrons were coupled electrotonically in the two-nephron simulation. The tubular variables and nephron blood flow oscillate in normotensive rats but are irregular in hypertensive animals, in which TGF gain is increased. We varied the strength of coupling between TGF and the myogenic mechanism to test whether an increase in this parameter could cause the change in the dynamics, and whether the experimental results represented deterministic chaos. Solutions of both one- and two-nephron models developed the irregularity at higher coupling strengths, but the range of coupling strengths that could cause the irregularity was larger in the two-nephron model.

These results confirm that the observed increase in coupling between TGF and the myogenic mechanism can cause the irregularities seen in experimental data from hypertensive rats and that the change in dynamics represents a bifurcation to deterministic chaos. Nephrons are normally coupled electronically to their neighbor nephrons, so the two-nephron result is more likely to represent the system dynamics in vivo.

The oscillations in normotensive animals show extensive synchronization, but this phenomenon is decreased in hypertensive animals, reflecting the operation of a chaotic system. The presence of periodic oscillations is likely to lead to the formation of ensembles of synchronized nephrons, and the absence of these oscillations in hypertensive animals can be

expected to reduce the size of such ensembles, and to reduce or eliminate the functional advantages such aggregation is likely to produce.

The strength of internephron coupling is also increased in hypertension, a change that models suggest can produce a bifurcation to chaos by itself. How the interaction between TGF and the myogenic mechanism affects the interaction between nephrons, and the effect of changes in both coupling strengths, remain to be studied.

GRANTS

The work of D. J. Marsh was supported by National Institutes of Health Grant EB-003508 and by a grant from the Lündbeck Foundation of Copenhagen, Denmark. O. V. Sosnovtseva and N.-H. Holstein-Rathlou received support from Det Frie Forskingsråd. J. Laugesen, O. V. Sosnovtseva, E. Mosekilde, and N.-H. Holstein-Rathlou acknowledge support from the European Union via the European Network of Excellence Biosim, Contract No. LSHB-CT-2004-005137.

DISCLOSURES

No conflicts of interest are declared by the authors.

REFERENCES

1. **Afraimovich VS, Shilnikov LP.** On invariant two-dimensional tori: their breakdown and stochasticity. *Am Math Soc Transl* 149: 201–209, 1991.
2. **Balanov A, Janson N, Postnov D, Sosnovtseva O.** *Synchronization: From Simple to Complex*. Berlin, Germany: Springer-Verlag, 2009.
3. **Barfred M, Mosekilde E, Holstein-Rathlou NH.** Bifurcation analysis of nephron pressure and flow regulation. *Chaos* 6: 280–287, 1996.
4. **Beach JM, Stewart WE, Pitman EB.** TGF-mediated dynamics in a system of many coupled nephrons. *Bull Math Biol* 71: 1482–1506, 2009.
5. **Chen YM, Yip KP, Marsh DJ, Holstein-Rathlou NH.** Magnitude of TGF-initiated nephron-nephron interactions is increased in SHR. *Am J Physiol Renal Fluid Electrolyte Physiol* 269: F198–F204, 1995.
6. **Chon KH, Chen YM, Marmarelis VZ, Marsh DJ, Holstein-Rathlou NH.** Detection of interactions between myogenic and TGF mechanisms using nonlinear analysis. *Am J Physiol Renal Fluid Electrolyte Physiol* 267: F160–F173, 1994.
7. **Davis MJ, Hill MA.** Signaling mechanisms underlying the vascular myogenic response. *Physiol Rev* 79: 387–423, 1999.
8. **Dilley JR, Arendshorst WJ.** Enhanced tubuloglomerular feedback activity in rats developing spontaneous hypertension. *Am J Physiol Renal Fluid Electrolyte Physiol* 247: F672–F679, 1984.
9. **Gonzalez-Fernandez JM, Ermentrout GB.** On the origin and dynamics of the vasomotion of small arteries. *Math Biosci* 240: 167, 1994.
10. **Hansen PB, Friis UG, Uhrenholt TR, Briggs J, Schnermann J.** Intracellular signalling pathways in the vasoconstrictor response of mouse afferent arterioles to adenosine. *Acta Physiol (Oxf)* 191: 89–97, 2007.
11. **Hansen PB, Friis UG, Uhrenholt TR, Briggs J, Schnermann J.** Intracellular signalling pathways in the vasoconstrictor response of mouse afferent arterioles to adenosine. *Acta Physiol (Oxf)* 191: 89–97, 2007.
12. **Holstein-Rathlou NH.** Synchronization of proximal intratubular pressure oscillations: evidence for interaction between nephrons. *Pflugers Arch* 408: 438–443, 1987.
13. **Holstein-Rathlou NH, He J, Wagner AJ, Marsh DJ.** Patterns of blood pressure variability in normotensive and hypertensive rats. *Am J Physiol Regul Integr Comp Physiol* 269: R1230–R1239, 1995.
14. **Holstein-Rathlou NH, Leyssac PP.** Differences in tubuloglomerular feedback–oscillatory activity between spontaneously hypertensive and Wistar-Kyoto rats. *J Hypertens Suppl* 3: S343–S345, 1985.
15. **Holstein-Rathlou NH, Leyssac PP.** TGF-mediated oscillations in the proximal intratubular pressure: differences between spontaneously hypertensive rats and Wistar-Kyoto rats. *Acta Physiol Scand* 126: 333–339, 1986.
16. **Holstein-Rathlou NH, Marsh DJ.** Oscillations of tubular pressure, flow, and distal chloride concentration in rats. *Am J Physiol Renal Fluid Electrolyte Physiol* 256: F1007–F1014, 1989.
17. **Holstein-Rathlou NH, Marsh DJ.** A dynamic model of the tubuloglomerular feedback mechanism. *Am J Physiol Renal Fluid Electrolyte Physiol* 258: F1448–F1459, 1990.
18. **Holstein-Rathlou NH, Yip KP, Sosnovtseva OV, Mosekilde E.** Synchronization phenomena in nephron-nephron interaction. *Chaos* 11: 417–426, 2001.
19. **Layton AT, Moore LC, Layton HE.** Multistable dynamics mediated by tubuloglomerular feedback in a model of coupled nephrons. *Bull Math Biol* 71: 515–555, 2009.
20. **Layton AT, Moore LC, Layton HE.** Multistability in tubuloglomerular feedback and spectral complexity in spontaneously hypertensive rats. *Am J Physiol Renal Physiol* 291: F79–F97, 2006.
21. **Layton HE, Pitman EB, Moore LC.** Nonlinear filter properties of the thick ascending limb. *Am J Physiol Renal Physiol* 273: F625–F634, 1997.
22. **Leyssac PP.** Further studies on oscillating tubulo-glomerular feedback responses in the rat kidney. *Acta Physiol Scand* 126: 271–277, 1986.
23. **Leyssac PP, Holstein-Rathlou NH.** Tubulo-glomerular feedback response: enhancement in adult spontaneously hypertensive rats and effects of anaesthetics. *Pflugers Arch* 413: 267–272, 1989.
24. **Marsh DJ, Martin CM.** Effects of diuretic states on collecting duct fluid flow resistance in the hamster kidney. *Am J Physiol* 229: 13–17, 1975.
25. **Marsh DJ, Osborn JL, Cowley AW Jr.** 1/f fluctuations in arterial pressure and regulation of renal blood flow in dogs. *Am J Physiol Renal Fluid Electrolyte Physiol* 258: F1394–F1400, 1990.
26. **Marsh DJ, Sosnovtseva OV, Chon KH, Holstein-Rathlou NH.** Nonlinear interactions in renal blood flow regulation. *Am J Physiol Regul Integr Comp Physiol* 288: R1143–R1159, 2005.
27. **Marsh DJ, Sosnovtseva OV, Mosekilde E, Holstein-Rathlou N-H.** Vascular coupling induces synchronization, quasiperiodicity, and chaos in a nephron tree. *Chaos* 17: 015114, 2007.
28. **Marsh DJ, Sosnovtseva OV, Pavlov AN, Yip KP, Holstein-Rathlou NH.** Frequency encoding in renal blood flow regulation. *Am J Physiol Regul Integr Comp Physiol* 288: R1160–R1167, 2005.
29. **Marsh DJ, Toma I, Sosnovtseva OV, Peti-Peterdi J, Holstein-Rathlou NH.** Electrotonic vascular signal conduction and nephron synchronization. *Am J Physiol Renal Physiol* 296: F751–F761, 2009.
30. **Mitchell KD, Navar LG.** Tubuloglomerular feedback responses during peritubular infusions of calcium channel blockers. *Am J Physiol Renal Fluid Electrolyte Physiol* 258: F537–F544, 1990.
31. **Mosekilde E.** *Topics in Nonlinear Dynamics*. Singapore: World Scientific, 1998.
32. **Mosekilde E, Maistrenko Y, Postnov D.** *Chaotic Synchronization: Applications to Living Systems*. Singapore: World Scientific, 2002.
33. **Navar LG, Champion WJ, Thomas CE.** Effects of calcium channel blockade on renal vascular resistance responses to changes in perfusion pressure and angiotensin-converting enzyme inhibition in dogs. *Circ Res* 58: 874–881, 1986.
34. **Ono H, Kokubun H, Hashimoto K.** Abolition by calcium antagonists of the autoregulation of renal blood flow. *Naunyn-Schmiedeberg's Arch Pharmacol* 285: 201–207, 1974.
35. **Oppermann M, Qin Y, Lai EY, Eisner C, Li L, Huang Y, Mizel D, Fryc J, Wilcox CS, Briggs J, Schnermann J, Castrop H.** Enhanced tubuloglomerular feedback in mice with vascular overexpression of A_1 adenosine receptors. *Am J Physiol Renal Physiol* 297: F1256–F1264, 2009.
36. **Pikovsky A, Rosenblum M, Kuerths J.** *Synchronization*. Cambridge, UK: Cambridge Univ Press, 2001.
37. **Pitman EB, Zaritski RM, Kesseler KJ, Moore LC, Layton HE.** Feedback-mediated dynamics in two coupled nephrons. *Bull Math Biol* 66: 1463–1492, 2004.
38. **Postnov D, Sosnovtseva O, Scherbakov P, Mosekilde E.** Multimode dynamics in a network with resource mediated coupling. *Chaos* 18: 015114, 2008.
39. **Postnov DE, Sosnovtseva OV, Mosekilde E.** Oscillator clustering in a resource distribution chain. *Chaos* 15: 13704, 2005.
40. **Quarteroni A, Valli A.** *Numerical Approximations of Partial Differential Equations*. Berlin, Germany: Springer Verlag, 1997.
41. **Sakai T, Craig DA, Wexler AS, Marsh DJ.** Fluid waves in renal tubules. *Biophys J* 50: 805–813, 1986.
42. **Schnermann J, Briggs JP.** Tubuloglomerular feedback: mechanistic insights from gene-manipulated mice. *Kidney Int* 74: 418–426, 2008.
43. **Schnermann J, Weihprecht H, Briggs JP.** Inhibition of tubuloglomerular feedback during adenosine1 receptor blockade. *Am J Physiol Renal Fluid Electrolyte Physiol* 258: F553–F561, 1990.
44. **Sosnovtseva OV, Pavlov AN, Mosekilde E, Holstein-Rathlou NH.** Bimodal oscillations in nephron autoregulation. *Phys Rev E Stat Nonlin Soft Matter Phys* 66: 061909, 2002.

45. **Sosnovtseva OV, Pavlov AN, Mosekilde E, Yip KP, Holstein-Rathlou NH, Marsh DJ.** Synchronization among mechanisms of renal autoregulation is reduced in hypertensive rats. *Am J Physiol Renal Physiol* 293: F1545–F1555, 2007.
46. **Sun D, Samuelson LC, Yang T, Huang Y, Paliege A, Saunders T, Briggs J, Schnermann J.** Mediation of tubuloglomerular feedback by adenosine: evidence from mice lacking adenosine 1 receptors. *Proc Natl Acad Sci USA* 98: 9983–9988, 2001.
47. **Wagner AJ, Holstein-Rathlou NH, Marsh DJ.** Internephron coupling by conducted vasomotor responses in normotensive and spontaneously hypertensive rats. *Am J Physiol Renal Physiol* 272: F372–F379, 1997.
48. **Wolf A, Swift JB, Swinney HL, Vastano JA.** Determining Lyapunov exponents from a time series. *Physica D* 16: 285–317, 1985.
49. **Yip KP, Holstein-Rathlou NH, Marsh DJ.** Dynamics of TGF-initiated nephron-nephron interactions in normotensive rats and SHR. *Am J Physiol Renal Fluid Electrolyte Physiol* 262: F980–F988, 1992.
50. **Yip KP, Holstein-Rathlou NH, Marsh DJ.** Mechanisms of temporal variation in single-nephron blood flow in rats. *Am J Physiol Renal Fluid Electrolyte Physiol* 264: F427–F434, 1993.
51. **Yip KP, Holstein-Rathlou NH, Marsh DJ.** Chaos in blood flow control in genetic and renovascular hypertensive rats. *Am J Physiol Renal Fluid Electrolyte Physiol* 261: F400–F408, 1991.
52. **Yip KP, Marsh DJ, Holstein-Rathlou N-H.** Low dimensional chaos in renal blood flow control in genetic and experimental hypertension. *Physica D* 80: 95–104, 1995.

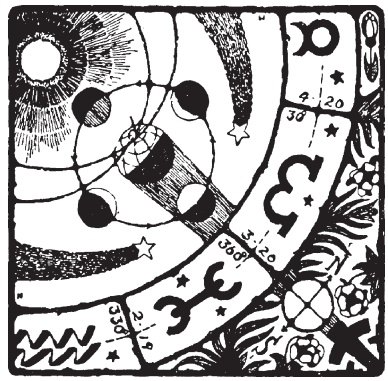

Publication P3:

Biosimulation and Computations in Systems Biology

Published in chapter 25 of *Handbook of Molecular Biophysics*, Ed. H. G. Bohr.

1
Biosimulation and Computations in Systems Biology

Olga Sosnovtseva[1], *Jakob L. Laugesen, and Erik Mosekilde*

1.1
Aiming to explain

Functioning of the human organism depends on regulatory processes that span an enormous range of spatial scales, from the nanometer scale of molecular conformation changes to the transmission of nerve signals over distances of the order of a meter. The fundamental elements of biochemical networks are nucleic acids (gene regulatory network), biomolecules (signaling networks) or small organic compounds (metabolic networks). The human genome may only have about 25000 genes, but these genes are used to make over 100000 proteins, many of which serve more than one function. Although some are more likely than others, the number of conceivable interactions between all the human genes and their protein products is completely incomprehensive. At the cellular level, biomolecular signaling networks implement a new set of functions, including signal transduction, rhythm generation, and intercellular signaling. Tissues and organs, the next level of biological organization, again display completely new properties. Communication among the cells lead them to function in a coordinated manner that can be very different from the isolated behavior of the cells that constitute the tissue. Biological complexity cuts across time as well as space. At the molecular level time scales of 10^{-9} seconds, characteristic of Brownian motion, are important, whereas aging processes and the development of diseases such as cancer and diabetes may involve time scales of the order of a human lifetime or 10^9 seconds.

Within this area of multi-disciplinary research, Systems Biology and Biosimulation are characterized by [17, 33, 34]:

- Global rather than local analysis, or holistic rather than reductionistic perspective. This refers to the attempt of System Biology to capture and analyze many interconnected aspects of a biological system simultaneously. This is in contrast to the reductionistic approach where one or a few aspects are studied at a time;

1) Corresponding author.

- The simultaneous study of different levels of biological organization, often with the aim of describing how new properties and functions arise through the coordinated interaction of many units;
- The investigation of biological reaction cascades and feedback networks, including gene regulatory, protein interaction as well as signaling and metabolic networks;
- The explicit incorporation of time in order to capture and analyze dynamical behaviors and stimuli-response patterns of biological systems and processes;
- The use of concepts and tools from engineering and control theory to examine the role of particular feedback regulations and to determine the significance and stability of such regulations;
- The direct involvement of concepts from non-linear dynamics and non-equilibrium thermodynamics to explain and describe observed temporal patterns, synchronization phenomena, and nonlinear wave propagation;
- The use of computational means to capture, model and simulate biological processes and systems.

Biosimulation, as we define it, is the application of Systems Biology to solve concrete problems in the pharmaceutical industry or the health sector at large [18]. Successful work in this area clearly requires close collaboration between pharmacists, medical doctors and modelers with a good understanding for feedback control, stability criteria, and nonlinear dynamics.

1.2 Approaches to a Systems Description

Computationally oriented biology involves two distinct approaches: (i) pattern recognition or data-mining that aims at extracting the hidden information from huge quantities of experimental data, in order to discover new phenomena, quantify their significance and formulate hypotheses about the involved processes [19] and (ii) simulation-based analysis (or hypothesis-driven research) that aims at establishing a dynamic model that captures the key features of a system and is consistent with all available experimental information [18].

Knowledge discovery and pattern recognition are used extensively within bioinformatics for such tasks as the prediction of exon-intron position and protein structure from a given sequence or the inference of gene regulatory

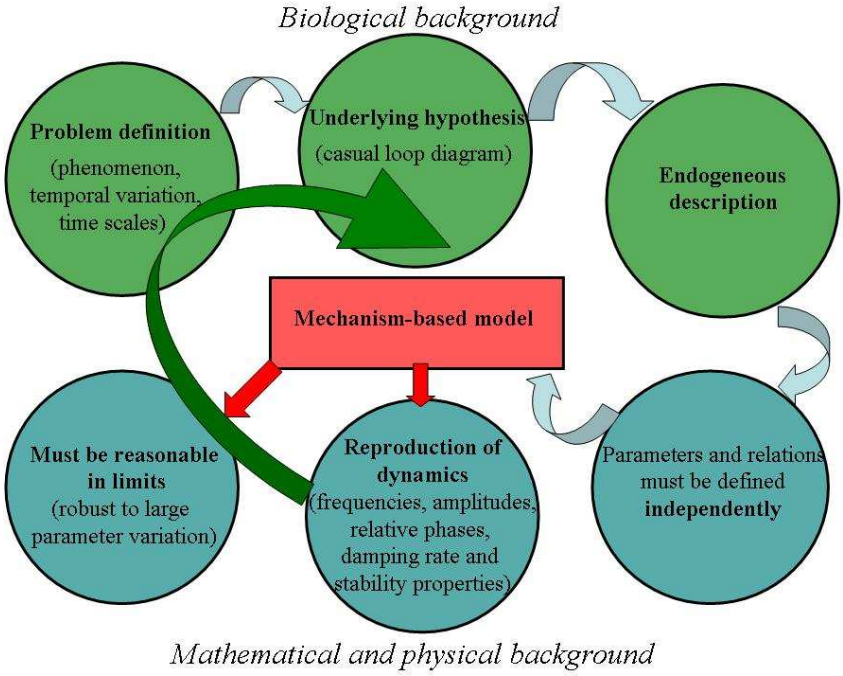

Fig. 1.1 Illustration of some of the main aspects of mechanism-based modeling as outlined in the main text. Note in particular the important role of problem definition. It is through this process that we can separate different time scales and decide what is important and what is not.

networks from expression profiles [19, 20]. These methods typically use predictions based on statistical discriminators that often involve sophisticated approaches (such as hidden Markov models) or other algorithms. In contrast, the simulation approach attempts to predict the dynamics of a system so that the validity of the underlying causal structures can be tested.

Although bioinformatics has long been used for genome analysis, protein structure determination and drug-likelyhood predictions, simulation-based approaches have so far received less attention. This now appears to change. Convincing results obtained with the systems approach have lead to a significant boost in interest, and combined with substantial advances in software and computational power this has enabled the creation and analysis of reasonably realistic, yet intricate biological models, such as the full-heart model developed by the universities in Oxford and Auckland [21, 22].

Mechanism-based modeling stems from engineering and other fields of science that have strong theoretical traditions. Computer simulation allows engineers to test the function of a new construction and compare it with other

possible constructions long before the first prototype is made. The results are enormous savings in time and money. Direct application of the same approach to biomedical problems is primarily restricted by the overwhelming complexity of living systems. From physics we have inherited the idea that one can separate processes and phenomena based on their temporal and spatial scales. This is obviously much more difficult for biological systems with their many and strongly coupled processes at overlapping time and space scales. Moreover, some of the most interesting problems are precisely to explain the coordination of processes that occur over separate time scales or to explain the properties of a tissue or the function of an organ in terms of the processes and interactions of the constituting cells or functional units.

A mechanism-based model is validated through its ability to generate behaviors with amplitudes, periodicities, phase relationships, response dynamics, damping characteristics, and stability properties in accordance with the experimentally observed dynamics [51]. At the end of the day, the model is validated by its ability to predict phenomena not previously experienced.

Two different paradigms can be recognized in the approach to model construction. In a bottom-up approach the individual base elements of the system are first described in great detail. These elements are then linked together to form larger subsystems, which in turn are linked, sometimes in many levels, until a complete model is developed at the top level. This strategy often resembles a "seed" model, where the beginning is small, but the model eventually grows in both complexity and coverage.

The theory of complex systems suggests that the rules by which parts of a system interact may be more important than the functioning of the individual parts. In a top-down approach an overview of the system is first formulated, specifying but not detailing relevant first-level subsystems. Each subsystem is then refined in yet greater detail, sometimes in many additional levels of subsystems, until the entire specification is reduced to basic elements. The top-down approach is most appropriate in a professional simulation environment that aims at developing a large, lasting and flawless model. The bottom-up approach is generally used in research environments where the goal is to test hypotheses and gain understanding. A judicious combination of the two, sometimes referred to as a "middle-out" approach, may turn out to be the most effective solution in some situations [18].

The purpose of the present chapter is to illustrate the use of mechanism based modeling and Biosimulation. We'll first demonstrate some of the basic aspects of the model building process by means of a strongly simplified description of the processes involved in regulation of the male sex hormone. Testosterone is found to be released in pulses with approximately two hour intervals, and we want to illustrate the possible role of feedback regulation in generating such ultradian oscillations. The second example provides a much

more detailed description of the mechanisms by which the individual nephron of the kidney regulates its afferent blood flow to compensate, for instance, for variations in the arterial blood pressure. Also this regulation is found to lead to self-sustained oscillatory dynamics.

1.3 Biological Rhythms and the Role of Feedback Regulation

Investigations performed during the last decades have revealed a great variety of rhythms of significance for the regulation and function of normal physiological systems. Hormonal secretion provides several illustrative examples with the release of luteinizing hormone [14], growth hormone [36], and insulin [37] displaying pronounced ultradian oscillations with 2-3 h periods. The release of insulin also displays a faster rhythm with a period of 9-15 min [38]. These rapid oscillations are likely to be of significance for the metabolic control processes in the liver, and there are a number of examples to support the idea that rhythmic administration of a hormone can be more effective than constant administration at the same average rate. It is also known that disruption of certain biological rhythms can lead to a state of disease [39] while, in other cases, synchronization of ultradian release processes can cause abnormal biological conditions such as, for instance, hot flashes [40].

Many hormonal secretion processes also exhibit strong 24 h or circadian components. This is true, for instance, for cortisol, antidiuretic hormone, and growth hormone. The secretion of growth hormone is markedly increased during the early periods of sleep, and the secretion of antidiuretic hormone also reflects the sleep-wake cycle. The stress hormone cortisol, on the other hand, shows a higher release rate during the last stages of sleep and in the early morning. This serves as a sort of wake-up call, and insulin secretion is similarly increased around the wakening hours in order to activate the body's muscular processes. The mechanisms underlying these oscillations can often be traced back to cyclical variations in the activity of the central nervous system [23, 24]. At the same time, the circadian rhythm modulates the above mentioned ultradian oscillations.

Feedback regulation is an important feature of all biological systems [25]. If a process has an effect on other processes and these processes again have an effect on the first process, then a "circular" relationship or "loop" exists. This generally helps a system to maintain stability. Regulation of the blood glucose concentration may serve as an example. Increasing concentration of glucose in the blood after a meal stimulates the pancreas to produce more insulin. The insulin is carried with the blood around in the body and diffuses through the capillary walls into the interstitial space, causing the cells to increase their

uptake of glucose. This in turn reduces the amount of glucose in the blood, thus bringing the system back towards its initial state.

The insulin-glucose feedback is said to be a negative feedback in that an initial increase in blood glucose concentration is counteracted by the release of insulin. Negative feedback regulations are generally considered as stabilizing to the system's dynamics. At the same time they reduce the significance of parameter variations, i.e., two individuals can have different values for the cellular sensitivity to insulin and yet function more or less in the same way. Positive feedback, on the other hand is destabilizing and leads to run-away phenomena. A typical example is the growth of cancer cells which often occurs in a nearly exponential fashion. Positive feedback regulation is not common in physiological systems. However, one can find examples where a temporary positive feedback helps to stimulate a fast activation. Peptides in the stomach, for instance, stimulate the release of chloric acid that breaks down proteins and thereby generate even more peptides. Similarly, during the release of an ovum from the ovary there is a phase in which some of the sex hormones enter into a positive feedback.

However, a negative feedback regulation is stabilizing only as long as the feedback is fast enough, i.e., the variables in the system must not change much before the change is registrated and corrections applied to the variables. If there is a delay in the feedback, the regulation may become unstable, and the system will start to oscillate. This is the situation in both of the two examples we are going to discuss in the present chapter. The presence of a delay is also the mechanism through which many other rhythmic phenomena arise in biological systems. We say that the system has undergone a Hopf bifurcation in which the original equilibrium point has become unstable (an unstable focus), and a self-sustained oscillation (or limit cycle) has taken over the role as the stationary solution [29].

1.4 Instabilities and Far-From-Equilibrium Conditions

From a physical point of view, the rhythmic phenomena are related to the fact that biological systems are maintained under far-from-equilibrium conditions through a continuous dissipation of energy [26]. However, non-equilibrium conditions can give rise to even more complicated behaviors. Chaotic dynamics, for instance, can arise either as a regular rhythmic process is destabilized and develops through a cascade of period-doubling bifurcations [41], by torus destruction in connection with the interaction of two or more rhythms with incommensurate periods [28], or via different types of intermittency [27].

Deterministic chaos is characterized by the facts that (i) the trajectory never repeats itself, but continues to find new ways to go, and that (ii) the dynamics is sensitive to small changes in the initial conditions [27]. Deterministic chaos may resemble random noise, and it can be difficult to distinguish the two. However, while a noisy system always responds in the same way to an external perturbation, the response of a chaotic system can vary significantly over the phases of its trajectory. In relation, for instance, to the medical treatment of a patient, this implies that while in a linear system the effect of a drug will always be the same, the precise timing of the administration may be significant for a rhythmic (or chaotic system). During certain phases of the oscillation, even a major dose may have little effect while a smaller dose may be highly effective (or perhaps even toxic) during other phases. Attempts to take advantage of this phenomenon are made, for instance, in experiments with chronotherapy of cancer and other diseases [47].

Synchronization is another universal phenomenon in nonlinear dynamical systems [30], a phenomena by which two (or more) rhythmic processes tend to adjust their dynamics relative to one another so as to attain a state where they are completely entrained or, alternatively, a state in which there is a rational relation between their periods. The synchronization of our circadian rhythm to the local time and the afore mentioned role of hormonal entrainment in the generation of hot flashes are typical examples. It is also well-known that the beating of the heart may synchronize with the respiration, typically with 1:3 or 1:4 relations between the two periods. By forcing an oscillating system with an external periodic signal and detecting the various synchronization regions, one can obtain information about the nonlinearities at play in the system. An example of this type of work is the investigation by Sturis *et al.* [42] of how the endogenous insulin secretion can synchronize with an externally forced periodic glucose infusion.

The significance of nonlinear dynamic phenomena seems to be even more pronounced at the cellular level. Coupling between the cells takes place via a variety of different mechanisms, including the short-range diffusive exchange of ions and small molecules through gap junction and the response of the individual cell to variations in the intercellular Ca^{2+}-concentration produced by the bursting activity of adjacent cells [43]. Hence, one can observe synchronization of the bursting activity between neighboring cells as well as waves of cytoplasmic calcium propagating across larger groups of pancreatic cells [45]. The above mentioned rapid oscillations in the secretion of insulin may be associated with a modulation of the bursting activity of the individual cells that arises from such intercellular interactions.

Synchronization of cellular activity is known from many other types of tissue, and transitions between different types of synchronization and between smaller and larger clusters of synchronized units may represent an impor-

tant component in the overall regulation of a physiological system. In their inactive state, smooth muscle cells, for instance, are found to exhibit incoherent waves of cytoplasmic Ca^{2+} produced by an instability associated with calcium-induced calcium release. When activated, however, the cells synchronize in a regular oscillatory pattern [46]. On the other hand, several cases are known where a similar transition is related to the development of a state of disease. It has long been recognized, for instance, that the onset of Parkinsonian tremor is associated with a synchronization of the firing activity for a group of cells in the brain [44].

1.5 Luteinizing Hormone

In this section we'll use a simple example of hormonal regulation to illustrate the basic principles of Systems Biology and feedback control. By means of a System Dynamics flow diagram [31] we build a model of the control of the production of the most important male sex hormone, testosterone, and we use this model to discus some of the aspects of the physiological mechanisms that cause the pulsatile behavior of the system.

System Dynamics [31] makes use of flow diagrams to illustrate the structure of interacting mechanisms that produces the dynamic phenomena we observe in managerial and economic systems. However, the same approach is applicable to biomedical systems. Flow diagrams can be considered as a language following a set of principles that must be used, in order to avoid ambiguous interpretations. In System Dynamics a system is described by a set of state variables, rates of change of these variables, auxiliary variables, exogenous variables and delays, each represented by a specific symbol in the flow diagrams.

1.5.1 Model of the pulsatile release of luteinizing hormone

In humans (and other mammals) the secretion of sex hormones, testosterone for males and estradiol and progesterone for females, are controlled by the production of luteinizing hormone, which again is controlled by the production of a releasing hormone called gonadotropin releasing hormone (GnRH). In turn the production of GnRH appears to be controlled by the amount of circulating testosterone [32].

A particular interesting aspect of the GnRH-LH-T system is that the hormone secretion takes the form of pulses. A GnRH-pulse is followed a few minutes later by an LH-pulse, while it takes approximately 30 minutes for LH to stimulate the production of T to its maximum. A pulsatile release of GnRH

is crucial for the system to function normally. It was shown by Knobil [12], that constant replacement of GnRH production fails to establish normal LH concentrations. On the other hand, various diseases, such as hypothalamic amenorrhea and hypogonadotropic hypogonadism, have been treated successfully with pulses of GnRH [13].

System Dynamics makes a clear distinction between amounts and concentrations with respect to their function in the models. The amounts of different hormones in their respective distribution volumes and their rates of change through production, degradation, transfer to other distribution volumes, etc., are the elements of the material conservation equations for the system, and they constitute the backbone of the models. Concentrations do not satisfy similar conservation equations, and use of concentrations as basic variables can only cause confusion in models with different or time-varying distribution volumes. On the other hand, biological effects are controlled by concentrations, and the concentration of various hormones therefore enter the model's causal relations. Concentrations are, of course, calculated from the corresponding amounts by division by the relevant distribution volume. In this way, causal relations will always start at a level (or state) variable and end at a rate variable.

When the concentration of GnRH increases it stimulates an increasing production of LH and, as long as the production of LH exceeds its rate of degradation in the organism, this leads to increasing amounts of LH. This first step in constructing a model is described by the flow diagram in Fig. 1.2, where the valves indicate the rates of production and decay. Rate related parameters, for instance hormone lifetimes, are indicated by dashed curves pointing into the valve. The boxes represent material accumulations of a given hormone. The solid straight arrows indicate flow direction and dashed curves indicate causal dependences. The rate of degradation depends both on the lifetime and on the amount of hormone, since the more hormone is present the more hormone will degrade per unit time. The rate of hormone production depends on the current concentration of the stimulating hormone through a non-linear relationship, which typically follows an S-shaped function. This implies that very little LH is produced at low concentrations of the stimulating hormone. Then follows a range of concentrations where the production of LH increases rapidly before it finally levels off at a maximum production rate.

In a similar way, stimulation of testosterone production in dependence of LH follows an S-shaped curve, such that increasing amount of LH stimulates an increasing production of T. An increase in T, on the other hand, is assumed to have an inhibitory effect on the production of GnRH. The system thus constitutes a negative feedback loop. A flow diagram of the described hormonal feedback system is shown in Fig. 1.4. Note, that material flows are expressed by fully drawn straight arrows and causal dependences, i.e.,

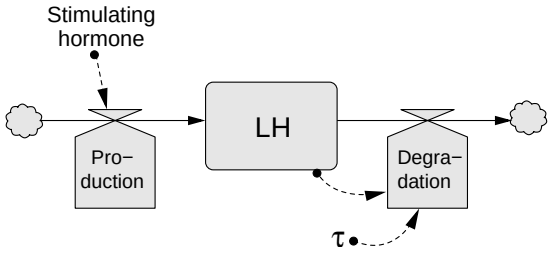

Fig. 1.2 Flow diagram of a production/degradation process. LH denotes the amount of hormone, and the arrows indicate flow directions with valves to illustrate that the flow is controlled by other variables or constants.

physical and chemical laws or biological control mechanisms, are described by dashed curves. Dashed curves always emanate from a state variable and end at a rate.

These three inter-hormonal dependences have been experimentally studied [35] and to a first approximation they follow the S-shaped curves shown in Fig. 1.3.

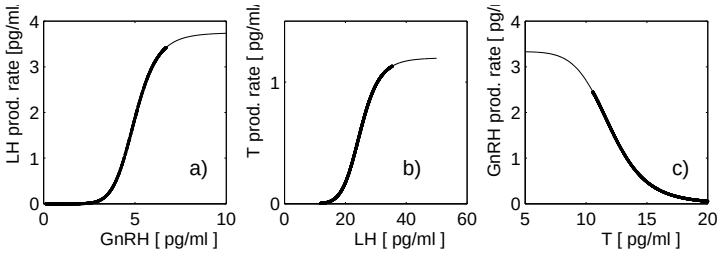

Fig. 1.3 S-shaped functions used to control the production of hormone in dependence on the concentration of the stimulating hormone. a) and b) are the functions controlling production of LH and T in dependence on GnRH and LH, respectively, while the negative sloped function in c) controls the suppression of GnRH production at high concentrations of T.

From a biological point of view the most appropriate functional relationship for the S-shaped curves are Hill-functions of the form

$$S(x) = \frac{Vx^n}{K^n + x^n}$$

where V is a saturation production rate, K is a constant that determines the position of the equilibrium point, and n a parameter that determines the slope of S at the equilibrium concentration x_0, which is also the turning point of the curve. Note, that the value of n is negative for $S_R(T)$.

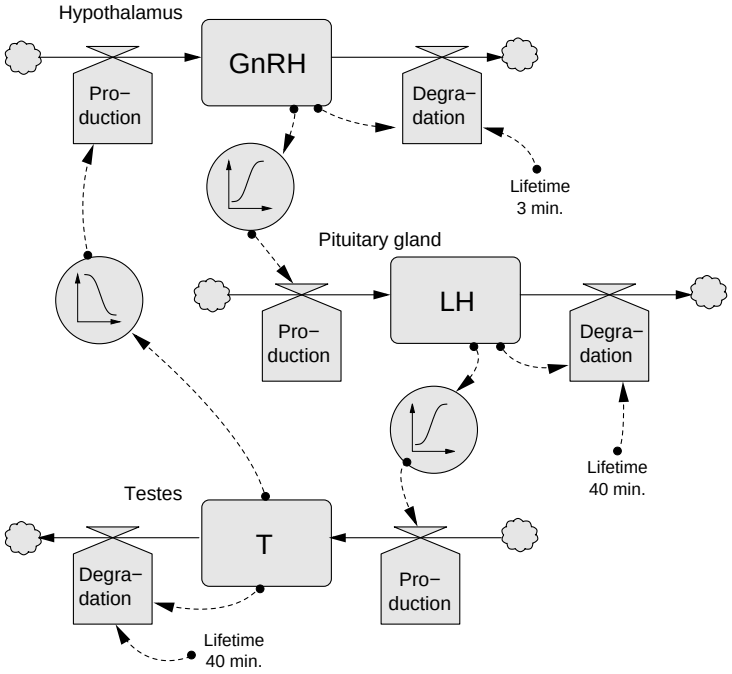

Fig. 1.4 Flow diagram describing the production of the releasing hormone (GnRH), luteinizing hormone (LH) and testosterone (T) and their mutual stimulatory effects are modeled by S-functions. The effect of T on GnRH is suppressing, and this makes the overall feedback negative.

The corresonding equations for the production of the three hormones are

$$\begin{aligned} \frac{dR}{dt} &= S_R(T) - R/\tau_R \\ \frac{dL}{dt} &= S_L(R) - L/\tau_L \\ \frac{dT}{dt} &= S_T(L) - T/\tau_T, \end{aligned}$$

where the parameters τ_R, τ_L and τ_T are hormonal lifetimes and $S(\cdot)$ are appropriately scaled S-shaped functions. Variables and indicies R, L and T refers to GnRH, LH and T. The equilibrium point of this system is found by requiring the flows vanish, whereby we find the equilibrium point

$$\begin{aligned} R_0 &= K_R \\ L_0 &= K_L \\ T_0 &= K_T \end{aligned}$$

The stability of the equilibrium is found by evaluating of the Jacobian matrix J at the equilibrium point

$$J = \begin{pmatrix} -1/\tau_R & 0 & n_R V_R/(4K_R) \\ n_L V_L/(4K_L) & -1/\tau_L & 0 \\ 0 & n_T V_T/(4K_T) & -1/\tau_T \end{pmatrix}$$

and taking the determinant to obtain the characteristic polynomium. For a third order system, the polynomium is also of third order $P(\lambda) = \lambda^3 + A\lambda^2 + B\lambda + C$, and for the present model the coefficients are

$$\begin{aligned} A &= \frac{1}{\tau_R} + \frac{1}{\tau_L} + \frac{1}{\tau_T} \\ B &= \frac{1}{\tau_R \tau_L} + \frac{1}{\tau_L \tau_T} + \frac{1}{\tau_T \tau_R} \\ C &= \frac{1}{\tau_R \tau_L \tau_T} - \frac{n_R n_L n_T}{64} \frac{V_L V_R V_T}{K_L K_R K_T}. \end{aligned}$$

The Routh-Hurwitz stability criterion [15] for a third order system states that the coefficients of the characteristic polynomium must fulfill the conditions

$$A > 0, B > 0, C > 0 \text{ and } AB - C > 0.$$

The first three conditions are clearly fulfilled for all physical relevant values of the delays constants τ_R, τ_L and τ_T. A more complete analysis of the system identifies the critical point, where $AB - C = 0$, as a Hopf bifurcation. The last equality can be explicitly written as

$$\frac{(\tau_T + \tau_L)(\tau_T + \tau_R)(\tau_R + \tau_L)}{(\tau_R \tau_L \tau_T)^2} > \frac{n_L n_R n_T}{64} \frac{V_L V_R V_T}{K_L K_R K_T}.$$

With experimentally measured lifetimes of τ_R=3 min, τ_L=40 min and τ_T=40 min [16] and equilibrium values of R_0 =5 pg/ml, L_0 =25 pg/ml and T_0 =12 pg/ml [14] we obtain the saturation values V_R =3.3 pg/(ml s), V_L =3.75 pg/(ml s) and V_T =1.2 pg/(ml s). The equilibrium point is stable for Hill exponents fulfilling the condition

$$|n_R n_L n_T| > 41.5.$$

By means of this inequality we can decide the values of the slopes such that the hormonal release over time shows an oscillating behavior. It is assumed that the response of L to R is fast since the hypothalamus and pituitary gland is located relative closely to the hypothalamus in the brain, while the response of T to L is slow since L must be transported over a significant distance to the testes where the production of T takes place. Realistic values would be $n_R = -6$, $n_L = 6$ and $n_T = 6$. The time evolution of the simulated hormone concentration with these values is shown in Fig. 1.5. Clearly, the behavior is oscillatory, however, the period is only approximately 50 minutes, which is more than a factor 2 too fast as compared with experimental findings. The parameters that most directly control the period are the lifetimes of the hormones. However, since the values have been measured experimentally there appears only to be one solution to the problem, namely to amend the production rate functions. The parameter V also influence the period, but this parameter have a strong influence on the amplitudes, and it is therefore not possible by varying this parameter to obtain both the amplitudes and the period correct at the same time. An alternative solution could be to examine the effect of delays that may be involved in the hormonal production. The presence of such delays could at one and and the same time provide a longer period and a more pulsatile dynamics.

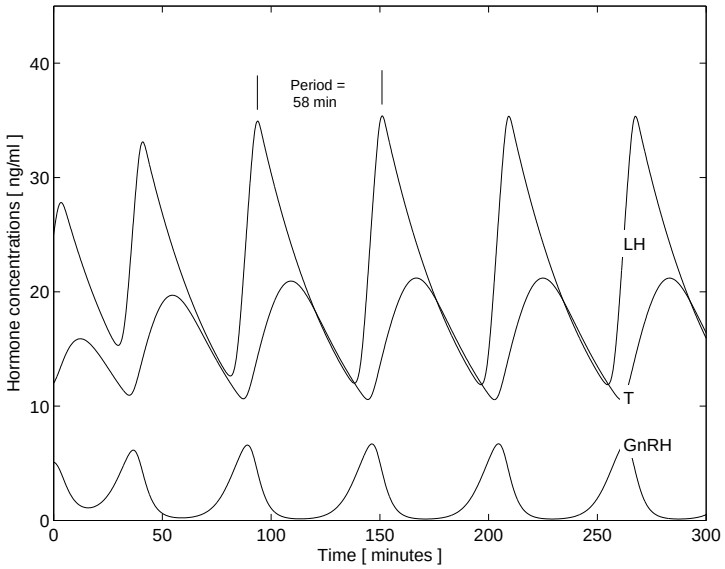

Fig. 1.5 Simulated time evolution for releasing hormone (GnRH), luteinizing hormone (LH) and testosterone (T). The parameters used in this simulation yield a period of 58 min between the bursts of LH secretion. In reality the period is closer to 2 h.

One possible way of increasing the period is to insert an extra delay in order to account for the time it takes to activate the cells to change their hormonal production.

A significant set of functions may fit the experimentally observed S-shaped hormone production response. However, few of them have a physiological interpretation in terms biochemical processes. For instance the logistic function, $V/(1+\exp\{K(x-x_0)\})$, could fit the relationship between hormone concentration and production rate quite well. But, it is not possible to relate the exponential function to the mechanisms that control the receptor dynamics. Hill functions, on the other hand, are accepted as a mechanistic model of receptor dynamics, since there is some correspondence between the parameters of the function with the chemical constants of the biological process.

Finally, we note that there might also be an inhibitory interaction between LH and GnRH, such that high concentrations of LH may slow down the production of GnRH, whereby the full development of a cycle is retarded.

1.6 Nephron Pressure and Flow Regulation

As an example of a more detailed application of the mechanism-based approach we'll consider a model that combines a description of nephron blood flow regulation with a description of the reabsorption of water and salts in the loop of Henle. A model of nephron autoregulation has previously been presented [5]. The purpose of that model was to examine the processes underlying the observed rhythmic and chaotic variations in pressures and flows observed for normotensive and hypertensive rats, respectively. Reabsorption of water and salts in the loop of Henle has been described in [8], but in a spatially extended model that is too complicated to allow detailed bifurcation analysis. The idea of the present study is to combine the two processes into a lumped model that retains sufficient simplicity to permit us to perform a more detailed bifurcation analysis.

1.6.1 Physiological background

By regulation the excretion of salts, water and metabolic end products, the kidneys play an important role in maintaining a suitable environment for the cells of the body. In particular, the kidneys control the plasma osmolality, the proportion of various blood solutes, the extracellular fluid volume, and the blood pressure. To protect their own function and secure a relatively constant blood flow, the kidneys also dispose of mechanisms that can compensate for variations in arterial blood pressure. It has long been recognized that this abil-

ity partly rests with controls in the individual nephron primarily the so-called tubuloglomerular feedback (TGF) [1]. This is a negative feedback that regulates the diameter of the afferent arteriole, and hence the incoming blood flow, in dependence of the chloride or sodium concentration of pre-urine leaving the loop of Henle.

The nephron may be considered as the functional unit of the kidney. The human kidney contains about 1 million nephrons, while the rat kidney contains some 30 thousand nephrons. However, the structural features, the main physiological processes, and the qualitative behavior appear to be similar to those of the human kidney. The differences are almost completely associated with the parameter values. The model we present here is a model of a single nephron initially formulated by Jensen *et al.* [6] and later studied in greater detail by Barfred *et al.* [7]. The intricacies of the nephron-nephron coupling, discussed in a number of recent studies [48], are neglected here.

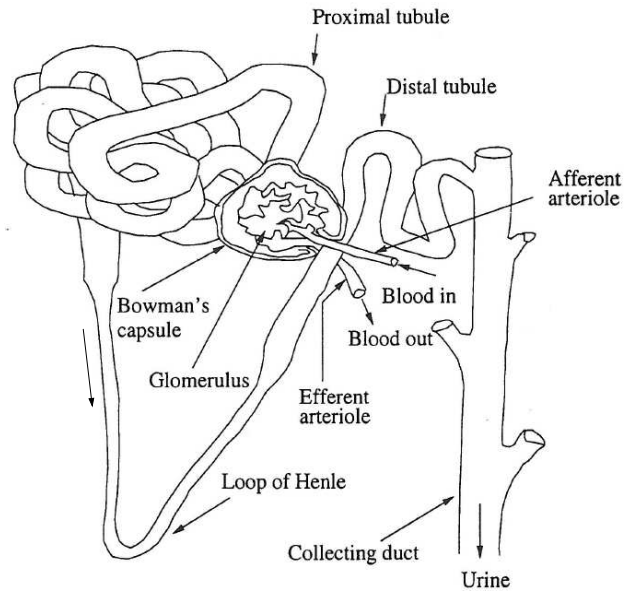

Fig. 1.6 Sketch of a nephron with its main components. The incoming blood from the afferent arteriole is filtered in the glomerulus. In the proximal tubulus a large part of the filtered fluid is reabsorbed and further reabsorption of water takes place in the descending limb of Henle, while salt reabsorption takes place in the ascending limb. At the point of contact between the distal tubulus and the glomerulus macula densa cells measure the salt concentration and send transmitters to the smooth muscle cells, which cause a constriction of the afferent arteriole at large salt concentrations.

Figure 1.6 shows the tubular structure of a nephron. The inset to the nephron from the body's vascular system is the afferent arteriole, originat-

ing from sequential branching of arteries. The blood enters the the glomerulus, which extracts water and various substance, except blood cells and proteins. The extracted fluid flows further into the convoluted proximal tubulus. Nearby 70% of the glomerular filtrate is reabsorbed from the proximal tubule into the capillary network and collected by the outgoing venous system. This isosmotic process is controlled completely by a hydrostatic pressure gradient. The residual fraction becomes important for the feedback mechanism later in the filtration. The remaining 30% of the filtrate enters the thin descending loop of Henle where additionally 15% of the water is reabsorbed giving rise to an increased concentration of NaCl as the limb is impermeable to salts. On passing the ascending limb the filtrate is again diluted as Na^+ and Cl^- are reabsorbed, while the limb is largely impermeable to water. At the end of Henle's loop, the tubulus comes into cellular contact with the afferent arteriole of the same nephron. At these points special cells, the so-called macula densa (MD) cells, sense the Na^+ concentration. If the rate of glomerular filtration, due for instance to an elevated arterial blood pressure, is too high, the active reabsorption of NaCl is not complete, and the salt concentration at the macula densa is too high. The macula densa cells then produce transmitter agents that cause the flow resistance of the afferent arteriole to increase by radial contraction, hence lowering the glomerular pressure and thereby reducing the filtration rate. A second mechanism that contribute to the autoregulation is the myogenic response of the afferent (and possibly the efferent) arteriole. Basicly it is an active response that counteracts increases in arteriolar pressure by increasing constriction/tension of the vessel caused by the smooth muscle cells in the arteriolar wall. The detailed chemical mechanics of the myogenic response are still not fully understood. In the present model a semi-empirical macro-physiological description of this process is adoted.

While most tissues in the organism dispose of a myogenic mechanism that allows them to control the incoming blood flow in relation to their metabolic and other needs, the TGF mechanism is specific to the nephrons of the kidney. This mechanism is seen as a way for the nephrons to protect their own function against variations in the arterial pressure. The causal loop diagram in Fig. 1.7 illustrates the main elements of the TGF mechanism as described above. The feedback is negative in that increasing arterial pressures lead to higher filtration rates which result in higher NaCl concentrations at the macula densa leading to arteriolar contraction and reduced filtration rates. However, the feedback involves a delay of approximately 12 s associated with the time it takes the filtrate to flow through the loop of Henle.

Early experiments by Leyssac and Baumbach [2] and by Holstein-Rathlou and Leyssac [3] demonstrated that the feedback regulation could become unstable and generate self-sustained oscillations in the proximal intratubular pressure with characteristic periods of 30-40 s. While for normotensive rats

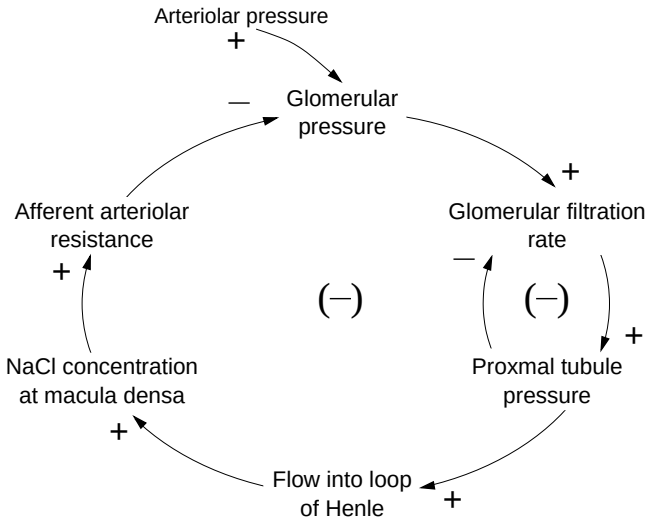

Fig. 1.7 Causal loops for TGF. Minus indicates a negative influence and plus indicates a positive influence in the arrow direction. Altogether the loop represents a negative feedback. However, due to the delay associated primarily with the fluid flow through the loop of Henle, and because of a relatively high gain factor the regulation tends to become unstable and produce self-sustained oscillatory dynamics.

the oscillations had the typical appearance of a limit cycle, highly irregular oscillations were found for spontaneously hypertensive rats (SHR). Oscillations were observed for 50-80% of the investigated nephrons. For non-oscillatory nephrons, self-sustained oscillations could be elicited by microperfusion with artificial tubular fluid, i.e., by artificially increasing the rate of flow through the loop of Henle. It has subsequently been observed that similar irregular oscillations can develop for normal rats, if the arterial pressure is increased by ligating the blood supply to the other kidney.

1.7 Single Nephron Model

In this section we construct the model step by step and collect the all the subsystems into one coherent description of the tubular and arteriolar system. We have already presented the fluid flow through the nephron above. In the following the total function of the nephron is grouped into specific submodels representing glomerular filtration rate (GFR), flow through the loop of Henle, the arteriolar resistance, and a macroscopic model of the smooth muscle cells in the afferent arteriole. This description will follow the structure of the corresponding flow diagram as depicted in Fig. 1.8.

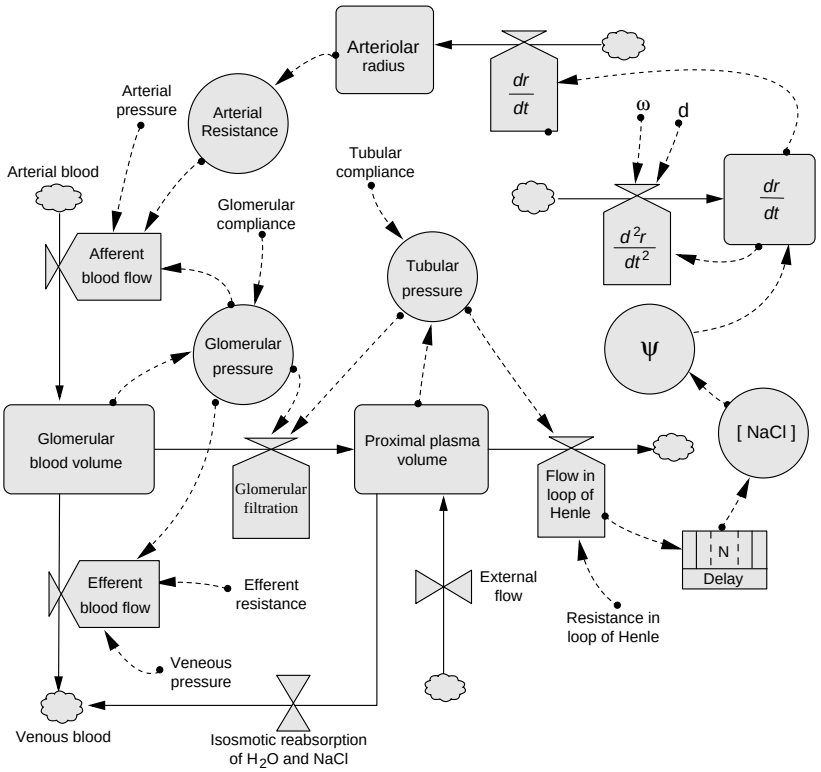

Fig. 1.8 Flow diagram for the single nephron model. The are four main flows in the diagram: 1) The blood flow through the glomerular capillaries, 2) the glomerular filtration, 3) the flow through the loop of Henle and 4) the rate of change of arterial radius and its second order rate of change. The feedback on the arterial blood flow is realized by the dependence of the arterial resistance on the arterial response to pressure. Description of the processes that take place in the loop of Henle is here reduced to a single flow rate and a delay. A lumped representation is shown in greater detail in Fig. 1.9.

To the left in the diagram we follow the flow of blood from the arterial system through the afferent arteriole, the glomerular capillaries, and the efferent arteriole to the venous system. The two arterioles are represented by their flow resistances of which the efferent resistance is assumed to be constant. The afferent flow resistance varies as part of the pressure and flow regulation. The blood flow through the glomerular capillaries is determined by the pressure difference between the arterial and venous sides and the two flow resistances. The glomerular capillaries are represented as a (small) compliant blood volume. The glomerular filtration rate depends on the difference between the glomerular pressure and the proximal tubular pressure accounting, of course, for the difference in protein osmotic pressure across the capillary

wall. It is assumed that the blood reaches pressure equilibrium before it leaves the glomerular capillaries. The equation for the proximal pressure is derived from the in- and outflows to the tubule

$$\frac{dP_t}{dt} = \left(F_{filt} - F_{reab} - F_H\right)\frac{1}{C_t},$$

where F_{filt} denotes the flow of filtrated fluid, F_{reab} the reabsorption, F_H the flow from the proximal tubule in the loop of Henle, and C_t is the proximal tubular compliance. The large reabsorption of both water and salt in this early tubule is represented in the flow diagram by the arrow pointing from the tubular fluid volume to the venous system. The salt concentration remains approximately constant in the proximal tubule as the tubular wall is equally permeable to water and salts.

The loop of Henle is modeled as a tube divided into a number of consecutive compartments, each with their specific physiological properties. In order to account for the mechanistic differences between water and salt reabsorption, the amounts of water and salt must be considered separately as shown in Fig. 1.9, where the upper part of the chain is the water volumes and flows between the compartments and the lower part represents the amounts of salt in the various compartments along the chain. Again, we model this system by the mass conservation of the filtrate for each compartment and apply our knowledge about the physical properties of the tube and fluid, which for instance are the compliance and resistance of the tube and the transit times between the compartments. The flow rate of water entering the first compartment of the thin descending limb from the proximal tubules is the inset to the flow diagram. This flow rate depends on the compliance and resistance of this compartment and on a delay time representing the time needed for the fluid to move from the proximal tubulus to the first compartment. Reabsorption of water into the the capillary system takes place through the interstitium, however this process is considered to fall outside the boundaries of the model, since it only has little influence on the TGF mechanism. Reabsorption of water is osmotic and therefore depends on the concentration difference across the tubular wall and on the permeability of the wall.

In Fig. 1.9 the lumped loop model is depicted with two descending compartments, each with reabsorption of water. The ascending limb is represented by three compartments. While there is no reabsorption of water in the ascending limb, reabsorption of salt takes place according to usual Michaelis-Menten kinetics. However, there is also an osmotic backleak of salt from the interstitium into the tubule. This backleak has only little influence on the dynamics of the model when operated in the normal working regime. However, if the flow through the loop becomes very small, the reabsorption of water will decrease, while the active salt reabsorption remains almost unchanged, giving rise to an increased salt gradient across the ascending limb. The backleak mechanism

seeks to re-establish the normal salt balance by allowing paracellular diffusion. At the end of the loop in Fig. 1.9 the amounts of both water and salt

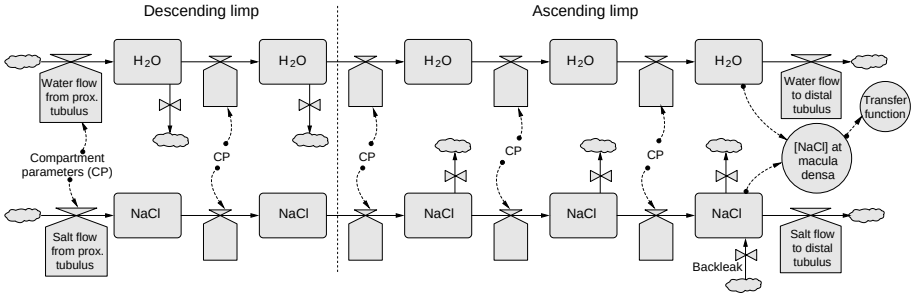

Fig. 1.9 Flow diagram with two descending and three ascending compartments in the loop of Henle. The incoming flows come from the proximal tubule and the outgoing flows enter the distal tubule close to the point where the macula densa cells are located. Reabsorption is symbolized by the rates between water/salt amounts and interstitial volume, which here is assumed to be an infinite sink.

yields a salt concentration which passes the macula densa cells at the intersect of the distal and juxta-glomerular apparatus, permitting the arteriolar model to respond to the NaCl concentration through the TGF transfer function.

Several experiments have shown that the radius of arterioles may perform spontaneous or self-sustained oscillations [9, 10], i.e. independent of the pressure variation due to TGF. According to Poiseuille's law the resistance of the arteriole is inversely proportional to the fourth power its radius. Hence, constrictions of the arteriolar radius cause a reduction in blood flow into the glomerulus. This mechanism is modeled by a second order differential equation of the form

$$\frac{d^2r}{dt^2} + d\frac{dr}{dt} = \omega^2 \frac{P_{trans}}{P_0}$$

where r is the normalized radius. d is a damping coefficient, P_{trans} the transmural pressure, ω a characteristic the angular frequency, and P_0 a normalization pressure. The transmural pressure is a quite complicated variable to describe for this system. It is expressed as the difference between the average pressure P_{av} of the fluid in the vessel and the equilibrium pressure P_{eq} for which the arteriole is in equilibrium with this pressure at its present radius and muscular tone.

$$P_{trans} = P_{av} - P_{eq}$$

On top of the elastic reaction of the arteriolar wall P_{el}, activation of the smooth muscle cells in this wall gives rise to an additional contribution ψP_{ac} to the

equilibrium pressure that the wall can sustain at a given radius, i.e.

$$P_{eq} = P_{el} + \psi([\mathrm{NaCl}])P_{ac}$$

Here, $\psi([\mathrm{NaCl}])$ is the the strength by which the active constriction takes place. If the salt concentration at the macula densa, [NaCl] is low, then ψ is also low, thus reducing the contraction of the afferent arteriole and, hence, increases the glomerular filtration. The dynamics of the active contribution, better known as the myogenic response, is shortly discussed below. The corresponding equations are represented in the flow diagram of Fig. 1.8 by two rates labeled d^2r/dt^2 and dr/dt with corresponding state variables.

The myogenic response is a process that is best understood on the cellular level. It is often observed that models on some space- and time level need to include processes on other levels. We have already seen one example of this: the Michaelis-Menten transport of salt in the ascending loop of Henle. This process can also be described on the chemical level, but the thermodynamic averages causes a macroscopic relationship to be a sufficient description of the process. By using a similar approach Feldberg *et al.* [11] have derived a macroscopic relationship between the constriction of arterioles and blood pressure, that includes the effect of the smooth muscle cells. The model is based on the assumption of nonlinear elastic stress-strain relationship and a linear relationship between the muscle tone and the stress.

The degree to which the afferent arterial resistance is changed due to an increased glomerular filtration is called the TGF transfer function (or loop gain). As mentioned above the values returned by the function is called the muscular tone. Actually, the TGF transfer function can be defined as a function of any variable along the loop of Henle, however, it is mechanistically most obvious to let it be a function of salt concentration at the site of the macula densa cells, since this is the terminal of the tubular system relevant for the autoregulation mechanism. The function is an S-shaped function with lower and upper limits, turning point and a slope at the turning point which can be determined by microperfusion experiments [5]. Especially the slope and upper limit of the function show characteristic differences between normotensive and hypertensive rats.

1.8 Simulation and Analysis

The model we have discussed in the preceding sections can be formulated mathematically as a set of ordinary differential equations. For the model with two descending and three ascending compartments of the loop of Henle 18 equations are required. Two of the equations describe the oscillations of the arterial wall and one describes the pressure in the proximal tubulus. Each

compartment, whether descending or ascending, is described by three equations representing fluid volume, amount of salt, and the delay of the fluid transport between the compartments. Computer simulations of the equations show a great variety in the dynamical behavior.

The TGF transfer function has been experimentally recorded by inserting a plug of wax in the middle of the proximal tubulus of the rat, so that the flow in the tubular system is blocked. On the other side of the wax plug a micropipette is inserted and artificial tubular fluid is infused at a constant rate. With time the system approaches a steady state and the pressure in the early proximal tubule is recorded.

With our mathematical model simulations of the microperfusion experiments can be made, by setting the glomerular filtration rate to zero and setting the flow into the loop of Henle to a constant rate, representing the externally forced infusion.

Complete bifurcation analyses are hard to perform on systems of the size of the present model. However, biological system are often infected by noise making it very difficult, if not impossible, to experimentally observe, for instance, a second period-doubling bifurcation after the first period-doubling has occurred. For the present model observations of a steady-state, a cycle, a cycle of double period and chaos, allow us to limit the analysis to bifurcations leading to these dynamical behaviors. Figure 1.10 shows a bifurcation analysis with the total delay time T and strength α of the TGF transfer function as the parameter. For small α values the system is in equilibrium with no time-dependent variations. As α is increased, the equilibrium point becomes unstable in a Hopf bifurcation, and a limit cycle is born. As it is clear from the figure a further increase of α may give rise to a cycle of double period followed by a period-doubling cascade leading to chaotic dynamics. The existence of all four types of behaviors is important for the validity of the model. But additional validation is required in order to claim that the model and parameters used are correct. As mentioned earlier, the period of the oscillations has been measured to be in the range of 30 to 40 seconds. The period of the simulated oscillations depends mainly on the delay time T. For delays in the range from 9 to 13 s the period resembles those measured experimentally, a range that partly covers the region with all of the four types of dynamics, see Fig. 1.10. The scan through the diagram at constant T =12.5 s is displayed Fig. 1.11 shows the dynamical behavior in more detail. The period doubling at $\alpha = 14$ is followed by a cascade of period doubling transitions leading to deterministic chaos. At larger α a reverse period doubling cascade terminate the chaotic region, a new cascade is initiated, and new regions with chaos appear. At $\alpha = 12.5$ and $\alpha = 17$ the periodic and chaotic attractors are shown, (A and B) of Fig. 1.11.

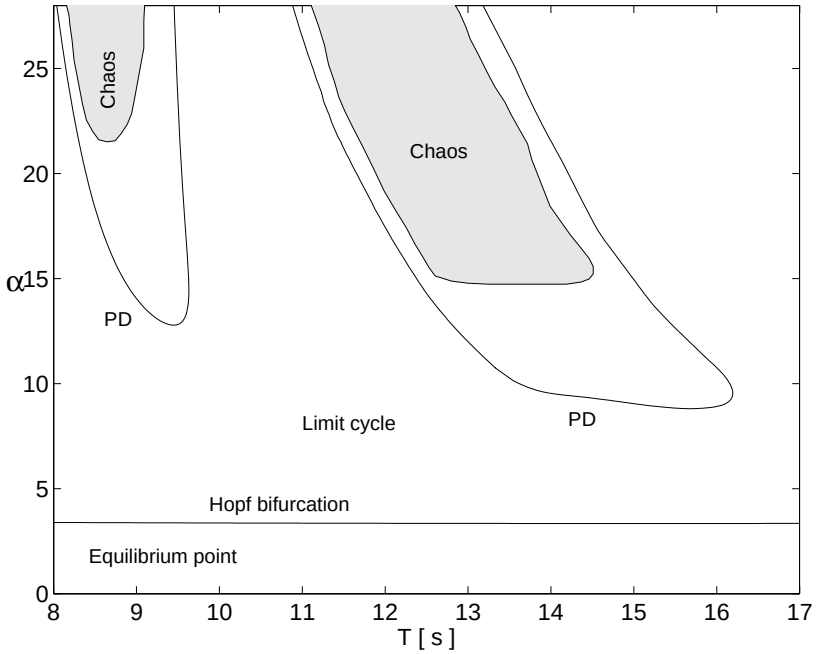

Fig. 1.10 Two-parameter bifurcation diagram for the extended nephron model showing the Hopf bifurcation at $\alpha \approx 4$, two tongues delineated by period-doubling bifurcations, and the regions dominated by chaotic dynamics.

Fast oscillations of the proximal pressure and arterial wall arise as a consequence of the pulsatile contractions of the smooth muscle cells when the arterial pressure is high. For the period-1 cycle shown in Fig. 1.11 the fast oscillations are clearly visible, as the orbit makes 5 fast cycles for each of the slow TGF-mediated oscillations. The number of fast oscillations per cycle of the slow oscillations depends on the parameters of the model, and as we increase the value of α (or T) we move from a region with 5:1 dynamics into a region with six oscillations for each slow oscillation.

The idea of creating a lumped model of the loop of Henle is to model the salt concentration along the loop. With the chosen number of compartments we obtain average concentrations within each compartment, and parameters specific to the tubules wall anatomy are either integrated over the compartment length if originally specified as a value per length or divided by the number of compartments if originally given as an effective parameter for the whole loop.

The temporal evolution of the tubular pressures along the loop is shown in Fig. 1.12 for a delay of $T = 12.5$s and a TGF feedback gain of $\alpha = 10$. For this value of the total delay the period is 38 s, and we also see that there is a phase shift of 11.5 s between the proximal pressure and the distal NaCl concentra-

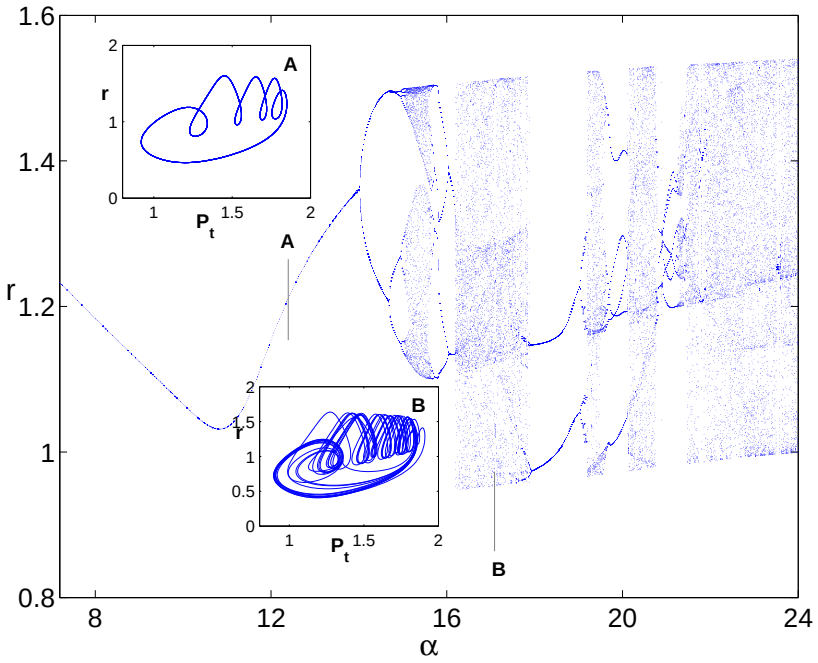

Fig. 1.11 Diagram showing the bifurcations and solutions as the TGF gain α is varied while the delay is kept constant at T =12.5 s. At low α the solution is oscillatory with a period of 38 s. As α increase a period doubling take place at $\alpha \approx 14$. Thereafter a cascade of period doublings lead to chaotic dynamics interrupted by periodic windows.

tion. The phase shift depends on the tubular compliances along the loop, since a highly compliant tubular segment can accommodate fluid at high pressure and release it as the pressure decreases. Also the decreasing amplitude of the pressure is accounted for by the relative large compliance in connection with the flow resistance.

Variation in time of the salt concentration along the loop is shown in Fig. 1.13. In the proximal tubule the concentration is defined constant equal to 150 mM in accordance with experimental knowledge. With appropriate absorption rates the concentration increases in the descending limb to 350 mM in the second compartment corresponding to the bend of the loop. In the subsequent compartments, that represent the ascending limb the Michaelis-Menten reabsorption of NaCl accounts for the decrease towards a concentration of 30 mM at the end of the loop.

Both this phase shift and the presence of period doubling and chaos depend on the compliance of the loop of Henle. For increasing compliance the phase shift increases and the period doubling and chaotic regions appear at larger values of α. Compliances measured in vitro [8] have indicated that the Henle

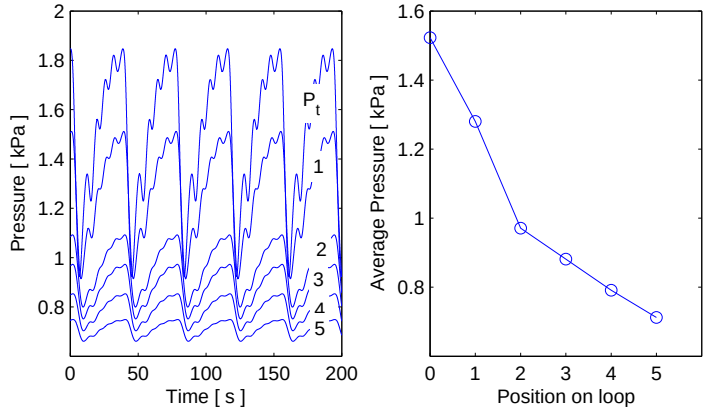

Fig. 1.12 Tubular pressures. *Left:* Time evolution of the pressures along the loop beginning with the proximal pressure (labeled P_t). Oscillations have a period of approximately 38 s. Note, how the amplitude of the oscillations is increasingly damped. *Right:* Time average of the pressures along the loop.

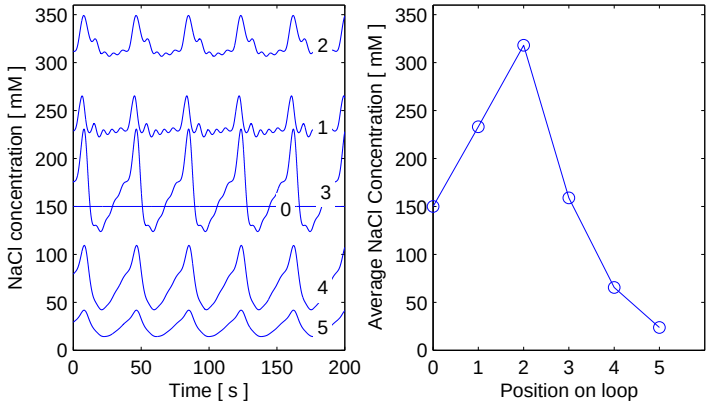

Fig. 1.13 NaCl concentrations. *Left:* The time evolution of the NaCl concentration along the loop, with the proximal concentration defined constant equal to 150 mM. Along the loop a phase shift evolves and at the distal tubulus the phase shift between the proximal pressure and the distal salt concentration is 11.5 s. *Right:* Time average of the concentrations. Clearly, the concentration increases in the descending limb (0-2) and decreases in the ascending limb (3-5).

compliance may be approximately 20 times larger than the proximal compliance. However, simulations with these larger values completely destroy the picture of the above findings. This seems to demonstrate that, when living tissue is taken out of its natural environment, the properties may change dras-

tically. One should also not forget that the tubular system of the nephron is surrounded by the tissue of the interstitium, which may have a large effect of the dynamical properties.

In the present chapter we have described a lumped model of a single nephron in the kidney. This model combines a description of the interacting myogenic and TGF-mediated mechanisms of nephron autoregulation with a description of the reabsorption of water and salts in the loop of Henle. The key features of nephron autoregulation we have aimed to reproduce are

- Four types of qualitative different dynamical behaviors: equilibrium state, oscillatory, oscillatory with double period and chaotic.
- A phase shift in the oscillation between the proximal pressure and distal NaCl concentration of 10-15 seconds.
- TGF transfer functions obtained by microperfusion experiments on normo- and hypertensive rats.
- Increasing NaCl concentration along the descending limb and decreasing NaCl concentration along the ascending limb of Henle's loop.
- Slow and fast oscillations of periods 30-40 s and 5-6 s, respectively, the fast oscillations being caused by the model for the afferent arteriole.

Other aspects of the nephronic system are described in our recent publications [49, 50].

1.9 The Promise of Systems Biology

Understanding the complex dynamic phenomena of the living world is one of the main scientific challenges of the coming decades. The way to acquire such understanding must necessarily involve a more direct and effective integration of experimental and computational research. Hypothesis-driven, or mechanism-based modeling is an approach in which the physiological, pathological and pharmacological processes of relevance to a given problem are represented as directly as possible. This approach allows us (i) to test whether assumed hypotheses are consistent with observed behavior, (ii) to examine the sensitivity of a system to parameter variation, (iii) to learn about processes not directly amenable to experimentation, and (iv) to predict system behavior under conditions not previously experienced. By virtue of the direct physiological interpretation of the involved parameters, mechanism based modeling provides a tool for translation between species and interpolation among

groups. This implies, for instance, that the pharmaceutical industry to a certain extent can predict human responses to a new drug from animal experiments by replacing the physiological parameters with parameters relevant to man.

Systems Biology is a scientific approach that seeks to understand how all the individual components of a biological system interact in time and space to determine the functioning of the system. This involves description of

- The structure of a biological system, i.e. the significant physiological components and their structural relationships at the appropriate spatial scale;
- The dynamical behavior of the system under different conditions and external perturbations;
- The mechanisms that control the states and behavior of the system;
- The causes of system changes in connection with various diseases and the methods by which such changes can be counteracted or compensated.

A model of a biological system can only be expected to reproduce experimentally observed features, if the mechanisms responsible for these features are implemented in the model. Therefore, a model can never be expected to reproduce all experimental findings. However, a model is usually build with the intension to model specific phenomena and behaviors. If some of these key features fail to be produced, a revision of the model is required.

Bibliography

1 Moore, L. C., Am. J. Physiol. 247 (**1984**), pp. F267-F276

2 Leyssac, P. P., Baumbach, L., Acta Physiol. Scand. 117, (**1983**), pp. 415-419

3 Holstein-Rathlou, N.-H., Leyssac, P. P., Acta Physiol. Scand. 126 (**1986**), pp. 333-339

4 Leyssac, P. P., Holstein-Rathlou, N.-H., Pflügers Archive 407, (**1986**), pp. 285-291

5 Leyssac, P. P., Holstein-Rathlou, N.-H., Pflügers Archive 413 (**1989**), pp. 267-272

6 Jensen, K. S., Holstein-Rathlou, N.-H., Leyssac, P. P., Mosekilde, E., Rasmussen, D. R., *Chaos in a system of interacting nephrons*, in *Chaos in Biological Systems*, Ed. H. Degn, A. V. Holden, and L. F. Olsen, Plenum, New York, **1987**

7 Barfred, M., Mosekilde, E., Holstein-Rathlou, N.-H., Chaos 6 (**1996**), pp. 280-287

8 Sakai, T., Craig, D. A., Wexler, A. S., Marsh, D. J., Biophysical Journal 50 (**1986**), pp. 805-913

9 Funk, W., Endrich, B., Messmer, K., Intaglietta, M., Int. J. Microcirc. Clin. Exp. 2 (**1983**), pp. 11Ű25

10 Aalkjær, C., Nilsson, H., British Journal of Pharmacology 144 (**2005**), pp. 605-616

11 Feldberg, R., Colding-Jorgensen, M., American Journal of Physiology 269 (**1995**), pp. F581-F593

12 Knobil, E., Recent Progress in hormone research 36 (**1980**), pp.53-88

13 Leyendecker, G., Wildt, L., Proceedings of the 3rd Ferring Symposiom, Noordwijk, Netherlands, september 11-13, (**1985**)

14 Smith, W. R., Bulletin of Mathematical Biology 42 (**1980**), pp. 57-78

15 Meirovitch, L., *Methods of Analytical Dynamics,* McGraw-Hill, New York, (**1970**)

16 Zolman, J., Am. J. Physiol. 248 (**1985**), pp. R312-R319

17 Alon, U., *An introduction to Systems Biology: Design Principles of Biological Circuits,* Chapman and Hall, London, (**2007**)

18 Bertau, M., Mosekilde, E., Westerhoff, H. (eds.), *Biosimulation in Drug Development,* Wiley-VCH, Weinheim, (**2008**)

19 Baldi, P., Brunak, S., *Bioinformatics: The Machine Learning Approach,* MIT Press, Massachusetts, (**1998**)

20 Kitano, H, *Foundations of Systems Biology*, MIT Press, Cambridge, (**2001**)

21 Hunter, P. J., Nielsen, P., Physiology 20 (**2005**), pp. 316-325

22 Noble, D., Science 295 (**2002**), pp. 1678-1682

23 Hastings, M. H., Reddy, A. B., Maywood, E. S., Nat. Rev. Neurosci. 4 (**2003**), pp. 649-661

24 Levi, F., Lancet Oncology 2 (**2001**), pp. 307-315

25 Murray, J. D., *Mathematical Biology,* Springer, New York, (**2002**)

26 Nicolis, G., Prigogine, I., *Self-Organization in Nonequilibrium Systems,* Wiley, New York, (**1977**)

27 Bergé, P., Pomeau, Y., Vidal, C., *Order within Chaos,* Wiley, New York, (**1984**)

28 Afraimovich, V. S., Shilnikov, L. P., Am. Math. Soc. Transl. 149 (**1991**), pp. 201-212

29 Thompson, J. M. T., Stewart, H. B., *Nonlinear Dynamics and Chaos,* Wiley, New York, (**1986**)

30 Pikovsky, A., Rosenblum, M., Kurths J., *Synchronization - A Universal Concept in Nonlinear Sciences,* Cambridge Univ. Press, New York, (**2001**)

31 Morecroft, J. D. W., Sterman, J. D., *Modeling for Learning Organizations,* Productivity Press, Portland, (**1994**)

32 Yen, S. S. C., Jaffe, R. B., Barbieri, R. L., *Reproductive Endocronology: Physiology, Pathophysiology, and Clinical Management,* Saunders, Philadelphia, (**1999**)

33 The Academy of Medical Sciences and the Royal Academy of Engineering., *Systems Biology: a Vision for Engineering and Medicine,* February, (**2007**)

34 European Science Foundation, *Systems Biology: a Grand Challenge for Europe,* August, (**2007**)

35 Veldhuis, J. D., *The hypothalamic-pituitary-testicular axis,* In:Reproductive Endocrinology (3rd ed.), Ed. S. S. C. Yen, R. B. Jaffe, Saunders, Philadelphia, (**1991**)

36 Bassett, N. S., Gluckman, P.D., J Endocrinol. 109 (**1986**), pp. 307-312

37 Polonsky, K. S., Given, B. D., Hirsch, L. J., Tillil, H., Shapiro. E. T., Beebe, C, Frank, B. H., Galloway, J. A., Van Cauter, E., N. Engl. J. Med. 318 (**1988**), pp. 1231-1239

38 Bergsten, P., Hellman, B., Biochem. Biophys. Res. Commun. 192 (**1993**), pp. 1182-1188

39 Glass, L., Mackey, M. C., *From Clocks to Chaos: The Rhythms of Life,* Princeton University Press, Princeton, (**1988**)

40 Kronenberg, F., Cote, L. J., Linkie, D. M., Dyrenfurth, I., Downey, J. A., Maturitas 6 (**1984**), pp. 31-43

41 Feigenbaum, M. J., Communications in Mathematical Physics 77 (**1980**), pp. 65-86

42 Sturis, J., Knudsen, C., O'Meara, N. M., Thomsen, J. S., Mosekilde, E., Van Cauter, E., Polonsky, K. S., Chaos 5 (**1995**), pp. 193-199

43 Chay, T. R., Biophysical Journal 73 (**1997**), pp.1673-1688

44 Tass, P. A., Biol. Cybern. 85 (**2001**), pp. 343-354

45 Gylfe, E., Grapengiesser, E., Hellman, B., Cell. Calcium. 12 **1991**, pp. 229-240

46 Peng, H., Matchkov, V., Ivasen, A., Aalkjaer, C., Nilsson, H., Circulation Research 88 (**2001**), pp. 810-815

47 Mormont, M. C., Levi, F., Cancer 97 (**2003**), pp. 155-169

48 Postnov, D. E., Sosnovtseva, O. V., Mosekilde, E., Holstein-Rathlou, N.-H., Int. J. Mod. Phys. B 15 (**2001**), pp. 3079-3098

49 Sosnovtseva, O. V., Postnov, D. E., Mosekilde, E., Holstein-Rathlou, N.-H., Chaos Solitons and Fractals 15 (**2003**), pp. 343-369

50 Sosnovtseva, O. V., Pavlov, A. N., Mosekilde, E., Yip, K.-P., Holstein-Rathlou, N.-H., Marsh, D., Am. J. Physiol. 293 (**2007**), pp. F1545-1555

51 Mosekilde, E., Sosnovtseva, O. V., Holstein-Rathlou, Basic Clinical Pharmacology and Toxicology 96 (**2005**), pp. 212-234